UNIVERSIDAD COMPLUTENSE DE MADRID
FACULTAD DE CIENCIAS FÍSICAS

TESIS DOCTORAL

Termodinámica e información en sistemas cuánticos abiertos

Thermodynamics and information in open quantum systems

MEMORIA PARA OPTAR AL GRADO DE DOCTOR

PRESENTADA POR

Jorge Tabanera Bravo

Director

Juan Manuel Rodríguez Parrondo

Madrid

© Jorge Tabanera Bravo, 2023

Universidad Complutense de Madrid
Facultad de Ciencias Físicas

Termodinámica e información en sistemas cuánticos abiertos

Thermodynamics and information in open quantum systems

Jorge Tabanera Bravo

Bajo la supervisión de

Juan Manuel Rodríguez Parrondo.

Universidad Complutense de Madrid

Facultad de Ciencias Físicas

Termodinámica e información en sistemas cuánticos abiertos

Thermodynamics and information in open quantum systems

Memoria presentada para optar al grado
de Doctor en Física por

Jorge Tabanera Bravo

Bajo la supervisión de

Juan Manuel Rodríguez Parrondo.

A mis padres.

Agradecimientos

Mi agradecimiento a mi director de tesis, Juan Manuel Rodríguez Parrondo, por darme esta oportunidad de iniciar mi carrera investigadora y por guiarme a lo largo de estos años con una paciencia inagotable. Realmente, yo no conocía a Juanma de nada el día que fui a su despacho, a principios de 2019, y le pregunté si sería posible hacer una tesis doctoral, pero de todas formas él me propuso este proyecto; todo lo que sigue es resultado de aquella confianza que depositó en mi.

Un agradecimiento muy especial a Natalia Ares y a todo el equipo de NanoQit, con quien he trabajado duramente estos años, Federico Fedele, Federico Cerisola, Kushagra Aggarwal, Jonathan Dexter, Joe Dunlop, Léa Bresque, Janet Anders, Alexia Auffèves y en particular a Florian Vigneau y a Juliette Monsel. Gracias también a Gerard Milburn, y a toda la gente que conocí en Oxford durante mis estancias allí por introducirme en un ambiente tan creativo.

Gracias a Massimiliano Esposito y a Felipe Barra por la colaboración que hemos llevado a cabo.

Gracias a todos mis amigos y compañeros de la Universidad Complutense, Miguel Barriuso y a Juan Pablo Miranda y a los profesores Ricardo Brito, Armando Relaño, Chantal Valeriani, Luis Dinis y Juan José Mazo, y a Carlos Mejía, de la Universidad Politécnica de Madrid.

Un reconocimiento muy sincero a José Martín Roca, por su ayuda y comentarios a la hora de preparar este manuscrito y en general, por nuestros continuos debates sobre termodinámica, programación y todo lo demás.

Gracias igualmente a Cristina Cabello, Roberto Ruiz, Andrés Agustí, Javier Faba y Javier Barranco por las muchas conversaciones interesantes que hemos tenido todos estos años, algunas de carácter científico, y por su revisión del manuscrito. A Elena Pascual Sánchez, por su asesoramiento emocional-socio-cognitivo-conductual durante todo el desarrollo de esta tesis.

Y, finalmente, gracias a mi más estrecho colaborador, Trasto, que durante los dos años de pandemia trabajó duramente a mi lado; nadie lo sabía en las reuniones online, pero siempre estuvo debajo de la mesa.

Nunca logro imponerme leer las escrituras de cabo a rabo ni examinar las transacciones que, a decir verdad, deberían necesariamente ser objeto de mi atención y de mi control. No es desdén filosófico por las cosas mundanas y transitorias... No, en realidad es por una pereza y una negligencia pueriles e inexcusables.

–Michel de Montaigne.

Contents

Resumen

Resumen

Entre las escalas macroscópica y microscópica existe una escala intermedia denominada mesoescala. A esta escala, los sistemas pequeños se ven influidos por su ruidoso entorno, siguen trayectorias fluctuantes y evitan las coherencias cuánticas. Los recientes avances en técnicas experimentales nos han permitido acceder a esta mesoescala, desvelando una rica fenomenología y proporcionando un control sin precedentes sobre nanodispositivos artificiales. El objetivo principal de esta tesis es describir la termodinámica de tales dispositivos, conectando modelos teóricos con novedosos hallazgos experimentales.

La primera parte de esta tesis se basa en el ámbito de la termodinámica de la información, una teoría física que se ha desarrollado en las últimas décadas. El papel de la información en la termodinámica ha sido objeto de debate desde los tiempos de Maxwell, pero ha cobrado renovada atención con la llegada de la teoría de la información de Shannon y los recientes avances experimentales y teóricos. El principio de Landauer establece un vínculo formal entre la disipación de energía y los procesos informáticos, sentando las bases de la termodinámica de la información.

En este trabajo, me centro en una implementación específica de un nanodispositivo, a saber, el resonador de un solo electrón. Este dispositivo implica un oscilador a nanoescala, como un nanotubo de carbono completamente suspendido, que es impulsado por la corriente estocástica de electrones que fluyen a través del tubo. La dinámica de este sistema puede describirse mediante una ecuación de Fokker-Planck, que engloba tanto el comportamiento del nanooscilador como el transporte ruidoso de electrones. Para probar este modelo pueden realizarse experimentos de autooscilación, en los que la excitación del oscilador es instantánea.

La termodinámica del resonador de un solo electrón puede deducirse directamente de la ecuación de Fokker-Planck. Nos permite definir magnitudes termodinámicas como el calor y el trabajo y derivar la desigualdad de Clausius, que encarna la segunda ley de la termodinámica. Sin embargo, debido a la naturaleza bipartita del sistema, la termodinámica puede describirse en términos de dos desigualdades distintas similares a la segunda ley -una para el oscilador y otra para el transporte de electrones- conectadas a través del flujo de información entre los subsistemas.

Por último, exploraré la física de los baños de colisión cuánticos para concluir el análisis. Estos modelos teóricos están diseñados para describir la interacción de un sistema cuántico con su entorno. La imagen intuitiva de un sistema de este tipo implica un sistema cuántico objetivo rodeado por un gas de partículas cuánticas más pequeñas, conocidas como ancillae, que colisionan ocasionalmente con el sistema objetivo. Sin

embargo, la termodinámica de estos modelos a veces puede ser incoherente, dando lugar a efectos espurios y dificultando la termalización. En mi investigación, examinaré la relación de los depósitos colisionales cuánticos y estableceré las condiciones mínimas necesarias para que estos modelos exhiban un comportamiento térmico genuino. Esta discusión abordará un problema fundamental en el campo de los sistemas cuánticos abiertos: el problema de lo local frente a lo global.

Abstract

Between the macroscopic and microscopic scales, there exists an intermediate scale known as the mesoscale. At this scale, small systems are influenced by their noisy environment, following fluctuating trajectories and avoiding quantum coherences. Recent advancements in experimental techniques have allowed us to access this mesoscale, unveiling a rich phenomenology and providing unprecedented control over artificial nano-devices. The primary objective of this thesis is to describe the thermodynamics of such devices, connecting theoretical models with novel experimental findings.

The first part of this thesis is grounded in the framework of information thermodynamics, a physical theory that has been developed over the past few decades. The role of information in thermodynamics has been a subject of debate since Maxwell's time, but it has gained renewed attention with the advent of Shannon's theory of information and recent experimental and theoretical progress. Landauer's principle provides a formal link between energy dissipation and computing processes, establishing the foundations of information thermodynamics.

In this work, I focus on a specific implementation of a nano-device, namely the single electron resonator. This device involves a nanoscale oscillator, such as a fully suspended carbon nanotube, that is driven by the stochastic current of electrons flowing through the tube. The dynamics of this system can be described by a Fokker-Planck equation, which encompasses both the behaviour of the nano-oscillator and the noisy electron transport. Self-oscillation experiments, where the excitation of the oscillator is instantaneous, can be conducted to test this model.

The thermodynamics of the single electron resonator can be derived straightforwardly from the Fokker-Planck equation. It allows us to define thermodynamic quantities such as heat and work and derive the Clausius inequality, which embodies the second law of thermodynamics. However, due to the bipartite nature of the system, the thermodynamics can be described in terms of two distinct second law-like inequalities—one for the oscillator and one for the electron transport—connected through the flow of information between the subsystems.

Finally, I will explore the physics of quantum collisional baths to conclude the analysis. These theoretical models are designed to describe the interaction of a quantum system with its surrounding environment. The intuitive picture of such a system involves a quantum target system surrounded by a gas of smaller quantum particles, known as ancillae, which occasionally collide with the target system. However, the thermodynamics of these models can sometimes be inconsistent, leading to spurious effects and hindering thermalization. In my investigation, I will examine the relationship of quantum collisional reservoirs and

establish the minimal conditions required for these models to exhibit genuine thermal behaviour. This discussion will address a fundamental problem in the field of open quantum systems—the local versus global problem.

Publicaciones

This thesis is based on the results published in

1. Tabanera, J., Luque, I., Jacob, S. L., Esposito, M., Barra, F., & Parrondo, J. M. (2022). Quantum collisional thermostats. New Journal of Physics, 24(2), 023018.

2. Vigneau, F., Monsel, J., Tabanera, J., Aggarwal, K., Bresque, L., Fedele, F., ... & Ares, N. (2022). Ultrastrong coupling between electron tunneling and mechanical motion. Physical Review Research, 4(4), 043168.

3. Tabanera-Bravo, J., Parrondo, J. M., Esposito, M., & Barra, F. (2023). Thermalization and dephasing in collisional reservoirs. Phys. Rev. Lett. 130, 200402

4. Tabanera-Bravo, J., Vigneau, F., Monsel, J., Aggarwal, K., Bresque, L., Fedele, F., ... & Ares, N. (2022). Stability of long-sustained oscillations induced by electron tunneling. arXiv preprint arXiv:2211.04074. *(Submitted to Phys. Rev. Lett.)*

In addition, along these years I had the opportunity to participate in the following work,

1. Dunlop, J., Cerisola, F., Tabanera-Bravo, J., & Anders, J. (2023). Multipurpose Quantum Thermodynamic Operations. arXiv preprint arXiv:2306.09088.

Part I.

Introduction

This thesis

This thesis focuses on the quantum thermodynamics of nanoscale systems, exploring its connection to information theory and its applicability to strongly coupled systems in specific limit situations. The thesis is divided into two parts.

The first part comprises the theoretical analysis conducted over the past few years, focusing on around an experimental device called the single electron resonator. In the initial chapter, I provide a comprehensive explanation of the properties of this resonator. The research undertaken was part of the collaborative international project known as FQxI-NanoQit, which afforded me the opportunity to collaborate with an experimental team and yield noteworthy findings. Notably, through a series of experiments, we were able to elucidate the mechanisms governing energy flow within the single electron resonator, unravelling the phenomenon of self-oscillations. The findings from these experiments are presented in the second chapter of this thesis.

In the third chapter, I utilize the aforementioned model to examine the system's thermodynamics from a foundational standpoint. Specifically, my aim is to comprehend how the principles of thermodynamics can be reinstated within the confines of this diminutive apparatus. Through my findings, I unveil the inherent connection between energy dissipation and the intricate exchange of information among the system's distinct components. As the first part culminates, I engage in a thoughtful discourse regarding the validity of the formalism known as *information flows*, which, despite its existence in the literature, remains largely unexplored.

In the second part of the thesis, I delve into the examination of *quantum collisional reservoirs* and their inherent characteristics. These reservoirs serve as simplified models aimed at capturing the interaction between a quantum system and its noisy environment. While the conventional approach of employing quantum master equations effectively describes situations where the system-environment coupling is weak, it fails to capture the essence of strong interactions. Within the fourth chapter of this thesis, I thoroughly discuss the salient features of collisional reservoirs and elucidate their implementation in order to restore thermal behaviour. Moving forward to the fifth chapter, I present the detailed design of two distinct *quantum collisional thermostats*, which are mechanisms specifically engineered to consistently restore thermal behaviour within collisional reservoirs. Finally, in the sixth chapter, I use the quantum collisional thermostats to address a fundamental problem in the realm of open quantum systems theory — the *local versus global* problem.

1. Thermodynamics of small systems

1.1. From classical to stochastic thermodynamics

Thermodynamics was born as a theoretical response to the development of technology during the industrial revolution. It is only natural that, now that nanoscience is growing enormously, we must rethink thermodynamics to adapt it to these new, uncharted lands.

In the 19th century, the main focus of physics researchers was on developing the mathematical foundations of Newtonian dynamics. Newtonian systems are described as sets of infinitely small massive points, moving along smooth trajectories in Euclidean space. While this approach was successful in describing the behavior of celestial objects, it fell short in explaining many phenomena we experience daily, especially the thermal properties of macroscopic objects. Furthermore, the study of heat lacked a rigorous treatment due to two main reasons: firstly, there were no thermometers and the concept of temperature was often subjective. Secondly, energy was not yet a well-defined notion.

Sadi Carnot (1796-1832) proposed the first rigorous formalism in his *Réflexions sur la puissance motrice du feu* (1824), which could systematically explain the behaviour of "fire machines," i.e., machines that could perform useful work from a thermal system (e.g., a piston). Even though there were only a few implementations of fire machines at that time, Carnot's formalism was intended to explain thermal behaviour "independently of any mechanism or agent," "applicable to all heat engines," and "whatever the working substance and whatever the method by which it is operated." It was this quest for abstraction in the treatment of thermal processes that defined classical thermodynamics. Carnot's analysis was remarkable in its depth and power: he demonstrated through intuitive reasoning that a thermal machine reaches maximum efficiency when it operates in a reversible manner[1], a fundamental result in the incipient industrial revolution.

The formalism following Carnot's analysis was further developed by William Thomson, Lord Kelvin (1824-1907), and Rudolf Clausius (1822-1888), who established the two principles of thermodynamics[2] in [Clausius, 1850].

- The *first law of thermodynamics*, or *energy conservation*, states that the change in the total energy of a thermal system is equal to the *work* performed on it plus the

[1] Otherwise, infinite energy could be extracted from a thermal bath by extracting work irreversibly and restoring the initial state reversibly.

[2] Thomson was the first to use the term *thermodynamics*, or the "dynamics of heat".

energy dissipated into the environment, called *heat*. To better understand what *heat* and *total energy* mean in this context, one can consider a system evolving adiabatically (without exchanging energy with its environment). In such a case, the work performed on the system, W_{ad} (measurable in the laboratory), *is a function only of the system state*, and not of the arbitrary working protocol. If the machine exchanges energy with the environment, the heat of a certain process, Q, is by construction the difference between this adiabatic work and the process work W:

$$Q = W_{ad} - W. \tag{1.1}$$

Since W_{ad} only depends on the initial and final state and not on the followed path, it is identified with the total energy exchange in the thermal machine $\Delta U = Q + W$, or *internal energy* exchange.

- The *second law of thermodynamics* or *increase of entropy* is based on Carnot's statement that a thermal machine must work between two heat sources at different temperatures; no machine could operate in contact with a single heat source. Moreover, the cold source could never cool down at the expense of spontaneously releasing heat to the hotter one. To formalize this statement, Clausius introduced the *entropy*[3] as a function of the system variable, which changes in a reversible process in contact with a thermal bath:

$$\Sigma = \Delta S - \frac{Q}{T}, \tag{1.2}$$

where T is the bath temperature, ΔS is the change in the entropy of the thermal machine[4]. The second law states that the entropy production is always positive: $\Sigma \geq 0$, being the equality reached only in reversible processes.

Notice that Carnot's definition of a thermodynamic system (a fire machine) is quite general. In classical thermodynamics, the definition of a *thermodynamic system* applies to macroscopic systems defined by a set of state variables (pressure, volume, magnetization, etc.) in contact with an environment at a certain temperature. Along this thesis, I will study how the laws of thermodynamics are recovered in increasingly smaller systems (nano-resonators, qubits) in contact with noisy environments.

1.1.1. Consequences of the second law

In his 1865 paper *On a universal tendency in nature to the dissipation of mechanical energy*, William Thomson deduced the absolute scale of temperatures, obtained the third

[3] In Clausius' words 'I prefer going to the ancient languages for the names of important scientific quantities, so that they may mean the same thing in all living tongues' [Clausius, 1865]. The word *en-tropy* comes from the Greek term "with-transformation", very similar to *en-ergy*, something like "with-work", also related to my name *Jorge–George*, from the Greek "earth-worker".

[4] Note that the second law is independent of the first law, but the entropy production requires the definition of heat. If the system evolves cyclically, $\Delta S = 0$. Expressing the second law using entropy implies the logical assumption of the first one.

law of thermodynamics, and proposed the unavoidable idea of universal thermal death, which states that the universe will eventually achieve the global thermal equilibrium state, where no work can be exchanged[5].

From a less fundamental scope, the second law is related to the efficiency of thermal processes. Since all the processes in practice dissipate energy into the environment, the second law sets a fundamental limit on how much useful energy we are going to get from so much energy invested. The ratio of energy gain to energy investment is called *thermodynamic efficiency*, and it is always less than one, avoiding the idea of the perpetual mobile. This would be any mechanism that, drawing energy from a single heat source, is capable of extracting useful energy. In any case, the consequences of the second law involve a system evolution, this is, the second law distinguishes between after and before, allowing the systems to evolve from one state to another, but never in the opposite sense, contrary to what happens in Newtonian mechanics.

Information and interpretation of the second law

The first work suggesting a paradox between the macroscopic second law of thermodynamics and the Newtonian microscopic description of matter involving fluctuations is attributed to James Clerk Maxwell, in correspondence with Peter Guthrie Tait [Knott and Tait, 1911],

"I do not know in a controversial manner the history of thermodynamics, that is, I could make no assertions about the priority of authors without referring to their actual works... Any contributions I could make to that study are in the way of altering the point of view here and there for clearness or variety, and picking holes here and there to ensure strength and stability.

" As for instance, I think that you might make something of the theory of the absolute scale of temperature by reasoning pretty loud about it and paying it due honor at its entrance. To pick a hole — say in the 2nd law of [...], that if two things are in contact the hotter cannot take heat from the colder without external agency.

" Now let A and B be two vessels divided by a diaphragm and let them contain elastic molecules in a state of agitation which strike each other and the sides.

" Let the number of particles being equal in A and B but let those in A have the greatest energy of motion. Then even if all the molecules in A have equal velocities, if oblique collisions occur between them their velocities will become unequal, and I have shown that there will be velocities of all magnitudes in A and the same in B, only the sum of the squares of the velocities is greater in A than in B.

" When a molecule is reflected from the fixed diaphragm CD no work is lost or gained.

" If the molecule instead of being reflected were allowed to go through a hole in CD no work would be lost or gained, only its energy would be transferred from one vessel to the other.

" Now conceive a finite being who knows the paths and velocities of all the molecules by simple inspection but who can do no work except open and close a hole in the diaphragm by means of a slide without mass.

" Let him first observe the molecules in A and when he sees one coming the square of whose velocity is less than the mean sq. vel. of the molecules in B let him open the hole and let it go

[5]Good news for the researchers in this field, since our labour will become trivial.

into B. Next let him watch for a molecule of B, the square of whose velocity is greater than the mean sq. vel. in A, and when it comes to the hole let him draw the slide and let it go into A, keeping the slide shut for all other molecules.

"Then the number of molecules in A and B are the same as at first, but the energy in A is increased and that in B diminished, that is, the hot system has got hotter and the cold colder, and yet no work has been done, only the intelligence of a very observant and neat-fingered being has been employed.

" Or in short if heat is the motion of finite portions of matter and if we can apply tools to such portions of matter so as to deal with them separately, then we can take advantage of the different motion of different proportions to restore a uniformly hot system to unequal temperatures or to motions of large masses.

" Only we can't, not being clever enough.

The image of a mechanism (*finite being*) breaking the laws of thermodynamics by acting on individual molecules was named *Maxwell demon*. In the early debates about its plausible implementation, the demon was understood as a kind of valve that let the particles of a gas circulate in unique directions, therefore something completely feasible, the second law of thermodynamics is a statistical artifice [Maxwell, 1990].

The first explicit proposal for a mechanism capable of extracting work using individual particles was given by Leo Szilard [Szilard, 1929]. Following in Maxwell's footsteps, he proposed a system consisting of a container in which a single molecule moves. By observing the position of the molecule and its velocity, a wall is conveniently arranged which will be pushed by the molecule, performing an adiabatic expansion and generating work. This started a historical discussion that we are currently engaged in.

The nature of fluctuations in thermodynamic systems was not treated rigorously until the work of Albert Einstein [Einstein, 1905] and Marian Smoluchowski [Von Smoluchowski, 1906] in the early 20th century. It is Smoluchowski himself who in 1912 proposed the first formal argument against the feasibility of Maxwell's mechanism [Smoluchowski, 1927]; according to him, fluctuations occur both to violate the second law and to recover it, preventing the extraction of energy on average.

1.1.2. Thermodynamics and information

Currently, the debate has been synthesized between Maxwell's initial idea –it is possible to violate the second law of thermodynamics in certain systems, and Smoluchowski's –fluctuations prevent the second law from being violated. For this, it is considered that an observer of the fluctuations, Maxwell's *finite being* or "Maxwell demon", when measuring the position of the molecules in the containers, reducing the system entropy at the cost of increasing his own entropy. The second law of thermodynamics is preserved as long as it applies to the whole system, but it is locally violated.

To express the precise relation between information and physical manipulation, in 1961 Rolf Landauer considered not a gas, but a system able to store information, a computer memory [Landauer, 1961]. The memory would contain information stored in the form of zeros and ones, represented by a certain number of *information-bearer* degrees of

freedom. When one performs a computation with that information, it manipulates those degrees of freedom, affecting the rest of the computer. Landauer's principle states *that in any logically irreversible operation, performed on the information-bearer degrees of freedom, involves a heat exchange with the rest of the system.* In the words of Landauer, *information is physical* [Landauer et al., 1991].

Under this assumption, Maxwell's finite being cannot extract useful energy from the system without dissipation, since it must erase its own memory [Bennett, 1982]. Following Landauer, the thermodynamic cost of rewriting a bit initialized in the state 0 or 1 indistinctly is given by the device entropy dissipation $\simeq kT \ln 2$, where k is the Boltzmann constant and T the environment temperature. This process is known as *Landauer's overwrite*. For a modern review on this topic, see [Wolpert, 2019].

Criticism

The thermodynamics of information following Landauer's principle is well established today. However, some criticisms remain that cannot be overlooked. Before continuing, I want to mention a few of them

1. If Maxwell's finite being is a physical system, Landauer's principle follows from the second law of thermodynamics and is therefore always fulfilled. If the finite being is not a thermodynamic system, then it is irrelevant. Therefore, the relationship between information and entropy is either trivially fulfilled by the second law, or it is irrelevant [Earman and Norton, 1999].

2. As Maxwell thought, it could be that the second law was a statistical artifice. In practice, the second law is never observed, since the energy lost in our laboratory apparatus far exceeds the efficiency limit set by Landauer's principle $\simeq T \ln 2$, which is never relevant [Bennett, 2003].

3. Introducing a macroscopic element such as a piston or a damper whose fluctuations are neglected is not a harmless action, but creates a non-equilibrium situation in the system, allowing the violation of the second law. This situation has been analyzed in detail in ref.[Alicki and Horodecki, 2019]. In this reference, it is established that any information bearer system must be *stable with respect to thermal or quantum noise*, and remarks that a system could have thermodynamic entropy but no information, making asymmetric the equivalence between the two.

Despite these criticisms, Landauer's principle continues to attract the attention of the scientific community, which refuses to abandon it. This is because it is a practical, useful, and quite pedagogical statement, as Charles Bennett points out in [Bennett, 2003].

With respect to (1), as we shall see in this thesis, one can derive the thermodynamics of a device departing from a microscopic model considering fluctuations, i.e. a Fokker-Planck equation; to do this, one requires to explicitly consider information exchanges within the device. In this sense, Landauer's principle is more fundamental than the second law. In the same line, with respect to (3) one can argue that microscopic models

can also deal with non-equilibrium phenomena, always recovering the second law in terms of information. With respect to (2) it is true that Landauer limit is far to be reached in several experimental implementations, where most part of the energy is dissipated in other processes, not related with information (electron conduction, heating, etc.) [Markov, 2014]. In the same line, multitask devices, where a single device is used to perform different computations [Bedingham and Maroney, 2016, Dunlop et al., 2023] depart from this limit; however, there exist important protocols where Landauer's limit is achieved when the computation is performed slow [Bérut et al., 2012]. In finite-time protocols, Landauer's limit can be approached up to a factor inversely proportional to the computing time [Aurell et al., 2012, Eckmann and Mejía-Monasterio, 2022]; very recent proposals focus on improving devices' efficiency beyond Landauer's limit at short times [Ray and Crutchfield, 2023].

Thermodynamics was constructed as a theory of energy economics during the 19th century, in situations where energy was a limiting resource. In nanotechnology, energy is not a limited resource but exists in excess, so *what is the point of doing thermodynamics at the nanoscale?* The answer is twofold: first, from an industrial point of view, we need to build more efficient computers, so maybe future transistor/neuron designs will indeed need to approach the Landauer limit [6]. In quantum technologies, it is also important to decrease the device's heating due to dissipation. Second, and from my point of view more interesting, the processes of Biology are indeed governed by well-optimized economic principles; probably the use of information has an important value in the development of living beings.

Thermodynamics of information

In 1948 Claude E. Shannon introduced a measure of uncertainty that one has about a random variable X, for instance, a message in a communication channel or a microstate of a physical system [Shannon, 1948][7]. Shannon entropy is defined as

$$S(X) = -\sum_x p_X(x) \ln p_X(x). \tag{1.3}$$

Here, $p_X(x)$ is the probability distribution of the random variable X. For a continuous variable, the sum is replaced by an integral [Cover et al., 1991]. This magnitude is measured in *bits* if the logarithm is in base 2, and in *nats* if we use the natural logarithm. In the rest of his work, we will consider the second case.

In some situations, it is not possible to directly observe the variable X and one is limited to measuring certain quantities Y. Measuring Y decreases our ignorance about X in

$$I(X:Y) = S(X) - S(X|Y). \tag{1.4}$$

[6] Just out of curiosity, the Landauer's limit to erase a single bit in thermal equilibrium at 300K is about 10^{-21}J [Landauer, 1961].

[7] See also [Brillouin, 2013].

This quantity is known as *mutual information*. The quantity $S(X|Y)$ is the uncertainty of the posterior distribution $p(x|y)$ averaged over all the measurement outcomes $Y \equiv y$,

$$S(X|Y) = -\sum_{x,y} p_{XY}(x,y) \ln p(x|y). \tag{1.5}$$

Using the relation $p_{XY}(x,y) = p(x|y)p_Y(y)$ one obtains

$$I(X:Y) = \sum_{x,y} p_{XY}(x,y) \ln \frac{p_{XY}(x,y)}{p_X(x)p_Y(y)} \tag{1.6}$$

We can observe that mutual information is symmetric, this is, measuring X provides the same information about Y than measuring Y about X. In addition, mutual information is a measure of the correlations between two variables: if the two variables are uncorrelated, this magnitude becomes zero, otherwise one can prove that it is positive, therefore

$$I(X:Y) = S(X) + S(Y) - S(X,Y) \geq 0. \tag{1.7}$$

The latter means that entropy is subadditive, and equality is achieved when systems are completely decorrelated.

The Shannon entropy is a candidate to represent the thermodynamic entropy in systems out of equilibrium. To relate the nats units with usual thermodynamic entropy units is enough to multiply the Shannon entropy by the Boltzmann constant k. The motivation for this is that, in thermal equilibrium, Shannon entropy coincides with Gibbs entropy. However, out of equilibrium, the equivalence between Shannon entropy and thermodynamic entropy is only true under certain circumstances; the reason for this is that Shannon entropy of an isolated system is constant since it follows Hamiltonian evolution. In order to obtain irreversible evolution, one must consider some loss of information, like the interaction with a noisy environment or a coarse-grained.

A physical system X in contact with a thermal environment E is described by the joint probability distribution $\rho(x,e)$. Here x and e represent the system and environment microstate, for instance, the position and velocities of the molecules of a gas in contact with a thermal bath. The thermal environment is a large system, that one could assume to be described by the thermal state

$$\rho_{\text{th}}(e;T) = \frac{e^{-\beta H_{\text{E}}(e)}}{\mathcal{Z}_{\text{E}}(T)}, \tag{1.8}$$

with $\beta = 1/kT$ the inverse temperature, and $\mathcal{Z}_{\text{E}}(T)$ the partition function. The joint system is then represented by

$$\rho(x,e) = \rho(x)\rho_{\text{th}}(e;T) \tag{1.9}$$

with

$$\rho(x) = \int de \rho(x,e). \tag{1.10}$$

Notice that the last assumption is taken because of our total ignorance of the global system microstate, due to the large bath size. In the following, we will prove that this assumption represents an information degradation compatible with the second law. Since the system and the environment are now defined by continuous variables, the entropy definition (1.3) can be calculated through the integral

$$\begin{aligned} S(X,E) &= -\int dx\ de\ \rho(x,e)\ln\rho(x,e) \\ &= -\int dx\ de\ \rho(x)\rho_{\text{th}}(e;T)\left[\ln\rho(x) - \ln\rho_{\text{th}}(e;T)\right] \\ &= -\int dx\ \rho(x)\ln\rho(x) + \int de\ \rho_{\text{th}}(e;T)\ln\rho_{\text{th}}(e;T) \\ &= S(X) + \beta E_{\text{th}}(T) + \beta\ln\mathcal{Z}_{\text{E}}(T). \end{aligned} \tag{1.11}$$

Here $E_{\text{th}}(T)$ is the average environment energy. If the temperature remains constant along a process, the total entropy produced is

$$\Delta S(X,E) = \Delta S(X) - \frac{Q}{kT}, \tag{1.12}$$

where $Q = E_{\text{th}}^{\text{init}} - E_{\text{th}}^{\text{fin}}$ is precisely the *heat* exchanged between the system X and the environment E. To prove that the last quantity is always positive, one can consider the state $\rho_{\text{H}}(x,e;t)$; this state is equal to $\rho(x,e)$ at the beginning of the process, $\rho(x,e)^{\text{init}} = \rho_{\text{H}}(x,e;t=0)$ and evolves following Hamiltonian evolution. Then

$$S[\rho] - S[\rho_{\text{H}}] = I(X:E) + \Delta S_{\text{E}} \geq 0. \tag{1.13}$$

Here $I(X:E)$, is the mutual information, Eq.(1.6), between the system and the environment contained in ρ_{H}, and $\Delta S_{\text{E}} = S[\rho_{\text{th}}] - S[\rho_{\text{HE}}]$ with

$$\rho_{\text{HE}}(e) = \int dx\ \rho_{\text{H}}(x,e). \tag{1.14}$$

Since Shannon entropy remains invariant along a Hamiltonian evolution $S[\rho_{\text{H}}] = S[\rho^{\text{init}}]$, obtaining the *Clausius inequation*

$$\Delta S(X) - \frac{Q}{kT} \geq 0. \tag{1.15}$$

From this result, we can conclude that the information degradation assumed in (1.9) is enough to recover thermodynamic reversibility. In addition, the identification of the Shannon entropy with the thermodynamic entropy supports Landauer's principle.

In a fluctuating system, the dynamics are given by a Fokker-Planck equation[8], in the case of continuous systems, or a master equation in discrete systems. Both equations

[8]This framework was developed in the works of Paul Langevin [Langevin, 1908], Adriaan Fokker [Fokker, 1914] and Max Planck [Planck, 1917] and later Hans Kramers [Kramers, 1940] or Kiyosi Itô [Ito, 1944] between others

can be written in an abstract way as $\dot{\rho} = \mathcal{L}[\rho]$. Using these equations, one can recover the concepts of *heat and work* [Sekimoto, 1998, Sekimoto, 2010], defining the *stochastic thermodynamics* of the system. To do this one considers the system time-dependent Hamiltonian H and probability distribution $\rho(x)$, and evaluates the average energy

$$E = \langle H \rangle = \int dx \rho(x) H. \tag{1.16}$$

Taking the time derivative

$$\dot{E} = \int dx \mathcal{L}[\rho] H + \int dx \rho(x) \dot{H}. \tag{1.17}$$

The first term is due to the unavoidable dissipation introduced by the Fokker-Planck, and therefore, it is identified as *heating* or *heat flow*, $\dot{Q}$. The second term is presented in the Hamiltonian time variation and is recognized as *work*, $\dot{W}$. A first law emerges assuming energy conservation, $\dot{E} = \dot{Q} + \dot{W} = 0$.

The preceding framework has been used to study from mesoscopic biological systems [Liphardt et al., 2002] to colloidal particles [Ciliberto et al., 2010], electric circuits [Ciliberto et al., 2013, Saira et al., 2012] and single-electron quantum dots [Küng et al., 2012, Koski et al., 2013] from a thermodynamical point of view. The relation with information systems, systems under measurements and external feedback Maxwell demons has been explored in several works [Esposito and Schaller, 2012, Sagawa and Ueda, 2012, Jacobs, 2009, Horowitz and Parrondo, 2011].

Now, one could be interested in *bipartite systems*. For instance, Maxwell's demon is composed of two different parts, the demon itself, and the gas. Under the action of the demon, the gas is apparently violating the second law and, therefore, the demon must be dissipating additional energy. To analyze this kind of system using stochastic thermodynamics with information, one must consider the two subsystems, let's call them X and Y, in contact with their respective individual thermal baths. Disregarding correlations with environments, the Shannon entropy of the complete system is

$$S_{\text{tot}} = S(X) + S(E_X) + S(Y) + S(E_Y) - I(X:Y). \tag{1.18}$$

If the interaction between both subsystems is weak, the local environment fluctuations prevent any correlation between X and Y. However, if the correlation is strong the mutual information $I(X:Y)$ remains in the last quantity. Taking the time derivative one obtains

$$\frac{dS(X)}{dt} + \frac{dS(Y)}{dt} + \frac{dI(X:Y)}{dt} - \frac{\dot{Q}_X}{kT_X} - \frac{\dot{Q}_Y}{kT_Y} \geq 0. \tag{1.19}$$

Here $\dot{Q}_X$ and $\dot{Q}_Y$ are the heat exchanged by the X and Y systems with their respective reservoirs at temperatures T_X and T_Y. The positivity of the last can be obtained in a similar way as I did in the one-environment case. In the steady state, both the entropy productions and the derivative of the information vanish, getting

$$-\frac{\dot{Q}_X}{kT_X} - \frac{\dot{Q}_Y}{kT_Y} \geq 0. \tag{1.20}$$

However, to gain a better understanding of the non-equilibrium processes taking place within the device it is useful to introduce the *information flows*

$$\dot{I}_X = \lim_{\tau\to 0} \frac{I(X(t+\tau);Y(t)) - I(X(t);Y(t))}{\tau} \tag{1.21}$$

and

$$\dot{I}_Y = \lim_{\tau\to 0} \frac{I(X(t);Y(t+\tau)) - I(X(t);Y(t))}{\tau}. \tag{1.22}$$

In the steady state, one has $dI(X:Y)/dt = \dot{I}_X + \dot{I}_Y = 0$ but the information flows are different from zero. In particular $\dot{I}_X = -\dot{I}_Y$. These properties allow us to interpret the thermodynamics of the system in terms of a subsystem measuring the other, for example, if $\dot{I}_X \geq 0$ the correlation between X and Y is increasing because of the evolution of $X(t)$ with fixed $Y(t)$. In this sense, X is gaining information or measuring Y.

Since both systems are in contact with separate thermal environments, one can prove the separate inequalities

$$\begin{aligned} -\dot{I}_X - \frac{\dot{Q}_X}{kT_X} &\geq 0, \\ \dot{I}_X - \frac{\dot{Q}_Y}{kT_Y} &\geq 0. \end{aligned} \tag{1.23}$$

The interest in bipartite systems has increased during the last two decades because of their ability to *exchange energy* and *communicate information*: these are composed of two distinct parts coupled by an interaction Hamiltonian modulating thermodynamic currents. For example, in [Allahverdyan et al., 2009, Rosinberg and Horowitz, 2016] the authors relate the internal energy exchange efficiency with the *information flow* of two coupled Brownian particles. In [Horowitz and Esposito, 2014] they do the same for discrete systems. Following this, in the first part of this thesis, I will study in detail the stochastic thermodynamics of a hybrid system –the single electron resonator– which is composed of a continuous system (a harmonic oscillator) coupled with a continuous system (a quantum dot).

1.2. Noisy quantum systems

Opposite to isolated quantum systems, which follow the deterministic and reversible Schrödinger equation, open systems evolve in contact with their environment, imposing a noisy irreversible evolution. There are several ways to model this kind of evolution, but the most usual tool is the *quantum master equations* (QME). In this thesis, I will develop a different framework, named *quantum collisional reservoirs*, which I introduce in the second part. However, in the rest of this introductory chapter, I start summarizing the main concepts of open quantum systems and quantum thermodynamics that I will require in the following chapters.

1.2.1. Open quantum systems

Any evolution of a quantum system, defined by a density matrix ρ, can be written in terms of a *quantum operation* or *quantum dynamical map*[9] as the most general transformation between quantum states,

$$\rho \to \rho' \equiv \mathcal{E}\rho. \tag{1.24}$$

Here $\mathcal{E}$ is a super-operator acting on ρ. In following sections we will consider Hilbert spaces with finite dimension, so we can refer both ρ and $\mathcal{E}$ to a certain vector basis,

$$\rho'_{i'j'} = \sum_{ij} \mathcal{E}^{ij}_{i'j'}\rho_{ij}. \tag{1.25}$$

The main example of such operations is the unitary evolution under a certain Hamiltonian H, $\rho'(t) = U(t)\rho U^\dagger(t)$, with $U(t) = \exp(-iHt)$. Here and in the following we take $\hbar = 1$.

The minimal physical condition one can impose on a quantum map is that it preserves the physical character of ρ, this is, it transforms quantum states into quantum states. Since any density matrix follows that: i) it is positive semi-definite and ii) it has unit trace, any quantum operation must verify:

1. Completely positive: if ρ is a positive matrix, $\mathcal{E}\rho$ is also positive. However, this is not sufficient to represent the action on multipartite systems, where the local action of a positive map is not enough to ensure the positive evolution of the global system. When the quantum operation $\mathcal{E}$ acts on a multipartite system, the global operation $\mathcal{E} \otimes \mathbb{I}$ must also be positive. The operator $\mathbb{I}$ is the identity acting on the rest of the multipartite system.

2. Trace preservation: the trace is preserved, $\mathrm{Tr}\,[\mathcal{E}\rho] = \mathrm{Tr}\,[\rho] = 1$.

3. Convex linearity: if $\sum_i \lambda_i\rho_i$ is a convex linear combination of a set of density matrices ρ_i, the map holds,

$$\mathcal{E}\sum_i \lambda_i\rho_i = \sum_i \lambda_i\mathcal{E}\rho_i. \tag{1.26}$$

A map following that desiderata is known as *completely positive trace-preserving map*, or CPTP map, and represents the most general operation of a quantum state.

The unitary evolution is of course a CPTP map. In particular, the unitary evolution is the unique CPTP transformation that can be inverted by another CPTP transformation. This is, for two CPTP maps $\mathcal{E}, \mathcal{E}^{-1}$,

$$\mathcal{E}\mathcal{E}^{-1} = \mathbb{I} \Longleftrightarrow \mathcal{E}, \mathcal{E}^{-1} \text{ unitary}. \tag{1.27}$$

Otherwise, at least one of the dynamical maps $\mathcal{E}, \mathcal{E}^{-1}$ we get this by doing thatates the positivity condition [Rivas and Huelga,].

[9] I use quantum operation and quantum dynamical map in an indistinct way. In the bibliography is usual the use 'quantum operation' to refer to any CPTP relation, and 'dynamical map' to refer to a explicit time propagation.

Other useful example of quantum operation is the dephasing channel $\mathbb{D}$, which erases the non-diagonal components of ρ in a certain basis, $\mathbb{D}^{ij}_{i'j'} = \delta_{i'j'}\delta_{ij}\delta_{i'i}$, then

$$\rho'_{i'j'} = \sum_{ij} \mathbb{D}^{ij}_{i'j'}\rho_{ij}. \tag{1.28}$$

An important CPTP map is generated by the interaction of the quantum system, denoted by S and an additional ancillary system A initially uncorrelated of S. The map

$$\mathcal{E}(0,t)\rho(0) := \rho(t) = \mathrm{Tr}_A\left[U_{SA}(t)\left(\rho(0)\otimes\rho_A\right)U^\dagger_{SA}(t)\right] \tag{1.29}$$

is also CPTP. U_{SA} is any unitary operator acting on the complete Hilbert space. In fact, any CPTP evolution, and therefore any quantum evolution, can be written in the form of Eq. (1.29) for a certain election of the ancillae system and unitary operation U_{SA} [Strasberg, 2022]. As a consequence, there exist infinite possible ancillae generating the same evolution of S, and therefore we can not infer the physical characteristics of a laboratory environment only by observing the evolution of S.

In addition, the map $\mathcal{E}(0,t)$ is only secured to be CPTP if the initial joint state $\rho(0)\otimes\rho_A$ is a tensor product. Otherwise, the total system could contain quantum correlations, and the evolution Eq. (1.29) is no longer CPTP, as it is not linear.[10]

The –quantum– Markovian property

Following the previous discussion, a system S following the evolution Eq. (1.29) is secure to be CPTP only if the initial state of A and S is uncorrelated. Then, consider three different times $t_2 > t_1 > t_0$, with the complete system uncorrelated at t_0, $\rho_{SA}(t_0) = \rho_S\otimes\rho_A$. The two maps $\mathcal{E}(t_0,t_2)$, $\mathcal{E}(t_0,t_1)$ generated by the evolution Eq. (1.29) are CPTP, but, as $\rho_{SA}(t_1) = U_{SA}\rho_{SA}(t_0)U^\dagger_{SA}$ could be quantum correlated, $\mathcal{E}(t_1,t_2)$ might not be CPTP. Then, the usual concatenation appearing in closed systems

$$\mathcal{E}(t_0,t_2) = \mathcal{E}(t_1,t_2)\mathcal{E}(t_0,t_1) \tag{1.30}$$

can no longer be written. The *Markovian property* in a quantum system implies that the last concatenation holds, this is, for any pair of times t_1, t_2 the map $\mathcal{E}(t_1,t_2)$ is CPTP.

1.2.2. Quantum master equations

A quantum master equation assumes differentiability in quantum evolution,

$$\dot{\rho} = \mathcal{L}\rho, \tag{1.31}$$

where $\mathcal{L}$ is any super-operator acting on ρ. It defines the evolution of ρ at arbitrary long times. This kind of equation can be phenomenologically written, or derived from a microscopical model. In the following, I will cite some examples

[10] In the presence of quantum correlation, the evolution Eq. (1.29) could create different quantum evolution departing from the same initial system (reduced) state.

CPTP quantum master equation

A CPTP quantum master equation is any equation with the form

$$\dot{\rho} = -i\left[H(t), \rho\right] - \sum_k \gamma_k(t)\left[J_k(t)\rho J_k^\dagger(t) - \frac{1}{2}\left\{J_k^\dagger(t)J_k(t), \rho\right\}\right] \tag{1.32}$$

since it always generates CPTP evolution. This equation was derived in parallel in [Lindblad, 1976] and [Gorini et al., 1976]. Here, the notation $\{A, B\} = AB + BA$ represents the anti-conmutator and $H(t)$ is a time-dependent Hamiltonian, $J_k(t)$ is an arbitrary set of operators acting on the system Hilbert space, and $\gamma_k(t)$ are positive rates. In addition, any continuous quantum evolution is Markovian at any time if and only if it is generated by a CPTP QME.

Born-Markov master equation

If a quantum system is weakly coupled to the environment, one can derive a quantum master equation departing from a microscopic model of the coupling. This derivation is a textbook exercise [11], so I will include only a few comments about it, as its result provides us with a good introduction for the next section.

It starts assuming a *weak* interaction between the system and a thermal bath of the form

$$V_{SA} = \sum_\alpha S_\alpha \otimes A_\alpha, \tag{1.33}$$

with S_α, A_α Hermitian operators acting on the system and bath respectively. The evolution of the complete system ρ_{SA} follows a unitary evolution, equivalent to the Liouville-von Neumann equation

$$\dot{\rho}_{SA} = \frac{-i}{\hbar}\left[H_{SA}, \rho_{SA}\right]. \tag{1.34}$$

The system state is recovered as $\rho = \mathrm{Tr}_A\left\{\rho_{SA}\right\}$. Since the interaction is weak, we integrate this equation following

$$\begin{aligned}\rho_{SA}(t) &= \rho_{SA}(0) - \frac{i}{\hbar}\int_0^t ds\left[H_{SA}(s), \rho_{SA}(s)\right] \\ &= \rho_{SA}(0) - \frac{i}{\hbar}\int_0^t ds\left[H_{SA}(s), \rho_{SA}(0)\right] \\ &- \frac{1}{\hbar^2}\int_0^t ds\int_0^s ds'\left[H_{SA}(s), \left[H_{SA}(s'), \rho_{SA}(s')\right]\right].\end{aligned} \tag{1.35}$$

The second equality is obtained by iterating the first one in its own integrand. The obtained result is, therefore, of second order in the weak potential V_{SA}.

After the last result, one must consider three steps,

[11] See, for example, [Rivas and Huelga, , Breuer et al., 2002].

1. Born approximation. Assume that the bath is much larger than the system S. Canonical examples of this are chains of a very large number of oscillators coupled to the system, initialized in a thermal state at inverse temperature β, $\pi_A = e^{-\beta H_A}/\mathcal{Z}_A$; in this case, the initial condition is factorized

$$\rho_{SA}(0) = \rho(0) \otimes \pi_A. \tag{1.36}$$

Born approximation moves a step further and considers the state factorized in arbitrary times,

$$\rho_{SA}(t) = \rho(t) \otimes \pi_A + O(V_{SA}). \tag{1.37}$$

Note that the order $O(V_{SA})$ prevents us from making predictions with higher precision than this quantity. In particular, a QME derived under this assumption could predict, for example, thermodynamic violations of this order.

2. Markov approximation. The effects of the bath will appear under correlation functions $\mathcal{C}_{\alpha\alpha'} = \mathrm{Tr}_A \{A_\alpha(t) A'_\alpha(0)\pi_A\}$. The Markov approximation implies that these correlation functions decay quickly with time. Under this approximation, the integral in the weak coupling equation can be extended to infinity, $t \to 0$. From a physical point of view, this assumption means that the time scales of the bath are much faster than that acting on the system, and therefore, it loses the information about the interaction instantaneously, becoming memory-less.

3. Jump operators. The system Hamiltonian can be written in terms of projectors associated with its energy levels, $H_S = \sum_i e_i \Pi_i$. Here e_i is a Hamiltonian energy level and Π is their associated projector. Then, we define

$$S_\alpha(\omega) = \sum_{e'_i - e_i = \omega} \Pi_i S_\alpha \Pi'_i. \tag{1.38}$$

Each sum is taken over the energy levels related by the same Bohr frequency ω. These operators have the following properties

$$\begin{aligned} S^\dagger_\alpha(\omega) &= A_\alpha(-\omega), \\ [S_\alpha(\omega), H_S] &= \omega S_\alpha(\omega), \\ S_\alpha(\omega)\pi_S &= e^{-\beta\omega}\pi_S S_\alpha(\omega). \end{aligned} \tag{1.39}$$

[12] The first property implies that the interactions with the environment conserve the total energy. The second property indicates that they are eigenoperators of H_S: the action of a jump operator transforms an eigenstate into another eigenstate. That point will be crucial in the following discussion.

[12] This definition might seem bizarre, but is just a fancy way to rewrite the ladder operators. In particular, if the system S is a single qubit, Hamiltonian could be $H_S = h\sigma_z$ and the jump operators are just the well-known $\sigma_\pm = \sigma_x \pm i\sigma_y$.

After consider the three steps, the weak interaction QME (in the interaction picture) takes the form

$$\dot{\rho} = \sum_{\omega,\omega'} \sum_{\alpha,\alpha'} e^{-i(\omega-\omega')t} \Gamma_{\alpha,\alpha'}(\omega) \left[S_{\alpha'}(\omega) \rho S_{\alpha}^{\dagger}(\omega') - S_{\alpha}^{\dagger}(\omega') S_{\alpha'}(\omega) \rho \right] + \text{h.c.}. \tag{1.40}$$

Here $\Gamma_{\alpha,\alpha'}$ is the Fourier transform of the correlation function $\mathcal{C}_{\alpha'\alpha}$. As they contain all the information of the temperature and coupling with the bath, they are interpreted as *rates* associated with the jumps operator. The last result is known as *Born-Markov equation*, or *Redfield equation*. This QME is largely extended in the literature. However, it is not a CPTP equation and therefore, it is known to predict non-physical evolution.

Secular Born-Markov equation

The secular terms of the last equation are that with $\omega \simeq \omega'$. These terms drive the system periodically, with very large periods, preventing the fast dissipation of energy due to the environment. The secular approximation considers (ironically) that the system has no secular terms. Therefore, the rates $\Gamma_{\alpha,\alpha'}$ timescales are slower than the exponential terms $e^{-i(\omega-\omega')t}$. In this case, one can substitute $e^{-i(\omega-\omega')t} \equiv \delta_{\omega,\omega'}$, and the Born-Markov equation becomes

$$\dot{\rho} = -i \sum_{\omega} \sum_{\alpha,\alpha'} \lambda_{\alpha,\alpha'}(\omega) \left[S_{\alpha}^{\dagger}(\omega) S_{\alpha'}(\omega), \rho \right] \tag{1.41}$$

$$+ \sum_{\omega} \sum_{\alpha,\alpha'} \gamma_{\alpha,\alpha'}(\omega) \left[S_{\alpha'}(\omega) \rho S_{\alpha}^{\dagger}(\omega) - \frac{1}{2} \left\{ S_{\alpha}^{\dagger}(\omega) S_{\alpha'}(\omega), \rho \right\} \right]. \tag{1.42}$$

Here $2i\lambda_{\alpha,\alpha'} = \Gamma_{\alpha,\alpha'} - \Gamma_{\alpha',\alpha}^{*}$ and $\gamma_{\alpha,\alpha'} = \Gamma_{\alpha,\alpha'} + \Gamma_{\alpha',\alpha}^{*}$. The first term is a renormalization of the eigenlevels of the Hamiltonian H_S, and it is known as *Lamb shift*. This part is usually discarded as the eigenenergies of H_S are usually measured in the experiment once the system is in contact with its environment, and therefore their correction is automatically introduced in the computation. On the other hand, the second term has the form of the dissipators introduced in the CPTP QME, and so, under secular approximation the Born-Markov master equation is CPTP. The secular approximation is known to fail if the frequencies of the system ω are close to degeneration [Cattaneo et al., 2019].

1.2.3. Fixed points and thermalization

One can ask how could a quantum system achieve a steady state: in fact, an isolated quantum system, described by a discrete set of levels following Schrödinger evolution, exhibits quasi-periodic dynamics, where the system continuously visits and leaves the same region of the Hilbert space; this is called *Poincaré recurrence*. In order to prevent it, one may consider the quantum system in contact with an extremely large environment, in such case the recurrence time becomes exponentially large, and the system reaches an apparent stationary state. Another option consists in considering some source of noise acting on the system, for example, continuous measures performed at random times

by an external observer: then the dynamics are no more unitary and the periodicity disappears.
The *fixed points* of a certain time-dependent quantum evolution $\mathcal{E}(t)$ are quantum states ρ_0 remaining invariant under the action of the map, $\mathcal{E}(t)\rho_0 = \rho_0$. In this part, I assume a unique fixed point for any dynamical map.

At this point, it is useful to introduce the Kullback-Leibler divergence relating two different arbitrary matrices ρ, ρ_0,

$$D_{KL}(\rho||\rho_0) = \mathrm{Tr}\left\{\rho\left(\ln\rho - \ln\rho_0\right)\right\}. \tag{1.43}$$

This quantity is interpreted as a statistical distance, since it quantifies how *far* are two density matrices. It is always positive and $D_{KL}(\rho||\rho_0) = 0 \Leftrightarrow \rho = \rho_0$. One can prove that the action of any quantum map always contracts the statistical distance [Rivas and Huelga,]

$$D_{KL}(\mathcal{E}(t)\rho||\mathcal{E}\rho_0) \leq D_{KL}(\rho||\rho_0). \tag{1.44}$$

The equality is only satisfied by unitary evolution, i.e. free Hamiltonian evolution. If ρ_0 is the fixed point of $\mathcal{E}$, this translates in

$$D_{KL}(\mathcal{E}(t)\rho||\rho_0) \leq D_{KL}(\rho||\rho_0), \tag{1.45}$$

which provides us with a notion of physical irreversibility. To derive an expression for the entropy production, one can rewrite the last as

$$\frac{D_{KL}(\mathcal{E}(\delta t)\rho||\rho_0) - D_{KL}(\rho||\rho_0)}{\delta t} \leq 0, \tag{1.46}$$

and finally

$$\sigma[\rho] = -\frac{d}{dt}D_{KL}(\rho(t)||\rho_0) \geq 0, \tag{1.47}$$

where, as before $\rho(t) = \mathcal{E}(t)\rho$. If the evolution follows a CPTP QME, the last expression implies

$$\sigma[\rho] = -\mathrm{Tr}\left\{\mathcal{L}(\rho)\ln\rho\right\} + \mathrm{Tr}\left\{\mathcal{L}(\rho)\ln\rho_0\right\} \geq 0. \tag{1.48}$$

The first term is nothing but the time derivative of the von Neumann entropy, $S_{VN}(\rho) = -\mathrm{Tr}\left\{\rho\ln\rho\right\}$; the second term is an entropy flow that we will denote J. Therefore,

$$\frac{dS_{VN}}{dt} + J \geq 0. \tag{1.49}$$

Notice that this result is closely related with the thermodynamics of information derived above, but generalized to the quantum case with an arbitrary environment. In fact, if the system is in contact with a thermal environment, the fixed point $\rho_0 \equiv \pi = \exp(-\beta H)/\mathcal{Z}$, with $\mathcal{Z} = \mathrm{Tr}\left\{\exp(-\beta H)\right\}$ is the thermal state, and one recovers the quantum Clausius inequality

$$J = -\beta\mathrm{Tr}\left\{\mathcal{L}(\rho)H\right\}. \tag{1.50}$$

In this case, one says that the system *thermalizes*.

Quantum heat and work

The notion of *heat* and *work* flows in quantum systems follows immediately from the previous result. First, I consider a time dependent Hamiltonian $H(t)$ acting on our system $\rho(t)$. Since the Hamiltonian changes, the fixed point of the evolution is also driven $\rho_0 \equiv \pi(t) = \exp(-\beta H(t))/\mathcal{Z}(t)$, with $\mathcal{Z}(T) = \mathrm{Tr}\{-\beta H(t)\}$.

The total internal energy of the system can be calculated as before, considering the average

$$U = \mathrm{Tr}\{H(t)\rho(t)\}. \tag{1.51}$$

Taking their time derivative, one obtains

$$\frac{dU}{dt} = \mathrm{Tr}\left\{H\frac{d\rho}{dt}\right\} + \mathrm{Tr}\left\{\frac{dH}{dt}\rho\right\}. \tag{1.52}$$

Observe that the first term appears due to the time variation of ρ, meanwhile, the second one depends on how the Hamiltonian is driven. Therefore, the second one is understood as a *controllable* energy exchange, id est, *work*

$$\dot{W} = \mathrm{Tr}\left\{\frac{dH}{dt}\rho\right\}. \tag{1.53}$$

In the autonomous case and in the absence of bias, the system achieves an equilibrium steady state with $\dot{W} = 0$. The first one is a *disordered energy exchange* or *heat flow*

$$\dot{Q} = \mathrm{Tr}\left\{H\frac{d\rho}{dt}\right\}. \tag{1.54}$$

Considering Eq. (1.31), the last quantity is

$$\dot{Q} = \mathrm{Tr}\{H\mathcal{L}[\rho]\}. \tag{1.55}$$

Comparing with Eq. (1.50) one obtains $J = -\beta\dot{Q}$, and we recover the second law of thermodynamics

$$\frac{dS_{VN}}{dt} - \beta\dot{Q} \geq 0. \tag{1.56}$$

1.2.4. Perspectives on quantum thermodynamics

In this chapter I explain the main features of quantum thermodynamics. Here, I offer a brief reflection on the recent themes and unresolved questions permeating quantum thermodynamics, drawing from my personal perspective accumulated over the past four years.

The community is doing a huge effort in designing and fabricating new platforms where perform new experiments; the first part of this thesis is a good example of it. The evolution of quantum thermodynamics is, of course, strongly related to near-future industrial applications (quantum communication, etc.), and as a consequence,

it is also related to our increasing capability to manipulate complex quantum systems [Trotzky et al., 2012].

The similarities between quantum and classical thermodynamics inspired the idea of *quantum thermal machines*, where a quantum working substance exchanges energy between several reservoirs representing the thermal bath, obtaining useful energy as a classical engine [Scovil and Schulz-DuBois, 1959, Geusic et al., 1967]. At present, quantum thermal machines are studied as useful examples of our knowledge of open quantum systems theory [Vinjanampathy and Anders, 2016]. The main difference between quantum and classical thermal machines rises when the thermal machine can use quantum correlations from the reservoirs to produce work [Gallego et al., 2014]. How to evaluate the efficiency of a thermal machine is a controversial topic [Manzano et al., 2020]. This debate is a remnant of classical thermodynamics: in fact, any measurement of the work or heat exchanged in a quantum machine requires a much larger energy investment than the measurement itself, which calls into question our notion of what is useful energy and what is not[13].

The next step consists of *introducing measurements in the thermodynamic scheme*. One can think of a quantum system following coherent evolution under measurements [Perarnau-Llobet et al., 2017], and recover the stochastic thermodynamics of the single trajectory, as one can do in classical physics. However, the measurement strategy followed by the observer disturbs the trajectory. The operational thermodynamics [Strasberg, 2022] was derived to conciliate the measurement scheme with thermodynamics in feedback experiments [Sayrin et al., 2011]. Indeed, using measurements results one can create a feedback loop between the system's stochastic dynamics and the external conditions favouring certain tasks [Wiseman and Milburn, 2009]; an open question in quantum thermodynamics is, precisely, to generalize the thermodynamics of information introduced in this chapter in terms of purely quantum evolution. Current research along these lines involves the generalization of fluctuation theorems [Funo et al., 2019], the role of measurements in that theorems [Micadei et al., 2020] and the analysis of diffusion in larger systems or networks [Kosloff, 2013].

Quantum thermometry tries to evaluate and control the temperature of quantum systems with increasing precision[Mehboudi et al., 2019]; however, the action of any thermometer disturbs the state of small systems, so one must infer the actual temperatures just from measurements statistics, which becomes prohibitive for large systems. The temperature estimation obtained from considering the global system is more precise, in general [Rubio et al., 2021], however, in the last decade the focus has been on *collisional thermometry* [Seah et al., 2019, O'Connor et al., 2021], where the temperature is estimated by the continuous bombarding of the target system with ancillary systems.

These collisional models can be used to implement *collisional quantum reservoirs* where the action of the environment on the system is emulated by repeated collisions with ancillae [Campbell and Vacchini, 2021]. The thermodynamic consistency

[13]During the 19th century, thermal machines had the exclusive task of converting thermal energy into useful energy, and *evolved* to become more efficient. In the current paradigm of nanotechnology, does it make sense to study the energetic efficiency of a machine in which *energy is not a limited resource*, and which does not evolve to improve industrial tasks?

of these models has been analyzed in several works [Barra, 2015, Jacob et al., 2021, Guarnieri et al., 2020]; in this thesis, I will present the improvements of these models published in [Tabanera-Bravo et al., 2022, Tabanera-Bravo et al., 2023].

The last open question in open quantum systems theory I want to mention is the *local versus global problem*, directly related to the derivation of CPTP quantum master equations. As I said, deriving a quantum master equation from a microscopic model requires imposing the secular approximation; otherwise, the Redfield approximation could predict non-physical evolution. In a multipartite system in contact with several local thermal reservoirs, the secular approximation could fail due to the strong coupling between parties, and the resulting CPTP QME fails. I will address this issue in depth in the last chapter of the thesis.

Part II.

Thermodynamics of information in the single electron resonator

2. The single electron resonator

In order to study thermodynamics of information, one may consider a *bipartite system*, where two individual subsystems are able to exchange energy and information. Some examples are superconducting qubits coupled to superconducting resonators, see [Clerk et al., 2020], phonon-driven trapped ions, [Cirac and Zoller, 2000], or mechanical systems coupled with solid-state systems (see below). Probably the most popular option in this field today are optomechanical devices, where a moving part of the system interacts with states of light, see for example [Barzanjeh et al., 2022, Aspelmeyer et al., 2014].

Some of these implementations consist in coupling a mechanical piece with a solid-state quantum system [Treutlein et al., 2014, Bachtold et al., 2022]. This can be done in several ways, for example, creating a superconducting circuit with a motile electrode [Schneider et al., 2012, Armour et al., 2002], confining an electron spin on a cantilever and manipulating it with magnetic fields [Degen et al., 2009, Rabl et al., 2009, Kolkowitz et al., 2012], coupling a quantum dot and one oscillator with a common cavity [Hammerer et al., 2009] or electric current [Bennett et al., 2010], or confining electric charge into a motile part of the system embedded in an electric field; the last examples are known as *electron resonators*, and will be the object of study of this work. In some works, this kind of device is also known as *mechanical electron shuttle* or *mechanical single-electron transistor* [Kindermann, 2011, Koenig et al., 2008]. Usual applications of the last example appear in metrology, being able to measure microscopic forces [Moser et al., 2013, Wang and Pistolesi, 2017, Wang et al., 2017] or in entanglement generation and quantum information manipulation [Palomaki et al., 2013, Reed et al., 2017].

Single-electron resonators are characterized by small masses, in the order of the attogram, and high resonating frequencies, in the order of the MHz. At very low temperatures, the single-electron resonators present very low quality factors > 1000 and, importantly, strong coupling between the electric transport and the mechanical oscillations.

In this chapter, I will study in depth the dynamical model of the single electron resonator. In section 2.1 I start presenting the basic features of electron conduction in nano-devices, taking the *single electron transistor* as a main example; all the electric transport features observed in the single electron resonator will be based on this example. In section 2.2 I expand the electron confinement and transport model using the WKB approximation. In section 2.3 I describe in detail the single electron resonator and elaborate on the relationship between the movement and transport. Finally, in section 2.4 I provide the dynamical model describing the complete device.

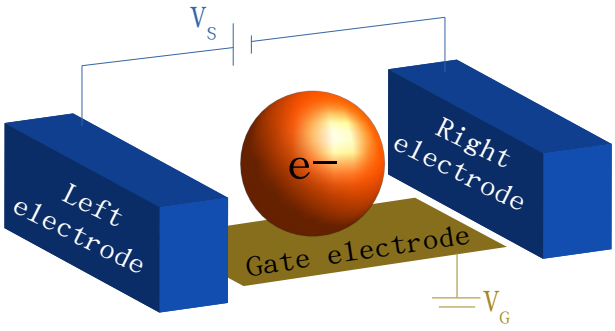

Figure 2.1.: Sketch of the single electric transistor. The quantum dot storing electrons (orange structure) exchanges charge with the right and left electrodes due to the bias voltage V_S. The gate electrode creates an electrostatic field, modulating electron transport.

2.1. The single electron transistor

A single electron transistor, or SET, is a transistor whose operation is based on single-electron tunnelling transitions filling and emptying a quantum dot [Wiseman and Milburn, 2009]. A sketch of the device is in fig.2.1. A quantum dot can be made of several sizes and materials using, for example, trapped molecules, metallic and superconducting pieces or electrostatic potential fields, nanotubes, nanowires, etc. [Hanson et al., 2007]. The electric current through the quantum dot is generated by putting the system in contact with two electrodes (usually named *left* and *right*) connected to a bias voltage V_S. A third electrode, called the gate, is connected to an electric potential V_G to control the transport by imposing an electrostatic field on the dot.

In this section, I introduce the essential operation of a single electron transistor independently of its construction. The central phenomenon observed in this kind of device is Coulomb blockade, which refers to the modification of the electric transport due to electron-electron Coulomb repulsion.

2.1.1. The quantum dot

A quantum dot, or metallic island, is a structure able to accommodate charge. In contrast to most models of transport, where electrons in conductors are regarded as non-interacting particles, the electrons filling the quantum dot interact with each other due to Coulomb repulsion.

In order to evaluate the electric current flowing through the device, one must first evaluate *how much energy is required to fill the charged dot with an additional electron?* This *adding energy* has two contributions,

1. The classical Coulomb repulsion. In a classical capacitor, the electrostatic energy depends on the current charge filling the device, Q and a device capacitance C,

$$E_{\text{est}} = \frac{Q^2}{2C} = E^0_{\text{est}} N^2. \tag{2.1}$$

   Here $Q = q_e N$, with q_e the elemental charge and N the number of electrons filling the device, and $E^0_{\text{est}} = q_e^2/2C$ is the device energy scale. In order to add a new electron, we must pay

$$\delta E_{\text{est}} = E^0_{\text{est}} N^2 - E^0_{\text{est}} (N-1)^2 = E^0_{\text{est}} (2N-1) \tag{2.2}$$

   because of Coulomb repulsion. The capacitance C decreases with the device length; as is noted in [Nazarov and Blanter, 2009], the charging energy vanishes in the usual thermodynamic limit, recovering the non-interacting model.

2. A quantum contribution. As we know from basic quantum physics, the single-particle energy is quantized in a bounded state; the discrete set of single-particle energy levels is ε_n. The quantum contribution to the total energy is

$$E_{\text{quantum}}(\{n_i\}, N) = \sum_i^N n_i \varepsilon_i, \tag{2.3}$$

   where the $n_i = 0, 1$ are the electron occupation of the i-th single-particle energy levels, $N = \sum_i n_i$. In order to add a new electron, we must pay $\delta E_{\text{quantum}} = \varepsilon_n$, just the next filled quantum level. The quantum levels ε_n depend on the geometry of the device.

The charge state energy is therefore,

$$E_{\text{ch}}(\{n_i\}, N) = E^0_{\text{est}} N^2 + \sum_i n_i \varepsilon_i. \tag{2.4}$$

In this chapter, I will evaluate both contributions but, since the classical part is dominant, I use the short notation $E_{\text{ch}}(\{n_i\}, N) \equiv E_{\text{ch}}(N)$. For larger and larger quantum dots, the quantum contribution becomes negligible [Nazarov and Blanter, 2009].

2.1.2. Creating the electron current

In the single electron transistor, the quantum dot is put in contact with two metallic electrodes named left and right (L and R respectively) defined by their chemical potential $\mu_{L,R}$ (also known as Fermi levels). The potential difference $q_e V_S = \mu_L - \mu_R$ is created by imposing the *bias potential*, a tunable electric potential difference generated between the electrodes.

Since the electrodes are macroscopic metallic pieces, they act as electron reservoirs in thermal equilibrium from where particles can be extracted. The probability

of exchanging energy with a certain electrode $b = L, R$ obeys *local detailed balance* [Van Houten et al., 1992]

$$\frac{\text{Prob}\{N \to N \pm 1\}}{\text{Prob}\{N \pm 1 \to N\}} \propto e^{-\beta_b(E_{\text{ch}}(N) - E_{\text{ch}}(N \pm 1) - \mu_b)}. \tag{2.5}$$

$\beta_{L,R}$ is the inverse temperature of the electrodes. Note that, at low temperatures, the isolated electrons filling the quantum dot could present coherent quantum effects; however, the strong coupling with the electrodes is a source of relaxation and decoherence [Hanson et al., 2007].[1]

For low temperature and $\mu_L = \mu_R$, the quantum dot is spontaneously filled with electrons until it reaches a charge state in chemical equilibrium, with N electrons, satisfying

$$E_{\text{ch}}(N) - E_{\text{ch}}(N \pm 1) - \mu_{L,R} \simeq 0. \tag{2.6}$$

If $\mu_R < \mu_L$, the quantum dot gets out of equilibrium, appearing an electron current from L to R. The difference $V_S = \mu_L - \mu_R > 0$ is known as *bias window* and coincides with the bias voltage; any charge state $E_{\text{ch}}(N)$ satisfying

$$\begin{aligned} E_{\text{ch}}(N) - E_{\text{ch}}(N+1) - \mu_L < 0, \\ E_{\text{ch}}(N+1) - E_{\text{ch}}(N) - \mu_R < 0, \end{aligned} \tag{2.7}$$

is inside the bias window, since it fills $(N \to N+1)$ from L and empties $(N+1 \to N)$ onto R, generating the current. The quantities $E_{\text{ch}}(N+1) - E_{\text{ch}}(N) = \varepsilon(N)$ are usually known as *electrochemical potential* level of the quantum dot with N electrons [Hanson et al., 2007].

The condition Eq. (2.7) is represented in fig.2.2. In this figure, we can observe the electrodes chemical potentials $\mu_{L,R}$ compared with the electrochemical potential of the quantum dot, for several values of N. Only the electrochemical level $\varepsilon(N)$ is in the bias window (represented by horizontal dashed lines), and electrons can move from L to R using only this level. The barriers $\Gamma_{L,R}$ represent the rate of tunnel events from each electrode.

2.1.3. Coulomb blockade

For large V_S, there exist many charge states within the bias window, contributing to create the electric current. However, in the low bias limit, even if V_S is not zero, the condition (2.7) could be not satisfied by any N: in this case, there exist a stable number of charges on the quantum dot, but no electric current. The last phenomenon is known as *Coulomb blockade*, since it is due to Coulomb's electric repulsion. As one can observe, this is a consequence of having a discrete set of charging energies, id est, a consequence of the discretization of electric charge.

[1] This point has been discussed several times in the bibliography [Armour et al., 2004] –and within the NanoQit project. Since the system works at very low temperatures, around 40 mK, one must not discard quantum effects in future implementations, but, at this moment, a classical model is able to recreate all the experimental phenomenology. *Hypotheses non fingo.*

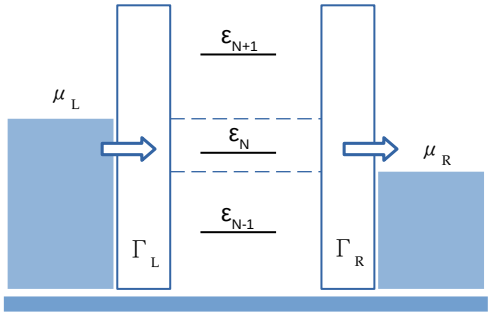

Figure 2.2.: Sketch of condition Eq. (2.7). Only the electromechanical level $\varepsilon(N)$ exists within the bias window, satisfying the conditions, and therefore, one observe single electron jumps.

In order to control the Coulomb blockade, the single electron transistor has a third electrode separated from the quantum dot, the gate electrode configured at gate voltage V_G. This electrode can not exchange electrons with the quantum dot, but modulates the electrostatic energy contribution E_{est},

$$E_{\text{est}} = E^0_{\text{est}} \left(N - \frac{q}{q_e} \right)^2 . \tag{2.8}$$

q is the electric charge induced by V_G and q_e is the elemental charge. The last equation is known as the *constant interaction model* [Van Houten et al., 1992].

Changing the gate voltage, one can force the quantum dot to satisfy the conditions eqs.(2.7) for arbitrary values of N, switching the electric current on and off at will. Increasing V_G implies dragging down all the electrochemical levels $\varepsilon(N)$ and vice versa since the gate voltage attracts more electrons.

The Coulomb blockade can be evidenced in the experiment by measuring the electric current as a function of V_S and V_G. Their main signature is the existence of blocked current regions named *Coulomb diamonds*, see figure 2.3.

2.1.4. Master equation

One can describe the evolution of the N charges within the quantum dot in a compact way using a master equation [Nazarov and Blanter, 2009]. For simplicity, here I consider the low bias regime, where there is a single charge state $E_{\text{ch}}(N)$ within the bias window. The unique allowed transitions are $N \longleftrightarrow N+1$, with energy change $E_{\text{ch}}(N+1) - E_{\text{ch}}(N) = \varepsilon$. The probability of a jump from $N+1$ to N per time unit is given by the tunnelling rate

$$\Gamma_{\text{out}} = \Gamma(\varepsilon)[1 - f_R(\varepsilon)], \tag{2.9}$$

and for the probability of jump from N to $N+1$,

$$\Gamma_{\text{in}} = \Gamma(\varepsilon) f_L(\varepsilon). \tag{2.10}$$

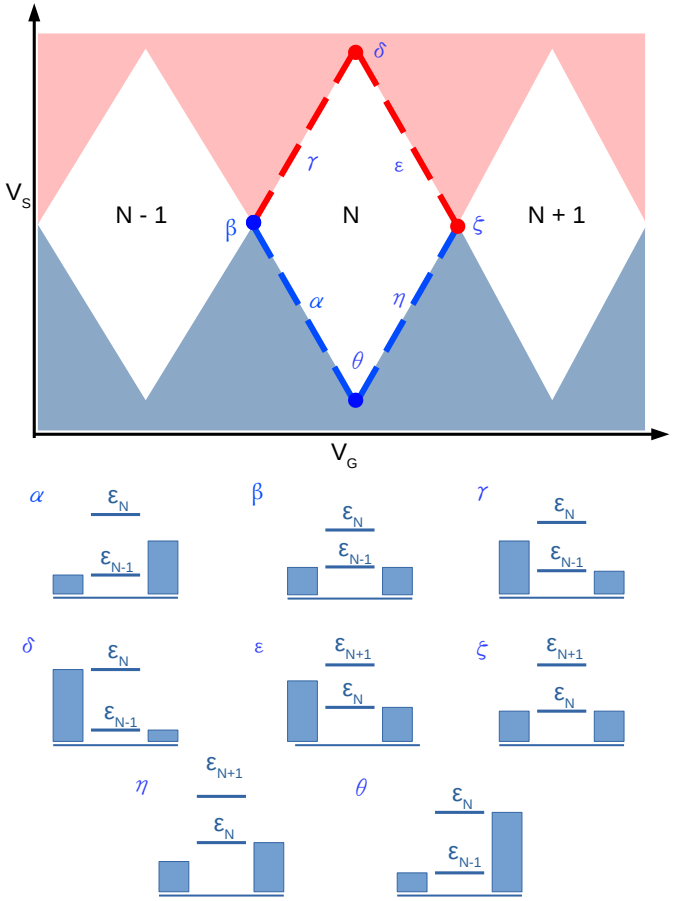

Figure 2.3.: (*up*) Sketch of the electric current along the SET as function of V_G and V_S, and (*down*) electrochemical configurations at different points. In the red region, $V_S = \mu_L - \mu_R > 0$ and therefore, the electrons flow from L to R; in the blue region $V_S < 0$ and the current flow from R to L. Within white diamonds, no electrochemical level is inside the bias window and the current is blocked. In the diamond borders (dashed lines), the electrochemical levels are aligned with one of the electrode chemical potentials (configurations $\alpha, \gamma, \varepsilon$ and η). At the points δ and θ, both levels ε_N and $\varepsilon_{N\pm1}$ are aligned with the chemical levels. At the points β and ζ, named the *Coulomb peaks*, the current is zero since $\mu_L = \mu_R$.

The functions $f_{L,R}$ are the Fermi functions

$$f_{L,R}(\varepsilon) = \frac{1}{1 + e^{-\beta_{L,R}(\varepsilon - \mu_{L,R})}}, \tag{2.11}$$

and $\Gamma(\varepsilon)$ is an energy-dependent function representing electron tunnelling. The local detailed condition Eq. (2.5) is provided by the Fermi functions.

The master equation

If $\mathcal{P}(N+1)$ and $\mathcal{P}(N)$ denote the probability of finding the system with $N+1$ or N electrons respectively, we can write the following master equations,

$$\frac{d\mathcal{P}(N+1)}{dt} = \Gamma_{\text{in}}\mathcal{P}(N) - \Gamma_{\text{out}}\mathcal{P}(N+1), \tag{2.12}$$

$$\frac{d\mathcal{P}(N)}{dt} = \Gamma_{\text{out}}\mathcal{P}(N+1) - \Gamma_{\text{in}}\mathcal{P}(N). \tag{2.13}$$

with the normalization constraint $\mathcal{P}(N+1) + \mathcal{P}(N) = 1$. The steady-state solution is

$$\mathcal{P}(N) = \frac{\Gamma_{\text{out}}}{\Gamma_{\text{out}} + \Gamma_{\text{in}}} \tag{2.14}$$

and

$$\mathcal{P}(N+1) = \frac{\Gamma_{\text{in}}}{\Gamma_{\text{out}} + \Gamma_{\text{in}}}. \tag{2.15}$$

The current

The number of electrons per time unit, flowing in a certain direction, corresponds to the electric current. In this case, the current takes the form

$$I = \Gamma_{\text{in}}\mathcal{P}(N) = \Gamma_{\text{out}}\mathcal{P}(N+1), \tag{2.16}$$

and electron flow from L to R. In the steady state, one obtains

$$I = \frac{\Gamma_{\text{in}}\Gamma_{\text{out}}}{\Gamma_{\text{out}} + \Gamma_{\text{in}}}. \tag{2.17}$$

2.2. Quantum confinement and transport

In the previous section, I described electron confinement from a macroscopic point of view. However, I made no comment about the behaviour of the electrons within the quantum dot, or about the transport mechanism. I will now describe the single electron transport from a completely quantum point of view, obtaining information about the electrochemical levels and the tunnelling ratios Γ_{in}. To describe their quantum dynamics, I will use the the Wentzel-Kramers-Brillouin *WKB approximation* [Nazarov and Blanter, 2009, Galindo and Pascual, 2012] of the Schrödinger equation.

2.2.1. The WKB approximation

Consider a single electron filling the SET. Its movement along the device follows the one-dimension Schrödinger equation

$$-\frac{\hbar^2}{2m_e}\frac{d^2\psi}{dx^2} + q_e V(x)\psi = E\psi, \tag{2.18}$$

where x is the position along the left-right axis of the system, $\psi = \psi(x)$ is a single-electron wave function with energy E, m_e is the electron mass and q_e the elemental charge. V is a complicated inhomogeneous electric potential created by the gate electrode, depending on the device geometry. This can be rewritten as

$$\hbar^2\frac{d^2\psi}{dx^2} + p^2(x)\psi = 0, \tag{2.19}$$

where

$$p(x) = \begin{cases} \sqrt{2m[E - q_e V(x)]} & E \geq q_e V(x), \\ i\sqrt{2m[q_e V(x) - E]} & E < q_e V(x). \end{cases} \tag{2.20}$$

This quantity is, precisely, the classical momentum of the particle.

Under the WKB approximation, the Schrödinger equation is treated using a certain ansatz, valid when the action scale of the system is larger than $\hbar$. Roughly speaking, this means that the amplitude of the wave function changes slowly in a de Broglie length, being a good approximation in semiclassical systems [Galindo and Pascual, 2012], and therefore in nanoscience. The WKB ansatz is

$$\psi(x) = A(x)e^{iS(x)/\hbar}, \tag{2.21}$$

where A and S are two functions representing the wave function amplitude and the phase, with the restriction $d^2A/dx^2 \simeq 0$. Inserting into Eq. 2.19,

$$\frac{dS}{dx} = \pm p(x), \tag{2.22}$$

$$\frac{d}{dx}\left(A^2 p\right) = 0. \tag{2.23}$$

The solution follows immediately

$$S(x) = \pm\int_{x_0}^{x} p(x)dx, \tag{2.24}$$

$$A(x) = \frac{C}{\sqrt{|p(x)|}}, \tag{2.25}$$

with C a constant. Note that if $E \geq q_e V(x)$ the phase S is real, and the electrons travel without damping. However, if $E < q_e V(x)$, the wave function is exponentially suppressed, corresponding with classically forbidden transport. The singular points x_p where $E = q_e V(x_p)$ are known as *tipping points* of the movement, as the amplitude A

diverges. These points represent a bounce in the classical movement, $p(x_p) = 0$; from a quantum point of view, the wave function changes from a suppressed to oscillatory behaviour.

To obtain further insight, consider a single-well potential $V(x)$ of length L and one electrons with energy E. The barriers are defined by the tipping points $0 < x_1 < x_2 < L$, since $E < q_e V(x)$ between x_1 and x_2. Inside the well $x \in [x_1, x_2]$, the wave function is

$$\psi(x) = \frac{\alpha_+}{\sqrt{|p(x)|}} e^{\frac{i}{\hbar}\int_{x_1}^{x} p(x)dx} + \frac{\alpha_-}{\sqrt{|p(x)|}} e^{-\frac{i}{\hbar}\int_{x_1}^{x} p(x)dx}, \tag{2.26}$$

where $\alpha_\pm$ are constants. In the left barrier $x < x_1$

$$\psi(x) = \frac{\alpha_L}{\sqrt{|p(x)|}} e^{\frac{i}{\hbar}\int_{x_1}^{x} p(x)dx}, \tag{2.27}$$

and in $x > x_2$,

$$\psi(x) = \frac{\alpha_R}{\sqrt{|p(x)|}} e^{-\frac{i}{\hbar}\int_{x_1}^{x} p(x)dx}. \tag{2.28}$$

The four constants $\alpha_\pm, \alpha_{L,R}$ must be tailored using continuity conditions of $\psi(x)$ in the tipping points.

Bounded states

One of the main applications of the WKB approximation consists in evaluating the quantum energy levels of a certain potential $V(x)$, denoted ε_n. In order to do this, we evaluate the bounded states in the system noting that, outside the well, the wave function eqs.(2.27) and (2.28) could diverge. Bounded states satisfy

$$\int_{x_1}^{x_2} \sqrt{\varepsilon_n - q_e V(x)} dx = 2\pi\hbar \left(n + \frac{1}{2}\right), \tag{2.29}$$

with n a positive integer. This condition prevents divergences [Galindo and Pascual, 2012]. Curiously, the *Bohr-Sommerfeld quantization condition* appeared in quantum physics decades before the WKB approximation, in 1916 [Sommerfeld, 1916].

The last equation can be analytically solved in some text-book cases, such as the harmonic oscillator [Galindo and Pascual, 2012], where the WKB approximation is exact, or the triangular well $V \sim |x|$ [Sakurai and Napolitano, 2014]. In more general applications, the spectrum can be obtained using numerical methods.

Transmission amplitudes

Using the WKB approximation, it is also possible to evaluate the transmission amplitudes of a given potential shape. Imagine an electron with energy E colliding with a potential barrier $E < q_e V(x)$ from $x = 0$ to x_1 the transmission amplitude is [Sakurai and Napolitano, 2014, Galindo and Pascual, 2012]

$$T(E) \simeq e^{-\frac{2}{\hbar}\int dx \sqrt{q_e V(x) - E}}. \tag{2.30}$$

Since the WKB approximation is semiclassical weak tunnel effects are expected and the reflection amplitude becomes classical $R \lesssim 1$ [Galindo and Pascual, 2012].

2.3. The single electron resonator

The single electron resonator is essentially a single electron transistor in which the quantum dot is a movable component. The device is characterized by the coupling between the motion of the quantum dot and electron transport. The varying position of the charge relative to the electrodes results in two effects: firstly, the tunnel rates and electrochemical levels are position-dependent, leading to electron transport that is influenced by the dot's instantaneous position. Secondly, the motion of the oscillator is driven by the electric force generated by the electrons. The subsequent phenomenology arises from this interplay.

Some examples of this are using nanoscale cantilevers [Yeo et al., 2014], nano-bridges [Wilson-Rae et al., 2004] and nanowires [Claudon et al., 2010]. The device used in [Vigneau et al., 2022, Tabanera-Bravo et al., 2022] is sketched in figure 2.4, we considered a GaAs carbon nanotube (CNT) horizontally suspended between two SET electrodes, L and R, in such a way that it can oscillate. The third gate electrode, G separated from the CNT, defines an electrostatic quantum dot confining the electric charge inside the oscillating tube. This quantum dot exchanges electrons with L and R via a quantum tunnel.

The last kind of devices have been widely studied in the last few years [Khivrich et al., 2019, Laird et al., 2012, Moser et al., 2014, Benyamini et al., 2014], noting their very high-quality factor ≥ 2000, with mechanical frequencies in the order of GHz. The typical temperature is in the order of 40 mK. In [Woodside and McEuen, 2002, Hüttel et al., 2010, Sazonova et al., 2004] it was noted that the electron current modulates the resonant mechanical frequency of the device; this effect can be explained from the explicit model of the position-dependent tunnel jump rates between the electrodes and the dot [Meerwaldt et al., 2012]. Following the experiments, some theoretical works start considering this particular implementation [Micchi et al., 2015, Micchi et al., 2016, Pistolesi et al., 2021]. The main result of that work was the explanation of the bistability appearing in the current due to the effective potential exerted by the electron flow on the nanotube, suggesting a robust implementation of a quantum qubit.

A major step forward in the development of these experiments was the introduction of the radio-frequency measurements and the linear signal amplifier [Ares et al., 2016, Wen et al., 2018] which allows us to observe and excite the mechanics of the CNT, generating the new family of experiments currently taking place. The immediate consequence was the discovery of the self-oscillations in the motion states [Urgell et al., 2020, Wen et al., 2020]. In these self-oscillations, the CNT starts oscillating, converting electrical into mechanical energy as a motor. Self-oscillation mechanism will be explained in the next chapters of this thesis. In contrast to the previous sections, I shall now focus on a particular implementation of a single electron resonator, specifically that employed in references [Vigneau et al., 2022, Tabanera-Bravo et al., 2022]. Nevertheless, our results can be easily extrapolated to a wide range of devices. I will begin this section by presenting the device's geometry, the parameters that define its operating regime and timescales, and the main phenomena observed in experiments. Following this, I will use the WKB approximation to assess the effects of mechanics on transport.

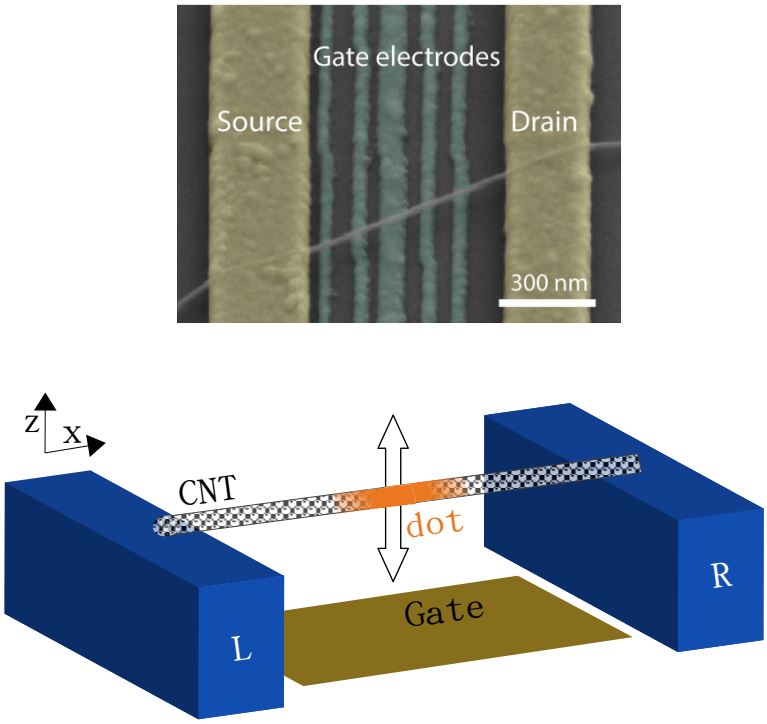

Figure 2.4.: Single electron resonator based on a carbon nanotube. In the upper image, one can observe the actual geometry of the device: the left and right electrodes (source and drain, respectively) appear in yellow, and the CNT in grey. In the lower figure, I represent the suspended CNT between the L and R electrodes, and the quantum dot electromagnetically defined by the gate electrode. The motion of the CNT is restricted to the vertical plane.

2.3.1. The device

In [Vigneau et al., 2022, Tabanera-Bravo et al., 2022], we utilized a single electron resonator based on a carbon nanotube (CNT). In this device, the quantum dot of the single electron transistor is defined on a carbon nanotube that is fully suspended, where the charge is confined within the CNT using the gate potential field. The movement of the quantum dot is provided by the oscillation of the nanotube.

In Fig.2.5 there is a sketch of the main geometry of the system used in [Vigneau et al., 2022, Tabanera-Bravo et al., 2022]. The gate electrode has been split into five smaller elec-

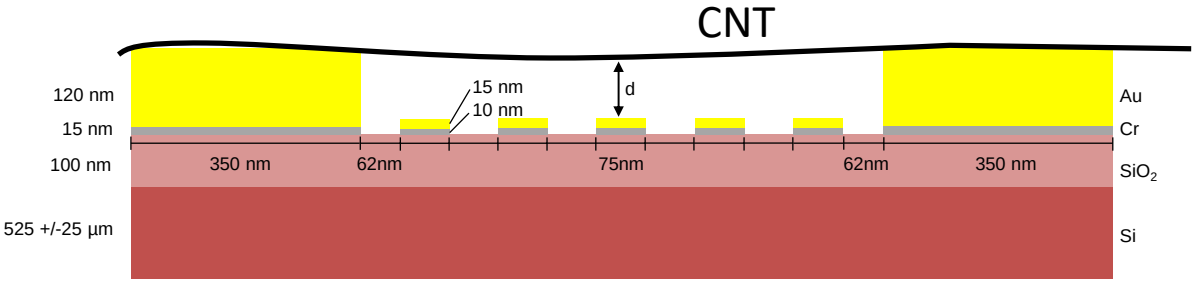

Figure 2.5.: Sketch of a vertical section of the device. The carbon nanotube CNT is fully suspended between two gold electrodes at a distance d from the bottom of the device. The gate voltage is generated by five independent equispaced gold gate electrodes. The bigger gold electrodes correspond with L (left) and R (right). Extracted from the supplemental material of [Vigneau et al., 2022].

trodes, $G1$, $G2$ ... $G5$, in order to gain control of the dot energy and the electron transport, or even create several dots along the same CNT [Benyamini et al., 2014].

An electron current I form L to R appears in the device once we impose a bias voltage V_S connected to the gold electrodes. Because of Coulomb blockade, the minimum bias voltage required to create the current depends on the number of charges filling the quantum dot and the gate voltage V_G. The blockade disappears once the bias voltage V_S is large enough or if the gate voltage V_G compensates the electric repulsion.

In the SET, the electrochemical levels of the quantum dot, ε_n, depend only on the number of charges and V_G. However, the mechanical oscillation affects the electrochemical levels (and thus the Coulomb blockade) through capacitive coupling. In the latter part of this section, I will provide a detailed description of this relationship.

The main device parameters appear in the following table.

The mechanical vibration is described by the CNT resonating frequency Ω, the effective oscillator mass m and the quality factor Q. [2]

The tunnel rates $\Gamma_{L,R}$ represent the number of electrons exchanged with L or R per unit time. Since $\Gamma_{L,R} \gg \Omega$, the electron transport is the fastest timescale. In the same

[2]The quality factor represents the friction with environment. The usual friction constant is given by

$$\gamma = m\frac{\Omega}{Q}. \tag{2.31}$$

Parameter	Name	Value
CNT height	d	100 nm
CNT lenght	L	936 ± 10 nm
Effective mass	m	61 ± 6 ag
Bias voltage	V_S/q_e	0.2 mV
Left tunneling rate	$\Gamma_L/2\pi$	1.0 ± 0.1 GHz
Right tunneling rate	$\Gamma_R/2\pi$	40 ± 5 GHz
Natural mechanical frequency	$\Omega/2\pi$	294.5 MHz
Mechanical quality factor	Q	≤ 2000
Coupling strength	$g/2\pi$	0.80 ± 0.04 GHz

Table 2.1.: Parameters of the device. Adapted from the supplemental material of [Vigneau et al., 2022].

way, the large quality factor Q implies that the oscillator is weakly damped by the environment. The coupling constant g describes the capacitive coupling strength; as we will see immediately, this is just the derivative of the electrochemical potential $\varepsilon(N)$ with the position. [3] The fact that $\Omega < g$ is known as *ultrastrong coupling*. In this regime, the feedback effects between the oscillator and the current becomes relevant.

As it was explained in the first section, the main evidence of single electron transport in a nanostructure is Coulomb blockade, revealed by a *Coulomb diamonds* pattern in $V_S - V_G$ space, as we can see in fig.2.6(left). Within the white regions, the electrostatic repulsion prevents electron transport, and the electron current I is blocked. Increasing the bias voltage V_S with positive (negative) value, the current is recovered in the red (blue) region.

Just to mention, the parallel lines in the current regions correspond to excited states of the quantum dot . As one can observe, the Coulomb diamond pattern is diffused in some points because of the mechanical motion. For example, one can observe electric current within the white diamonds promoted by oscillations.

In the same way, the electron transport affects the oscillation frequency. To observe this in an experiment, one can measure the resonant frequency of the oscillating CNT as a function of the gate voltage [Woodside and McEuen, 2002, Hüttel et al., 2010, Sazonova et al., 2004, Meerwaldt et al., 2012]. This measure appears in fig.2.6(right), where we plot the resonant frequency for very low bias when the gate crosses through a Coulomb peak. As a result, the resonant frequency decreases just in the peak, remaining constant in the blocked regions. [4]

[3] By convention, g is sometimes expressed in frequency units. This is useful to compare with the mechanical timescale Ω; the actual coupling constant (in units of force) is obtained recovered using

$$g[\text{ GHz}] = \frac{g[\text{ eV/nm }]}{\sqrt{2\hbar m\Omega}}. \tag{2.32}$$

[4] The actual resonant frequency ω in the device is measured by driving the CNT with a microwave tone at certain frequency ω_e and drive power P_0. Reached resonance $\omega_e = \omega$, I exhibits a sharp step due

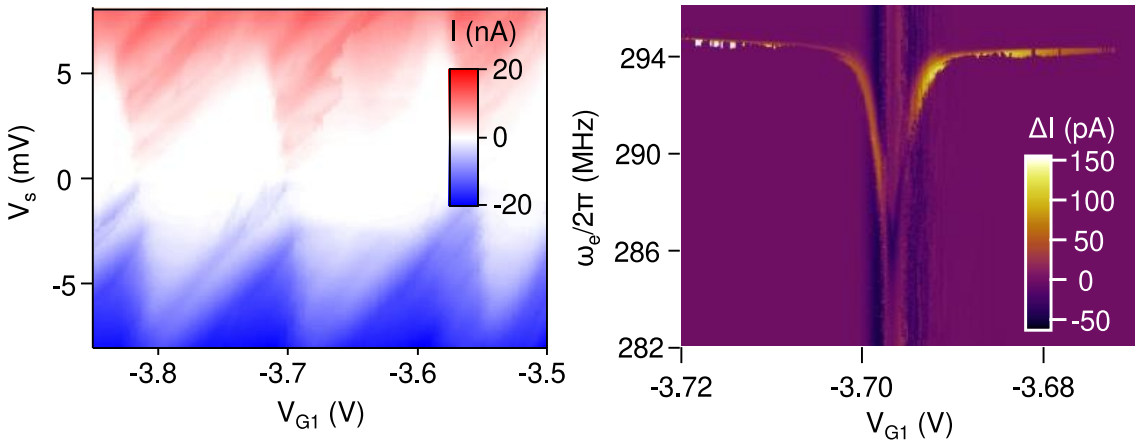

Figure 2.6.: *Left*: current measured in the device as function of V_{G1} and V_S revealing Coulomb diamonds, with $V_{G2} = 0\text{V}, V_{G3} = -4\text{V}, V_{G4} = 0\text{V}, V_{G5} = -3.95\text{V}$. *Right*: current measured as function of V_{G1} and the driving frequency, revealing the resonant frequency dip. Adapted from [Vigneau et al., 2022]

Capacitive coupling

The exposed feedback between electron transport and mechanical motion is due to the inhomogeneity of the electric field generated by the gate voltage, and therefore, it is known as *capacitive coupling*. Indeed, meanwhile the CNT oscillates, the electrons filling the quantum dot change their distance to the gate electrode and therefore, the charge confinement is weaker when the system CNT is up, and harder when it is down. To describe the electrostatic potential field in the device, $V(z, x)$, in [Vigneau et al., 2022] we solve numerically the Laplace equation $\nabla^2 V(z, x) = 0$ with certain boundary conditions. Here x is the horizontal position of the device (from L to R) and z is the vertical position, see fig.2.7. We only consider the vertical section of the device containing the CNT.

The geometry of the device was taken from fig.2.5. The boundary conditions represent the voltage configuration at which the experiment is configured; they are sketched in fig.2.7: we set the L, R electrodes and the experiment floor at zero voltage, and the gates $V_{G1} = V_{G3} = V_{G5} = 2V$ and $V_{G2} = V_{G4} = 0$. The top boundary of the simulation must be set to zero volts for the calculation to converge. For this reason, the grid on which the simulation is carried out must have a large height with respect to the size of the experiment. In the simulation, we considered the top border at 2000 nm from the gate electrodes.

to the mechanical work performed. In the figure, we represent the derivative $dI/d\omega_e$ numerically calculated from experimental data along a Coulomb peak $V_S \sim 0$. The resonance appears around the natural frequency of the device $\omega_e = \omega = \Omega$. In the peak $\omega_e = \omega < \Omega$ as a consequence of the transport.

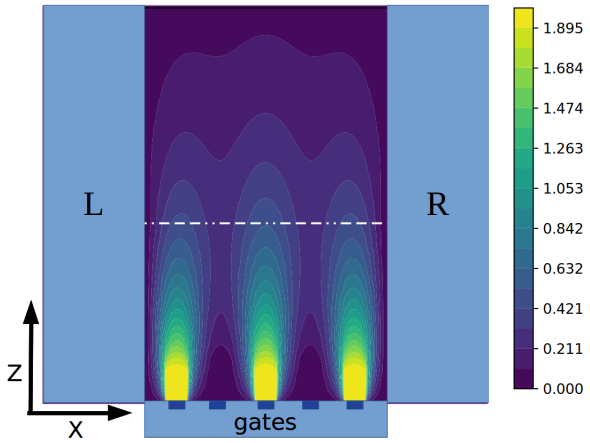

Figure 2.7.: Electrostatic potential $V(z, x)$ in a vertical section of the device with boundary conditions $V_{G1} = V_{G3} = V_{G5} = 2$ V and $V_{G2} = V_{G4} = 0$ V. The horizontal dashed line represents the position of the CNT. From [Vigneau et al., 2022]

2.3.2. WKB approximation and electronic levels

I consider now the dynamics of the single electrons passing through the CNT embedded in $V(z, x)$. Since the electrons are confined within the tube, their movement is described by a one dimensional Schrödinger equation

$$i\hbar\frac{\partial\psi(x,t)}{\partial t} = -\frac{\hbar^2}{2m_e}\frac{\partial^2\psi(x,t)}{\partial^2 x} + q_e V(d,x)\psi(x,t). \tag{2.33}$$

Here as before m_e and q_e are the electron mass and charge respectively, and $\psi(x,t)$ is the electron wave function. The potential V is restricted by the CNT geometry $z = d$, with d a certain height from the gates (see fig.2.5).

One can apply the WKB approximation, exposed in previous sections, to solve the Schrödinger equation and obtain the quantum energy levels of the electric potential [Heinze et al., 2002, Heinze et al., 2003]. To do this, I use Eq. (2.29)

$$\int_{x_1}^{x_2} dx\sqrt{2m_e\left[\varepsilon_n(d) - q_e V(d,x)\right]} = 2\pi\hbar\left(n + \frac{1}{2}\right), \tag{2.34}$$

with $n = 0, 1...$ an integer. The quantities ε_n represent the discrete set of quantum energy levels of the Schrödinger equation Eq. (2.33). As we know from the previous sections, they contribute to the electrochemical levels ε_N of the SET.

Since V lacks analytical expression, the quantum energy levels ε_n must be numerically solved, for every height d. As in Eq. (2.29), the tipping points $x_{1,2}$ are that where the electron energy E satisfies $E(d) = q_e V(d, x_{1,2})$. Solving numerically the last equation requires, therefore, finding the tipping points for all the values of d.

In fig.2.8, extracted from [Vigneau et al., 2022], we plot the quantum energy levels of the dot, for several values of d and n. As one can observe, when the CNT height is low, the quantum energy levels are negative, and the electrons filling the quantum dot are

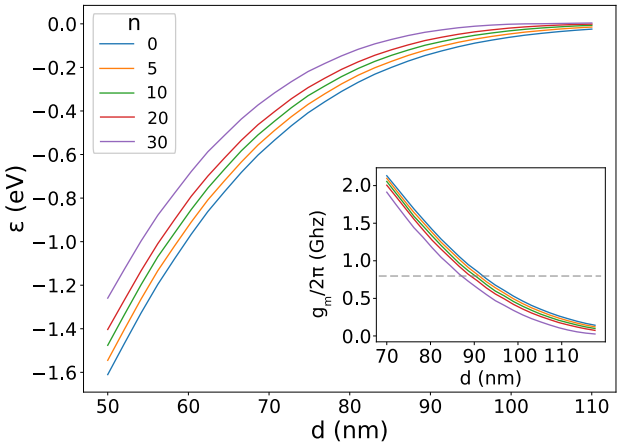

Figure 2.8.: Several quantum energy levels of the dot as function of the distance d. The configuration is the same as in fig.2.6. (Inset) Coupling constant g as function of d. The dashed line represents the value of g at the actual CNT height. The gate configuration is the same as in figure 2.6. From [Vigneau et al., 2022].

strongly confined in the device. Once the CNT is separated from the dot, confinement is reduced until become negligible at high d.

Coupling constant

The first quantity one can evaluate from the previous analysis is the coupling constant, g, quantifying the strength of the capacitive coupling. It is defined as

$$\varepsilon_n(d) \equiv \varepsilon_n(d_0) + \left.\frac{\partial \varepsilon_n}{\partial d}\right|_{d_0} d \quad \rightarrow \quad g = \left.\frac{\partial \varepsilon_n}{\partial d}\right|_{d_0}, \tag{2.35}$$

where d_0 is the actual position of the CNT in the experiment. In 2.8 (inset) we evaluate $\partial\varepsilon_n(d)/\partial d$ for several values of n and d. The mechanical-measured value $g_m = 0.80$Ghz (see tab.2.1) is obtained for $d = 90$nm, a value compatible with the geometry of the device, fig.2.5.

Tunnel barriers

The second quantity one can obtain from the WKB approximation is the intensity of a certain tunnel barrier at a given position z, which can be evaluated using Eq. (2.30). This (making some assumptions about the junction) was already done in [Korotkov and Nazarov, 1991, Bezryadin et al., 1997] and successfully applied in [Meerwaldt et al., 2012],

$$\Gamma_{\mathrm{L,R}}(z) = \Gamma_{\mathrm{L,R}} e^{\alpha_{\mathrm{L,R}} z}. \tag{2.36}$$

Here $\Gamma_{\mathrm{L,R}}$ are constant depending on the barrier size, controlling the number of electron jumping per time unit. The constants $\alpha_{\mathrm{L,R}}$ define the "triangular shape" of the barrier.

2.4. Dynamical model

In the previous section, I described the transport in the single electron resonator and obtained information about the strong coupling between mechanics and electric current, but it lacks an equation predicting the evolution of the oscillator. In this section, I present the *dynamical model* describing how the electronics affect the mechanics and vice versa.

It consists of three elements:

1. A Langevin equation representing *mechanical oscillations*, this is, an equation of motion representing the evolution of the vertical position z of the oscillating CNT, considering the thermal fluctuations induced by the nanotube environment.

2. A master equation representing electron transport in Coulomb blockade, similar to Eq. (2.13). Since all the experiments are performed in Coulomb blockade regime, I will consider a single electrochemical level ε within the bias window.

3. The capacitive coupling relation. A relation between the quantum dot electromechanical level ε and the vertical displacement z of the CNT. For small oscillations, this relation is approximately linear

$$\varepsilon(z) = \varepsilon_0 + gz, \tag{2.37}$$

with ε_0 a constant and g the coupling constant already evaluated.

A similar model has been proposed for several electron resonators devices, not always based on CNT [Gorelik et al., 1998, Isacsson et al., 1998, Weiss and Zwerger, 1999, Wächtler et al., 2019, Nord et al., 2002].

In fig.2.9, I sketch the main parts of the model.

Mechanical oscillations

As the CNT is a large object, this issue is akin to the classic problem of a rope suspended and fixed at both ends. Nonetheless, the electric force produced by electrons on the CNT is plainly localized on the quantum dot. The entire motion is depicted by the dot's vertical position on the CNT, z. Owing to the large quality factor Q, the nanotube oscillation adheres to an underdamped Langevin equation.

$$dz = vdt, \tag{2.38}$$
$$dv = F(z, v, p)/mdt + \sigma dB_t. \tag{2.39}$$

v is the vertical velocity of the dot. The term σdB_t is a Wiener process representing the effect of the thermal environment times $\sigma = \sqrt{2Dm^2}$, $D = \gamma/\beta_{zv}m^2$ the diffusion coefficient of the thermal environment with inverse temperature β_{zv} and dB_t a Wiener process. $\gamma = m\Omega/Q$ is the friction constant. The force acting on the oscillator is

$$F = -\partial_z U(x) - \gamma v - g_0 N + f_f(t). \tag{2.40}$$

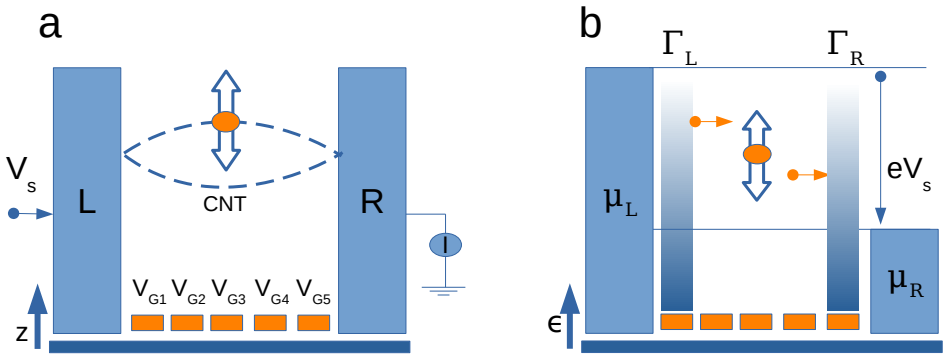

Figure 2.9.: Sketch of the device model. The mechanical part (a) consists of the carbon nanotube CNT suspended between the L, R electrodes; the electric current I between the electrodes is generated by a bias voltage $q_e V_S$. Five gate electrodes $V_{\text{G 1-5}}$ define the electrostatic quantum dot on the CNT (orange circle) with vertical position z. The transport part (b) represents the energy of the dot ε. The electron exchange (orange arrows) between the quantum dot and the L, R electrodes takes place within the bias window $q_e V_S = \mu_L - \mu_R$, Through the energy-dependent tunnel barriers $\Gamma_{L,R}(\varepsilon)$.

The first term represents the recovering force; for small displacements $U(z) = -m\Omega^2 z^2/2 - \lambda z^4$. The anharmonic constant $\lambda \geq 0$ only appears if the displacement increases enough, this is when the CNT is externally driven. It is known that this anharmonic term is responsible for a bistable oscillation amplitude [Wen et al., 2020]. $f_f(t)$ takes into account a time-dependent external forcing, generated by microwave pulses injected by the gates. The term $-gN$ represents the electric force exerted by electrons occupying the quantum dot due to the external electric field (capacitive coupling). g is known as *coupling constant* and N is the number of electrons occupying the dot.

Master equation in Coulomb blockade

I will consider the low bias regime, where there exists a single dot electrochemical level satisfying $\varepsilon \in [\mu_L, \mu_R]$ (only this level is inside the bias window). Due to the Coulomb blockade, its electron occupation is restricted to the two states $p = 0$ (empty level) or $p = 1$ (full level). The evolution of the occupation number p is given by the energy-dependent tunnel rates $\Gamma_{\text{in}}^{\text{L, R}}(\varepsilon), \Gamma_{\text{out}}^{\text{L, R}}(\varepsilon)$, id est, the probabilities of an electron tunnel jump per time unit, between any of the L, R electrodes and the quantum dot. The rates depend on both the geometry of the device [see Eq. (2.36)] and on the electrode material. If the electron density within the electrode is high, the quantum dot can fill with an electron quickly, but it is impossible for it to get empty; since the electrodes are gold (metallic) pieces at very low temperatures, the electron density is given by the Fermi

functions

$$f_{\mathrm{L,R}}(\varepsilon) = \frac{1}{\exp[(\varepsilon - \mu_{\mathrm{L,R}})\beta_{\mathrm{L,R}}] + 1}. \tag{2.41}$$

Here $\beta_{\mathrm{L,\,R}}$ are the inverse temperatures of the L, R electrodes and $\mu_{\mathrm{L,\,R}}$ is their chemical potential or Fermi levels. One can write the rates as

$$\Gamma_{\mathrm{in}}^{\mathrm{L,R}} = \Gamma_{\mathrm{L,R}}(\varepsilon) f_{\mathrm{L,R}}(\varepsilon), \tag{2.42}$$

$$\Gamma_{\mathrm{out}}^{\mathrm{L,R}} = \Gamma_{\mathrm{L,R}}(\varepsilon)(1 - f_{\mathrm{L,R}}(\varepsilon)). \tag{2.43}$$

Note that, in these definitions, I am considering a single electromechanical level ε in the bias window. The total tunnelling is just $\Gamma_{\mathrm{in}} = \Gamma_{\mathrm{in}}^{\mathrm{L}} + \Gamma_{\mathrm{in}}^{\mathrm{R}}$, $\Gamma_{\mathrm{out}} = \Gamma_{\mathrm{out}}^{\mathrm{L}} + \Gamma_{\mathrm{out}}^{\mathrm{R}}$.

In an infinitesimal time interval dt the occupation variation is

$$dp = (1 - p)dp_{01} - pdp_{10}. \tag{2.44}$$

The quantities dp_{01} are Poissonian random increments taking the values $0, 1$ with average values $\langle dp_{01}\rangle = \Gamma_{\mathrm{out}}(\varepsilon)dt$ and $\langle dp_{10}\rangle = \Gamma_{\mathrm{in}}(\varepsilon)dt$.

Capacitive coupling

The consequence of the capacitive coupling on the mechanics is the presence of the occupation-dependent force $-gN$ in the Langevin equation. The respective effect on the transport is the dependence of the electromechanical potential of the dot, ε, with the oscillator position z.

The explicit relation has been evaluated in figure 2.8 using the WKB approximation but, for most applications, one can assume the linear small-displacement approximation [5]

$$\varepsilon(z) = \varepsilon_0 + gz. \tag{2.45}$$

This is in accordance with the electric force defined in Eq. (2.39) since $-gp = -d(\varepsilon p)/dz$. I remark that the last approximation prevents the $N - p$ fixed charges from affecting the motion. These additional charges exert a constant force $-g(N - 1)$ just shifting the CNT equilibrium position. In the following sections, I will assume last relation and use the short notation $\Gamma[\varepsilon(z)] \equiv \Gamma(z)$ for any function Γ of ε.

2.4.1. System Hamiltonian and Fokker-Planck equation

The dynamical model can be written in a compressed way using a Fokker-Planck equation. Previously note that the total energy of the system can be expressed using a single Hamiltonian depending on the height z and velocity $v = \dot{z}$ and the occupation N,

$$H(z, v, p) = \frac{1}{2}mv^2 + \frac{1}{2}kz^2 + \varepsilon_0 p + gpz. \tag{2.46}$$

[5] Typical oscillation amplitude is, as we will see in the next chapter, less than half a nanometre, so this approximation is strongly justified in any realistic case.

This Hamiltonian is very similar to that in optomechanics, see for example [Elouard et al., 2015]. In the following chapters, I will combine this Hamiltonian with the stochastic equations of motion in order to obtain the system's thermodynamics.

The Fokker-Planck equation describes the evolution of the joint probability density function of the system, $\rho = \rho(z, v, p)$

$$\begin{aligned}\partial_t \rho = &-v\partial_z \rho - \partial_v \left[f(t) - D\partial_v\right] \rho \\ &+ (2p-1)\left[\Gamma_{\text{in}}\rho(z,v,0) - \Gamma_{\text{out}}\rho(z,v,1)\right].\end{aligned} \tag{2.47}$$

Here, $f = F/m$ is the force per unit mass. The last term contains the jump processes of the occupation modulated by the tunnel rates. Obtaining Eq. (2.47) from the Langevin equation Eq. (2.39) is a text-book exercise [Wächtler et al., 2019, Gardiner et al., 1985]. It can be written in a compact way

$$\partial_t \rho(z, v, p) = -\partial_z j_z - \partial_v j_v - j_p. \tag{2.48}$$

in terms of the probability currents,

$$\begin{aligned} j_z &= v\rho(z, v, p), \\ j_v &= \left[f - D\partial_v\right]\rho(z, v, p), \\ j_p &= -(2p-1)\left[\Gamma_{\text{in}}\rho(z,v,0) - \Gamma_{\text{out}}\rho(z,v,1)\right]. \end{aligned} \tag{2.49}$$

I remark that the number of particles within a system is conserved, $j_1 + j_0 = 0$. However, the instantaneous electric current measured in a laboratory by the Ampere meter connected to L or R is not j_p (which has no definite direction) but the number of particles exchanged with the connection electrode. If the Ampere meter is connected to R, for example, the measured current is

$$i \equiv j_p^R = (2p-1)\left[\Gamma_{\text{in}}^R \rho(z,v,0) - \Gamma_{\text{out}}^R \rho(z,v,1)\right]. \tag{2.50}$$

2.4.2. Mean Field and adiabatic approximations

In the following, I will explain two approximations useful to explain several experimental facts observed in the lab. The experiments working regime was resumed in table 2.1. As one can see, the dot occupation, governed by the tunnel rates $\Gamma_{\text{L,R}}$ evolves faster than the CNT, whose timescale is given by Ω.

The first approximation, known as *mean field*, consists in neglecting both environment and current noise. Environment noise is neglected when the inertia of the oscillator is large with respect to the environmental fluctuations, and therefore, the position and velocity z, v behave as deterministic variables. The only source of noise acting in this case comes from the occupation p. If $\Omega \ll \Gamma_{L,R}$, the electron exchange occurs much faster than mechanical oscillations, happening a great number of electron jumps in a single mechanical period. Then, neglecting fluctuations also in the occupation p, we can describe the dynamics in terms of the average position, velocity, and instantaneous occupation, $n \equiv \langle p \rangle$.

Taking the average over samples [6] values of the variables in the Fokker-Planck equation, we obtain the system of equations

$$\begin{aligned} \langle \dot{z} \rangle &= \langle v \rangle, \\ \langle \dot{v} \rangle &= \frac{1}{m} \langle F(z, v, p) \rangle, \\ \dot{n} &= \langle \Gamma_{\text{in}}(z) \rho(z, v, 0) - \Gamma_{\text{out}}(z) \rho(z, v, 1) \rangle. \end{aligned} \tag{2.52}$$

I use the notation

$$n = \langle p \rangle = \int dz dv \rho(z, v, 1). \tag{2.53}$$

Within the approximation, one can discard the correlations between the dynamical variables up to the first order to obtain

$$\langle \Gamma_{\text{out}}(x) \rho(z, v, 1) \rangle \sim \Gamma_{\text{out}}(\langle z \rangle) n, \tag{2.54}$$

and

$$\langle \Gamma_{\text{in}}(x) \rho(z, v, 0) \rangle \sim \Gamma_{\text{in}}(\langle z \rangle)(1 - n), \tag{2.55}$$

obtaining the following non-linear dynamical system

$$\begin{aligned} \langle \dot{z} \rangle &= \langle v \rangle, \\ \langle \dot{v} \rangle &= \frac{1}{m} \langle F \rangle, \\ \dot{n} &= \Gamma_{\text{in}}(\langle z \rangle)(1 - n) - \Gamma_{\text{out}}(\langle z \rangle) n. \end{aligned} \tag{2.56}$$

Replacing the bracket average notation with the more suitable z_M, v_M, n, I obtain the deterministic dynamical system of equations

$$\begin{aligned} \dot{z}_M &= v_M, \\ \dot{v}_M &= \frac{1}{m} F(z_M, v_M, n), \\ \dot{n} &= \Gamma_{\text{in}}(z_M)(1 - n) - \Gamma_{\text{out}}(z_M) n. \end{aligned} \tag{2.57}$$

In this approximation, the instantaneous electric current, defined in Eq. (2.50) is given by the instantaneous values of n and z_M,

$$i_M = \Gamma^R_{\text{in}}(z_M)(1 - n) - \Gamma^R_{\text{out}}(z_M) n. \tag{2.58}$$

The second approximation is known as *adiabatic approximation*. It appears in the limit of infinite tunnelling rates, where the quantum dot occupation is instantaneously

[6] The average of a certain dynamical variable f over samples is defined as

$$\langle f \rangle = \sum_p \int dz dv f(z, v, p) \rho(z, v, p). \tag{2.51}$$

equilibrated, this is $\dot{n} = 0$ at any time. Under this approximation, the occupation of the dot depends only on the mean value z_M, denoted as $n \equiv \pi(z_M)$. Using Eq. (2.57) I obtain

$$\Gamma_{\text{in}}(z_M)(1-\pi) - \Gamma_{\text{out}}(z_M)\pi = 0, \tag{2.59}$$

then

$$n = \pi(z_M) = \frac{\Gamma_{\text{in}}(z_M)}{\Gamma_{\text{in}}(z_M) + \Gamma_{\text{out}}(z_M)}. \tag{2.60}$$

2.5. Conclusion

In this chapter, I have introduced the basic model describing a single electron resonator. To do this, I have returned to the well-known single electron transistor electrostatic model, which will serve as an illustrative example hereafter. I have proposed to extend the single electron transistor model by considering the WKB approximation to describe the quantum states of the system.

After this, I give details on the construction of the single electron resonator we have been working in the laboratory and include a numerical characterization of the electrostatic fields involved in its operation. From this characterization, I have used the theoretical results obtained from the WKB approximation to evaluate the energy levels of the system, and their dependence on the geometry of the device. Finally, I have introduced the dynamical system that combines the state of the oscillator with the number of electrons inside the device, obtaining a set of equations of motion capable of explaining the experimental phenomenology. From this model, I have obtained two approximations, mean-field and adiabatic, which are useful in regimes where thermal and electric current fluctuations are negligible.

3. Self-oscillations in electron resonators

The non-linear coupling between the oscillator and electronic transport gives rise to several phenomena, such as the frequency softening studied in the previous chapter. In this chapter, I will explain in detail the phenomenon of self-oscillations. Self-oscillations occur when an oscillator is excited without any human interaction or external signal, leading to self-sustained oscillations [Jenkins, 2013].

Self-oscillations appear in many natural systems, generated by various mechanisms. Limiting ourselves to nanoscience, they have been reported, for example, in Brownian oscillators [Filliger and Reimann, 2007, Chiang et al., 2017] or thermal engines [Roulet et al., 2017, Fogedby and Imparato, 2018], and resonators [Chiang et al., 2017, Marchegiani et al., 2016, Serra-Garcia et al., 2016]. In these implementations, self-oscillations are fuelled by a thermal gradient. In single-electron resonators, self-oscillations occur due to the effect of electric transport on the mechanical part, as reported in [Eichler et al., 2011, Schmid et al., 2012, Schmid et al., 2015, Urgell et al., 2020, Willick and Baugh, 2020, Wen et al., 2020].

Recent experiments have sparked a series of theoretical studies that describe the system's thermodynamics [Wächtler et al., 2019] or characterize the electromechanical noise [Bashkirtseva et al., 2015, Usmani et al., 2007, Blanter et al., 2004, Bennett and Clerk, 2006] using a model similar to that described in the previous chapter. Some applications of this work include describing collective behaviour in systems [Wächtler et al., 2020] and thermodynamic machines [Strasberg et al., 2021, Elouard et al., 2015] in terms of self-oscillating devices, or attempting to emulate neural behaviour [Lin et al., 2018, Stoliar et al., 2021, Rocco et al., 2022] using this type of system.

In this chapter, I will explain the results of [Tabanera-Bravo et al., 2022]. In this work, we experimentally prove that self-oscillations in the single-electron resonator are bistable, meaning that self-oscillations can spontaneously appear or disappear under certain conditions. This bistability can be explained using the mean-field approximation model, Eq. (2.48).

The structure of this chapter is as follows: in 3.1, I will explain the physical origin of self-oscillations from an intuitive perspective. The presence of self-oscillations can be predicted by the mean-field model, eqs.(2.57), and thus, they are independent of electric or thermal noise. In section 3.1.3, I propose a numerical method capable of predicting the appearance, bistability, and amplitude of self-oscillations. In brief, this method involves evaluating the amount of energy the oscillator gains in a single oscillation period due to the electron current. Finally, in section 3.2, I explain the experimental results obtained in ref.[Tabanera-Bravo et al., 2022] and compare them with the theoretical model.

3.1. The origin of self-oscillations

To explore the physical origin of self-oscillations in the single electron resonator, I will start from the mean-field equations describing the evolution of our single-electron resonator, eqs.(2.57),

$$\begin{aligned} \dot{z} &= v, \\ \dot{v} &= \frac{1}{m}\left(-m\Omega^2 z - \gamma v - gn\right), \\ \dot{n} &= \Gamma_{\text{in}}(z)(1-n) - \Gamma_{\text{out}}(z)n. \end{aligned} \tag{3.1}$$

These mean field equations average the thermal and electric noise, becoming completely deterministic. As there is no place for confusion, I remove the subscript z_M used in the previous chapter. Since the amplitude of the oscillations is not so large[1], one can neglect the non-linear term λz^3.

3.1.1. Intuition: delay

Once the oscillator is moving, it imposes a time modulation on the occupation n which, in response, drives the oscillator. If the oscillation of z and n is perfectly synchronized, such as a harmonic oscillator, no energy is extracted at all. In order to extract energy, both oscillations must be delayed.

For a very large tunnelling rate Γ,[2] the occupation n is instantaneously equilibrated to the adiabatic value given by Eq. (2.60); in this situation, $n = \pi(z)$ is only a function only of z and the delay is impossible. For a lower Γ, the occupation requires some time [3]to equilibrate, delaying n with respect to z.

This is proved in figure 3.1, where I represent the value of n in front of z in three situations: when the oscillator is moving up (blue line), moving down (orange line), and in the adiabatic case (green line). As we can observe, the average occupation depends not only on z but on the carbon nanotube velocity. Both predictions are close to the adiabatic value. Following this idea, one can take the approximation

$$n \simeq \pi(z - v/\Gamma), \tag{3.2}$$

where the dependence $z - v/\Gamma$ delays the current position $z(t)$ in respect to the occupation. For small oscillations, one can expand

$$n \simeq \pi(0) + \left.\frac{d\pi}{dz}\right|_{z=0} (z - v/\Gamma)\,. \tag{3.3}$$

The last term, inserted in eqs.(3.1) drives the oscillator frequency and damping constants

$$m\Omega^2 \;\to m\Omega^2 + g\left.\tfrac{d\pi}{dz}\right|_{z=0}, \tag{3.4}$$

$$\gamma \;\to \gamma - \tfrac{g}{\Gamma}\left.\tfrac{d\pi}{dz}\right|_{z=0}. \tag{3.5}$$

[1]This is justified by the following experimental results.

[2]The tunnelling rates were defined in Eq. (2.36). In this section I will consider $\Gamma = \Gamma_L = \Gamma_R$ for simplicity.

[3]At least, a time $1/\Gamma$.

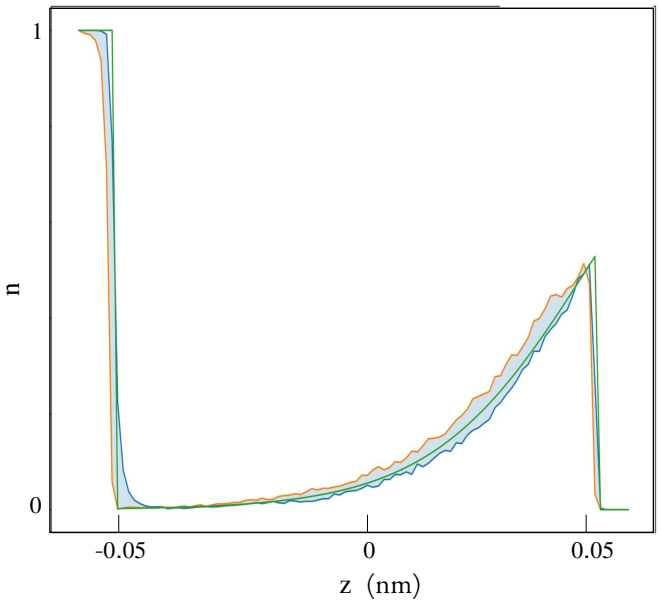

Figure 3.1.: Adiabatic occupation $\pi(z)$ as function of z along one period (green line). Average occupation predicted by the complete Fokker-Planck Eq. (2.48) depending on the sign of v; $v > 0$ (blue line) $v < 0$ (orange line). All the parameters are taken from table 2.1 and $\Gamma = 50\Omega$.

Note that the softening of Ω doesn't depend on Γ, appearing even within the adiabatic approximation. However, the driving of γ disappears if $\Gamma \gg g$. The derivative $d\pi/dz$ can be negative because of the energy-dependent tunnel barriers, Eq. (2.36). Therefore, for small friction coefficient γ and strong coupling g, the effective friction acting on the system becomes negative, giving place to anti-damped oscillations, id est, self-oscillations.

Perturbative solution

One can obtain a more precise solution by solving the last equation of eqs.(3.1) for large Γ,

$$n(t) = \pi(z(t)) + \delta n(t). \tag{3.6}$$

δn is a perturbation. Taking the time derivative and using Eq. (2.57) I obtain

$$\dot{\delta n} = -\Gamma_t(z(t))\delta n - \dot{\pi}. \tag{3.7}$$

With $\Gamma_t(z(t)) = \Gamma_{\text{in}}(z(t)) + \Gamma_{\text{out}}(z(t))$. This is an inhomogeneous linear equation admitting a solution of the form

$$\begin{aligned}\delta n &= e^{-\int_0^t dt'\Gamma_t(t')}\left[\delta n(0) - \int_0^t dt'\pi(t')e^{\int_0^{t'} dt''\Gamma_t(t'')}\right] \\ &= -\int_0^t dt'\dot{\pi}(t')e^{-\int_{t'}^t dt''\Gamma_t(t'')}.\end{aligned} \tag{3.8}$$

I have taken $\delta n(0) = 0$, and used the shorthand notation $\pi(t) \equiv \pi(z(t))$. The exponential in the integral goes quickly to zero for large Γ except for $t' \sim t$, and we can substitute the dependence in t' both in $\dot{\pi}(t')$ and $\Gamma_t(t')$. We obtain

$$\delta n = -\dot{\pi}(t)\int_0^t dt' e^{-\Gamma_t(t)(t-t')} = -\frac{\dot{\pi}(t)}{\Gamma_t(t)}. \tag{3.9}$$

With this,

$$n(t) = \pi(z(t)) - \frac{1}{\Gamma_t(t)}\frac{d\pi}{dz}\dot{z}. \tag{3.10}$$

For small oscillations, the first term can be expanded,

$$n(t) = \pi(0) + \frac{d\pi}{dz}z - \frac{1}{\Gamma_t(t)}\frac{d\pi}{dz}\dot{z}. \tag{3.11}$$

This is in agreement with the delay result, but now corrected with the instantaneous $\Gamma_t(t)$.

3.1.2. Linear stability analysis

To complete the analysis of the origin of self-oscillations, I will introduce the linear stability analysis. This consists of linearizing the dynamics of the system near its fixed points to determine whether these are stable or unstable. Since the parameter space of the single-electron resonator is large (in particular, the tunable parameters of the tunnel barriers, $\Gamma_{L,R}$, $\alpha_{L,R}$), this analysis can be used to numerically determine the region where self-oscillations occur.

A steady point (z_s, v_s, n_s) of eqs.(3.1) is defined by the conditions $\dot{z} = \dot{v} = \dot{n} = 0$, this is $v_s = 0$, $z_s = -gn_s/m\Omega^2$ and $n_s = \Gamma_{\text{in}}(z)/(\Gamma_{\text{in}}(z) + \Gamma_{\text{out}}(z))$. Note that since the tunnel barriers depend on z, this solution depends on the explicit form of the barriers, Eq. (2.36), and the system can have zero, one, or multiple steady points satisfying these conditions. These points can be numerically determined.

Once those points are determined, the stability analysis comes as follows. First, we linearize the system of equations, eqs.(3.1) around a certain steady point,

$$\begin{pmatrix}\dot{z}\\ \dot{v}\\ \dot{n}\end{pmatrix} = J(z_s, v_s, n_s)\begin{pmatrix}z\\ v\\ n\end{pmatrix} + ... \tag{3.12}$$

Here $J(z, v, n)$ is the Jacobian matrix with components

$$J_{ij}(z, v, n) = \frac{\partial \dot{z}_i}{\partial x_j} \tag{3.13}$$

and $x_i = z, v, n$. Let $\lambda_J \in \mathbb{C}$ be the 3 eigenvalues of the matrix $J(z_s, v_s, n_s)$, at the steady point (z_s, v_s, n_s). The solution of the linearized system close to a steady point is proportional $\exp(\lambda_J t)$; then if the real part of all the eigenvalues is negative, $\Re\{\lambda_J\} < 0$, any deviation from the steady point will be spontaneously recovered, suppressing any oscillation. However, if any λ_J becomes positive, $\Re\{\lambda_J\} > 0$, a small deviation of the system from the steady state will be exponentially augmented, generating spontaneous oscillations.

The *instability region* is that region of the parameter space where the system Eqs.(3.1) at least, one eigenvalue that has a positive real part, creating self-oscillation [4]. In Fig.3.2 I plot the instability region of Eqs.(3.1) as function of α_L and Γ_L, and compare it with the delay prediction Eq. (3.5) and the perturbation solution Eq. (3.11). As we can observe,

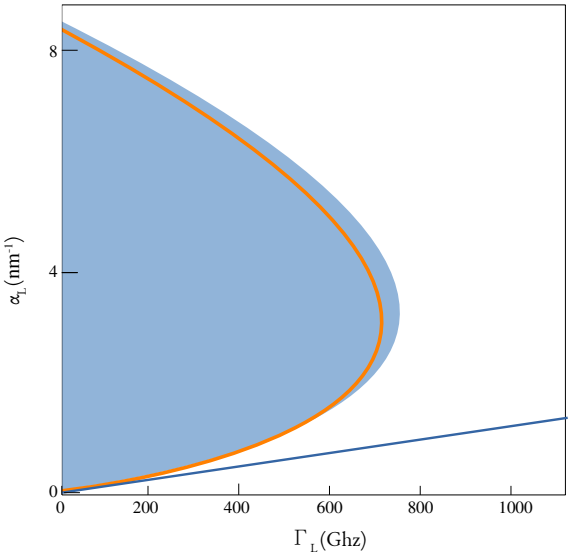

Figure 3.2.: Limits of the instability region of the dynamical system as a function of α_L and Γ_L, predicted by the linear stability analysis (shaded region), Eq. (3.5) (blue line) and Eq. (3.11). Other parameters are taken from table 2.1.

the instability region (blue) appears for low values of Γ_L. For $\Gamma_L > 800$Ghz the adiabatic approximation dominates, and the anti-damping effects disappear. For high values of α_L, the system becomes stable, opposite to the delay prediction. All the approximation coincides for low α_L, Γ_L.

[4] An unstable fixed point is sufficient to create self-oscillations; however, the actual amplitude of the oscillation depends on friction and on the voltage configuration, as we will see.

3.1.3. The energy balance

I discuss the origin of the self-oscillations in electron resonators as feedback between electron transport and oscillation. The main conclusion of that section was that the occupation n must depend both on z and v in order to promote the self-oscillations; in particular, the oscillator must transport electric charge from up to down: ascends empty, descends full.

However, the linear stability analysis gives no information about the actual amplitude of the oscillations; in fact, this amplitude depends on a balance between the friction and the self-oscillation mechanism.

To see this, one can consider the oscillator mechanical energy

$$E(z,v) = \frac{1}{2}mv^2 + \frac{1}{2}m\Omega^2 z^2, \tag{3.14}$$

and use eqs.(3.1) to evaluate their derivative

$$\frac{dE}{dt} = mv\dot{v} + m\Omega^2 z\dot{z} = -\gamma v^2 - gnv. \tag{3.15}$$

In one period of time, $T = 2\pi/\Omega$, the energy change is

$$\Delta E = -\int_0^T dt[\gamma v^2(t) + gn(t)v(t)]. \tag{3.16}$$

with $v(t)$ and $n(t)$ two solutions of the dynamical system eqs.(3.1) determined by certain initial conditions z_0, v_0, n_0.

For low coupling g, this quantity is always negative, and the system dissipates all its energy in terms of friction after some periods. However, as we saw in Fig.3.1, the instantaneous average occupation n depends on v, and therefore, the nv term could give a positive contribution.

In the central part of the oscillation in Fig.3.1, the energy gain is positive because there is more charge transported downward than upward. However, at the points $z = \pm 0.05$nm, the occupation sharply changes, transporting current above the Fermi levels, absorbing energy.

Self-oscillations amplitude can be determined by the energy balance condition $\Delta E = 0$, which in the following will be evaluated considering harmonic solutions.

3.2. Experimental results

In [Tabanera-Bravo et al., 2022], we conducted experiments to observe the appearance of self-oscillations in the single-electron resonator shown in Fig.2.5. We discovered that the self-oscillations are bistable, meaning they can spontaneously start or stop. In the laboratory, it is possible to detect this bistability by measuring the electric current because the self-oscillations draw their energy from the electric current flowing through the quantum dot.

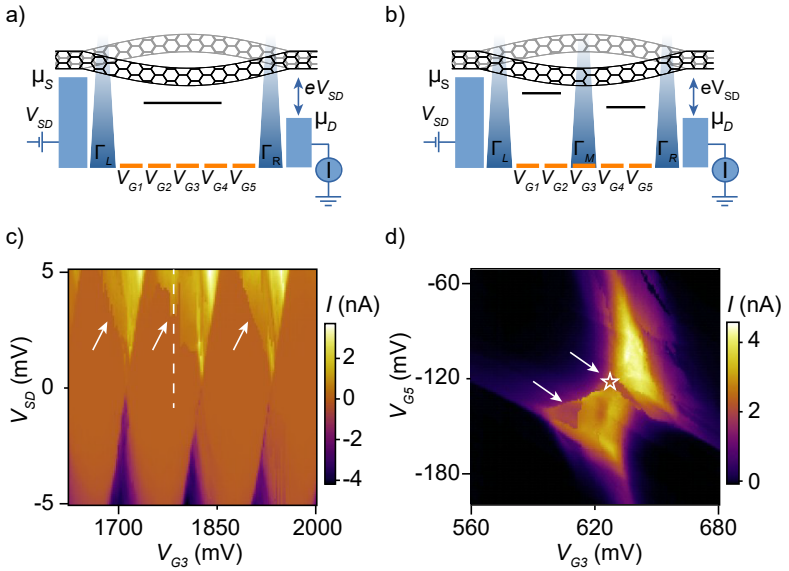

Figure 3.3.: Single dot (a) and double dot (b) configurations. Right, left, and interdot tunnel rates are indicated, and the associated tunnel rates are labeled Γ_R, Γ_L and Γ_M. c) Coulomb diamonds in the current in the single-dot configuration as a function of the gate voltage V_{G3} and bias voltage V_S. White arrows point at features that indicate the presence of self-oscillations. The current traces in Fig.3.4a were taken along the dashed vertical line. d) Current measured in the double-dot configuration by sweeping V_{G5} and stepping V_{G3} with $V_{SD} = 1.8$ mV. White arrows point at current features which indicate the presence of self-oscillations. The white star indicates a triple point, where we observe the hysteresis in current as a function of V_{SD} in Fig.3.8a. From [Tabanera-Bravo et al., 2022]

.

The experimental setup is illustrated in Fig.3.3. We first set up the device to observe single-electron transport, as shown in Fig.3.3(a). As explained in the previous chapter, the quantum dot defined on the CNT has a single electrochemical level within the bias window created by the bias voltage V_{SD}. The corresponding Coulomb diamond structure, as shown in Fig.3.3(c), resembles that in ref.[Vigneau et al., 2022], showing diamonds of blocked current (orange) and single-level current (yellow and purple regions). The first sign of self-oscillations is the distorted edges in the Coulomb diamonds (white arrows), indicating that the blocked current is restored because the self-oscillations drive the quantum dot level within and outside the bias window.

All the experiments can be repeated in a double-dot configuration, Fig.3.3(b). In this configuration, the gate voltages define two different quantum dots along the CNT, which can exchange electrons with both left and right electrodes and between them. The inter-dot electron exchange takes place through an intermediate tunnel barrier denoted

Γ_M.

The current blockade in this configuration is similar to the single-electron configuration Coulomb blockade. However, in order to restore the inter-dot current, both quantum dots must have similar electrochemical levels. This results in a blockade pattern in the gate voltages configuration space, Fig.3.3(d). This pattern is usually called *Coulomb triangles* [Hanson et al., 2007]. [5] The spots in this pattern (white arrows, star) are also due to the self-oscillations; in this situation, the oscillation of the CNT is able to change both the alignment of the two dots and their position with respect to the bias window.

3.2.1. Single-electron configuration

We start analyzing the self-oscillations in single-dot configuration, Fig.3.3(a, c). To do this, we set the gate voltage configuration with $V_{G3} = 1.8$V [white dashed line in Fig.3.3(c)] and measure the current along the dashed line, first increasing, and then decreasing V_{SD}. The result is in Fig.3.4(a). Note that the value of measured current changes if we measure increasing V_{SD} (red arrow) or decreasing it (blue arrow), defining a hysteresis region (II). In regions (I, III) the current makes no distinction between the curves. Region (I) is within the Coulomb diamond, where the absence of current prevents the self-oscillations. If we increase V_{SD}, self-oscillations remain inactive in region (II). Once we enter in region (III), the quantum dot enters the bias window and the current is restored, generating self-oscillations. If we start decreasing V_{SD}, we enter again in (II) but, since the self-oscillations are activated, they recover the current in this region. This happens because the dot expends a part of the oscillation period inside the Coulomb diamond, and a part inside the bias window. Back in (I), the oscillation is too weak to recover the current, and the self-oscillations disappear.

We can use the theory exposed above to describe the three regions of self-oscillations and obtain information about the oscillation amplitude. To do this, we must compute the energy gain ΔE defined in Eq. (3.16) in the three regions (I, II and III) for several oscillation amplitudes. Evaluating this integral in terms of the oscillation amplitude can be cumbersome because we must previously solve the complete system dynamics, eqs.(3.1). This step can be simplified considering harmonic mechanical oscillations

$$z(t) = A\cos(\Omega t), \tag{3.17}$$

$$v(t) = -A\Omega\sin(\Omega t), \tag{3.18}$$

along a period $\tau \in [0, 2\pi/\Omega)$. A is the amplitude. Then, the master equation in eqs.(3.1) can be solved numerically using this trajectory, and its result, $n(t)$ inserted in Eq. (3.16) to obtain ΔE. In Fig.3.4(b) we represent ΔE as a function of V_{SD} and A using this method.[6]

[5] Coulomb triangles are analogous to the Coulomb blockade of the single-dot configuration. As one can observe, in Fig.3.3(d) the current gets blocked within the black regions because the electrochemical levels are misaligned or outside the bias window.

[6] Note that under this ansatz, the quantity ΔE only depends on the amplitude A and thus, on the current mechanical energy $E = m\Omega^2 A^2/2$.

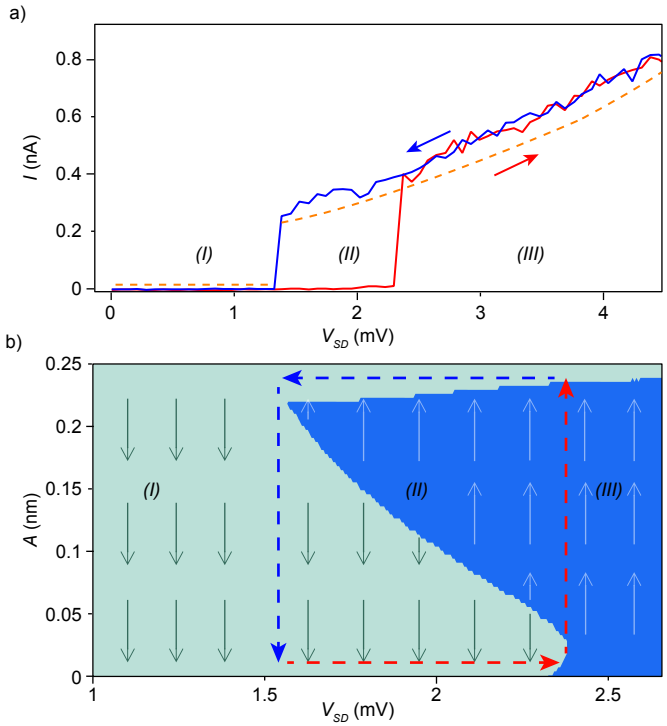

Figure 3.4.: a) Current switch hysteresis as a function of V_{SD} measured in the single dot regime following the dashed line ($V_{G3} = 1.8$ V) in Fig.3.3c. The red and blue arrows indicate the direction of each current sweep. The orange dashed line is the current calculated from Eq. (3.19). The numerals (I, II, III) indicate regions of no oscillations, bistability, and self-oscillations, respectively. b) Stability diagram: the dark (light) blue areas indicate $\Delta E > 0$ ($\Delta E < 0$) for different values of A and V_{SD}. Small arrows indicate the direction in which A would change in each area, given the sign of ΔE. Blue and red arrows delimit regions (I), (II), and (III) and indicate a similar hysteresis cycle as that shown in panel a). We use $\Omega/2\pi = 270$ MHz, $g_{\,\mathrm{m}} = 0.01$ eV/nm, $m = 2 \times 10^{-22}$ kg, and $Q = 1000$, $\Gamma_L = 400$ GHz, $\Gamma_R = 18$ GHz, $\alpha_L = 4$ nm^{-1}, and $\alpha_R = 0$. From [Tabanera-Bravo et al., 2022]

In the region (I), $\Delta E < 0$ (light blue region) for any amplitude. Since there is no current in this region, the mechanical friction absorbs all the energy from the oscillator, damping the oscillations (downward arrows). In (II), some amplitudes show $\Delta E > 0$ (dark blue region); in this zone, the energy obtained from electric transport is greater than the friction and the self-oscillations are sustained. In this region, the zero amplitude oscillations, $A = 0$, are stable since any small amplitude deviation is suppressed. At $A \simeq 0.25$ nm, the oscillator energy balance is zero, $\Delta E = 0$ corresponding with the actual amplitude of stable self-oscillations. Finally, in region (III) the current Coulomb blockade fails, and the self-oscillations always exist. In this region, any fluctuation at zero amplitude becomes unstable due to the current.

Dashed arrows in Fig.3.4(b) represent the same hysteresis cycle as Fig.3.4(a) revealing the relation between the current and the mechanical state: the red arrows starts with no oscillations in regions (I) and (II). Once it achieves region (III) oscillations are spontaneously generated and the current starts, acquiring $A \simeq 0.25$nm. From that region, the blue curve descends with stable self-oscillations until reaches (I) where the mechanical energy is immediately dissipated.

In order to compare the theoretical model with the current, we evaluated the theoretical current with the experimental measurements. The theoretical instantaneous value of the current is given by Eq. (2.58), and therefore, the average current is given by

$$I = \frac{1}{T}\int_0^T \left[\Gamma^R_{\text{out}}(z(t))(1-n) - \Gamma^R_{\text{in}}(z(t))n\right] dt. \tag{3.19}$$

In order to evaluate this integral, we also considered harmonic trajectories with amplitude $A = 0.25$ nm. The resulting prediction is in Fig.3.4, where we can observe how the current is zero in the region (I), as we expect in the absence of oscillations, and increases in (II) and (III) according to the experiment.

In the bistability region, self-oscillations remain for several seconds, corresponding approximately to $\sim 10^9$ times the natural period $2\pi/\Omega$. For longer times, they can vanish or get spontaneously generated.

In Fig.3.5, we present self-oscillations duration along the three regions. To measure this duration we applied the following protocol: first, we initialize the experiment with no oscillations, killing them by switching off the bias voltage, $V_{SD} = V_{\text{KILL}} \sim 0$, see Fig.3.5(a, blue curve). The bias voltage is then recovered for 10 seconds with probing value $V_{SD} = V_{\text{PROBE}}$; at this time, we observe the electric current to determine if self-oscillations appear spontaneously or not. After this, we activate artificially the self-oscillation by switching the bias voltage for one second to an activation value $V_{SD} = V_{\text{PUMP}}$. After that, we recover $V_{SD} = V_{\text{PROBE}}$ again to observe the self-oscillations decay.

In Fig.3.5(b) we plot the electric current against the time for several values of V_{PROBE}. In (I), the current is completely blocked, and self-oscillations are never generated. The region (II) has been split into two parts: in (IIa), self-oscillations never appear spontaneously after the kill step but are activated by the pump, recovering the current. As we can observe, the oscillation remains for some time after disappearing. The self-oscillation duration goes from a few seconds to more than 25 seconds; this duration seems to increase

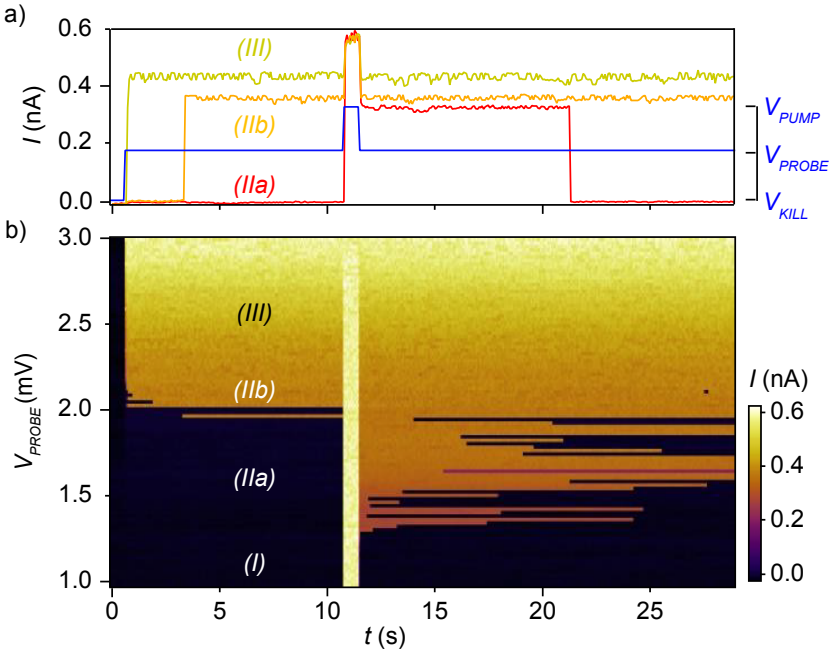

Figure 3.5.: a) The sequence of bias voltages V_{SD} applied (blue) and observed current during the protocol for $V_{\mathrm{PROBE}} = 1.6$ mV (IIa), 1.98 mV (IIb), and 2.5 mV (III), selected from panel b). The device is in the single-dot configuration (see Fig.3.3a). V_{SD} is initially set to $V_{\mathrm{KILL}} = 0$ mV to start the protocol with the CNT at rest. Then V_{SD} is increased up to V_{PROBE} for a given time. self-oscillations are pumped by setting V_{SD} to $V_{\mathrm{PUMP}} = 3$ mV. Finally, the persistence of the self-oscillations is measured by setting V_{SD} back to V_{PROBE}. b) Observed current during the protocol for different values of V_{PROBE}. We identify four regions: (I) absence of self-oscillations; (IIa) self-oscillations observed after the pumping step and spontaneously decaying after a random time; (IIb) self-oscillations spontaneously appearing at a bias potential $V_{SD} = V_{\mathrm{PROBE}}$; and (III) stable self-oscillations. Figure from [Tabanera-Bravo et al., 2022].

with V_{PROBE}. In region (IIb), self-oscillations are generated spontaneously before the pump step, after a few seconds. In (III), self-oscillations appear immediately once we switch on the bias voltage and never decay.

Discussion

Before proceeding to explain the experiments in the double dot configuration, I will do a brief discussion of these results. In particular, I will try to explain how a nanomechanical device (working in the timescale of a few gigahertz) is able to behave in the timescale of a few seconds.

Imagine the system in the region (II) once the self-oscillations have been activated, recovering the electric current. As we see in Fig.3.4 their mean amplitude is around $A = 0.25$ nm. A strong thermal or electrical fluctuation could drive the system to lower amplitudes, even below the $\Delta E > 0$ region. If this happens, the self-oscillations can not be recovered and are damped by friction. In the opposite case, if the oscillations are inactive, $A = 0$, a thermal fluctuation can promote the amplitude into the $\Delta E > 0$ region, activating the self-oscillations.

The activation/deactivation mechanism is therefore governed by the fluctuations. However, since the electrical fluctuations only operate during the self-oscillations, it is easier for the system to destroy the oscillation than to create them. Self-oscillations are more easily destroyed close to $V_{SD} = 1.5$ mV because the $\Delta E > 0$ region is narrower at this point, and they are easier created close to $V_{SD} = 2.3$ mV since the region approaches $A = 0$.

This explains the increasing time of the self-oscillations in the region (IIa) and the spontaneous generation in (IIb). However, an explanation of the 20 seconds timescale is needed. As I will prove, this problem is very similar to that classical textbook problem where a Brownian particle is confined in a double well potential. In this problem, the average time the particle needs to jump the barriers due to the fluctuations increases exponentially following the Arrhenius law [Gardiner et al., 1985]. In this problem, it is well-known that the jumping times become much longer than any system time scale.

In order to establish our analogy between both problems, I will consider that the oscillator mechanical energy E varies slowly along a mechanical period. Then, I define the magnitude

$$U(E) = -\frac{1}{T}\int_0^E \Delta E(E')dE'. \tag{3.20}$$

$T = 2\pi/\Omega$ is the period of oscillation and ΔE is computed using Eq. (3.16). Then, the mechanical energy E follows the approximated evolution

$$\frac{dE}{dt} \simeq \frac{\Delta E}{T} + \xi(E) = -\frac{dU}{dE} + \xi(E). \tag{3.21}$$

The last approximation is valid under a timescale separation, this is when the energy E varies slowly along one period T. Otherwise, the quantity $U(E)$ could depend on time. $\xi(E)$ is an energy-dependent noise containing thermal and electric fluctuations.

Note that the quantity $U(E)$ represents a sort of potential in the energy space, and that Eq. (3.21) is analogous to the Langevin equation describing a particle in the double well potential. In Fig.3.6 we plot $U(E)$ revealing their double well structure for a certain value of V_{PROBE}. To evaluate the integral in ΔE, I consider again harmonic trajectories

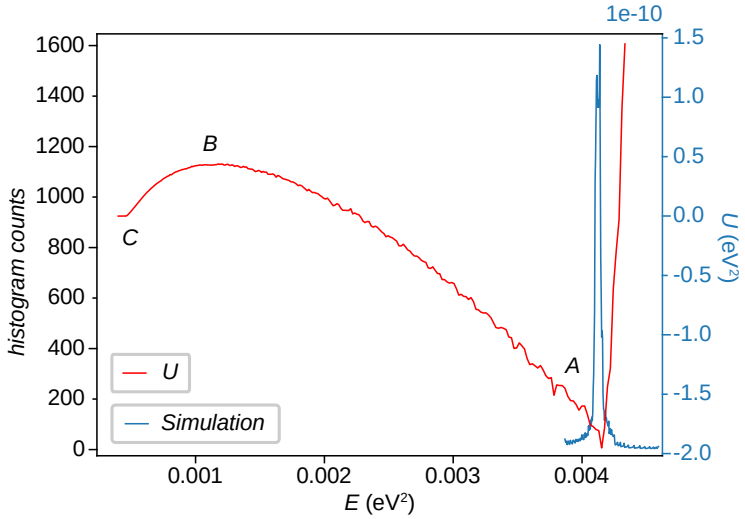

Figure 3.6.: Numerical computation of the effective potential $U(E)$ (red) stochastic simulation of a single trajectory (blue) as a function of the mechanical energy for the one dot-configuration. The sharp peak in U at point A is due to the borders of the conduction region of the device. Letters A, B, and C indicate the stable oscillation points of the oscillation (A, C) and the tipping point between both regimes (B). The parameters are $\Omega/2\pi = 270$ MHz, $g_{\text{m}} = 0.01$ eV/nm, $m = 2 \times 10^{-22}$ kg, $Q = 1000$, $\Gamma_L = 400$ GHz, $\Gamma_R = 18$ GHz, $\alpha_L = 4$ nm^{-1}, and $\alpha_R = 0$.

$z(t) = A\cos(\Omega t)$ with $A = \sqrt{2E/m\Omega^2}$.

The left well in Fig.3.6, labeled C, corresponds to the zero amplitude oscillations. The right well, A, corresponds with self-oscillation energy. To activate/deactivate the self-oscillations, a fluctuation must drive the system over the maximum B.

Since it is hard to analytically evaluate the thermal and electric noise using the complete Fokker-Planck equation, Eq. (2.48), I performed a simulation of the stochastic dynamics contained in that equation using the stochastic Heun algorithm. [7] The blue line in Fig.(3.6) represents the histogram of a single trajectory for 10^4 oscillation periods T.

[7]The Heun algorithm is a numerical method for solving differential equations. However, it can be extended to stochastic differential equations such as Eqs.(2.39)[Toral and Colet, 2014]. Given the (perhaps multi-dimension) stochastic differential equation

$$dx = a(x)dt + b(x)dB_t \tag{3.22}$$

with dB_t a Wiener process, the Heun scheme consists of discretizing the solution $x(t)$ in steps x_t

As we can observe, the trajectory remains localized inside the well A, explaining the timescale separation between the oscillation period, and the bistability times.

3.2.2. Double dot configuration

In the double-dot configuration, two dots are situated in series along the carbon nanotube. While this implementation is well-established in the literature for static dot devices [Hanson et al., 2007], limited knowledge exists concerning its impact on the oscillator. Analogous to the Coulomb diamond structure observed in the electric current of the single-dot configuration, the current structure in the double-dot configuration takes the form of a honeycomb pattern in gate voltage space (see [van der Wiel et al., 2002] and the figure below). The hexagons, however, are distorted by the capacitive coupling between the two dots.

Breaking the Coulomb blockade requires both dots to possess an electrochemical level within the bias window. Additionally, for electric current to flow between the dots, both electrochemical levels must align, a phenomenon known as *elastic transport* [Nazarov and Blanter, 2009, Hanson et al., 2007]. Should the bias voltage increase, electrons may leap between misaligned levels, giving rise to spurious current within the hexagons, referred to as *inelastic transport*. This is due to second-order phenomena such as phonon absorption and cotunnelling. The bias triangles observed in Fig.3.3(d) arise at the vertices of the honeycomb structure, where elastic current is restored.

In Fig.3.7, extracted from [Tabanera-Bravo et al., 2022] we plot the electric current in the device in a large region of the gate voltages configuration space. In the upper part of the plot, the straight lines reveal the single dot configuration [8]. In the lower left part, the lines collide, and the honeycomb structure appears. The triangles in Fig.3.3 have been taken from this part of the plot.

We repeat the previously explained experiments in the double-dot configuration. First, in Fig.3.8 we observe the hysteresis cycles moving the bias voltage up and down (red and blue lines). In this case, two different bistable regions appear, (ii) and (iv). These regions are separated by stable self-oscillations (iii). Regions (i) and (v) are stable and exhibit no oscillations. In contrast to the single-dot case, an additional spurious current appears in regions (iii, iv, v) for high values of bias voltage, even if the self-oscillations are not present. To explain this, we generalize the theoretical model of self-oscillations by assuming one of the dots to be static. The latter is justified since the configuration is generated by the gate electrodes $G5$, just below the fixed border of the nanotube, and $G3$, below the moving part of the nanotube. In that case, the equations of movement

with time interval Δt following

$$x_{t+1} = x_t + \frac{a(x_t) + a(\bar{x}_t)}{2}\Delta t + \frac{b(x_t) + b(\bar{x}_t)}{2}\Delta B, \tag{3.23}$$

where $\bar{x}_t = x_t + a(x_t)\Delta t + b(x_t)\Delta B$ and ΔB is a Gaussian random variable with zero mean and variance Δt.

[8] The straight lines pattern appears because both V_{G5} and V_{G3} are acting on the same dot, being manipulated indistinctly by the two.

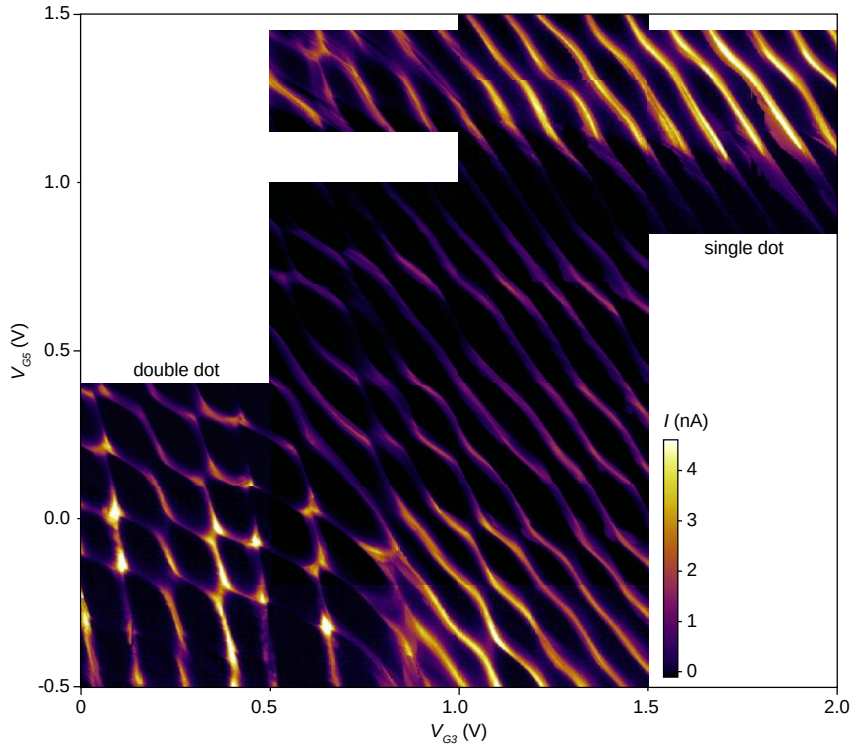

Figure 3.7.: Stability diagram containing the single quantum dot and double quantum dot regime measured at $V_{SD} = 3$ mV. Extracted from [Tabanera-Bravo et al., 2022].

eqs.(3.1) remain formally unchanged. Only the explicit form of $\Gamma_{\text{in/out}}$ change. In [Tabanera-Bravo et al., 2022] we propose

$$\Gamma_{\text{in}}(z) = \Gamma_L(z) f_L(\epsilon(z)) + \Gamma^{\text{ie}}(V_S) \tag{3.24}$$

$$\Gamma_{\text{out}}(z) = \Gamma_L(z)[1 - f_L(\epsilon(z))] + \Gamma_{\text{dot-dot}}(z) + \Gamma^{\text{ie}}(V_S). \tag{3.25}$$

The last model represents the moving dot exchanging charges with the L electrode, as in the single dot configuration. However, it doesn't pour its charge directly into the R electrode, but into the static dot with rate $\Gamma_{\text{dot-dot}}(z)$. This depends on the electrochemical alignment

$$\Gamma_{\text{dot-dot}}(z) = \Gamma_{\text{M}} \exp\left[-(z - z_{\text{d}})^2/\sigma^2_{\text{dd}}\right]. \tag{3.26}$$

Here, z_{d} represents the oscillator position in which both dots are aligned, and σ_{dd} represents the effective width of the dot.

The stability diagram in Fig.3.8(b) was obtained by evaluating again ΔE with harmonic trajectories, distinguishing a region with $\Delta E > 0$ (dark blue) and $\Delta E < 0$ (light blue). Dashed arrows represent the same trajectories from Fig.3.8(a). As one can observe, in region (i) the moving dot is outside the bias window, and therefore, no current is measured at all. The bistability of the regions (ii) and (iv) is explained by the presence

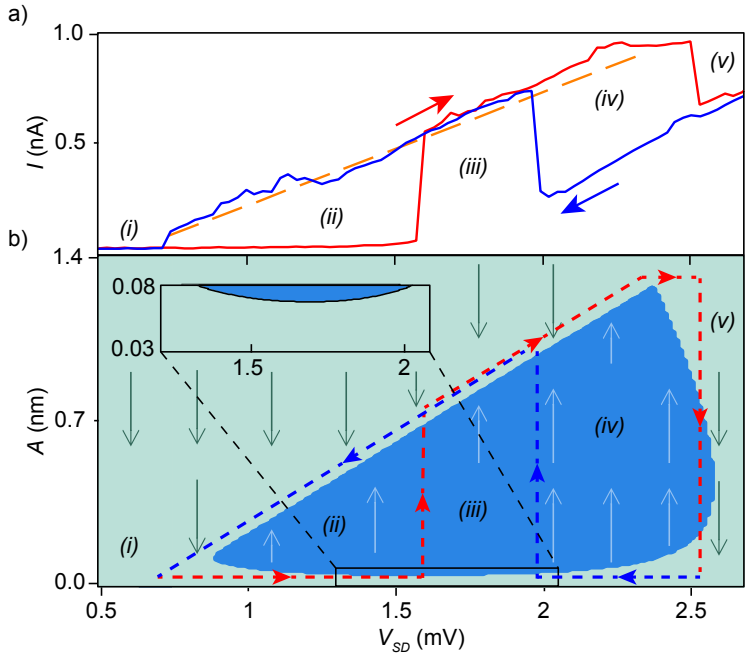

Figure 3.8.: a) Current switch hysteresis as a function of V_{SD} in the double-dot configuration, measured at the white star location in Fig. 3.3d ($V_{G3} = 620$ mV, $V_{G5} = -120$ mV). Red and blue arrows indicate the direction of each current sweep. The dashed orange line shows the current calculated from Eq. (3.19) with $\Gamma_M = \Omega$, $\sigma = 0.1$ nm and amplitude 1 nm. The numerals (i, ii, iii, iv, v) indicate different regions in the stability diagram. b) Stability diagram: the dark (light) blue areas indicate $\Delta E > 0$ ($\Delta E < 0$) for different values of A and V_{SD}. Small arrows indicate the direction in which A would change in each area, given the sign of ΔE. Blue and red dashed lines delimit regions (ii), (iii), and (iv). Blue and red arrows indicate a similar hysteresis cycle as that shown in panel a). Inset: zoom in on areas approaching zero amplitude. We use $\Omega/2\pi = 270$ MHz, $g_m = 0.01$ eV/nm, $m = 2 \times 10^{-22}$ kg, and $Q = 1000$.

of a zone with $\Delta E > 0$, obtaining two stable solutions, one with $A = 0$, and one with self-oscillations recovering the current. Note that the amplitude of self-oscillations increases proportionally to V_{SD}. In region (iii) self-oscillations are always generated, even if the mean-field model predicts a stable solution with $A = 0$. The discrepancy occurs due to thermal fluctuations, which, when the solution $A = 0$ is extremely close to the $\Delta E > 0$ region, are able to activate the self-oscillation almost instantaneously. This is the case, precisely in the region (iii), see Fig.3.8(b, inset).

In region (v), the bistability disappears and the current is only due to inelastic transport. The absence of self-oscillations in this region can be explained, precisely by the action of this inelastic current. To understand this, I remark that equation Eq. (3.16) predicts self-oscillations because the term $-n(t)v(t)$ becomes positive, id est, because the quantum dot descends almost full, and ascends almost empty. This correlation is destroyed by the

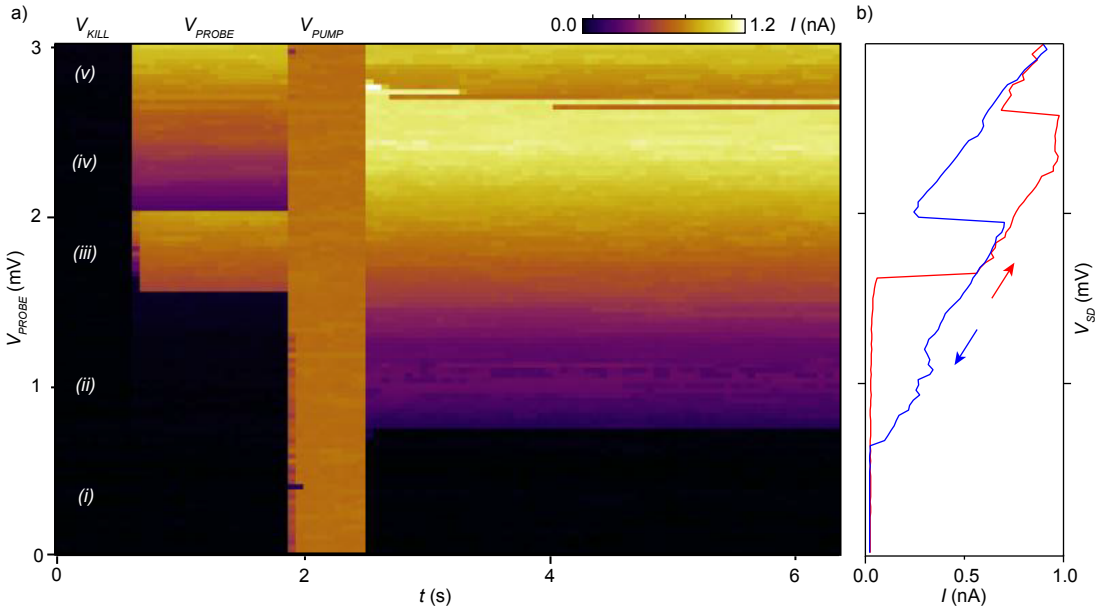

Figure 3.9.: a) Current measured by repeating the sequence shown in panel a) for different V_{PROBE}. The different behaviour is classified in five areas: (i) absence of self-oscillations, (ii) self-oscillations observed after the pumping step, (iii) self-oscillations spontaneously appearing, (iv) self-oscillations observed after the pumping step and spontaneously decaying after a random time, (v) absence of self-oscillations. b) IV measurement with the two sweep direction in the configuration of panel a) showing the current switch hysteresis; same as Fig. 4(a) of the main text.

inelastic transport, which does not distinguish the velocity, preventing self-oscillations. In Fig.3.9(a) we measure the self-oscillations duration following the same activation protocol as in Fig.3.5. As we can observe, in regions (ii) and (iv) self-oscillations are very stable, remaining active for all the measurement time, and in (iii) they activate spontaneously before the pump. The spontaneous decay is observed only in the border between regions (iv) and (v), where the unstable region $\Delta E > 0$ in Fig.3.8 becomes narrower. In region (v) we only observe inelastic current.

3.3. Discussion and conclusion

In this chapter, I have applied the model developed in the previous chapter to study the phenomenon of self-oscillations appearing in a series of experiments in [Tabanera-Bravo et al., 2022]. As I have shown, mechanical self-oscillations are produced by feedback between oscillator motion and modulation of electron transport and can be addressed using a mean-field deterministic model. In particular, self-oscillations are generated because the occupation of the dot is higher when descending than ascending, extracting energy from the gate electric field.

Our first result has been the experimental and theoretical description of the bistability of the self-oscillations, which, as we have seen, is due to the Coulomb blocking of the current, both in the single-dot and the double-dot configurations. The activation and deactivation of self-oscillation are due to thermal and electrical fluctuations. Strong enough fluctuations can drive the system from a motionless state into a self-sustained oscillation and vice versa; however, since the self-oscillations undergo electrical fluctuations while the motionless state does not, self-oscillations are more likely to be destroyed than created. From an energetic point of view, self-oscillations are transforming electric current, coming from the bias voltage, into mechanical energy dissipated in the environment, as an electrical motor. In the absence of mechanical load, this energy is dissipated into the environment

These results are very interesting from an experimental point of view. In fact, further experiments could employ the self-oscillating living time to characterize the electric and thermal noise from the environment, extracting from them information about the environment temperature. To do this one considers the double-well potential problem of figure 3.6 and Arrhenius law, which relates the average bistability time with the potential shape and the fluctuations temperature [Gardiner et al., 1985].

In [Tabanera-Bravo et al., 2022] (see Supplemental material) we explored the role of temperature on the self-oscillations. The mechanical dispersion due to thermal fluctuations can be estimated as $\sigma_x^{\text{therm}} = \sqrt{k_B T/m\Omega^2}$. For a temperature $T = 60\text{mK}$, the dispersion is $\sigma_x^{\text{therm}} \simeq 3.7 \times 10^{-2}$ nm, orders of magnitude smaller than the amplitude of self-oscillations, so that they are not so relevant for the oscillations. We have observed that as the temperature increases, the fluctuations become larger and larger, preventing self-oscillations, but our results are not sufficient to predict exactly at what temperature the oscillations disappear, so there is plenty of room for further experiments. In other self-oscillation systems has been shown that thermal fluctuations have been related to fluctuations in the oscillating period; these fluctuations decay with the average oscillation energy [Aminzare et al., 2019], making them excellent clocks. It will be interesting to prove if our device can replicate this, considering the electric noise.

The bistability observed in the experiment is very similar to that predicted in [Pistolesi et al., 2021]; the main difference is that the reference considers a system with two motion-less states, and we are considering a motion-less and an oscillation state. Following that reference, one could try to implement a mechanical qubit based on the robust self-oscillations/motion-less states. For example, if we consider the self-oscillations state with the logical value 0 and motion-less state with value 1, switching on the self-oscillations (figure 3.5) is equivalent to performing the logical erasure[9].

[9]Also known as Landauer's erasure. This is a logical operation defined by the action of rewriting a memory to $0\ 0, 1 \to 0$.

4. Thermodynamics of the single electron resonator

In the introduction chapter, I have presented the general framework of the thermodynamics of information. This framework has been applied to several models close to the single electron resonator in [Wächtler et al., 2019, Elouard et al., 2015, Strasberg et al., 2021] establishing the definitions of heat, work and entropy production precisely in the self-oscillation regime. In this chapter, I will apply this theory to the previous model of a single electron resonator, analyzing the thermodynamic efficiency of the different working regimes. I will start by introducing SET thermodynamics as an illustrative example, proposing the *electron pump mechanism*. After that, I will consider the single electron resonator thermodynamics, where the *information flows* formalism provides a clear image of the role of information in the operation of the device. My final result is the existence of the *information engine* working regime where the device performance can be only explained by the information exchange, very similar to Maxwell's demon.

I will do a very brief survey about the fluctuation theorems defining the stochastic behaviour of the device. I want to understand the role of information flow in these theorems, but this is just an incomplete part of future research, and I don't want to give more than a shallow motivation.

The chapter comes as follows: in section 4.1 I establish the SET thermodynamics and discuss some applications. I continue in section 4.2 showing the single electron resonator thermodynamics and discuss their applications in the non-autonomous 4.2.2 and the autonomous 4.2.3 cases. In the last case, I explore the information engine regime. Finally, in section 4.3 I explore the possible application of the information flows to the fluctuation theorems.

4.1. SET thermodynamics

Consider a single electron transistor in the low bias regime, with a single electrochemical level ε inside the bias window. The electron occupation in this situation follows the master equation Eqs.(2.13),

$$\begin{aligned} \frac{d\mathcal{P}_1}{dt} &= \Gamma_{\text{in}}\mathcal{P}_0 - \Gamma_{\text{out}}\mathcal{P}_1, \\ \frac{d\mathcal{P}_0}{dt} &= \Gamma_{\text{out}}\mathcal{P}_1 - \Gamma_{\text{in}}\mathcal{P}_0. \end{aligned} \tag{4.1}$$

Here, I take $N = 0$, so $\mathcal{P}_{0,1}$[1] represents the probability of having $0, 1$ electrons filling the electrochemical level ε. Since $\mathcal{P}_1 + \mathcal{P}_0 = 1$, both variables are dependent $\mathcal{P} = \mathcal{P}_1 = 1 - \mathcal{P}_0$. Remember that the ratios depend on ε and the Fermi distributions, $\Gamma_{\text{in}} = \Gamma_L(\varepsilon)f_L(\varepsilon) + \Gamma_R(\varepsilon)f_R(\varepsilon)$, $\Gamma_{\text{out}} = \Gamma_L(\varepsilon)[1 - f_L(\varepsilon)] + \Gamma_R(\varepsilon)[1 - f_R(\varepsilon)]$.

In a macroscopic system, the energy exchanges are expressed in terms of well-defined *heat and work*, depending on the energy source. If the energy is injected into the system in a controlled way by an external agent, it is identified as work, meanwhile, if it is exchanged with a thermal environment, it is identified as heat. The main difference between macroscopic and microscopic dynamics is the presence of fluctuations: a microscopic device gives and receives energy through stochastic particle exchange and random environment interactions but, as I will do in the following, is it possible to recover the notion of (fluctuating) heat and work considering only the microstates.

In the case of the SET, the easiest way to do this is from the latter master equation, containing all the information we need, and the definition of the device energy. The instantaneous SET energy is

$$H(\varepsilon, \mathcal{P}) = \varepsilon\mathcal{P}. \tag{4.2}$$

The dot has no energy when the occupation is zero, and gains ε once an electron fills it. Taking the time derivative, we obtain two terms,

$$\frac{dH}{dt} = \frac{d\varepsilon}{dt}\mathcal{P} + \varepsilon\frac{d\mathcal{P}}{dt}. \tag{4.3}$$

The first term only appears if the electrochemical level ε depends on time. This happens, for example, when the gate voltage V_G is driven following a certain protocol. In this sense, this term represents a controlled energy extraction, identified as thermodynamic work,

$$\dot{W} = \frac{d\varepsilon}{dt}\mathcal{P}. \tag{4.4}$$

The second contribution depends on the electron exchange with the electrodes. To evaluate this term, let's write it as

$$\varepsilon\frac{d\mathcal{P}}{dt} = (\varepsilon - \mu_L + \mu_L)\frac{d\mathcal{P}^L}{dt} + (\varepsilon - \mu_R + \mu_R)\frac{d\mathcal{P}^R}{dt}, \tag{4.5}$$

where

$$I^b \equiv \frac{d\mathcal{P}^b}{dt} = \Gamma^b_{\text{in}}(1 - \mathcal{P}) - \Gamma^b_{\text{out}}\mathcal{P} \tag{4.6}$$

are the electron current flowing from the L, R electrodes. Then, the chemical work created by the bias voltage is[2]

$$\dot{W}_{ch} = \mu_L I^L + \mu_R I^R. \tag{4.7}$$

[1]The N electrons filling the device impose a constant force on the CNT, shifting their equilibrium position. However, it is impossible to measure this shift in the experiment.

[2]This definition looks artificial, but it will be justified with the derivation of the second law.

In the steady state, $d\mathcal{P}/dt = 0$, therefore $I^L = -I^R$, and the chemical work is proportional to the bias voltage $\dot{W}_{ch} = q_e V_S I^L$.

The rest of the energy flow represents the heat provided by the electrodes

$$\dot{Q} = \dot{Q}_L + \dot{Q}_R = (\varepsilon - \mu_L) I^L + (\varepsilon - \mu_R) I^R. \tag{4.8}$$

If the total energy is conserved, one can take $dH/dt = 0$, from where the *first law of thermodynamics* follows trivially

$$\dot{W} + \dot{W}_{ch} + \dot{Q}_L + \dot{Q}_R = 0. \tag{4.9}$$

In order to derive a second law of thermodynamics, one must consider the Shannon entropy of the device,

$$S(\mathcal{P}) = -\sum_{p=0,1} \mathcal{P}_p \ln \mathcal{P}_p, \tag{4.10}$$

and measured in nats (here ln is the natural logarithm). This is a quantity coming from Information theory, and quantifying the uncertainty of a certain probability distribution; the main property related to thermodynamics consists in the fact that, if the system is in equilibrium, the Shannon entropy reduces to the Gibbs entropy. To derive the second law one takes the time derivative, and using the master equation again,

$$\frac{dS}{dt} = -\left(I^L + I^R\right) \ln\left(\frac{\mathcal{P}}{1-\mathcal{P}}\right). \tag{4.11}$$

To recover the second law, one must use the property

$$\begin{aligned} -I^b \ln\left(\frac{\mathcal{P}}{1-\mathcal{P}}\right) - \beta_b \dot{Q}_b &= I^b \ln \frac{(1-\mathcal{P})\Gamma^b_{\text{in}}}{\mathcal{P}\Gamma^b_{\text{out}}} \\ &= \left(\Gamma^b_{\text{in}}(1-\mathcal{P}) - \Gamma^b_{\text{out}}\mathcal{P}\right) \ln \frac{(1-\mathcal{P})\Gamma^b_{\text{in}}}{\mathcal{P}\Gamma^b_{\text{out}}} \geq 0, \end{aligned} \tag{4.12}$$

with $b = L, R$. In the first step, I have used the local detailed balance condition Eq. (2.5)

$$\ln \frac{\Gamma^b_{\text{in}}}{\Gamma^b_{\text{out}}} = -\beta_b(\varepsilon - \mu_b), \tag{4.13}$$

with $\beta_{L,R}$ the electrodes inverse temperature. The inequality comes from the property $(a-b)\ln(a/b) \geq 0$ for positive reals a, b. Using this, one finally obtains the second law

$$\frac{dS}{dt} - \beta_L \dot{Q}_L - \beta_R \dot{Q}_R \geq 0. \tag{4.14}$$

The term dS/dt represents the entropy change of the SET, and $-\beta_b \dot{Q}_b$ is the entropy created by the electrons flowing into the electrodes.

4.1.1. Applications

The SET as a computer

Since the SET occupation states $p = 0, 1$ make a classical bit, one can use it to store and manipulate logical information, id est, the SET can be regarded as the smallest binary computer implementation. The occupation-bit state can be manipulated in a controlled way using the gate and bias voltages, driving the system out of equilibrium. However, according to Eq. (4.14), the information processing implemented in any protocol will require a certain amount of heat dissipation in the electrodes due to the current noise. This is, precisely, the Landauer principle exposed in the introduction (note that, in this interpretation, the Shannon entropy represents both the thermodynamic entropy of the system and the information entropy of the computer) from a philosophical point of view.

Let's initialize the SET state in a certain state $\mathcal{P}$ with a certain Shannon entropy. If one starts moving the gates and bias voltage following a certain desired *computing protocol*, the information stored in $\mathcal{P}$ changes. If we reduce $dS/dt < 0$ implies that we 'gain information' about our bit, but also that we dissipate heat $\beta_L \dot{Q}_L + \beta_R \dot{Q}_R < 0$. In the opposite case, any heat absorption from the electrodes $\beta_L \dot{Q}_L + \beta_R \dot{Q}_R > 0$ $dS/dt > 0$ requires an 'information loss' in the bit. This highlights the relationship between thermodynamics and logical operation in physical devices.

The main example of this kind of operation is the *Landauer's overwrite*; in this operation, one has one bit in a high entropy state, for example, a bit prepared in the maximal entropy state $\mathcal{P} = 1/2$, and operates to put it into a minimal entropy state, $\mathcal{P} = 0$. Along this operation, one gain one bit of information but, following Eq. (4.14) one must pay

$$-\beta \Delta Q \geq \ln 2, \tag{4.15}$$

where for simplicity $\beta = \beta_L = \beta_R$ and $\Delta Q < 0$ is the total heat dissipated dissipated in the electrodes.

Thermoelectricity

In this example, I will recover a typical case from classical thermodynamics. If one has $\beta_L \neq \beta_R$ and $\varepsilon = \text{cte.}$ (the gate is performing no work on the system) a positive bias voltage $q_e V_S = \mu_L - \mu_R > 0$ generates an electron current flowing from L to R, consuming work. However, If the temperature gradient is large enough, the conduction can be reversed due to electrothermal effects. The thermal current takes place because the Fermi distributions on the electrodes start to fill the higher energy levels, allowing electron conduction even in the Coulomb blockade. This situation is sketched in Fig.4.1 The thermodynamic analysis of this situation is straightforward. Since $\varepsilon = \text{cte.}$ the system achieves a non-equilibrium steady (NESS) state after a short transient; in this state we have $dS/dt = 0$ even if we have non-zero heat flows $\dot{Q}_b$. Also, from their definition, we observe that the heat flows are proportional to the electric current, $\dot{Q}_L = (\varepsilon - \mu_L) I^L$ and $\dot{Q}_L = -(\varepsilon - \mu_R) I^L$, something that does not happen if ε depends on time. The last is called *tight coupling*. Thermoelectric effects in this kind of device were studied in detail in [Turek and Matveev, 2002, Matveev and Andreev, 2002].

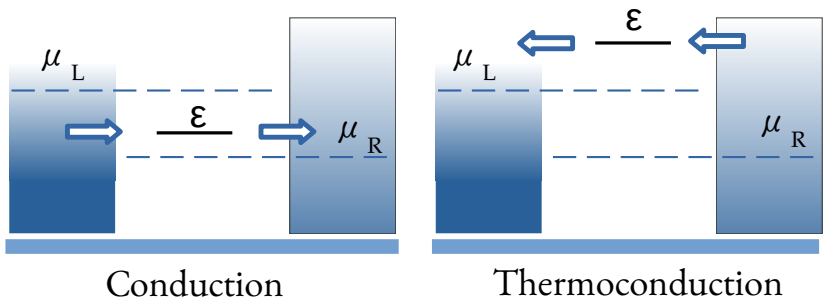

Figure 4.1.: Electron conduction when $\beta_L > \beta_R$ and $V_S > 0$. *Right*: if the electrochemical level is inside the bias window, the bias voltage generates a current from L to R. *Left*: opposite of that, if the level is above the bias window, the current is reversed due to the temperature gradient.

From the first and second laws of thermodynamics, $\dot{Q}_L + \dot{Q}_R + \dot{W}_{ch} = 0$, and one obtains the efficiency of the process

$$\eta = \frac{-\dot{W}_{ch}}{\dot{Q}_R} \leq \eta_C, \tag{4.16}$$

where $\eta_C = 1 - \beta_R/\beta_L$ is the Carnot efficiency.

Electron pumping

In the isothermal case, the electrons can be pumped against the bias voltage, by externally driving the electrochemical level up and down. The pumping protocol driving ε is sketched in Fig.4.2, and opposite to thermoelectricity, requires the asymmetry of the energy-dependent tunnel barriers to work. From the thermodynamic point of view, we are performing work on the system $\Delta W \geq 0$ and extracting energy in terms of chemical work $\Delta W_{ch} < 0$. Since the process is cyclic, the system entropy remains constant, $\Delta S = 0$, and the first law is

$$\Delta Q_L + \Delta Q_R + \Delta W_{ch} + \Delta W = 0, \tag{4.17}$$

combined with Eq. (4.14) gives us $|\Delta W_{ch}| \leq \Delta W$. A similar mechanism has been studied in [Sánchez and Büttiker, 2011, Mayrhofer et al., 2021] in the case where the SET is autonomously driven by a second external dot.

4.1.2. SET stochastic thermodynamics

Although the thermodynamic description explained above is useful to analyze the efficiency of certain processes, such as I did with computation, thermoelectricity, or electron

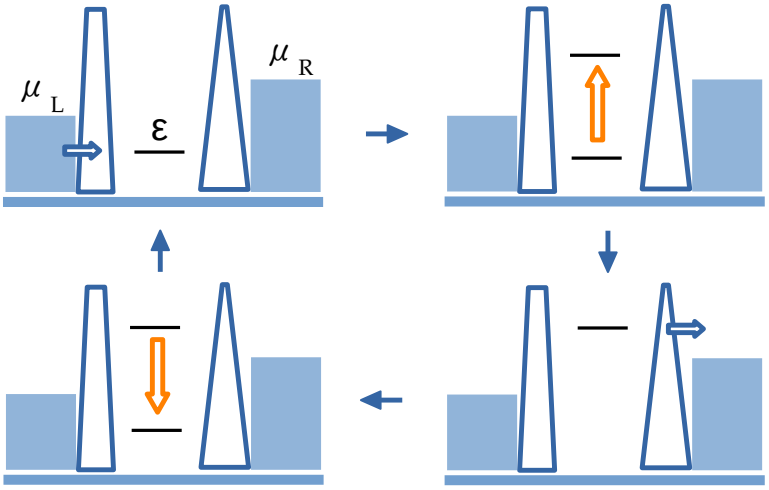

Figure 4.2.: Electron pumping cyclic protocol. The tunnel barriers are asymmetric; when the protocol starts (top, left) the dot fills from L since this barrier is thinner at this energy. The electrochemical level is pushed up (orange arrow, up, right) using the bias voltage and unfills onto R (bottom, right). The electrochemical level comes to its original position (orange arrow, bottom, left).

pumping, it provides little information about the effects of the fluctuations acting on the system. In fact, if we continuously observe the system state, the trajectory obtained [3] will be affected by fluctuations; *how can we extract information about thermodynamics from this single trajectory?*

Stochastic thermodynamics consists in redefine the thermodynamic quantities in terms of the microscopic details of the system, containing fluctuations, along a single trajectory. The usual thermodynamics are recovered by averaging over all the possible trajectories.

Let's define a single trajectory as the set $X = \{p_0, p_1, ...p_N\}$ of instantaneous occupations p followed by the SET. If the system is non-autonomous ε is a function of time, and the system receives work. The amount of work received in a time interval dt is $\eth W = d\varepsilon/dtp_t dt$, where p_t is the occupation in this time interval. The SET exchanges heat each time an electron fills/unfills the quantum dot; then, the heat exchanged with each electrode $b = L, R$ in the time interval is $\eth Q_b = (\varepsilon - \mu_b)dp^b$, where $dp^b = \pm 1$ each time an electron jumps in/out the quantum dot into the b electrode.

The previous definitions represent the "instantaneous" heat and work exchange; in fact, these definitions help us to describe the system if there are, for example, large fluctuations driving the system. To do the same with the entropy production, one can

[3] A trajectory is, for example, the series of 0 and 1 extracted by observing the SET occupation evolution.

define the *stochastic entropy* as

$$\mathcal{S}(p) = -\ln \mathcal{P}_p. \tag{4.18}$$

Note that, opposite to the Shannon entropy, this quantity depends on the instantaneous occupation p, in addition to the density function $\mathcal{P}$. In a single electron jump, $p \to p'$, the stochastic entropy changes

$$d\mathcal{S}(p) = [\mathcal{S}(p) - \mathcal{S}(p')]\, dt. \tag{4.19}$$

The total entropy exchanged by the trajectory X is

$$\Delta S[X] = \int_z d\mathcal{S}(p). \tag{4.20}$$

The point of this is that this quantity can be positive or negative. The second law is recovered by taking the average of the produced entropy along all the compatible trajectories X,

$$\Delta S = \int_X \mathcal{D}X \Delta S[X], \tag{4.21}$$

where the symbol $\mathcal{D}X$ represents the path integral in the trajectories space. This entropy production coincides with the average result (4.14).

The heat exchange in a single electron jump is given by the quantity

$$\eth Q^b = \pm(\varepsilon - \mu_b) dt, \tag{4.22}$$

where $b = L, R$ and the $\pm$ sign depends on the jump ($+$ if the electron fills the SET, $-$ if the electron leaves).

One can be interested in describing *how many times* a trajectory shows a negative entropy production. Imagine a trajectory starting at initial occupation p_0 with probability $\pi(p_0)$ and evolving $\{p_0, p_1, ..., p_N\}$. Its probability to appear is

$$\begin{aligned} \mathcal{P}[X] =& \pi(p_0)\mathcal{P}(0 \to 1)\mathcal{P}(0 \to 0)...\mathcal{P}(p_{N-1} \to p_N) \\ =& \pi(p_0) \prod_{p_i, p_j \in X} \mathcal{P}(p_i \to p_j). \end{aligned} \tag{4.23}$$

The transition probabilities $\mathcal{P}(p_i \to p_j)$ are proportional to the tunneling rates $\Gamma_{\text{in/out}}$, and therefore, they obey local detailed balance, $\mathcal{P}(0 \to 1)/\mathcal{P}(1 \to 0) = \exp[-\beta(\varepsilon - \mu_b)]$ with $b = L, R$.

Let us consider the *backward trajectory* $\bar{X}$ from the definition of X. This trajectory starts with p_N and runs over the same occupations of X but in the opposite sense, $\bar{X} = \{p_N, p_{N-1}, ..., p_0\}$ absorbing an entropy equal to $\Delta S[\bar{X}] = -\Delta S[X]$.

The probabilities of each trajectory are related by the equality

$$\begin{aligned} \ln \frac{\mathcal{P}[X]}{\mathcal{P}[\bar{X}]} =& \ln \frac{\pi(p_0)}{\pi(p_N)} + \sum_{p_i, p_j \in X} \ln \frac{\mathcal{P}(p_i \to p_j)}{\mathcal{P}(p_j \to p_i)} \\ =& \Delta S[X] - \beta \Delta Q[X]. \end{aligned} \tag{4.24}$$

Here, I assumed π to be the thermal equilibrium state. $\Delta S[X]$ represents the SET entropy exchange and ΔQ the total heat exchanged along the trajectory X. In the second step, I considered the local detailed balance of the transition probabilities. The last equality is known as *fluctuation theorem* [Seifert, 2005]. As one can see, the probability of observing a trajectory decreasing entropy decays exponentially with the total entropy production, decreasing for very long trajectories.

4.2. Thermodynamics of the single electron resonator

The thermodynamics of the single electron resonator follows straightforwardly from the SET thermodynamics. As in the previous case, one must consider the system energy, already expressed in Eq. (2.46),

$$H(z,v,p) = \frac{1}{2}mv^2 + \frac{1}{2}m\Omega^2 z^2 + \varepsilon(z)p, \tag{4.25}$$

with $\varepsilon(z) = \varepsilon_0 + gz$, and the master equation defining the system evolution, in this case, the complete Fokker-Planck equation, Eq. (2.48). From the joint density function, $\rho(z,v,p)$ one can evaluate the average energy of the system,

$$E \equiv \langle H \rangle = \sum_p \int dzdv\ H(z,v,p)\rho(z,v,p). \tag{4.26}$$

Taking their time derivative, and using Eq. (2.48) we obtain

$$\frac{dE}{dt} = -\gamma\langle v^2 \rangle + mD - \sum_p \int dzdv\ \varepsilon(z) p j_p. \tag{4.27}$$

The definition of heat and work follows straightforward. If we consider no time-dependent force acting on the resonator, all the energy exchanged with the CNT environment can be defined as heat

$$\dot{Q}_{zv} = mD - \gamma\langle v^2 \rangle. \tag{4.28}$$

This quantity is just the heat exchanged by an underdamped oscillator in a thermal environment [Sekimoto, 2010]. The first term represents the energy provided by the environmental thermal fluctuations, while the second term represents the friction losses. If the system is oscillating, for example, in self-oscillations, all the energy is dissipated in terms of friction, and $\dot{Q}_{zv} < 0$. However, in the absence of oscillations, and if the mechanics are overheated, one could observe a heat flow from the mechanics into the electrodes $\dot{Q}_{zv} > 0$. In thermal equilibrium, both contributions exactly compensate and one recovers a fluctuation-dissipation theorem $\langle v^2 \rangle = mD/\gamma$.

The last term in Eq. (4.27) is completely analogous with that appearing in the single electron transistor containing both the chemical work and the heat dissipated in the

electrodes. Following that example, I define chemical work as

$$\begin{aligned}\dot{W}^b_{\rm ch} &= \mu_b \int dzdv \left[\Gamma^b_{\rm in}\rho(z,v,0) - \Gamma^b_{\rm out}\rho(z,v,1)\right] \\ &\equiv \mu_b I_b,\end{aligned} \tag{4.29}$$

where the quantities I_b are the electron currents flowing from the $b = L, R$ electrode.

$$I_b = \sum_p \int dzdv\ \Gamma^b_{\rm in}(z)\rho(z,v,0) - \Gamma^b_{\rm out}\rho(z,v,1) \tag{4.30}$$

flowing from the $b = L, R$ electrode. If the system achieves a non-equilibrium steady state, $I_L = -I_R$, and the total chemical work is proportional to the total electron current flowing through the device, $\dot{W}_{\rm ch} = \dot{W}^L_{\rm ch} + \dot{W}^R_{\rm ch} = q_e V_S I_L$.

The heat dissipated in the electrodes is simply

$$\dot{Q}^b = \int dzdv(\varepsilon(z) - \mu_b)\left[\Gamma^b_{\rm in}\rho_0 - \Gamma^b_{\rm out}\rho_1\right]. \tag{4.31}$$

In the absence of other energy sources, one can take $dE/dt = 0$, recovering the first law of thermodynamics

$$\dot{Q}^L + \dot{Q}^R + \dot{W}^L_{\rm ch} + \dot{Q}_{zv} = 0. \tag{4.32}$$

Internal energy currents

In the previous chapter, I defined the quantity ΔE, Eq. (3.16), to predict the presence and amplitude of self-oscillations; this quantity represents the energetic balance in the oscillator between the friction loss and energy received from the electric transport. To conclude this section, I will describe the energy currents flowing through the device and related to heat and work exchange.

In order to do this, I consider separately the energies of the system and oscillator,

$$H_{zv}(z,v) = mv^2/2 + m\Omega^2 z^2/2, \tag{4.33}$$

$$H_p(p) = \varepsilon_0 p, \tag{4.34}$$

whose average values, $E_{zv} = \langle H_{zv}\rangle$ and $E_p = \langle H_p\rangle$, evolve following the Fokker-Planck equation, Eq. (2.48),

$$\frac{dE_{zv}}{dt} = -\gamma\langle v^2\rangle + mD - g\langle pv\rangle, \tag{4.35}$$

$$\frac{dE_p}{dt} = \varepsilon_0\left(I_L + I_R\right). \tag{4.36}$$

These equations can be written in terms of the previous definitions of heat and work,

$$\frac{dE_{zv}}{dt} = \dot{Q}_{zv} + e_{zv}, \tag{4.37}$$

$$\frac{dE_p}{dt} = \dot{Q}^{\rm L} + \dot{Q}^{\rm R} + e_p, \tag{4.38}$$

where the energy currents are

$$e_{zv} = -g\langle pv\rangle, \tag{4.39}$$

$$e_p = -g\int dxdv\ x\left[\Gamma^b_{0\to1}\rho(0) - \Gamma^b_{1\to0}\rho(1)\right] \tag{4.40}$$

representing the internal energy exchange between the electron transport and the oscillator. Note that

$$\frac{dE}{dt} = \frac{dE_{zv}}{dt} + e_{zv} + \frac{dE_p}{dt} + e_p. \tag{4.41}$$

In a steady state, all the exact time derivatives $dE/dt = dE_{zv}/dt = dE_p/dt = 0$ vanish, but not the energy currents, which only vanish in thermal equilibrium. From Eq. (4.41) one can prove that the internal energy currents are equal with opposite sign $e_{zv} = -e_p \equiv e$. From Eq. (4.38) we obtain

$$\dot{Q}_{zv} + e = 0, \tag{4.42}$$

$$\dot{W}_{\rm ch} + \dot{Q}^{\rm L} + \dot{Q}^{\rm R} - e = 0. \tag{4.43}$$

One can recover the usual (global) expression of the first law, Eq. (4.32) by taking the sum of the last two. Observe that the first line is, precisely, the condition $\Delta E = 0$ from where I obtained the amplitude of self-oscillations in the last chapter.

4.2.1. System entropy and Information flows

The Shannon entropy of the joint probability density function $\rho(z, v, p)$ is

$$S(t) = -\sum_p \int dzdv\ \rho(z, v, p)\ln\rho(z, v, p). \tag{4.44}$$

This quantity can be identified as the thermodynamic entropy of the whole device, from which one can derive the second law. However, one could be interested in describing the local entropy productions, this is how the mechanics and the transport produce entropy in contact with their own thermal baths. To give this detailed description, one can use the following property of the Shannon entropy,

$$S = I(zv : p) - S_{zv} - S_p. \tag{4.45}$$

The last two terms appearing on the right-hand side are, precisely, the local entropy production on the oscillator, S_{zv}, and on the quantum dot S_p. They are defined as the Shannon entropy of the marginal distributions $\rho_p = \int dzdv\rho(z, v, p)$ and $\rho_{zv} = \sum_p \rho(z, v, p)$,

$$\begin{aligned} S_{zv} &= -\sum_p \int dzdv\ \rho(z, v, p)\ln\rho_{zv}, \\ S_p &= -\sum_p \int dzdv\ \rho(z, v, p)\ln\rho_p. \end{aligned} \tag{4.46}$$

An observer with partial access to the system would not be able to evaluate the total entropy, but the local ones.

The quantity

$$I(zv:p)=\sum_p\int dzdv\ \rho(z,v,p)\ln\frac{\rho(z,v,p)}{\rho_p\rho_{zv}}. \tag{4.47}$$

is the mutual information shared between the oscillator degrees of freedom and the dot occupation. As the Shannon entropy, this magnitude comes from the Information theory, it is symmetric and positive, vanishing when the variables are statistically independent. Therefore, it represents the correlation between two random variables. In this case, the random variables compared by mutual information are the movement coordinates (vertical position and velocity can be regarded as a unique variable) and the occupation.

Given these definitions, I will proceed to derive the second law. Taking the time derivative of S one has

$$\frac{dS}{dt}=\frac{dS_{zv}}{dt}+\frac{dS_p}{dt}-i_{zv}-i_p. \tag{4.48}$$

The first two terms on the right-hand side are the local entropy productions. The last terms are the *information flows*, coming from the time derivative of the mutual information $dI/dt=i_{zv}+i_p$. Their explicit expression can be obtained from Eqs.(4.47) and (2.48),

$$\begin{aligned} i_{zv}&=\sum_p\int dzdv\ \left(j_x\frac{\partial}{\partial x}\ln\frac{\rho_{zv}}{\rho}+j_v\frac{\partial}{\partial v}\ln\frac{\rho_{zv}}{\rho}\right),\\ i_p&=-\sum_p\int dzdv\ j_p\ln\frac{\rho_p}{\rho}. \end{aligned} \tag{4.49}$$

Using these definitions, as well as Eqs.(4.28) and (4.31), after a calculation one obtains the two inequalities

$$\begin{aligned} \frac{dS_{zv}}{dt}-i_{zv}-\beta_{zv}\dot{Q}_{zv}\geq 0,\\ \frac{dS_p}{dt}-i_p-\beta_L\dot{Q}^L-\beta_R\dot{Q}^R\geq 0. \end{aligned} \tag{4.50}$$

As one can note, each inequality represents a second law of thermodynamics for each component of the global system, but they are related through the information flows. The usual form second law in terms of a single inequality can be recovered by summing the last and using Eq. (4.48)

$$\frac{dS}{dt}-\beta_{zv}\dot{Q}_{zv}-\beta_L\dot{Q}^L-\beta_R\dot{Q}^R\geq 0. \tag{4.51}$$

I will use the information flows in order to analyze different uses of the single electron resonator. However, there are some questions to address about how to interpret these results. First, notice that in a steady state, all the total derivatives vanish, $dS/dt=$

$dS_{zv}/dt = dS_p/dt = 0$; however, the information flows can be different from zero. From Eq. (4.48) one obtains that, in this case, they become equal and with different sign $i_{zv} = -i_p$. This recovers the notion of one subsystem acting on the other.

Second, the information flows are actually information. Even if I gave the mathematical expression of the information flow using mutual information, this is not a reason to identify them as physical information. In fact, information is something that is exchanged between an observer and a physical system, not between inanimate objects. Now, imagine a thermal device working under continuous measuring; if we use the result of these measures (which is actual physical information) to improve the working efficiency in a feedback process the entropy of the device changes in $\Delta S_{\text{measure}} = I(X : M)$, where $I(X : M)$ is the mutual information between the device state X and the measurement result M [Parrondo et al., 2015]. I conclude that mutual information is a good measure of physical information.

Third, the definitions I used in this chapter are completely equivalent to that I provide in the introduction for a general bipartite system $\mathcal{X}$ and $\mathcal{Y}$,

$$i_{\mathcal{X}} = \lim_{\tau \to 0} \frac{I(\mathcal{X}(t+\tau) : \mathcal{Y}(t)) - I(\mathcal{X}(t) : \mathcal{Y}(t))}{\tau}, \tag{4.52}$$

$$i_{\mathcal{Y}} = \lim_{\tau \to 0} \frac{I(\mathcal{X}(t) : \mathcal{Y}(t+\tau)) - I(\mathcal{X}(t) : \mathcal{Y}(t))}{\tau}. \tag{4.53}$$

According to these expressions, a positive flow $i_{\mathcal{X}} > 0$ means that $\mathcal{Y}(t)$ is more correlated with $\mathcal{X}(t+\tau)$ than with $\mathcal{X}(t)$, as if $\mathcal{Y}$ were gaining control on $\mathcal{X}$ [Allahverdyan et al., 2009].

4.2.2. Non-autonomous device

At the beginning of this chapter, I described the relation between thermodynamics and computing by considering a certain protocol (Landauer's overwrite) on the SET. In that case, I proved that the energy required to erase a certain amount of information was given by the change in the Shannon entropy. Now, I want to do the same with the single electron resonator, whose electron occupation $p = 0, 1$ can be used as a classical bit in a similar way. The main difference between the two implementations is how can we manipulate the occupation: in the SET, we change the gate voltage in order to modify the average occupation, but, in the resonator, one can do this using the oscillation. In this sense, the resonator is a minimal computer where both the memory and the computer state are noisy[4].

To manipulate the occupation-bit using the resonator, one can drive the CNT acting on it with a harmonic external force $f_f(t) = f_0 \cos(\Omega t)$, with f_0 a constant. This force can be applied, for example, by injecting a radio-frequency current pulse in the gate electrodes. This force drives the system out of equilibrium and prevents the system to

[4]This could seem artificial at first glance because we are used to thermo-stable macroscopic computers, but, for example in quantum computing, the noise is generated by the computer itself. One can also find important examples of this in biophysics, where the molecular systems responsible for sharing the information are at room temperature.

achieves a steady state. Instead of that, after a short transient the system achieves a time-dependent state $\rho(z, v, p)$ evolving cyclically with driving phase $\varphi = \Omega t \mod 2\pi$.

In Fig.4.3(top), I represent this evolution of the system with $\mu_L = \varepsilon_0$. As one can observe, the average position (red curve) approximately follows a harmonic oscillation. When the CNT ascends, the quantum dot is driven out of the bias window and the occupation falls to zero. Once the CNT descends, the dot enters the bias window again, recovering the average occupation $\langle p \rangle = 1/2$. I have considered energy-independent barriers in order to prevent self-oscillations; indeed, energy-dependent barriers could affect information exchange. The state of occupation and the oscillation are only correlated

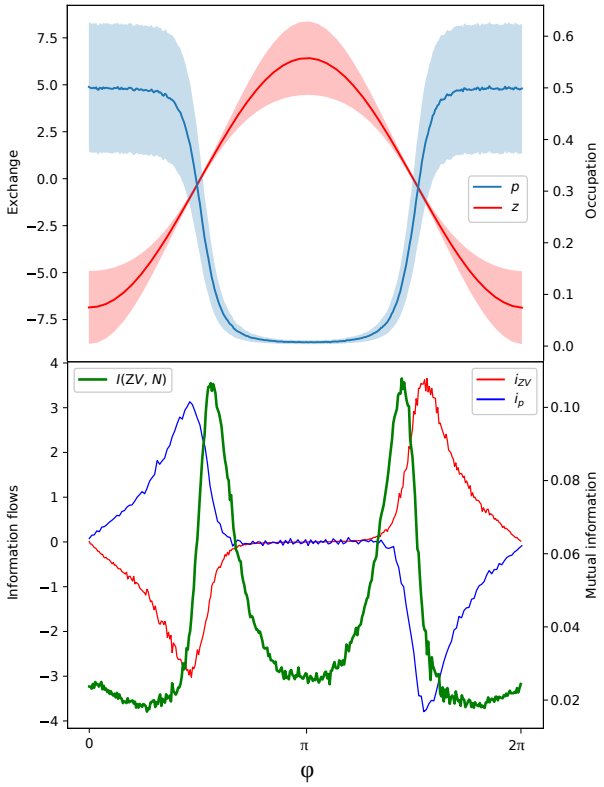

Figure 4.3.: Non-autonomous implementation of the device. *Up*: Average position (red) and occupation (blue) of the system along the oscillations in terms of the stroboscopic phase ϕ. *Down*: Mutual information (green) and information flows i_{zv} (red) and i_p (blue) along the oscillation. $\Omega/(2\pi) = 270$ MHz, $g = 0.01$ eV/nm, $m = 2 \times 10^{-22}$ kg, and $Q = 1000$. $\Delta\mu = 1$ eV and $\beta_L = \beta_R = \beta$ in terms of the force phase φ. I also consider homogeneous tunnel barriers, $\alpha_{\mathrm{L,R}} = 0$ and $\Gamma_{\mathrm{L,R}} = 100\Omega$. In this configuration, the dot switches between a state with average occupation $\langle p \rangle = 0.5$ and $\langle p \rangle = 0$ each time the oscillator moves through $x = 0$.

in these moments, giving place to two maxima of mutual information, Fig.4.3(bottom).

From the thermodynamic point of view, we can see this operation as the cyclic application of two different computation processes [Elouard et al., 2015]. First, form $\varphi = 0$ to $\varphi = \pi$, the CNT-computer changes the bit from a state with maximal entropy $S_p = \ln 2$ into a state with $S_p = 0$. This is, precisely, a Landauer's overwrite process. Integrating the second line of (4.50) on time along this process, one obtains

$$-\ln 2 - \Delta i_p - \beta(\Delta Q^L + \Delta Q^R) \geq 0. \tag{4.54}$$

The last result coincides with the usual formulation of Landauer's principle, also found in the SET, with a correction given by the total information exchange Δi_p.

In Fig.4.3(bottom) I represent both the mutual information and the information flows as a function of time; note that, since we are not in a steady state, the information flows are not equal with opposite signs. In this figure, we can observe that if the quantum dot is completely inside or outside the bias window, the occupation and position are completely uncorrelated, sharing no mutual information. The occupation and movement correlate when the quantum dot moves through the bias window border (at $z = 0$), creating a maximum in the mutual information at $\varphi = \pi/2$, where the rewrite is taking place. In this process, the information flow i_p is positive, and therefore $-\Delta i_p$ is negative. The consequence of this is that the total energy required to erase the bit, given Eq. (4.54) is *larger* than that obtained in the SET. In fact, one must invest more energy in computing using a noisy computer because one must erase not only the bit but also a part of the computer's state.

The second process takes place from $\varphi = 0$ to $\varphi = 3\pi/2$. Along this process, the oscillator recovers its original position, increasing the quantum dot entropy in $\ln 2$. Integrating again the second inequality of (4.56) along this process one obtains

$$\ln 2 - \Delta i_p - \beta(\Delta Q^L + \Delta Q^R) \geq 0. \tag{4.55}$$

Along this process, one can use this entropy generation to recover a part of the invested energy [Elouard et al., 2015], acting as a motor. In this case, as we $\Delta i_p \leq 0$ a part of the recovered information must be invested in recovering the correlation.

4.2.3. Autonomous systems

Since the oscillator environment represents an additional thermal bath, the single electron resonator can implement many more thermodynamic processes than the SET in the autonomous regime. To conclude my analysis of the device, I will do a systematic analysis of all the possible implementations and their relation with information exchange. In their free evolution, the system evolves until it reaches a steady state, vanishing all the exact derivatives in (4.50). This state is out of equilibrium as we impose a bias voltage $\Delta\mu$ or a thermal gradient between the electrodes and the ambient. The steady-state electron currents $I^{L,R}$ satisfy the charge conservation $I^L = -I^R$ and the energy currents within the device $e_{zv} = -e_p = e \neq 0$. Since $dI/dt = 0$ the mutual information takes a steady non-zero value and, $i_{zv} = -i_p = i$ and are constant values satisfying

$$\begin{aligned} -i - \beta_{zv}\dot{Q}_{zv} &\geq 0, \\ i - \beta_L \dot{Q}^L - \beta_R \dot{Q}^R &\geq 0. \end{aligned} \tag{4.56}$$

To express these inequalities in terms of measurable quantities, I restrict myself to the experimental condition $\beta_L = \beta_R = \beta$ (I ignore the thermocurrent cases, already explained in the SET). Under this condition, and using conservation of energy,

$$\begin{aligned} -i - \beta_{zv}\dot{Q}_{zv} &\geq 0, \\ i + \beta\dot{Q}_{zv} + \beta\Delta\mu J &\geq 0. \end{aligned} \tag{4.57}$$

Here $J = I^L - I^R$ is the total current flowing through the device, considered positive when flowing rightward, and $\Delta\mu = \mu_L - \mu_R$.

Let's start analyzing the case $\Delta\mu J > 0$. In this case, the bias voltage forces the electrons to flow from the L to R electrode, using this energy to exchange heat with the environment. In the case $\dot{Q}_{zv} < 0$, the system extracts energy from the electrodes in terms of chemical work and dissipates the energy into the oscillator environment, heating the mechanics, for example in the case of *self-oscillations*. The case $\dot{Q}_{zv} > 0$ implies that the mechanics are hotter than the electrodes, and therefore the system is *cooling the mechanics*. In both cases, all the entropy generation comes from the electron current: as one can see in the second line of Eqs.(4.57), this term provides the positive term ensuring that the second law is always satisfied.

The opposite case, $\Delta\mu J < 0$, requires charge pumping. This is, the device makes use of some mechanism to create an electric current against the bias voltage. The microscopic mechanism allowing this is the same explained in the SET and sketched in Fig.4.2 but, in this case, the quantum dot is autonomously driven by the mechanics. Note that in this regime we expect no self-oscillations, which only appear if $\Delta\mu J > 0$, and so, the pumping cycle takes place through the thermal fluctuations driving the CNT up and down. From the point of view of thermodynamics, the unique thermodynamic force feeding this pump is the thermal gradient between the electrodes and the environment, $\beta_{zv} \neq \beta$. By doing an electron pump, we are extracting chemical work.

If $\beta_{zv} < \beta$ the device absorbs heat from the environment, $\dot{Q}_{zv} > 0$, using this energy to generate the current and heat the electrodes. In this case, all the entropy production in Eqs.(4.57) comes from the term $\beta\dot{Q}_{zv} > 0$, as it could happen in macroscopic *thermocurrent*.

Opposite to this, the case with $\beta_{zv} < \beta$ and $\Delta\mu J < 0$ belongs exclusively to an *information engine*, this is, a device where the information takes a fundamental role in the operation. This happens because the only positive term in the second line of (4.57) is, precisely, the information flow

$$i \geq \beta|\dot{Q}_{zv} + \Delta\mu J| \geq 0. \tag{4.58}$$

In the next table, I summarize the conditions leading to each regime I remark that in any regime some information flow can be observed, and indeed this will be the common case. However, any regime can operate without information flow, except for the information engine. In the information engine, the CNT operates as a Maxwell demon performing measures in order to obtain chemical work.

$\dot{Q}_{zv}$	$\Delta\mu J$	Regime
> 0	> 0	*Cooling the mechanics*
> 0	< 0	*Thermocurrent*
< 0	< 0	*Information engine*
< 0	> 0	*Self-oscillations*

The information engine

I will study the operation of the resonator in the thermocurrent and the information engine regimes using numerical simulations. Apart from the already cited [Horowitz and Esposito, 2014], a very similar mechanism has attached a lot of attention during the last years in systems of two couple dots [Schaller et al., 2010, Sánchez et al., 2010, Sánchez and Büttiker, 2011, Rutten et al., 2009, Bulnes Cuetara et al., 2011, Mayrhofer et al., 2021]; in these works, the CNT is substituted by a second quantum dot, providing a similar thermodynamic approximation [Strasberg et al., 2013].

The left and right tunnel barriers are tuned to be asymmetric; for simplicity, we choose $\Gamma_L(\varepsilon) = \Gamma$ and $\Gamma_R(\varepsilon) = \Gamma e^{\alpha x}$. Γ and α are tunable parameters. In Fig.4.4 I plot the electron current flowing from L to R as function of Γ/Ω and T/T_{zv}, where $T = 1/\beta$ is the electrodes temperature and $T_{zv} = 1/\beta_{zv}$ the oscillator environment temperature. In this figure, consider no bias voltage.

In the region $T < T_{zv}$ the system works extracting heat from the environment $\dot{Q}_{zv} > 0$ and the pumps occur from L to R, $J > 0$. Therefore activating the bias $\Delta\mu < 0$ in this region one can generate the *thermocurrent* regime explained in the section above. The current maximizes when $\Gamma \sim \Omega$. In the region $T > T_{zv}$, the system takes energy from the

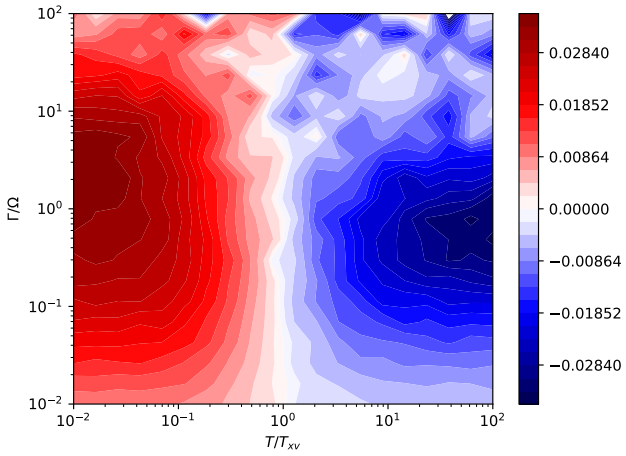

Figure 4.4.: Current flowing along the device at zero bias, $\Delta\mu = 0$ for different values of Γ/Ω and leads and oscillator temperatures ($T = 1/\beta$, $T_{zv} = 1/\beta_{zv}$) in electrons per cycle. $\Omega/(2\pi) = 270$ MHz, $g = 0.01$ eV/nm, $m = 2 \times 10^{-22}$ kg, and $Q = 1000$, $\Gamma_L = 400$ GHz, $\Gamma_R = 18$ GHz, $\alpha_R = 4$ nm^{-1}, and $\alpha_L = 0$

electrodes and dissipates heat into the environment, $\dot{Q}_{zv} < 0$, and the same pumping mechanism reverses the sign of current, $J < 0$. In this region, a positive bias voltage $\Delta\mu \gtrsim 0$ gives place to the expected *information-fuelled regime*. If $T = T_{zv}$, the system reaches thermal equilibrium and the current disappears.

As one can observe in the figure, the current is larger when $\Gamma \simeq \Omega$; at these points, the electron transport and the mechanics timescales are similar and the information becomes maximal. Indeed, for larger values of Γ the quantum dot occupation approaches the adiabatic approximation prediction Eq. (2.60) vanishing the information flows. For high values of Ω, the quantum dot remains in the same occupation state $p = 0, 1$ for several periods, avoiding again any correlations.

4.3. Information and fluctuations

A Maxwell's demon continuously measuring a fluctuating system will obtain a fluctuating amount of information from each measurement. In fact, in this chapter I have introduced the trajectory-dependent stochastic entropy, heat and work considering the SET, so one expects a similar trajectory-dependent *fluctuating information exchange*. To conclude this chapter, I will introduce the concept of fluctuating information exchange considering the single electron resonator as an example. This has been studied, for example, in feedback continuous systems [Maitland et al., 2015, Rosinberg and Horowitz, 2016] and discrete systems [Shiraishi and Sagawa, 2015] during the last decade on the basis of Sagawa and Ueda work [Sagawa and Ueda, 2010]. In the development of this thesis I have not been able to go too deeply into this theoretical approach as it has been hard to connect it directly with the experiment, so following should be understood as the motivation for future work.

I will start considering the total energy of the single-electron resonator, given by the Hamiltonian, $H(z, v, p) = mv^2/2 + kz^2/2 + \varepsilon_0 p + H_{int}(z, v, p)$. Inserting Eqs.(2.39) one obtains

$$dH(z, v, p) \doteq -\gamma v^2 dt + mv\sigma dB_t + DdB_t^2 + (\varepsilon_0 + g_0 x)dp. \tag{4.59}$$

The notation $\doteq$ indicates that we are defining the white noise dB_t in the Itô interpretation. $dp = dp^L(z, v, p) + dp^R(z, v, p)$ is the occupation increment in the time interval dt, this is $dp^{L(R)} = 1, -1$ if the dot fills/unfills from left (right). From the last result, one can define the stochastic heat and work as

$$\begin{aligned} \eth Q_{zv} &\doteq -\gamma v^2 dt + mDdB_t^2, \\ \eth Q^b &= (\varepsilon_0 + g_0 x - \mu^b)dp^b, \\ \eth W_{ch}^b &= \mu_b dp^b. \end{aligned} \tag{4.60}$$

As before, $b = L, R$. These quantities represent stochastic heat and work exchanges along a single trajectory, the average thermodynamic quantities are recovered just by averaging these quantities over trajectory realizations.

A single trajectory is defined by the set $X = \{(z, v, p)_t\}_{t=0}^{t_f}$ of values of position z, v and occupation p that the system takes along their time evolution, starting at $t = 0$ and

ending at $t = t_f$. Along this trajectory X, the total heat exchange is evaluated as the integral

$$Q[X] = \int_X \eth Q, \tag{4.61}$$

and analogous to any other thermodynamic quantity.

The entropy and the information exchanges are obtained from the probability density function $\rho(z, v, p)$. One can define stochastic entropy and information,

$$\begin{aligned} \mathcal{S} &= -\ln \rho(z, v, p), \\ \mathcal{I} &= \ln \frac{\rho(z, v, p)}{\rho_p(p)\rho_{zv}(z, v)}. \end{aligned} \tag{4.62}$$

Eq. (4.44) and Eq. (4.47) are the ensemble average of these quantities. The stochastic quantities depend on the instantaneous values of z, v and p, but also in the function $\rho(z, v, p)$. Again, the stochastic mutual information allows us to write

$$d\mathcal{S} = d\mathcal{S}_{zv} + d\mathcal{S}_p - \eth\mathcal{I}_{zv} - \eth\mathcal{I}_p. \tag{4.63}$$

As before, $d\mathcal{I} = \eth\mathcal{I}_{zv} + \eth\mathcal{I}_p$ define the information flows. In order to identify each term, we expand the entropy production $dS(z, v, p)$ using Ito calculus,

$$d\mathcal{S} \doteq \partial_x\mathcal{S}dz + \partial_v\mathcal{S}dv + \frac{1}{2}\partial_v^2\mathcal{S}dv^2 + \sum_{k=1} \frac{\mathcal{S}^{(k)}}{k!}dp^k. \tag{4.64}$$

The last term must be treated carefully [Wächtler et al., 2019] [5]. Before treating it directly, we can write the occupation change in terms of the Poissonian process $dP(p', p)$, this is $dp(z, v, p) = \sum_{p'}(p' - p)dP(p', p)$. The Poissonian takes the values $dP(0, 1) = 1$ and $dP(1, 0) = 1$ with probability $\Gamma_{\text{in/out}}dt$ respectively; in other words, it contributes only during the electron jumps. Notice that the Poissonian processes are idempotent, $[dP(p', p)]^k = dP(p', p)$, allowing us to compute

$$\sum_{k=1} \frac{\mathcal{S}^{(k)}(p)}{k!}dp^k = \sum_{p',k=1} \frac{\mathcal{S}^{(k)}(p)}{k!}(p' - p)^k dP(p', p)^k = \sum_{p'} \left[\mathcal{S}(p') - \mathcal{S}(p)\right] dP(p', p). \tag{4.65}$$

Here we used the short notation $\mathcal{S}(p) \equiv \mathcal{S}(z, v, p)$. With this, the stochastic thermodynamics of the system follows

$$d\mathcal{S} \doteq \partial_x\mathcal{S}dz + \partial_v\mathcal{S}dv + \frac{1}{2}\partial_v^2\mathcal{S}dv^2 + \sum_{p'} \ln \frac{\rho(z, v, p)}{\rho(z, v, p')}dP(p', p). \tag{4.66}$$

[5] Here the notation $f^{(k)}$ refers to the k-th derivate of the function f. The last term implies the complete expansion of the entropy function because the increments dp have a finite value, and therefore the series expansion will not converge.

Comparing this with the entropy generation of the marginal distributions $\rho_{zv}(z,v)$,$\rho_p(p)$ following

$$\begin{aligned} d\mathcal{S}_{zv} &\doteq \partial_x \mathcal{S}_{zv} dz + \partial_v \mathcal{S}_{zv} dv + \frac{1}{2}\partial_v^2 \mathcal{S}_{zv} dv^2, \\ d\mathcal{S}_p &= \sum_{p'} \ln \frac{\rho_p(p)}{\rho_p(p')} dP(p',p), \end{aligned} \tag{4.67}$$

I obtain

$$\begin{aligned} d\mathcal{I} \doteq \partial_x \ln \frac{\rho_{zv}}{\rho(z,v,p)} dz + \partial_v \ln \frac{\rho_{zv}}{\rho(z,v,p)} dv + \frac{1}{2}\partial_v^2 \ln \frac{\rho_{zv}}{\rho(z,v,p)} dv^2 \\ + \sum_{p'} \ln \frac{\rho(z,v,p)\rho_p(p')}{\rho(z,v,p')\rho_p(p)} dP(p',p). \end{aligned} \tag{4.68}$$

From where one can define trajectory-level information flows as

$$\eth\mathcal{I}_{zv} \doteq \partial_x \ln \frac{\rho_{zv}}{\rho(z,v,p)} dz + \partial_v \ln \frac{\rho_{zv}}{\rho(z,v,p)} dv + \frac{1}{2}\partial_v^2 \ln \frac{\rho_{zv}}{\rho(z,v,p)} dv^2 \tag{4.69}$$

and

$$\eth\mathcal{I}_p = \sum_{p'} \ln \frac{\rho(z,v,p)\rho_p(p')}{\rho(z,v,p')\rho_p(p)} dP(p',p). \tag{4.70}$$

Fluctuation theorem

This discussion is based on the work of Rosinberg and Horowitz [Rosinberg and Horowitz, 2016] After defining the stochastic quantities, I will motivate a fluctuation theorem. To do this, consider again the trajectory $X = \{(z,v,p)_t\}_{t=0}^{t_f}$. Now, imagine an experiment where one can just measure the instantaneous occupation p, gaining no information about the oscillator state. The observed trajectory in this case is $X_p = \{p_t\}_{t=0}^{t_f}$, with probability

$$\mathcal{P}[X_p] = \pi(z_0,v_0,p_0) \prod_{z_t,v_t,p_t \in X} \rho(z_t,v_t,p_t)\mathcal{P}(p_t \to p_{t+dt}|z_t,v_t). \tag{4.71}$$

Here, π is the initial distribution of the variables. To simplify, I will consider a single electrode exchanging electrons with the quantum dot; however the final result can be immediately generalized.

Let $\bar{X}$ denote the backward trajectory, this is, that trajectory starting at z_{t_f}, v_{t_f} and p_{t_f}, running over the same values of z,v,p in the opposite sense. The occupation trajectory follows

$$\mathcal{P}(\bar{X}_p) = \pi(z_{t_f},v_{t_f},p_{t_f}) \prod_{z_t,v_t,p_t \in \bar{X}} \rho(z_t,v_t,p_t)\mathcal{P}(p_t \leftarrow p_{t+dt}|z_t,v_t). \tag{4.72}$$

The probability of measuring the forward and backward trajectories follow

$$\ln \frac{\mathcal{P}(X_p)}{\mathcal{P}(\bar{X}_p)} = \ln \frac{\pi(z_0,v_0,p_0)}{z_{t_f},v_{t_f},p_{t_f}} + \sum_{z_t,v_t,p_t \in X} \ln \frac{\rho(z_t,v_t,p_t)\mathcal{P}(p_t \to p_{t+dt}|z_t,v_t)}{\rho(z_t,v_t,p_{t+dt})\mathcal{P}(p_t \leftarrow p_{t+dt}|z_t,v_t)}. \tag{4.73}$$

If the rates $\mathcal{P}(p_t \to p_{t+dt}|z_t, v_t)$ obey local detailed balance $\mathcal{P}(0 \to 1)/\mathcal{P}(0 \to 1) = \exp[-\beta(\varepsilon_0 + g_0 x - \mu)]$, using Eq. (4.70) one obtains[6]

$$\sum_{z_t, v_t, p_t \in X} \frac{\rho(z_t, v_t, p_t)\mathcal{P}(p_t \to p_{t+dt}|z_t, v_t)}{\rho(z_t, v_t, p_{t+dt})\mathcal{P}(p_t \leftarrow p_{t+dt}|z_t, v_t)} = \mathcal{I}_p[X] + \mathcal{S}_p[X] - \beta Q[X]. \tag{4.74}$$

Here $\mathcal{I}_p[X]$, $\mathcal{S}_p[X]$ and $Q[X]$ are the total information flow exchanged by the quantum dot, the total entropy generated in the quantum dot and the heat exchange with the leads. Finally, one obtains the fluctuation theorem

$$\frac{\mathcal{P}(X_p)}{\mathcal{P}(\bar{X}_p)} = e^{\Delta\mathcal{I}_p[X] + \Delta\mathcal{S}_p[X] - \beta\dot{\Delta}Q[X]}. \tag{4.75}$$

4.4. Discussion and conclusion

In this chapter, I have analyzed the thermodynamic aspects of the single electron resonator, identifying energy exchanges as thermodynamic heat and work. Subsequently, I derived the second law of thermodynamics, proving the positive production of Shannon entropy. By acknowledging the Shannon entropy as the non-equilibrium entropy, one can directly relate energy dissipation to information processing, thus recovering Landauer's principle. Stochastic thermodynamics eventually strays from macroscopic thermodynamics when dealing with complex systems. In fact, when I examined the bipartite nature of the single electron resonator, I realized that a comprehensive description of the system necessitates additional quantities, such as internal energy currents and information flows, that lack a macroscopic analogy.

Using information theory, I was able to classify the possible thermodynamic performances of the single electron resonator into one table including the *information engine*. Within this working regime, the CNT extracts chemical work, and unlike other operating regimes, information exchange is essential. Consequently, this phenomenon would never occur in a macroscopic system.

I also studied the autonomous performance of the device, in particular, I evaluated the ability of the device to implement Landauer's overwrite of one bit of information and proved that the thermodynamic efficiency of the protocol is reduced due to the information flow. The following step in this analysis can be similar to that in [Miller et al., 2020]; here the authors consider a quantum system (a qubit) under Landauer's overwrite protocol and determine the effects of quantum coherence on the heat and work distributions. They show that the quantum nature of the system implies long-tail distribution of these quantities due to extreme fluctuations. In our classical system, these extreme fluctuations could be promoted by the information flow.

[6] I am implicitly assuming that the process is Markovian, which is realistic when both the oscillator and the quantum dot are weakly coupled, and the action of the electrodes and environment is enough to destroy the system memory. However, a rigorous proof of this theorem requires a complete description of the fluctuating dynamics, and therefore I don't want to claim this result to be definitive.

I want to remark that if the system is at a very low temperature β diverges, and therefore one can not write the Clausus inequality Eq. (4.50). This limit becomes relevant if the thermal-mechanical dispersion as well as the thermal distribution of the electrodes become negligible with respect to the oscillator zero point motion. However, considering the Shannon entropy one can always derive an inequality. This is, precisely, what I did in Eq. (4.12) but, at zero temperature the balance Eq. (4.13) is not true, and one doesn't recover the second law in terms of thermodynamic heat. The physical interpretation of Eq. (4.12) requires to consider of the steady state of the dynamics [Esposito and Van den Broeck, 2010]. An option to do this consists of recovering Eq. (4.13) for a certain effective temperature due to the electric noise [Kewming and Shrapnel, 2022], but it has never been done in a bipartite system such as the single electron resonator.

Part III.

Quantum collisional thermostats

5. Quantum collisional reservoirs

In classical statistical physics of macroscopic systems, thermal reservoirs are represented by large collections of particles in thermal equilibrium, but quantum experiments require a much more sophisticated model of the environment. The CPTP quantum master equations I explained in the introduction of this thesis, in particular the secular Born-Markov approximation, are the most common tool to describe the interaction between the quantum system and the environment. However, in the derivation of these equations, one assumed certain restrictions, such as a weak coupling between the system and the environment or the secular approximation; these restrictions prevent the derivation of master equations in a lot of cases.

Collisional reservoirs based on repeated interactions, introduced in [Rau, 1963, Caves, 1986, Caves and Milburn, 1987] appear as an alternative reservoir model in these situations. The intuitive image of these models consists of the quantum system under study, named $\mathcal{S}$, embedded in a gas of quantum particles at a certain temperature. The gas particles are named *ancillae* and eventually collide with $\mathcal{S}$, exchanging energy with it. After several collisions, the system $\mathcal{S}$ equilibrates at bath temperature. In this chapter, I explain the basic mathematical models of collisions between the system and the ancillae and discuss how can these systems be applied to quantum thermodynamics. Remark that these models are useful to modelize both classical and quantum systems [Ehrich et al., 2020], as the Andersen thermostat in molecular dynamics [Hünenberger, 2005].

These models allow us to manipulate the strength of the coupling between the system and the environment, depending on how we model the individual collisions, and how frequent the collisions are. In a very dilute gas, the collisions take place one by one, and the system evolves freely most of the time. If the gas is dense, the system is continuously colliding with the ancillae, even with several of them at the same time. In the latter case, two different ancillae could get correlated, generating non-Markovian evolution out of equilibrium. In this work, I will always consider the dilute gas situation, preventing this kind of effect.

From the laboratory perspective these are very suitable models, for example, of the experiments bombarding a cavity with a beam of atoms coming from an oven in a thermal state [Rempe et al., 1990]. The interest in these experiments has increased in the last decade [Haroche and Raimond, 2006] given their ability to manipulate the intensity of the coupling and the bombarding rate [Camposeo et al., 2001]. Also, collisional models can explain the loss of quantum coherence in large molecules [Hackermüller et al., 2004, Hornberger et al., 2003, Hornberger and Sipe, 2003].

Most of the theoretical applications of collisional reservoirs are in the field of quantum thermodynamics. In [Strasberg et al., 2017], the authors evaluated the energy exchange between the quantum system and the collisional reservoir in terms of thermodynamic heat

and work, deriving the second law of thermodynamics. The non-equilibrium effects created by some collision models have been studied, for example, in [Rodrigues et al., 2019, Guarnieri et al., 2020]. These non-equilibrium effects prevent the collisional models from behaving as appropriate thermal reservoirs [Barra, 2015], and therefore, the models must be treated carefully. In recent works [Jacob et al., 2021, Ehrich et al., 2020], the authors study in detail the different models of single collisions, giving more realistic models recovering thermal behaviour, the *scattering models*. The following works [Tabanera-Bravo et al., 2023, Tabanera et al., 2022], which are part of this thesis, make use of that models to implement a well-behaved thermal collisional reservoir; in that papers, we also study the minimal conditions for a collisional system guaranteeing thermal behaviour.

The application of collisional models has gone beyond thermal reservoirs, applying to other types of quantum reservoirs [Manzano et al., 2022] or implementing non-markovian effects [Ciccarello et al., 2022].

In this chapter, I will introduce the main physics of collisional reservoir models and evaluate their suitability to represent thermal behaviour, presenting or avoiding non-equilibrium effects. The chapter comes as follows. In the first section 5.1, I explain how the single collisions affect the target quantum system $\mathcal{S}$. This effect is represented by a quantum map –the collision map $\mathbb{S}_{\mathcal{A}}$– acting on the system density matrix ρ. After this, I explain the effect of the continuous bombarding, represented by the repeated application of the collision map, and represent the whole process using a Poissonian master equation. In section 5.2 I present the interaction-time model: this is the most common model of single collisions. Within the interaction-time model, the collision map $\mathbb{S}_{\mathcal{A}}$ is obtained using unitary evolution. In 5.3 I present the more realistic scattering model, where the collision map is obtained by solving the complete scattering problem. Finally, in section 5.4 I explain the conditions required by any model to recover thermal behaviour, avoiding non-equilibrium effects.

At the end of the section 5.4 I include a discussion on how the repeated interaction and the scattering models can implement a thermal reservoir. The conclusion of this discussion is that the interaction-time model can only predict thermal behaviour under very restrictive conditions. The scattering model can be applied in more general situations.

5.1. Systems under continuous bombarding

In this section, I will study the dynamics of a target system under continuous bombarding with ancillae. Let be $\mathcal{S}$ our target quantum system; this is the system we want to manipulate. $\mathcal{S}$ is described by a density matrix ρ, and evolves under the action of the Hamiltonian $H_{\mathcal{S}}$. The set of auxiliary quantum systems forming the collisional reservoir, the *ancillae*, is denoted $\{\mathcal{A}_t\}$. Each ancilla evolves independently of the others under its own Hamiltonian $H_{\mathcal{A}}$ and is initialized in a certain state $\rho_{\mathcal{A}}$.

At random times, a single ancilla $\mathcal{A}_t$ collides with $\mathcal{S}$, interacting with it for a certain time t_{int}, and it is then traced out. The effect of every single collision is represented by a

quantum collision map $\mathbb{S}_{\mathcal{A}}$ acting the state of $\mathcal{S}$,

$$\rho \to \mathbb{S}_{\mathcal{A}}\rho. \tag{5.1}$$

This map will depend on how one models the collision. In the following sections, I will elaborate on the two most important collision models.

Between two consecutive interactions, the system $\mathcal{S}$ must wait a time τ_t until the next ancillae $\mathcal{A}_t$ arrives. This time is a random variable following a Poissonian distribution with rate Γ. For very high rates, the system is continuously interacting with ancillae, even with several of them at the same time. This could generate quantum correlations between the system $\mathcal{S}$ and the collisional environment. In the opposite case, for low values of Γ, the system rarely interacts with the environment, and the effect of consecutive collisions is completely uncorrelated. Only in the last case, the system evolution is completely Markovian.

During the random times τ_t, the system $\mathcal{S}$ evolves unitarily under its own free Hamiltonian $H_{\mathcal{S}}$. Therefore, the state of $\mathcal{S}$ after n collisions are described by its density matrix

$$\rho(t) = \langle \mathcal{U}(\tau_n)\mathbb{S}_{\mathcal{A}} \quad ... \quad \mathcal{U}(\tau_1)\mathbb{S}_{\mathcal{A}}\mathcal{U}(\tau_0)\mathbb{S}_{\mathcal{A}}\rho(0)\rangle\,. \tag{5.2}$$

Here, $\rho(0)$ represents the initial state of $\mathcal{S}$, and t is the total time. The super-operator $\mathcal{U}(\tau_t)\rho = e^{-iH_S\tau_t}\rho e^{iH_S\tau_t}$ represents the unitary evolution, and the notation $\langle\cdot\rangle$ denotes the average over realizations of Poissonian random times τ_t. A similar mechanism of repeated interaction interspersed with unitary evolution has been used to analyze quantum thermodynamic in large systems [Mejía-Monasterio et al., 2005].

5.1.1. Master equation

The collisional scheme is useful and intuitive to implement numerical simulations of quantum systems. From a more analytical perspective, one can describe the average evolution of ρ in Eq.(5.2) by deriving a master equation. To do this, I consider Poissonian distributed random times τ_t with a small rate Γ. In particular $1/\Gamma \gg t_{\text{int}}$, where t_{int} is the collision duration. As I mention before, this condition implies that the system $\mathcal{S}$ spends most of the time evolving free and that the collisions $\mathbb{S}_{\mathcal{A}}$ occur almost instantaneously; this approximation is in accordance with a variety of experiments [Haroche and Raimond, 2006], and prevents non-Markovian correlation between $\mathcal{S}$ and the reservoir (see section 1.2.1).

Dividing the evolution time t in N short time steps of duration Δt, $t = N\Delta t$, satisfying the condition $1/\Gamma \gg \Delta t \gg t_{\text{int}}$, in a time step Δt the system $\mathcal{S}$ evolves following

$$\rho \to \begin{cases} \mathcal{U}(\Delta t)\rho & \text{with prob. } 1-\Gamma\Delta t, \\ \mathbb{S}_{\mathcal{A}}\rho & \text{with prob. } \Gamma\Delta t. \end{cases} \tag{5.3}$$

Taking the average,

$$\rho(t+\Delta t) = (1-\Gamma\Delta t)\mathcal{U}(\Delta t)\rho(t) + \Gamma\Delta t\mathbb{S}_{\mathcal{A}}\rho(t). \tag{5.4}$$

One can expand the evolution operator up to first order in Δt, $e^{-iH_{\mathcal{S}}\Delta t} \sim \mathbb{I} - iH_{\mathcal{S}}\Delta t$ and take an infinitesimal Δt to obtain the *Poissonian master equation*

$$\dot{\rho} = -i\left[H, \rho\right] + \Gamma\left[\mathbb{S}_{\mathcal{A}} - \mathbb{I}\right]\rho, \tag{5.5}$$

where $\mathbb{I}$ is the identity super-operator $\mathbb{I}\rho = \rho$. In the following sections, I will use this equation in two tasks. First, I will derive a CPTP QME describing the interaction-time models. Doing this, I will reproduce a common technique in literature [Guarnieri et al., 2020]. After that, I use Eq.(5.5) to study analytically the steady state of systems under collisional evolution, defined by $\dot{\rho} = 0$.

5.2. The interaction-time model

The simplest model representing the collision $\mathbb{S}_{\mathcal{A}}$ is the interaction-time model based on unitary evolution. This model is common in the literature, see for example [Strasberg et al., 2017, Guarnieri et al., 2020, Barra, 2015]. Before the collision, an ancilla $\mathcal{A}_t$ is extracted from the reservoir in a certain initial state $\rho_{\mathcal{A}}$. This state will depend on the different applications of the collisional reservoir. In quantum thermodynamics, the collisional reservoir is in thermal equilibrium at temperature $1/\beta$, therefore, the ancilla is initialized in the canonical ensemble $\rho_{\mathcal{A}} = e^{-\beta H_{\mathcal{A}}}/\mathcal{Z}_{\mathcal{A}}$, with partition function $\mathcal{Z}_{\mathcal{A}} = \mathrm{Tr}_A\{e^{-\beta H_{\mathcal{A}}}\}$.

Then, $\mathcal{A}_t$ is put in contact with $\mathcal{S}$ during a short time t_{int}. During this time, the complete system $\mathcal{S} + \mathcal{A}_t$ evolves unitarily under the action of the total Hamiltonian

$$H_{\mathrm{tot}} = H_{\mathcal{S}} + H_{\mathcal{A}} + V, \tag{5.6}$$

where $H_{\mathcal{S}}$ and $H_{\mathcal{A}}$ the target system and ancilla free Hamiltonian respectively and V is the interaction. After that, the ancilla is traced out. The action of the collision on $\mathcal{S}$ is obtained from

$$\rho \to \mathbb{S}_{\mathcal{A}}\rho := \mathrm{Tr}_A\left\{e^{-iH_{\mathrm{tot}}t_{\mathrm{int}}}\left(\rho \otimes \rho_{\mathcal{A}}\right)e^{iH_{\mathrm{tot}}t_{\mathrm{int}}}\right\}. \tag{5.7}$$

Here the notation $\mathrm{Tr}_A\{\}$ denotes the partial trace on the ancilla.

CPTP quantum master equation

Using the interaction-time model, one can write Eq.(5.5) in the more familiar form of a CPTP QME by expanding the exponential operator in the map $\mathbb{S}_{\mathcal{A}}$, Eq.(5.7) up to second order [Guarnieri et al., 2020, Ciccarello et al., 2022],

$$e^{-iH_{\mathrm{tot}}t_{\mathrm{int}}} \sim \mathbb{I} - iH_{\mathrm{tot}}t_{\mathrm{int}} - H_{\mathrm{tot}}^2 t_{\mathrm{int}}^2/2. \tag{5.8}$$

With this [1] ,

$$\begin{aligned}\mathbb{S}_{\mathcal{A}}\rho = & \\ = \mathrm{Tr}_A\left\{\rho \otimes \rho_{\mathcal{A}} - i\left[H_{\mathrm{tot}}, \rho \otimes \rho_{\mathcal{A}}\right]t_{\mathrm{int}} + \left(H_{\mathrm{tot}}\rho \otimes \rho_{\mathcal{A}}H_{\mathrm{tot}} - \frac{1}{2}\left\{H_{\mathrm{tot}}^2, \rho \otimes \rho_{\mathcal{A}}\right\}\right)t_{\mathrm{int}}^2\right\},\end{aligned} \tag{5.9}$$

[1] In this expression, $\{a, b\}$ denotes the anticonmutator. This should be not confused with $\mathrm{Tr}\{a\}$, denoting the trace.

and inserting this expression in the master equation Eq.(5.5), one obtains

$$\dot{\rho} = -i\,[H, \rho] + \mathcal{D}_A[\rho], \tag{5.10}$$

with the diffusive term

$$\mathcal{D}_A[\rho] = \Gamma t_{\text{int}}^2 \text{Tr}_A \left\{ H_{\text{tot}} \rho \otimes \rho_{\mathcal{A}} H_{\text{tot}} - \frac{1}{2} \left\{ H_{\text{tot}}^2, \rho \right\} \right\}. \tag{5.11}$$

The diffusive term is proportional to Γt_{int}^2 which, in the studied regime, is extremely small. Since only the interaction Hamiltonian V can give arbitrarily strong contributions, only terms proportional to V^2 give a significant contribution in Eq.(5.11),

$$\mathcal{D}_A[\rho] = \Gamma t_{\text{int}}^2 \text{Tr}_A \left\{ V \rho \otimes \rho_{\mathcal{A}} V - \frac{1}{2} \left\{ V^2, \rho \otimes \rho_{\mathcal{A}} \right\} \right\}. \tag{5.12}$$

Similar to what I did in Eq.(1.33), it is always possible to split the interaction Hamiltonian in terms of Hermitian operators,

$$V = \sum_{ij} \mathfrak{S}_i \otimes \mathfrak{A}_j, \tag{5.13}$$

with $\mathfrak{S}_i$ and $\mathfrak{A}_j$ Hermitian operators acting on the system $\mathcal{S}$ and ancilla $\mathcal{A}_t$ respectively. With this the diffusive terms become

$$\mathcal{D}_A[\rho] = \Gamma t_{\text{int}}^2 \sum_{ij} \gamma_{i,j} \left(\mathfrak{S}_i \rho \mathfrak{S}_j^\dagger - \frac{1}{2} \left\{ \mathfrak{S}_i^\dagger \mathfrak{S}_j . \rho \right\} \right), \tag{5.14}$$

Only the correlation coefficients $\gamma_{ij} = \text{Tr}_A \left\{ \mathfrak{A}_i^\dagger \mathfrak{A}_j \rho_{\mathcal{A}} \right\}$ contain information about the initial state of the ancilla bath, and, as one can observe, can be designed in several ways from different choices of $\rho_{\mathcal{A}}$ depending on what collisional system we are modelling. The last result has the form of a CPTP quantum master equation, Eq.(1.32) and therefore, it guarantees Markovian CPTP physical evolution.

Observe that this equation is quite different from the Born-Markov CPTP QME Eq.(1.42), which is a strong model of open quantum systems. In particular, the Hermitian operators $\mathfrak{S}_i$ don't satisfy the jump operator properties Eqs.(1.39) in general. The non-equilibrium properties found in this kind of model [Guarnieri et al., 2020] come, precisely, from this fundamental difference. In the following section 5.4 I will continue this discussion in the particular example of thermal reservoirs.

5.3. The scattering model

The scattering model $\mathbb{S}$ is a more realistic model for the collision map [2]. In this model, each ancilla $\mathcal{A}_t$ is described by a kinetic degree of freedom x, and the total Hamiltonian

[2] In this chapter, I used $\mathbb{S}_{\mathcal{A}}$ to denote any kind of collisional map. In the following, I use $\mathbb{S}$ to distinguish the scattering map in particular.

describing the collision with $\mathcal{S}$ takes the form

$$H_{\text{tot}} = \frac{p^2}{2m} + H_{\mathcal{S}} + \chi_{[0,L]}(x)V. \tag{5.15}$$

Here, p is the linear momentum operator and m is the ancilla mass. Unlike the repeated-interaction model, the interaction Hamiltonian V acts exclusively on the target system $\mathcal{S}$; the index function $\chi_{[0,L]}(x)$ defines the region of interaction between the system and the ancilla, being 1 in the interval $[0, L]$ and 0 otherwise. As before, $H_{\mathcal{S}}$ is the system $\mathcal{S}$ Hamiltonian. We assume that the Hamiltonian, $H_{\mathcal{S}}$ has a discrete set of eigenenergies given by the equation $H_{\mathcal{S}} |s_j\rangle = e_j |s_j\rangle$. Similarly, it is useful to define the basis $(H_{\mathcal{S}} + V) |s'_j\rangle = e'_j |s'_j\rangle$.

The complete system evolves unitarily until $\mathcal{A}_t$ crosses the interaction interval $[0, L]$. After that, it is traced out. Since the time required for the ancilla to cross the interval, the main difference between this and the interaction-time model is the absence of a well-defined interaction time t_{int}.

5.3.1. The scattering map

In this section, I derive the explicit expression of the scattering map $\mathbb{S}$ after a cumbersome calculation. Before proceeding, it is convenient to write the map by components in the particular eigenbasis of $H_{\mathcal{S}}$,

$$\rho_{ij} \quad \to \quad \rho'_{i'j'} = \sum_{ij} \mathbb{S}^{ij}_{i'j'} \rho_{ij}. \tag{5.16}$$

Here $\rho = \sum_{ij} \rho_{ij} |s_i\rangle \langle s_j|$ is the density matrix of $\mathcal{S}$. The map is defined at arbitrary times t by tracing the ancilla after unitary evolution with H_{tot},

$$\mathbb{S}^{ij}_{i'j'}(t) = \langle s_{i'}| \operatorname{tr}_X \left\{ U(t) \left(|s_i\rangle \langle s_j| \otimes \rho_{\mathcal{A}} \right) U^\dagger(t) \right\} |s_{j'}\rangle . \tag{5.17}$$

Here $U = \exp(-iH_{\text{tot}}t)$ is the unitary evolution operator and $\rho_{\mathcal{A}}$ represents the ancilla initial state.

In order to evaluate the scattering map, one needs to compute the eigenstates of H_{tot}. These states are known as scattering states

$$H_{\text{tot}} |\Psi_i(k)\rangle = E_i(k) |\Psi_i(k)\rangle . \tag{5.18}$$

Since the scattering states represent a composed state of $\mathcal{S}$ and $\mathcal{A}_t$, they are characterized by two quantities representing the initial conditions: the index i representing the initial state of $\mathcal{S}$ before the collision, and the initial linear momentum k of the ancilla. The total energy associated with them is

$$E_i(k) = e_i + \frac{k^2}{2m}. \tag{5.19}$$

Note that this initial energy is conserved through the collision. In position representation, the scattering states are written as [3]

$$|\psi_i(k,x)\rangle = \begin{cases} \sum_j \left(\alpha_{ji}e^{ik_{ji}x} + \beta_{ji}e^{-ik_{ji}x}\right)|s_j\rangle & x<0, \\ \sum_j \left(\alpha'_{ji}e^{ik'_{ji}x} + \beta'_{ji}e^{-ik'_{ji}x}\right)|s'_j\rangle & x\in[0,L], \\ \sum_j \left(\alpha''_{ji}e^{ik_{ji}x} + \beta''_{ji}e^{-ik_{ji}x}\right)|s_j\rangle & x>L. \end{cases} \tag{5.20}$$

Since this represents the system initialized in the state $|s_i\rangle$ and the initial linear momentum k, I take $\alpha_{ji}=\delta_{i,i}$ and $\beta''_{ji}=0$. The constants k_{ji} are calculated from the energy associated with the state,

$$E_i(k) = e_j + \frac{k_{ji}^2}{2m} = e'_j + \frac{k_{ji}'^2}{2m} = e_i + \frac{k^2}{2m} \tag{5.21}$$

for all j. The last equalities define the relations

$$k_{ji}(k) = \sqrt{2m\left(\frac{k^2}{2m} + e_i - e_j\right)}. \tag{5.22}$$

The complex amplitudes $\beta_{ji}, \alpha'_{ji}, \beta'_{ji}$ and α''_{ji} are determined by the four continuity conditions

$$\begin{aligned} |\psi_i(k,0^-)\rangle &= |\psi_i(k,0^+)\rangle\,, \\ |\psi_i(k,L^-)\rangle &= |\psi_i(k,L^+)\rangle\,, \\ \partial_x|\psi_i(k,0^-)\rangle &= \partial_x|\psi_i(k,0^+)\rangle\,, \\ \partial_x|\psi_i(k,L^-)\rangle &= \partial_x|\psi_i(k,L^+)\rangle\,. \end{aligned} \tag{5.23}$$

In a certain eigenbasis, these conditions represent a system of equations for the coefficients that can be numerically solved. In the next chapter, I will explain an approximated method to evaluate them.

The initial state of the system, $|i\rangle\langle j|\otimes\rho_{\mathcal{A}}$, can be decomposed in terms of the scattering states,

$$|s_i\rangle\langle s_j|\otimes\rho_{\mathcal{A}} = \int dkdk'\rho_{\mathcal{A}}(k,k')\,|\Psi_i(k)\rangle\langle\Psi_j(k')|\,, \tag{5.24}$$

immediately obtaining their unitary evolution

$$U(t)\left(|i\rangle\langle j|\otimes\rho_{\mathcal{A}}\right)U^\dagger(t) = \int dkdk'\rho_{\mathcal{A}}(k,k')e^{-iE_i(k)t}\,|\Psi_i(k)\rangle\langle\Psi_j(k')|\,e^{iE_j(k')t}. \tag{5.25}$$

Using the position representation Eq.(5.20), one can trace out the ancilla obtaining

$$\begin{aligned} &\mathrm{Tr}_A\left\{U(t)\left(|i\rangle\langle j|\otimes\rho_{\mathcal{A}}\right)U^\dagger(t)\right\} = \\ &= \int dxdkdk'\rho_{\mathcal{A}}(k,k')e^{-iE_i(k)t}\,|\psi_i(k,x)\rangle\langle\psi_i(k',x)|\,e^{iE_j(k')t}. \end{aligned} \tag{5.26}$$

[3] Remember that in this expression, k is the initial momentum and x is a coordinate.

Finally, inserting this result in Eq.(5.17),

$$\begin{aligned}\mathbb{S}^{ij}_{i'j'} &= \langle i'| \operatorname{Tr}_A \left\{U(t) \left(\rho_{\mathcal{A}} \otimes |i\rangle \langle j|\right) U^\dagger(t)\right\} |j'\rangle = \\ &= \int dx dk dk' \rho_{\mathcal{A}}(k,k') t_{i'i}(k) t^*_{j'j}(k') e^{-i(E_i(k)-E_j(k'))t} e^{-i(k_{j'j}(k')-k_{i'i}(k))x}.\end{aligned} \tag{5.27}$$

The coefficients $t_{i'i}(k) \equiv \alpha''_{i'i}$ are called transition amplitudes. In the last term, one can recognize the Dirac delta property

$$\int dx e^{-i[k_{j'j}(k)-k_{i'i}(k')]x} = 2\pi\delta[k_{i'i}(k) - k_{i'i}(k')]. \tag{5.28}$$

In Appendix A.2.1 we use properties of Dirac delta to prove the identity

$$\delta[k_{j'j}(k') - k_{i'i}(k)] = \frac{k_{i'i}(k)\delta(k'-\kappa)}{\kappa}, \tag{5.29}$$

with

$$\kappa(k) = \sqrt{k^2 + 2m(e_i - e_j + e_{j'} - e_{i'})}. \tag{5.30}$$

Using this identity the scattering map is finally determined

$$\mathbb{S}^{ij}_{i'j'}(t) = \int dk \rho_{\mathcal{A}}(k,\kappa) \frac{k_{ji}(k)}{\kappa} t_{i'i}(k) t^*_{j'j}(\kappa) e^{-i[E_i(k)-E_j(\kappa)]t}. \tag{5.31}$$

The last exponential, including the time dependence, can be simplified using the identity

$$E_i(k) - E_j(\kappa) = e_{i'} - e_{j'}, \tag{5.32}$$

from which we get

$$e^{-i(E_i(k)-E_j(\kappa))t} = e^{-i(e_{i'}-e_{j'})t}, \tag{5.33}$$

which does not depend on the momentum. This is, precisely, the free unitary evolution of the system $\mathcal{S}$ between two consecutive collisions. Since this evolution has been already introduced Eq.(5.2) using the superoperators $\mathcal{U}$, one can omit this term. The map representing the collision between $\mathcal{S}$ and $\mathcal{A}_t$ in Eq.(5.31) is simply

$$\mathbb{S}^{ij}_{i'j'} = \int dk \rho_{\mathcal{A}}(k,\kappa) \frac{k_{ji}(k)}{\kappa} t_{i'i}(k) t^*_{j'j}(\kappa). \tag{5.34}$$

This map doesn't depend on time[4], only on the transition amplitudes and the initial state of $\mathcal{A}_t$.

Let me remark that the scattering map preserves the initial energy during the collision, as one can see from Eq.(5.21). From a physical point of view, this happens because the ancilla is initialized out of the interaction region $[0, L]$, and it is traced out once it is far from there. Since asymptotically far from $[0, L]$ the scattering states Eq.(5.20) are both eigenstates of $H_{\mathcal{S}} + H_{\mathcal{A}}$ and $H_{\mathcal{S}}$, no energy can be exchanged by the interaction V in that regions.

[4]In this development, I have defined the transition coefficients as $t_{i'i}(k) \equiv \alpha''_{i'i}$. Doing this, I assumed that the ancilla $\mathcal{A}_t$ crosses the region $[0, L]$ almost instantaneously; the last is true in our studied regime, where the system $\mathcal{S}$ spent the most part of time evolving free, and the collisions are almost instantaneous. In a regime where the ancilla spent a lot of time within the interaction region, one can not directly extract the Dirac delta, preserving the time dependence during the collision.

5.4. Thermodynamics of collisional reservoirs

Until now, I have explored the general properties of collisional reservoirs. In this section, I apply this theory to thermal systems. In quantum thermodynamics, the collisional reservoirs are used to model thermal reservoirs in some cases where, for example, the strong interaction between the quantum system and the environment prevents the derivation of a Born-Markov CPTP QME, or where the microscopic nature of the environment is unknown.

If the collisional reservoir acts as a thermal reservoir, any target system $\mathcal{S}$ in contact with it will exchange energy until achieving the thermal equilibrium, defined by the canonical ensemble

$$\pi_{\mathcal{S}} = \frac{e^{-\beta H_{\mathcal{S}}}}{\mathcal{Z}}, \tag{5.35}$$

where $\mathcal{Z} = \mathrm{Tr}\left\{e^{-\beta H_{\mathcal{S}}}\right\}$ is the system partition function, and β is the inverse temperature of the thermal reservoir. This process is known as *thermalization*. According to that, the master equation Eq.(5.5) governing the collisional process must satisfy

$$-i[H, \pi_{\mathcal{S}}] + \Gamma[\mathbb{S}_{\mathcal{A}} - \mathbb{I}]\pi_{\mathcal{S}} = 0. \tag{5.36}$$

Since the canonical ensemble $\pi_{\mathcal{S}}$ is diagonal in the eigenbasis of $H_{\mathcal{S}}$, the first term is always zero,

$$[H_{\mathcal{S}}, \pi_{\mathcal{S}}] = 0, \tag{5.37}$$

and the collisional reservoir satisfies that $\pi_{\mathcal{S}}$ is a fixed point of the collisional map [Tabanera-Bravo et al., 2023]

$$\mathbb{S}\pi_{\mathcal{S}} = \pi_{\mathcal{S}}. \tag{5.38}$$

If the collisional reservoir is not thermal, the last equation is not satisfied, and the system achieves a non-diagonal ($[H_{\mathcal{S}}, \rho] \neq 0$) non-equilibrium ($\mathbb{S}_{\mathcal{A}}\pi_{\mathcal{S}} \neq \pi_{\mathcal{S}}$) steady state.

5.4.1. Conditions for thermalization

The last condition, Eq.(5.38) is sufficient to ensure that a collisional reservoir is working as a genuine thermal reservoir. However, in order to understand why is this true and the suitability of each model, it is instructive to split it into two more intuitive statements, one for the diagonal elements, and one for the quantum coherence (non-diagonal elements).

1. **Local detailed balance**. In the eigenbasis of $H_{\mathcal{S}}$ and in the absence of coherence terms, the diagonal elements evolve following a Markov chain,

$$\rho_{ii} \to \sum_j \mathbb{S}_{ii}^{jj} \rho_{jj}. \tag{5.39}$$

The canonical ensemble Eq.(5.35) is a fixed point of the map if it satisfies

$$\mathbb{S}_{ii}^{jj} = e^{-\beta \Delta_{ij}} \mathbb{S}_{jj}^{ii} \tag{5.40}$$

for any values of i, j. Here $\Delta_{ij} = e_i - e_j$, with e_i, e_j two different eigenenergies of $H_{\mathcal{S}}$.

2. **Absence of coherence**. The collisional map generates no coherence terms from a diagonal density matrix. This means,

$$\mathbb{S}^{ii}_{i'j'} = 0 \tag{5.41}$$

for $i' \neq j'$. In a few words, this means that non-diagonal elements can not appear from a diagonal state.

The first condition can be checked in several energy-preserving systems. The reason for this is that the ubiquitous unitary evolution follows *microreversivility* property. Suppose a system and ancilla discrete spectrum $H_{\mathcal{S}} |e_i\rangle = e_i |e_i\rangle$ and $H_{\mathcal{A}} |a_i\rangle = a_i |a_i\rangle$, microreversibility means that the probability $\mathcal{P}$ of a given transition between two quantum states, $|e_i, a_i\rangle$ and $|e_j, a_j\rangle$, is symmetric under time reversal in a single collision [5],

$$\mathcal{P}(e_i, a_i \to e_j, a_j) = \mathcal{P}(e_i, a_i \leftarrow e_j, a_j) \tag{5.42}$$

with $e_i + a_i = e_j + a_j$. The main example is unitary evolution,

$$\mathcal{P}(e_i, a_i \to e_j, a_j) = |\langle e_j, a_j| e^{-iH_{\rm tot} t_{\rm int}} |e_i, a_i\rangle|^2. \tag{5.43}$$

Using the microreversibility property, it is easy to prove that

$$\begin{aligned} \mathcal{P}(e_i \to e_j) &= \sum_{a_i, a_j} \mathcal{P}(e_i, a_i \to e_j, a_j)\mathcal{P}(a_i) = \\ &= \sum_{a_i, a_j} \mathcal{P}(e_j, a_j \to e_i, a_i)\mathcal{P}(a_j)\frac{\mathcal{P}(a_i)}{\mathcal{P}(a_j)}. \end{aligned} \tag{5.44}$$

Assuming the ancilla in thermal equilibrium at inverse temperature β,

$$\mathcal{P}(a_i)/\mathcal{P}(a_j) = e^{-\beta \Delta_{ji}}, \tag{5.45}$$

as well as energy conservation $e_i + a_i = e_j + a_j$, one immediately obtains local detailed balance for transitions in the target system $\mathcal{S}$,

$$\mathcal{P}(e_i \to e_j) = e^{-\beta \Delta_{ji}} \mathcal{P}(e_j \to e_i), \tag{5.46}$$

equivalent to Eq.(5.40).

[5] In quantum mechanics, time reversal operations are implemented by the anti-unitary operator $\mathcal{T}$ acting on the system Hilbert space. Any anti-unitary operator can be written $\mathcal{T} = C\mathcal{U}$, where C is the conjugation of coordinates and $\mathcal{U}$ is a unitary operator. $\mathcal{T}$ depends on the physical nature of the system, for example, since angular momentum is an odd magnitude under time reversal, a spin 1/2 system inverts all the spin components under the action of $\mathcal{T}$, id est, $\mathcal{T}\sigma_i\mathcal{T}^\dagger = -\sigma_i$, being σ_i the Pauli matrices [Sachs, 1987]. If the system is a wave function in momentum representation, the action of $\mathcal{T}$ reverses the momentum sign, formally $\mathcal{T}\phi(p) = \phi(-p)$ [Taylor, 2006]. Microreversibility is obtained in those systems where the total Hamiltonian commutes with the total time reversal operator $\mathcal{T}_{\mathcal{S}} \otimes \mathcal{T}_{\mathcal{A}}$, $[H_{\rm tot}, \mathcal{T}_{\mathcal{S}} \otimes \mathcal{T}_{\mathcal{A}}] = 0$. In those cases, one recovers Eq.(5.42)[Jacob et al., 2021, Tabanera et al., 2022].

5.4.2. Discussion

What is the relationship between the interaction-time and scattering models with thermalization conditions? A naive image of the collisional models can lead one to think that both models are suitable in order to obtain genuine thermal behaviour because the ancilla is initialized in a thermal state $\rho_{\mathcal{A}}$, but this is not true. In fact, the interaction-time model is not autonomous and is therefore susceptible to performing work on the system, breaking the equilibrium state. The scattering model is energy-preserving, but may create quantum correlations. In the two following remarks, I elaborate on the pros and cons of these models.

First remark. Let's start discussing the thermal behaviour of the interaction-time model. The main point of this discussion will be that any collisional reservoir based on this model will fail in most cases because it does not conserve energy and generate quantum correlations.

From the point of view of quantum master equations, the thermalization process of the system $\mathcal{S}$ is described by the CPTP quantum master equations with diffusive term Eq.(5.14). If the Hermitian operators $\mathfrak{S}_i$ within this term satisfy the conditions Eqs.(1.39), the diffusive term $\mathcal{D}_A$ generates quantum jumps between different eigenstates of $H_{\mathcal{S}}$, creating no quantum coherence (the density matrix remains diagonal). This satisfies the second thermalization condition, Eq.(5.41).

In addition, the jump rates are given by the coefficients γ_{ij} in $\mathcal{D}_A$. If the ancilla $\mathcal{A}_t$ is in a thermal equilibrium state, the coefficients obey

$$\gamma_{ij}(-\omega) = \gamma_{ji}(\omega)e^{-\beta\omega}. \tag{5.47}$$

Here, ω represents the energy exchange between the ancilla $\mathcal{A}_t$ and $\mathcal{S}$ in a single collision. In conclusion, Eq.(5.2) obeys local detailed balance, and the conditions for thermalization are satisfied.

If conditions Eqs.(1.39) are not met, the Hermitian operators $\mathfrak{S}_i$ may create a quantum jump from an eigenvalue of $H_{\mathcal{S}}$ into an arbitrary linear combination of them, creating quantum coherence. The diffusive term, Eq.(5.14) generates non-diagonal terms in the system density matrix, preventing thermalization.

From the thermodynamics perspective, the explanation is much simpler [Barra, 2015]. In fact, the interaction-time thermostat is not an autonomous system because each time an ancilla interacts with the system $\mathcal{S}$, the interaction Hamiltonian V in Eq.(5.7) must be switched on and off. This time dependence in the total Hamiltonian performs energy in the form of thermodynamic work on the system, preventing thermalization. According to the definition Eq.(1.53), the work performed in a single collision is (see also ref.[Guarnieri et al., 2020])

$$W_{\text{coll}} = \text{Tr}\left\{\left(e^{iH_{\text{tot}}t_{\text{int}}}Ve^{-iH_{\text{tot}}t_{\text{int}}} - V\right)(\rho\otimes\rho_{\mathcal{A}})\right\}. \tag{5.48}$$

In order to recover thermalization in the target system $\mathcal{S}$, one can impose the condition

$$[H_{\mathcal{S}} + H_{\mathcal{A}}, V] = 0, \tag{5.49}$$

which vanishes the performed work W_{coll}. Then, the total energy is conserved and one recovers the local detailed balance.

As a conclusion of this point, I observed in two ways, one from dynamics and one from thermodynamics, that a collisional reservoir based on repeated interactions Eq.(5.7) can behave as a thermal reservoir only under a certain choice of the interaction Hamiltonian V. This is a major limitation in terms of applications, as it restricts us to a limited number of models.

Second remark. I continue by studying the thermodynamics of the scattering model derived in the last section. As we will see, this model guarantees thermal behaviour under more general conditions than the repeated interaction thermostat.

To start with the analysis, I remark that opposite to the repeated interactions model, the scattering evolution Eq.(5.34) conserves the total initial energy. As I explained, the physical reason for this is that each ancilla is initialized far from the interaction interval $[0, L]$, and it is traced once it crosses it. Then, switching on and off the Hamiltonian V injects no energy into the system. A second observation is that the scattering evolution obeys microreversibility

$$\mathcal{P}(e_i, k \to e_j, k') = \mathcal{P}(e_j, k' \to e_i, k), \tag{5.50}$$

where e_i is the state of $\mathcal{S}$ and k is the linear momentum of the ancilla $\mathcal{A}_t$. This fact comes from the unitary evolution in the definition Eq.(5.17)[6].

In the following, it will be useful to denote the probability in terms of the total energy $E = k^2/2m + e_i$, $\mathcal{P}(e_i, k \to e_j, k') = \mathcal{P}_{ji}(E)$. With this, the microreversibility property is written as $\mathcal{P}_{ji}(E) = \mathcal{P}_{ij}(E)$.

Since the system obeys microreversibility and conserves energy, we can recover local detailed balance by averaging the ancilla degree of freedom

$$\begin{aligned}
\mathcal{P}(e_i \to e_j) &= \int \mu(k_i) \mathcal{P}_{ji} \left(\frac{k_i^2}{2m} + e_i \right) dk_i \\
&= \int \mu\left(k_i\left[E\right]\right) \mathcal{P}_{ji}\left(E\right) \frac{dk_i}{dE} dE \\
&= \int \mu\left(k_i\left[k_j\right]\right) \mathcal{P}_{ij} \left(\frac{k_j^2}{2m} + e_i \right) \frac{dk_i}{dk_j} dk_j.
\end{aligned} \tag{5.51}$$

To perform this calculation, from the energy $k_i^2/2m + e_i = k_j^2/2m + e_j$, one can prove $dk_i/dk_j = k_j/k_i$.The initial linear momentum of the ancillae comes from a distribution $\mu(k)$. In order to obtain detailed balance $\mathcal{P}(e_i \to e_j) = e^{-\beta \Delta_{ij}} \mathcal{P}(e_j \to e_i)$, the distribution of moments must follow

$$\frac{\mu\left(k_i\left[k_j\right]\right)}{k_i} = e^{-\beta \Delta_{ij}} \frac{\mu(k_j)}{k_j}. \tag{5.52}$$

Interestingly, this is not the Gibbs distribution $e^{-\beta k_i}/\mathcal{Z}$, but the *effusion distribution*

$$\mu(k) \propto k e^{-\beta \frac{k^2}{2m}}. \tag{5.53}$$

[6]In this thesis, I will always assume invariant Hamiltonians under time reversal, see footnote 5.

Therefore, this system needs no work injection preventing thermalization, and the system is able to reach equilibrium in general cases even in $[H_{\mathcal{S}} + H_{\mathcal{A}}, V] \neq 0$.

However, the scattering map is able to create quantum coherence, breaking the second condition for thermalization. We can observe this from the expression of the terms $\mathbb{S}^{ii}_{i'j'}$ with $i' \neq j'$: these terms creates non-diagonal elements from a diagonal state,

$$\mathbb{S}^{ii}_{i'j'} = \int dk \rho_{\mathcal{A}}(k, \kappa) \frac{k}{\kappa} t_{i'i}(k) t^*_{j'i}(\kappa) \neq 0. \tag{5.54}$$

In order to prevent these coherences to be created, one has two options. First, one can recover the restrictive condition $[H_{\mathcal{S}} + H_{\mathcal{A}}, V] = 0$ again. The other option consists in design a suitable ancillae initial state $\rho_{\mathcal{A}}$ satisfying $\rho_{\mathcal{A}}(k, \kappa) \sim \delta(k - \kappa)$.

In conclusion of this point, the scattering map satisfies local detailed balance due to energy preservation and microreversibility, becoming a good candidate to implement thermal collisional reservoirs. However, in some circumstances, this map creates spurious quantum coherences.

5.5. Conclusion

In this chapter, I present the main aspects of collisional reservoir models, discussing their relationships with quantum thermodynamics. I prove that the usual interaction-time model fails to predict thermal behaviour since switching on and off the interaction potential between the system and the ancillae performs thermodynamic work, preventing thermalization. Then, I propose the scattering map as a more realistic model for collisions. In the second section of this chapter, I derive the explicit form of the scattering map and prove that it can be used to obtain genuine thermal behaviour. In the last part of the first section, I give the minimal conditions required for a system to thermalize.

6. Quantum thermostats implementation

In the previous chapter, I studied the basic physical properties of collisional reservoirs and I give the minimal conditions required by a collisional reservoir in order to recover thermal behaviour. In this chapter, I will be concerned about the particular implementation of collisional reservoirs satisfying those conditions. Such an implementation is named a *thermostat*. To do this, I will start studying how can the random Poissonian bombarding remove the –unavoidable– quantum coherence created by the collisional maps; in particular, I will prove that the quantum coherence is damped by the random bombarding at a low bombarding rate. Provided with this result, I build the *Poissonian thermostat* using the scattering model. The results of this section are extracted from [Tabanera-Bravo et al., 2023].

I will continue by demonstrating a useful property of the scattering reservoirs: as we will see, if the ancillae are very localized in the momentum space (they are narrow wave packets in the momentum space) the scattering map is not allowed to create quantum coherence and, therefore, the system thermalizes for arbitrary bombarding rates. Using this result, I will implement the *wave packet thermostat* published in [Tabanera et al., 2022].

The outline of the chapter is as follows. In section 6.1 I derive the transmission amplitudes expression using the transfer matrix method: this is a useful approximation, simplifying our calculations at high reservoir temperatures. In 6.2 I study the relationship between the Poissonian bombarding and the quantum coherence introduced by the scattering map, proving that the coherence is damp at low bombarding rates Γ. Using this, I will test the Poissonian thermostat using numerical simulations. In the last section 6.3 I show that the ancillae localized in the momentum space are not allowed to create quantum coherence and implement the wave packet thermostat in numerical simulations.

6.1. The transfer matrix method

Before presenting the thermostat implementation, I introduce an approximation useful to evaluate the transmission amplitudes, the *transfer matrix method*. As I show in the last chapter, these amplitudes t_{ji} in the scattering map $\mathbb{S}$, Eq. (5.34), are introduced in the scattering states eqs.(5.20). In order to evaluate them, one must impose the continuity conditions Eq. (5.23) and solve all the coefficients $\beta_{ji}, \alpha'_{ji}, \beta'_{ji}$ and α''_{ji}. The coefficients $\alpha_{ji} = \delta_{j,i}$ and $\beta''_{ji} = 0$ were determined by the initial conditions. However, this procedure becomes cumbersome when the Hilbert space of $\mathcal{S}$ is larger and larger. In the appendices,

I included a section with more details about this method.

The four continuity equations, eqs.(5.23) governing the transmission amplitudes can be expanded as

$$\begin{aligned}\sum_j (\delta_{ij} + \beta_{ij}) |s_j\rangle &= \sum_j \left(\alpha'_{ij} + \beta'_{ij}\right) |s'_j\rangle \,, \\ \sum_j (k_{ij}\delta_{ij} - k_{ij}\beta_{ij}) |s_j\rangle &= \sum_j \left(k'_{ij}\alpha'_{ij} - k'_{ij}\beta'_{ij}\right) |s'_j\rangle \,,\end{aligned} \tag{6.1}$$

at $x = 0$ and

$$\begin{aligned}\sum_j \left(\alpha'_{ij} e^{ik'_{ij}L} + \beta'_{ij} e^{-ik'_{ij}L}\right) |s'_j\rangle &= \sum_j \alpha''_{ij} e^{ik_{ij}L} |s_j\rangle \,, \\ \sum_j \left(k'_{ij}\alpha'_{ij} e^{ik'_{ij}L} - k'_{ij}\beta'_{ij} e^{-ik'_{ij}L}\right) |s'_j\rangle &= \sum_j k_{ij}\alpha''_{ij} e^{ik_{ij}L} |s_j\rangle \,.\end{aligned} \tag{6.2}$$

at $x = L$. A useful way to manipulate it defining the *wave vector operators*,

$$\mathbb{K}_0(E) = \sqrt{2m(E - H)}, \tag{6.3}$$

$$\mathbb{K}(E) = \sqrt{2m(E - H - V)}. \tag{6.4}$$

Here $E(e_i, k) = k^2/2m + e_i$ is the incident energy. As one can see, the eigenvalues of these operators are nothing but the momentum appearing in scattering states, Eq. (5.20), defined in Eq. (5.22). In terms of these operators, the last conditions are

$$\begin{aligned}|a\rangle + |b\rangle &= |a'\rangle + |b'\rangle \,, \\ \mathbb{K}_0 \left(|a\rangle - |b\rangle\right) &= \mathbb{K} \left(|a'\rangle - |b'\rangle\right)\end{aligned} \tag{6.5}$$

and

$$\begin{aligned}e^{i\mathbb{K}L} |a'\rangle + e^{-i\mathbb{K}L} |b'\rangle &= e^{i\mathbb{K}_0 L} |a''\rangle \,, \\ \mathbb{K} \left(e^{i\mathbb{K}L} |a'\rangle - e^{-i\mathbb{K}L} |b'\rangle\right) &= \mathbb{K}_0 e^{i\mathbb{K}_0 L} |a''\rangle \,.\end{aligned} \tag{6.6}$$

At high temperatures, the kinetic energy of the particles is higher than the level spacing of the system, and we can make the approximation $\mathbb{K}^{-1}\mathbb{K}_0 \sim \mathbb{I}$ to obtain the approximation

$$t_{ij}(k) \equiv \alpha_{ij} = \begin{cases} \langle e_j | \, e^{-i\mathbb{K}_0 L} e^{i\mathbb{K}L} \, |e_i\rangle & E > e_{\max}, \\ 0 & E \leq e_{\max}. \end{cases} \tag{6.7}$$

This result is derived in the appendix in the appendix Ap.A. Eq. (6.7) is known as *wave vector operator approximation.* Here $e_{\max}$ is the largest eigenvalue between $H_{\mathcal{S}}$ and $H_{\mathcal{S}} + V$. [1]

[1] In the previous chapter, I introduced the system Hamiltonian $H_{\mathcal{S}}$ acting on the target system $\mathcal{S}$, with eigenenergies e_i and eigenstates $|e_i\rangle$. V is the interaction Hamiltonian between the system and the ancilla, and k was the ancillae initial linear momentum.

The minimum energy $e_{\max}$ is introduced to avoid transitions through "closed channels". A closed channel occurs when the energy of the ancilla is too low: as a result of this, some coefficients k_{ij} in Eq. (5.20) become complex, damping the quantum transport. Then, the ancillae bounce, leaving the system $\mathcal{S}$ unchanged.

The main property of this approximation is that it preserves microreversibility. In fact,

$$\mathcal{P}_{ij}(E) \equiv |t_{ij}(k)|^2 = \mathcal{P}_{ji}(E), \tag{6.8}$$

where $\mathcal{P}_{ij}(E)$ is the probability of the transition $e_j, k \to e_i, k'$ at constant energy $E = k^2/2m + e_j$. Remember that the microreversibility property recovers local detailed balance if the system conserves the total energy.

For even higher temperatures, $E \gg H_{\mathcal{S}}, V$, we arrive at an even simpler expression. In these conditions, one can expand the operator $\mathbb{K}$ up to the first order

$$\mathbb{K}(E) \simeq \sqrt{2mE} - \sqrt{\frac{m}{2E}}(H + V), \tag{6.9}$$

and insert this into Eq. (6.7), obtains

$$t_{i'i} \simeq \langle e_{i'}| \, e^{-i\tau_i(k)(H+V)} \, |e_i\rangle \, . \tag{6.10}$$

Here,

$$\tau_i(k) = \begin{cases} \dfrac{L}{\sqrt{2E/m}} & E > e_{max}, \\ 0 & E \leq e_{\max} \end{cases} \tag{6.11}$$

plays the role of an effective energy-dependent interaction time. Interestingly, it is the time required by a classical particle with velocity k/m to pass completely through the interaction region $[0, L]$. We call the latter the *time of flight*. Again, this interaction preserves microreversibility.

6.2. The Poissonian thermostat

I will now introduced the Poissonian thermostat. As I introduce in the previous chapter, under Poissonian bombarding the quantum system $\mathcal{S}$ evolves following the master equation Eq. (5.5); in this case, the collisional map will be given by the scattering map Eq. (5.34). The scattering map guarantees that the collisions obey local detailed balance, even if they could create quantum coherence. As I will immediately prove, this quantum coherence is suppressed by the Possonian bombarding.

6.2.1. Thermalization under Poissonian bombarding

The evolution of the system $\mathcal{S}$ follows the master equation, Eq. (5.5). After a short transient, this system achieves an equilibrium state defined by the algebraic equation

$$\dot{\rho} = -i[\rho, H_{\mathcal{S}}] + \Gamma[\mathbb{S} - \mathbb{I}]\rho = 0, \tag{6.12}$$

where $\mathbb{S}$ is the scattering map, Γ the Poissonian bombarding rate and $H_{\mathcal{S}}$ the system Hamiltonian. If the scattering map generates no coherence, the steady state is represented by a diagonal matrix in the eigenbasis of $H_{\mathcal{S}}$, and each term in the last equation vanishes independently, $[\rho, H_{\mathcal{S}}] = [\mathbb{S} - \mathbb{I}]\rho = 0$; this situation is independent of the bombarding rate Γ.

In the other case, if $\mathbb{S}$ creates quantum coherence, none of the terms are zero and the density matrix is non-diagonal. Opposite to the previous situation, the non-diagonal terms in the steady state depend on Γ, decreasing for low Poissonian rates. This suggests that quantum coherence can be avoided by reducing the frequency of collisions.

In order to prove this, one can expand the solution of Eq. (5.2) in a polynomial series on Γ,

$$\rho = \rho^0 + \Gamma\rho^1 + \Gamma^2\rho^2 + ... \tag{6.13}$$

Here, each term ρ^n represents the nth term of the series. Inserting it in the Poissonian master equation Eq. (5.2) and taking $\dot{\rho} = 0$ one obtains

$$-i\left[H_{\mathcal{S}}, \rho^0\right] - i\Gamma\left[H_{\mathcal{S}}, \rho^1\right] + \Gamma\left[\mathbb{S} - \mathbb{I}\right]\rho^0 + \Gamma^2\left[\mathbb{S} - \mathbb{I}\right]\rho^1 + ... = 0. \tag{6.14}$$

For small Γ respect to the eigenfrequencies of $H_{\mathcal{S}}$, each power in the equation is zero independently,

$$\begin{aligned} -i\left[H_{\mathcal{S}}, \rho^0\right] &= 0, \\ -i\left[H_{\mathcal{S}}, \rho^1\right] + \left[\mathbb{S} - \mathbb{I}\right]\rho^0 &= 0, \\ -i\left[H_{\mathcal{S}}, \rho^2\right] + \left[\mathbb{S} - \mathbb{I}\right]\rho^1 &= 0... \end{aligned} \tag{6.15}$$

In the eigenbasis of the system Hamiltonian, $H_{\mathcal{S}}\left|e_i\right\rangle = e_i\left|e_i\right\rangle$, the last equations take the form

$$\begin{aligned} -i\Delta_{ij}\rho^0_{ij} &= 0, \\ -i\Delta_{ij}\rho^1_{ij} + \sum_{kl}\left[\mathbb{S} - \mathbb{I}\right]^{kl}_{ij}\rho^0_{kl} &= 0, \\ -i\Delta_{ij}\rho^2_{ij} + \sum_{kl}\left[\mathbb{S} - \mathbb{I}\right]^{kl}_{ij}\rho^1_{kl} &= 0... \end{aligned} \tag{6.16}$$

Here $\Delta_{ij} = e_i - e_j$ represents the eigenfrequencies of the Hamiltonian $H_{\mathcal{S}}$. If $\mathcal{S}$ does not degenerate, we can deduce from the first one that ρ^0 is diagonal. From the second one, one obtains

$$\sum_{jj}\mathbb{S}^{jj}_{ii}\rho^0_{jj} = \rho^0_{ii}. \tag{6.17}$$

This means that the diagonal elements of the density matrix are the fixed points of a Markov chain obtained from the scattering map. Since the scattering map obeys detailed balance (see later chapter), this means that ρ^0 is precisely, the thermal equilibrium state $\rho^0 = \pi_{\mathcal{S}}$.

The non-diagonal terms of the density matrix are dominated by ρ^1. From the previous equations, with $i \neq j$,

$$\rho^1_{ij} = -\frac{i}{\Delta_{ij}}\sum_{kl}\left[\mathbb{S} - \mathbb{I}\right]^{kl}_{ij}\rho^0_{kl}. \tag{6.18}$$

As one can observe, the coherences decay with Γ, vanishing when the system bombarding is very slow. However, if the system degenerates $\Delta_{ij} = 0$ for some energy levels, and Eq. (6.18) diverges, generating unavoidable coherent quantum effects, preventing thermalization.

6.2.2. An example

I will now test the Poissonian thermostat using numerical simulations of a particular example. The quantum system $\mathcal{S}$ will be represented by a single qubit

$$H_{\mathcal{S}} = \frac{\Delta}{2}\sigma_z, \tag{6.19}$$

where Δ is the qubit energy gap and σ_z is the Pauli matrix. This Hamiltonian has two non-degenerated eigenstates: the excited state $|e\rangle$ and the ground state, $|g\rangle$ respectively. The ancilla Hamiltonian is, as in the previous chapter $H_{\mathcal{A}} = p^2/2m$, where p is the kinetic momentum and m is the mass. The interaction Hamiltonian between the two is

$$\chi_{[0,L]}(x)V, \tag{6.20}$$

with χ the indicator function, L the length of the interaction region, x is the position operator and $V = \lambda(\sigma_y + \sigma_x)$ acts on $\mathcal{S}$. λ represents the intensity of the coupling and $\sigma_{x,y}$ are also Pauli matrices.

Under the ancillae bombarding, the system $\mathcal{S}$ evolves following Eq. (5.2), where the collision map is evaluated using the scattering model Eq. (5.34),

$$\rho(t) = \langle \mathcal{U}(\tau_N)\mathbb{S} \quad ... \quad \mathcal{U}(\tau_1)\mathbb{S}\mathcal{U}(\tau_0)\mathbb{S}\rho(0)\rangle\,. \tag{6.21}$$

As before, the unitary evolution times τ_t are Poissonian distributed random variables with rate Γ; Eq. (5.5) is also valid for scattering $\mathbb{S}$.

In [Tabanera-Bravo et al., 2023] we initialized the ancillae in a mixed Gaussian state localized around the position $x_0 \ll 0$ with dispersion Δx. In order to recover local detailed balance, the initial momentum is distributed according to the effusion distribution Eq. (5.53). This initial state ρ_A can be defined using the Wigner function [Jacob et al., 2022]

$$W(k,x) = \frac{\mu(k)}{\sqrt{2\pi\Delta x^2}} e^{-(x-x_0)^2/(2\Delta x^2)} \tag{6.22}$$

where $\mu(k)$ is the effusion distribution. [2]

[2] As I mention in the previous chapter, for very large values of Γ, two different ancillae could collide at the same time with $\mathcal{S}$, creating quantum correlations between the system and environment. To prevent this, the value of Γ must satisfy the condition

$$L\Gamma \ll \sqrt{\frac{1}{\beta m}}. \tag{6.23}$$

To derive this condition, I've considered that the typical velocity of a particle whose momentum is given by the effusion distribution is, precisely $\sqrt{1\beta m}$. Then, $t_{\text{class}} = L\sqrt{\beta m} \ll 1/\Gamma$ is the time required for a classical particle to cross the interaction region.

The density matrix in the momentum space is defined by

$$\rho_A(k,k') = \int dx\, W\left(\frac{k+k'}{2}, x\right) e^{-i(k-k')x/\hbar}$$
$$= \mu\left(\frac{k+k'}{2}\right) \exp\left[-\frac{\Delta x^2 (k-k')^2}{2\hbar^2} - i\,\frac{(k-k')x_0}{\hbar}\right]. \tag{6.24}$$

Since the initial state must be in agreement with the Wigner uncertainty principle, the last state is only valid if $4\pi\Delta x\sqrt{m/\beta} \geq \hbar$ [Hillery et al., 1984].

In fig.6.1, extracted from [Tabanera-Bravo et al., 2023], we represented the population of the ground state of H_S as a function of time for several values of the Poissonian rate Γ. The red line in fig.6.1 corresponds to erasing the non-diagonal elements of ρ in the

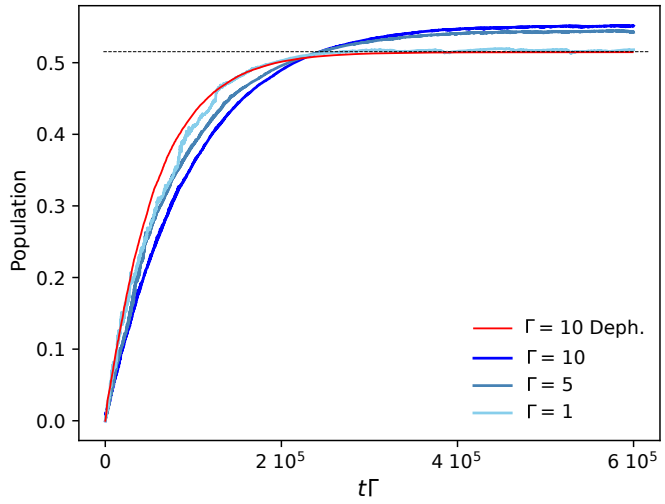

Figure 6.1.: Time evolution of the diagonal element ρ_{00} when we intercalate the dephasing super-operator $\mathbb{D}$ (red), and with Poissonian bombarding with rates $\Gamma = 10, 5, 1$. The black dashed line represents the thermal equilibrium state. In units such that $\hbar = 1$, the rest of parameters are: $\Delta = 0.6$, $\beta = 0.1$, $m = 0.1$, $\lambda = L = \hbar = 1$, $\Delta x = 1$ and $x_0 = -10$.

basis of H_S generated by the scattering map $\mathbb{S}$, after each collision. This is

$$\rho(t) = \langle \mathcal{U}(\tau_N)\mathbb{D}\mathbb{S} \quad \ldots \quad \mathcal{U}(\tau_1)\mathbb{D}\mathbb{S}\mathcal{U}(\tau_0)\mathbb{D}\mathbb{S}\rho(0)\rangle\,, \tag{6.25}$$

with $\mathbb{D}$ the dephasing channel introduced in Eq. (1.28).

The black dashed line corresponds with the equilibrium state $\rho = \frac{e^{-\beta H_S}}{\mathcal{Z}}$, with $\mathcal{Z} = \mathrm{Tr}\left\{e^{-\beta H_S}\right\}$ the partition function.

As one can observe in the figure, after a transient the population following both the dephasing evolution (red line), and the $\Gamma = 1$ curve coincide with the equilibrium state. For $\Gamma = 5, 10$, the prediction departs from the equilibrium state.

The physical interpretation of this fact is as follows: for the dephasing and $\Gamma = 1$ trajectories, both conditions for thermalization (section 5.4.1) are satisfied, and the equilibrium state is recovered, id est, the system thermalizes. In the two other trajectories $\Gamma = 5, 10$, the scattering map obeys local detailed balance but also creates coherence preventing thermalization.

This is in accordance with the prediction Eq. (6.18), where we prove that quantum coherence decays with Γ. For $\Gamma = 5, 10$, these non-diagonal elements are large and prevent thermalization. For $\Gamma = 1$ the coherence is damped, and the thermalization is recovered.

This result is supported by figure 6.2. In that figure, we represented the diagonal elements of the density matrix ρ, ρ_{00} (blue line), and ρ_{11} (red line) in the steady state. The green line represents the non-diagonal element $|\rho_{10}|$, and the black dashed lines represent the thermal equilibrium state. In order to obtain this equilibrium state, we numerically solved Eq. (5.5) with $\dot{\rho} = 0$. According to what we saw in fig.6.1, at high values of

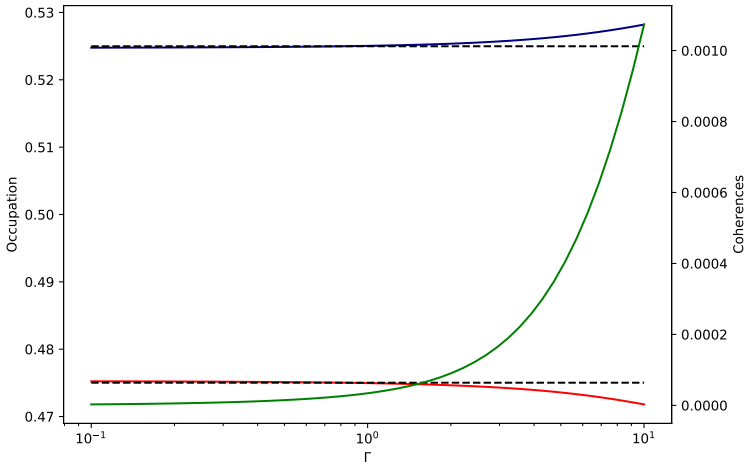

Figure 6.2.: Numerical solution of (5.5) in the case of a single qubit as a function of Γ: ρ_{00} (blue), ρ_{11} (red) and $|\rho_{10}|$ (green). In units such that $\hbar = 1$, the rest of the parameters are: $\Delta = 0.6$, $\beta = 0.1$, $m = 0.1$, $\lambda = L = \hbar = 1$ and $\Delta x = 1$, $\Delta x = 1$ and $x_0 = -10$. Extracted from ref.[Tabanera-Bravo et al., 2023]

.

Γ, the continuous bombarding with ancillae creates quantum coherence, preventing thermalization. However, the Poissonian dephasing at lower Γ damps this coherence quickly, bringing the system to equilibrium.

After clarifying the role of Γ in the dephasing mechanism, I will treat systematically the other relevant variables in the problem of thermalization. These variables are the energy gap of the bombarded qubit Δ, and the ancilla width Δx.

As I mentioned at the beginning of this section, the scattering map Eq. (5.34) can generate quantum coherence if $\rho_A(k, \kappa) \neq 0$ for $k \neq \kappa$. Using the definition Eq. (6.24),

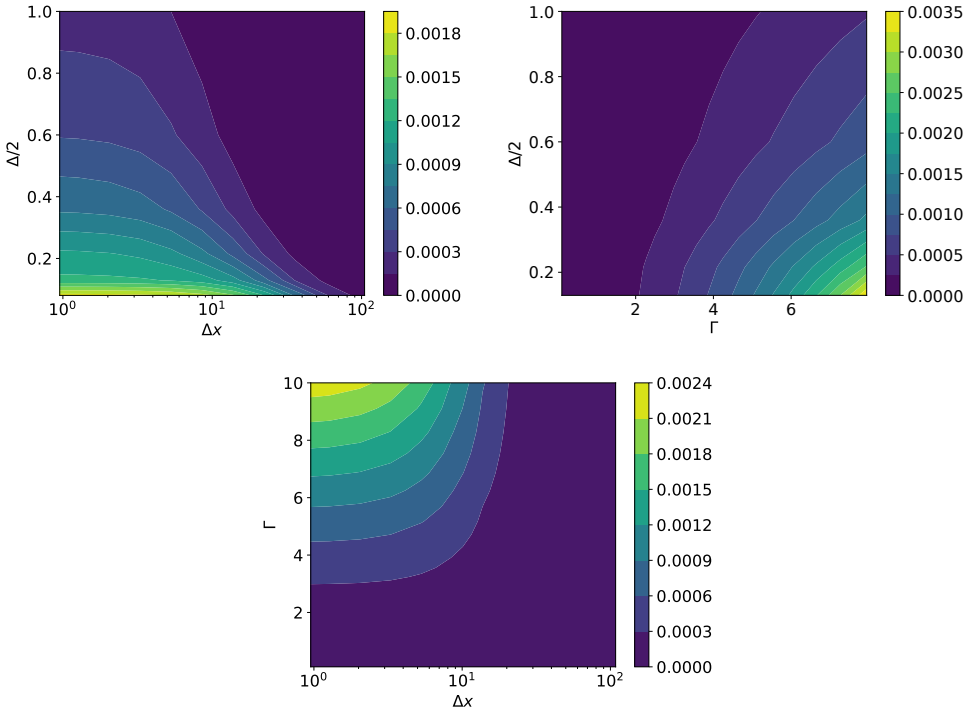

Figure 6.3.: Diagonal element $|\rho_{01}|$ from the numerical solution of Eq. (5.5) in the case of a single qubit as a function of Δ and Δx with $\Gamma = 5$, as a function of Δ and Γ with $\Delta x = 1$ and as a function of Γ and Δx with $\Delta/2 = 0.6$. $\beta = 0.1$, $m = 0.1$, $\lambda = L = \hbar = 1$ and $\Delta x = 1$ and $x_0 = -10$, in units such that $\hbar = 1$. Adapted from ref.[Tabanera-Bravo et al., 2023].

one can prove that this occurs for finite Δx; in particular, for $\Delta x \to 0$ the coherence generation is maximized.

In the same line, for large values of energy gap Δ, the scattering map Eq. (5.34) can not generate quantum coherence. However, following the approximation Eq. (6.18), for low values of Δ, the qubit almost degenerates and quantum coherences are unavoidable.

In figure 6.3, extracted from ref.[Tabanera-Bravo et al., 2023] we represented the element $|\rho_{01}|$ at the steady state of Eq. (5.5), as function of Γ, Δ and Δx.

Supporting our prediction, in fig.6.3(top) one can observe how the quantum coherence vanishes for higher values of Δ and Δx, increasing for higher values. Fig.6.3(middle) is in agreement with fig.6.2 since the lower values of Γ damps the non-diagonal element. In this figure, it becomes clear that thermalization prevails when $\Delta/\hbar \sim \Gamma$. That means that, for example, a 1 GHz qubit thermalizes under a bombarding of 10^9 collisions per second, compatible with experimental implementations [Camposeo et al., 2001]. Fig.6.3(bottom) is in agreement with the last two.

6.3. The wave packets thermostat

A different way to prevent coherence term using the scattering model consists in select properly the initial ancilla state ρ_A, avoiding that which creates quantum coherence. In this section, I will start proving that if the ancillae are very localized in the momentum space, they are not able to create quantum coherence. "Very localized" means that their dispersion in the momentum space is small with respect to the H_S level spacing (see details below). The physical reason for this is that an ancilla with well-defined energy, measured after the collision, will always[3] determine the physical state of the system, so the system collapses each time the ancilla is traced out. Another physical consequence is that the ancillae are extremely extended objects; in fact, if the target system almost degenerates, the ancillae must be infinitely extended waves.

6.3.1. Thermalization under wave packets

I start probing thermalization under narrow packets. To do this, I start defining explicitly the initial state ρ_A. [4] A single ancilla is initialized in a pure state, $\rho_{\mathcal{A}} = |\Psi_{k_0}\rangle\langle\Psi_{k_0}|$ with $|\Psi_{k_0}\rangle = \int dx \Psi_{k_0}(x)|x\rangle$ and

$$\Psi_{k_0}(x) = \int f(k-k_0)e^{-ik(x_0-x)}dk. \tag{6.26}$$

The quantity $f(k-k_0)$ is an arbitrary function peaked around the central momentum k_0. The last quantum state is a wave packet state centered around the position x_0, with linear momentum k_0. In appendix B I summarize the time evolution of wave packets related to the scattering problem. The scattering map Eq. (5.34) takes the form

$$\mathbb{S}_{ij}^{i'j'}(k_0) = \int dk \frac{k_{ji}(k)}{\kappa} t_{i'i}(k) t^*_{j'j}(\kappa) f(k-k_0) f^*(\kappa-k_0). \tag{6.27}$$

The central momentum k_0 represents the linear momentum of the wave packet as if it was a classical particle. Each time a particle is extracted from the thermal bath, it will come out with a random linear momentum k_0 following the effusion distribution Eq. (5.53), $\mu(k_0)$.

Since $f(k-k_0)$ decay quickly around k_0, the integrand in $\mathbb{S}$ will be small except for that k satisfying $k \sim \kappa$, where both functions f overlap. Only that points contribute to the integral. If the function $f(k-k_0)$ has width Δk, this condition is equivalent to

$$\begin{aligned} k_0 - \Delta k < k < k_0 + \Delta k, \\ k_0 - \Delta k < \kappa < k_0 + \Delta k. \end{aligned} \tag{6.28}$$

[3] In the absence of Bohr degeneracy.

[4] In the Poissonian thermostat I built the ancilla initial state ρ_A using the Wigner function. In this chapter, I will build a different state because of two reasons: first, the wave packets are more intuitive. Second, because we wrote ref.[Tabanera et al., 2022] did not know about the Wigner function.

For a given element $\mathbb{S}_{ij}^{i'j'}$, one can eliminate k form the previous inequalities and obtain the condition

$$\Delta k > \frac{m}{2k_0} \left| \Delta_{i'i} - \Delta_{j'j} \right| . \tag{6.29}$$

If $\mathbb{S}_{ij}^{i'j'}$ does not satisfy this condition it will be damped by the functions $f(k - k_0)$, becoming negligible. A *narrow packet* is that with Δk small to only allow the elements $\mathbb{S}_{ij}^{i'j'}$ satisfying $\Delta_{i'i} = \Delta_{j'j}$. With this condition, the scattering map $\mathbb{S}(k_0)$ reduces to

$$\mathbb{S}_{i'j'}^{ij}(k_0) \simeq t_{i'i}(k_0) t_{j'j}^*(k_0) \left[\delta_{i'i}\delta_{j'j} + \delta_{ij}\delta_{i'j'} - \delta_{i'i}\delta_{j'j}\delta_{ij}\delta_{i'j'} \right] . \tag{6.30}$$

The integral has been evaluated considering the contributions of that points $k = k_0$.

The condition $\Delta_{i'i} = \Delta_{j'j}$ limits the possible transitions to two cases: the case $i = j \to i' = j'$ representing transitions between diagonal elements and the case $i = i' \to j = j'$. This structure of transitions guarantees thermalization. In order to see this, I will derive the two conditions for thermalization introduced in section 5.4.1. Since the transitions between diagonal elements have the form $\mathbb{S}_{i'j'}^{ij}(k_0) \simeq t_{i'i}(k_0) t_{j'j}^*(k_0) \equiv \mathcal{P}(e_i \to e_j | k_0)$, every collision obeys microreversibility,

$$\mathcal{P}(e_i \to e_j | k_0) = \mathcal{P}(e_j \to e_i | k_0'). \tag{6.31}$$

k_0' is recovered using energy conversion $k_0^2/2m + e_i = {k_0'}^2/2m + e_j$. Taking the average on k_0, one recovers the local detailed balance

$$\begin{aligned} \mathcal{P}(e_i \to e_j) &= \int dk_0 \frac{\beta k_0}{m} e^{-\beta k_0^2/2m} \mathcal{P}(e_i \to e_j | k_0) \\ &= \int dk_0 \frac{\beta k_0}{m} e^{-\beta ({k_0'}^2/2m + e_j - e_i)} \mathcal{P}(e_j \to e_i | k_0') \\ &= e^{-\beta ({k_0'}^2/2m + e_j - e_i)} \mathcal{P}(e_j \to e_i). \end{aligned} \tag{6.32}$$

The second condition for thermalization is trivially followed since the narrow packets always satisfy $\mathbb{S}_{j'j}^{ii} = 0$. In conclusion, if the ancillae are narrow wave packets, the collisional reservoir recovers thermal behavior. I implement this thermostat in the following example using numerical simulations. I remark that since the thermalization is guaranteed, the bombarding rate Γ plays no role in the steady state of the dynamics.

6.3.2. An example

As in the previous example, the target system $\mathcal{S}$ is a single qubit, $H_\mathcal{S} = \Delta_\mathcal{S}/2\sigma_z$. In addition, the ancillae are narrow wave packets satisfying the conditions eqs.(6.28), obeying the Hamiltonian

$$H_{\text{Atot}} = \frac{k^2}{2m} + H_\mathcal{A}. \tag{6.33}$$

Here, the Hamiltonian $H_\mathcal{A}$ implies that the ancillae can have additional degrees of freedom. In fact, this is the case in experimental applications, where the systems are composed of atoms or molecules. For simplicity, I choose $H_\mathcal{A} = H_\mathcal{A}\sigma_z^{(\mathcal{A})}$.

The notation $\sigma_z^{(\mathcal{S},\mathcal{A})}$ represents that the Pauli operator is acting on the system $\mathcal{S}$ or the ancilla $\mathcal{A}_t$ Hilbert space, respectively. In the same way, I define the basis

$$\begin{aligned} H_{\mathcal{S}} |e_i\rangle &= e_i |e_i\rangle , \\ H_{\mathcal{A}} |a_i\rangle &= a_i |e_i\rangle , \\ (H_{\mathcal{S}} + H_{\mathcal{A}}) |e_I\rangle &= e_I |e_I\rangle . \end{aligned} \tag{6.34}$$

I reserve capital letters I, J to denote the eigenstates of the total Hamiltonian, and lower case i, j to denote the individual eigenstates $H_{\mathcal{S}} + H_{\mathcal{A}}$. The interaction Hamiltonian is $V = J_x \sigma_x^{(\mathcal{S})} \sigma_x^{(\mathcal{A})} + J_y \sigma_y^{(\mathcal{S})} \sigma_y^{(\mathcal{A})}$.

The scattering map Eq. (6.35) is therefore,

$$\mathbb{S}^{IJ}_{I'J'}(k_0) \simeq t_{I'I}(k_0) t^*_{J'J}(k_0) \left[\delta_{I'I}\delta_{J'J} + \delta_{IJ}\delta_{I'J'} - \delta_{I'I}\delta_{J'J}\delta_{IJ}\delta_{I'J'}\right] . \tag{6.35}$$

Since the ancilla internal degrees of freedom can be initialized following an arbitrary distribution, the last statement doesn't imply thermalization. One can, for example, initialize the internal degrees of each ancilla non-equilibrium state, so that refresh the ancilla state after the collisions breaks global equilibrium. However, if the ancilla is initialized in thermal equilibrium [5] , the eigenstates of the complete Hamiltonian $H_{\mathcal{S}} + H_{\mathcal{A}}$ thermalize to the equilibrium state

$$\pi_{\mathcal{SA}} = \frac{e^{-\beta(H_{\mathcal{S}} + H_{\mathcal{A}})}}{\mathcal{Z}_{\mathcal{SA}}}, \tag{6.37}$$

with $\mathcal{Z}_{\mathcal{SA}} = \mathrm{Tr}\{e^{-\beta(H_{\mathcal{S}} + H_{\mathcal{A}})}\}$ after few collisions.

In fig.6.4 we plot the steady state of the system $\mathcal{S}$ under the action of the scattering map $\mathbb{S}$ using both the wave vector operator approximation Eq. (6.7) and the time of flight approximation Eq. (6.11). Additionally, we compare it with the exact numerical result of eqs.(5.23) and compare it with the equilibrium distribution. Additionally, in fig.6.4 we also included the result obtained by considering the classical time of flight, this is, we considered

$$t_{i'i} = \langle e_{i'}| \, e^{-i\tau(k_0)(H_{\mathcal{S}} + H_{\mathcal{A}} + V)} \, |e_i\rangle , \tag{6.38}$$

with $\tau(k_0) = mL/k_0$. Note that this result is, precisely, the repeated-interaction model explained in the previous chapter, with random k_0.

Since they obey microreversibility, the occupation predicted by the WVO approximation, the exact transmission amplitudes, and the time of flight approximations coincide with the thermal equilibrium for any value of the interaction $J_y = 1, 0, -1$.

The interaction-time model breaks microreversibility at low temperatures, achieving a non-equilibrium state. If $J_x = J_y$, the interaction-time model achieves equilibrium. In fact, this case satisfies the condition (5.49) required for the interaction-time model to perform

[5] This means that the ancilla is initialized in the state

$$|\Psi_{k_0}\rangle \langle \Psi_{k_0}| \otimes \rho_{\mathcal{A}}, \tag{6.36}$$

where $\rho_{\mathcal{A}} = e^{-\beta H_{\mathcal{A}}}/\mathcal{Z}_{\mathcal{A}}$ is an equilibrium state with $\mathcal{Z}_{\mathcal{A}} = \mathrm{Tr}\{e^{-\beta H_{\mathcal{A}}}\}$.

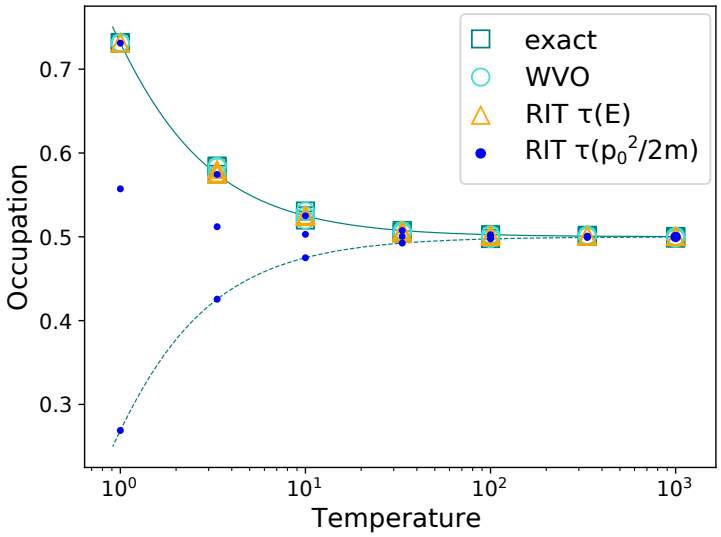

Figure 6.4.: Stationary occupation of the ground state of the qubit for $J_y = 1, 0, -1$, $J_x = 1$ and $\Delta_{\mathcal{S}} = \Delta_{\mathcal{A}} = 1$, $m = 0.1$, and $L = 50$. We depict the exact solution of the scattering problem numerically solving the scattering states (B.4) (dark green squares) and the populations given by different models: the wave-vector-operator model given by Eq. (6.7) (green circles) and the random-interaction-time model given by Eq. (6.11) (orange triangles). The exact solution and the two models induce thermalization at the same temperature as the bath, as expected. We also show the population if the interaction time is chosen as $\tau_{\text{packet}} \equiv \tau(k_0^2/(2m)) = Lm/k_0$ (dark blue dots, $J_y = 1, 0, -1$ from top to bottom), which clearly departs from the thermal state and even exhibits negative absolute temperatures or population inversion for $J_y = -J_x = -1$. The continuous and dashed light green curves depict the population of the fundamental level in the canonical ensemble with positive and negative temperatures, respectively. From [Tabanera et al., 2022].

no work, allowing thermalization. If $J_x = -J_y$ system is completely out of equilibrium, even reaching a canonical state with negative effective temperature $-\beta$. This is an artefact of the system Hamiltonian; in the appendix C I include a detailed explanation of the non-equilibrium states of this particular system. At very high temperatures, all the models make the same prediction.

6.4. Discussion and conclusion

In this chapter, I describe two implementations of collisional reservoirs recovering thermal behaviour, id est, two thermostats. The first one makes use of the scattering model of collisions, guaranteeing local detailed balance. The spurious quantum coherence

created in the single collisions is removed by the Poissonian random collision time, recovering thermalization in any case. For a given system, the coupling strength with the environment is conditioned by the bombarding rate Γ: for a low bombarding rate, any quantum coherence is removed from the system, but the transient state until reaching the equilibrium becomes larger and larger. If the target quantum system degenerates, quantum coherence becomes unavoidable.

The second thermostat consists in bombarding the target system with narrow wave packets in the momentum space, which prevents any coherence generation. In this case, the evolution of the system always leads to thermalization regardless of the bombarding rate. In order to vanish the quantum correlation, the dispersion of the wave packets in the momentum must be negligible with respect to the system level spacing. Again, as the system degenerates, the ancillae must become plane waves in order to recover thermalization, which can not be implemented by any finite experimental device, and so this thermostat cannot avoid quantum coherence in this case either. The scattering is a very realistic model since it contains the complete evolution of the system during the collision. Therefore, both thermostats are powerful models to understand experimental implementations.

7. Local thermalization

Quantum thermodynamics and quantum information comprise several instances of multipartite systems in contact with their *local* environment, for example, the study of energy transport along a spin chain heated by their boundaries, or any quantum communication device. Due to quantum entanglement between the parties, these interactions produce global effects.

In cases where the coupling between the parties of a system, denoted by ε, is small, it is possible to describe the dissipation of the entire system using a local CPTP quantum master equation, such as equation (1.32), which includes independent diffusive terms that only affect a local subsystem of the complete Hilbert space. Typically, it is feasible to derive a Born-Markov equation, like equation (1.42), that only affects each individual subsystem of the system from a microscopic model. These equations are referred to as *local master equations* (LME) or "phenomenological master equations".

In the opposite case, when the system parties are strongly coupled, using local diffusive terms in the quantum master equation becomes inconsistent as the conditions in Eq. (1.39) are no longer satisfied. As explained in the previous chapters, violating these conditions leads to a lack of thermal behavior and the emergence of quantum coherence. The solution to this issue is to diagonalize the global system and describe the diffusion using *global* quantum master equations, where the diffusion takes place in the global system eigenbasis. The equations following this approach are called *global master equations* (GME). However, deriving a GME can be very challenging since one must diagonalize the complete system Hamiltonian, which is often a difficult task for large systems, especially when starting from a microscopic model.

The discrepancy between the two different approaches has been studied in [Hofer et al., 2017], where the authors consider two coupled harmonic oscillators coupled to respective thermal baths, comparing the LME and GME predictions with an exact result. In this case, the thermal baths are large collections of harmonic oscillators at different temperatures. Their conclusions are that the LME predict correct thermal currents when the oscillators are weakly coupled but fail for strong coupling, where the GME coincides with the exact result. However, GME fails in some non-equilibrium circumstances [Cattaneo et al., 2019]. Interestingly, although one could expect GME to be precise for arbitrary coupling, it fails for low coupling; the reason for this is that secular approximation, underlying the GME, fails.

Secular approximation was introduced at the beginning of this thesis in order to derive the Secular Born-Markov equation, Eq. (1.42). Within this approximation, one considers that the oscillating terms in the Redfield equation evolve much faster than the quantum jumps and, therefore, one can drop these terms; however, if the system degenerates, some oscillation terms start oscillating infinitely slowly (the secular terms),

invalidating the approximation. In [Cattaneo et al., 2019] they consider both the local master equation and the global master approximation with full-secular approximation and with partial-secular approximation (only the non-secular terms are removed from the Redfield equation). In this case, confirming the previous statement, the GME with partial-secular approximation is always valid.

In addition, GME predict quantum transitions between global energy levels obeying detailed balance, and therefore, they will always lead to the correct equilibrium steady state, id est, global thermalization. However, even in autonomous situations, they fail to predict the transient evolution [Scali et al., 2021].

In [Barra, 2015] the author approaches the problem using a collisional reservoir. In particular, he uses the interaction-time collision model introduced above to study the thermodynamics of a spin chain driven by its boundary. As a result, he finds that the local master equation obtained from the interaction-time model predicts spurious energy currents violating the second law. This effect is a result of the work performed by the interaction-time model, by switching on and off the interaction, as I explained in chapter 5. In [De Chiara et al., 2018] the authors recover the thermodynamic consistency by explicitly considering this work contribution.

The main objective of this chapter is to analyze the behavior of a system (a qubit chain) heated by its boundary by the Poissonian thermostat developed in the last chapter. The main advantage of this thermostat is that it is able to recover thermalization without performing spurious work. However, I must warn that this chapter is part of a work in progress, that these results have not yet been consolidated and published, and that the conclusions I will draw are still subject to debate. My aim with this chapter is precisely to lay the ground for future work, assessing the relevance of collisional reservoirs to the problem of local and global master equations. I also find these results to be of great aesthetic value.

In section 7.1, I will apply the Poissonian thermostat to a qubit chain to study both the transient and the stationary phenomena. To recreate local effects during the transient, the reservoir will be applied exclusively to the first qubit of the chain; during this transient, if the inter-qubit coupling is small, the thermostat will drive only the first qubit to *local* thermalization, id est, to the Gibbs state given by its local Hamiltonian, without affecting the rest of spins. Nevertheless, in the steady state, the action of the thermostat affects the whole chain, thermalizing the global system. The parameters I am considering to study local thermalization are the inter-dot coupling, the bombarding rate determining the coupling strength with the bath, and the ancillae width. The contribution of this study to the system lies in the realistic evolution provided in the Poissonian thermostat: in fact, the Poissonian thermostat can be regarded as a microscopic model of the interaction between a system and the environment.

In section 7.2 I will derive two quantum master equations using the Poissonian collisional thermostat and obtain an analogy between narrow and broad packets with the usual global and local quantum master equations.

7.1. Boundary driven system

I start considering the target system $\mathcal{S}$ as an XY-qubit chain described by the following Hamiltonian,

$$H_{\mathcal{S}} = \frac{h}{2}\sum_{q=1}^{N}\sigma_z^{(q)} + \varepsilon\sum_{q=1}^{N-1}\left(\sigma_x^{(q)}\sigma_x^{(q+1)} + \sigma_y^{(q)}\sigma_y^{(q+1)}\right). \tag{7.1}$$

Here, each one of the N qubits is defined by its local energy h, and interacts with its first neighbours with a coupling strength ε. For low values of ε, the Hamiltonian almost degenerates.

As in the previous chapter, the system is bombarded with ancillae at Poissonian random times with rate Γ. Each collision follows the Hamiltonian

$$H = \frac{p^2}{2m} + H_{\mathcal{S}} + \chi_{[0,L]}(x)V, \tag{7.2}$$

where p is the ancilla momentum and $\chi_{[0,L]}$ is the index function representing the interaction region $[0, L]$. The thermostat acts exclusively on the first spin, $V = \lambda\left(\sigma_x^{(1)} + \sigma_y^{(1)}\right)$.

It is useful to define two different bases of eigenvectors: the *global basis* is that of the system Hamiltonian, $H_{\mathcal{S}}\left|e_i\right\rangle = e_i\left|e_i\right\rangle$, depending ε. On the other hand, the *local basis* is that of the local Hamiltonian part $H_{\text{loc}} = h/2\sum_q \sigma_z^{(q)}$, this is $H_{\text{loc}}\left|\epsilon_I\right\rangle = \epsilon_I\left|\epsilon_I\right\rangle$. Note that V generates no quantum coherence on the global basis but on the local one. The eigenenergies ϵ_I will always degenerate. In this work I denote the local eigenstates $\left|\epsilon_I\right\rangle$ in terms of the $\sigma_z^{(q)}$ eigenvalues, using computational notation, $\left|\epsilon_0\right\rangle = \left|00...00\right\rangle$, $\left|\epsilon_1\right\rangle = \left|00...01\right\rangle$, ... $\left|\epsilon_{2^N}\right\rangle = \left|11...11\right\rangle$.

Under the thermostat, the qubit chain $\mathcal{S}$ evolves following Eq. (5.5), $\dot{\rho} = -i[H_{\mathcal{S}}, \rho] + \Gamma\left[\mathbb{S} - \mathbb{I}\right]\rho$, where ρ is the system density matrix and $\mathbb{S}$ is the scattering map defined in Eq. (5.34),

$$\mathbb{S}^{ij}_{i'j'}(k_0) = \int dk \frac{k_{ji}(k)}{\kappa} t_{i'i}(k) t^*_{j'j}(\kappa) f(k - k_0) f^*(\kappa - k_0). \tag{7.3}$$

$f(k - k_0)$ are Gaussian functions centered around k_0 with dispersion Δk. The scattering map is obtained by taking the average of the central momentum k_0,

$$\mathbb{S}^{ij}_{i'j'} = \int dk_0 \mu(k_0) \mathbb{S}^{ij}_{i'j'}(k_0), \tag{7.4}$$

where $\mu(k_0)$ is the effusion distribution .

7.1.1. Transient dynamics

The system has two different timescales. The first one is given by the system-thermostat strength: for constant parameter λ, the diffusive evolution of the chain is determined by the bombarding rate Γ[1]. The second one is given by the inter-qubit coupling ε. If both

[1]The characteristic time of a quantum system is related with its characteristic energy by the constant $\hbar$, which I consider to be 1 in this chapter. Therefore, one can determine the timescale using a frequency –such as Γ– or an energy –such as ε.

timescales are fast, the diffusion created by the thermostat immediately affects the whole chain and the system achieves a global steady state, whereas if the coupling with the environment is strong and the inter-qubit coupling is weak, the first qubit may achieve a local steady state while the rest of the qubits remain evolving.

To illustrate this, in fig.7.1 I consider a chain of $N = 3$ qubits and plot the evolution of the populations in the local basis as a function of time for constant bombarding rate, and varying the coupling ε. As one can observe, when the inter-qubit coupling is large,

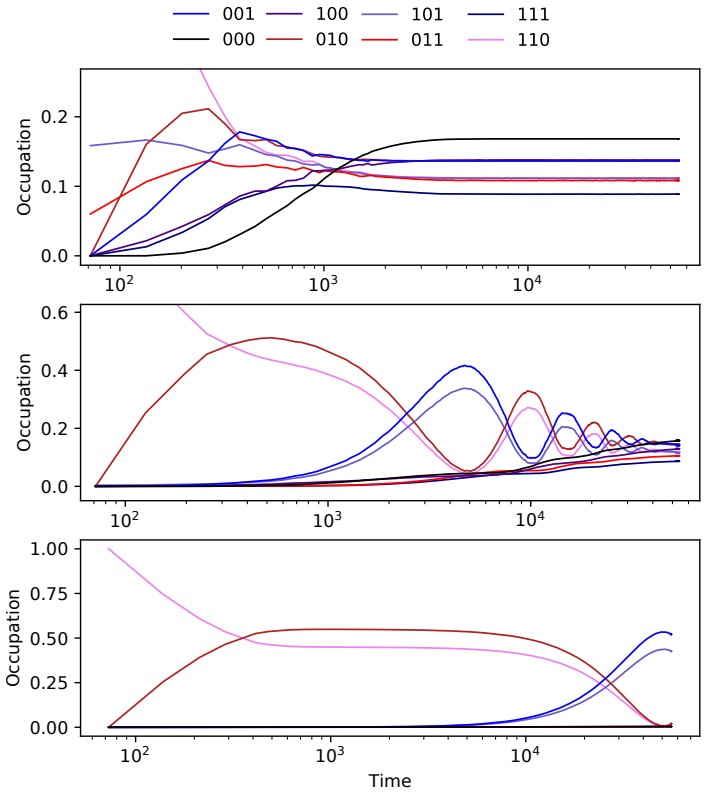

Figure 7.1.: Time evolution of the diagonal elements of the system density matrix during the transient state for different values of ε: (top) $\varepsilon = 10^{-2}$, (middle) $\varepsilon = 10^{-3}$, (bottom) $\varepsilon = 10^{-4}$. $\Gamma = 1/20$, $h = 2$, $\lambda = 1$, $\beta = 0.1$, $m = 0.1$, $L = 100$ and $\Delta k = 0.01$.

the transient is short and the system achieves a global steady state. When I reduce ε, the transient becomes larger and starts exhibiting damped oscillations before the global steady state. Interestingly, these oscillations start when the two levels $|110\rangle$ and $|010\rangle$ are occupied, leaving the rest empty. This indicates that only the first qubit is being activated by the thermostat, achieving a local steady state for a while. After that, the rest of the spin chain is activated filling the levels $|101\rangle$ and $|001\rangle$. Note that along these oscillations the second qubit and third qubit are slowly oscillating between their local states $|0\rangle$ and $|1\rangle$. This phenomenon is similar to the quantum synchronization observed

in bipartite systems sharing a common bath [Giorgi et al., 2013], or the quantum beats observed in tuned quantum dots [Ficek et al., 1987, Gross and Haroche, 1982].

For the lowest value of ε, the transport along the qubit chain is almost frozen, giving place to a long-lasting local steady state.

In order to understand these results, in fig.7.2 (top left) I represent all the possible transitions generated by the thermostat acting on the first qubit (orange arrows) and that generated by the inter-qubit coupling ε, between the levels represented in the local eigenbasis. For $N = 3$ qubits the system presents a ground state $|000\rangle$, an excited state $|111\rangle$ and two degenerated triplets $\{|100\rangle, |010\rangle, |001\rangle\}$ and $\{|101\rangle, |110\rangle, |011\rangle\}$. The energy difference between the levels and the separated triplets is of order h, therefore, the system can only jump between these subspaces by a collision with an ancilla. Otherwise the levels $|111\rangle$ and $|000\rangle$ remain stable. The degeneracy of the triplet levels is broken by the coupling ε; the quantum jumps within both subspaces take place during the free unitary evolution between two ancilla collisions, under the global Hamiltonian $H_{\mathcal{S}}$. When $\varepsilon \simeq 0$, the orange arrow transitions immediately equilibrate, while the system starts exploring the rest of the states space through the blue arrows. The oscillations take place because the system is exploring the square formed by $|101\rangle, |001\rangle, |010\rangle$ and $|110\rangle$, and decay once the system moves away from this subspace.

In order to quantify the characteristics of the oscillations, one can write the master equation, Eq. (5.5) as a dynamical system of equations. To do this, I express the master equations components of the $H_{\mathcal{S}}$ eigenbasis,

$$\dot{\rho}_{ij} = -i\Delta_{ij}\rho_{ij} + \Gamma \sum_{kl} \left[\mathbb{S} - \mathbb{I}\right]^{kl}_{ij} \rho_{kl}. \tag{7.5}$$

Here $\Delta_{ij} = e_i - e_j$. The last result can be expressed as the dynamical system $\dot{\bar{\rho}} = \mathbb{M}\bar{\rho}$ if one expresses the $2^N \times 2^N$ matrix ρ_{ij} as a 2^{2N} vector $\bar{\rho} \equiv \rho_\alpha$, with $\alpha = 2^N i + j$. The $2^{2N} \times 2^{2N}$ matrix $\mathbb{M}$ is defined by

$$\mathbb{M}^{\beta}_{\alpha} = \left[-i\Delta_{ij} + \Gamma\left[\mathbb{S} - \mathbb{I}\right]^{kl}_{ij}\right]^{\beta=2^N k+l}_{\alpha=2^N i+j}. \tag{7.6}$$

The complex part of the eigenvalues of $\mathbb{M}$ governs the oscillations frequency of the 'normal modes' of ρ, while the real part determines the decay of these modes into the global steady state. For $N = 3$ qubits there exists $2^6 = 64$ complex eigenvalues.

In figure 7.2 (top, right) I represent the real part of the eigenvalues of $\mathbb{M}$ for several values of ε. Since the lower eigenvalues are quickly damped by the dynamics, I just represent the 6 upper (less damped) eigenvalues. As one can see, there always exists one eigenvalue with zero real part: this mode represents the global steady state, which is always stable. For large values of ε the rest of the eigenvalues are very negative, damping immediately any dynamics apart from the global steady state. This confirms what we see in fig.7.1(top). If ε decreases, the eigenvalues start approaching zero, allowing the coexistence of the oscillation modes for a longer time, and creating the transient in fig.7.1(middle, down). In fact, these long-lived modes are the secular modes preventing the secular approximation to be applied when deriving a GME. When $\varepsilon \to 0$, all these modes become stable, and the oscillations are not damped anymore.

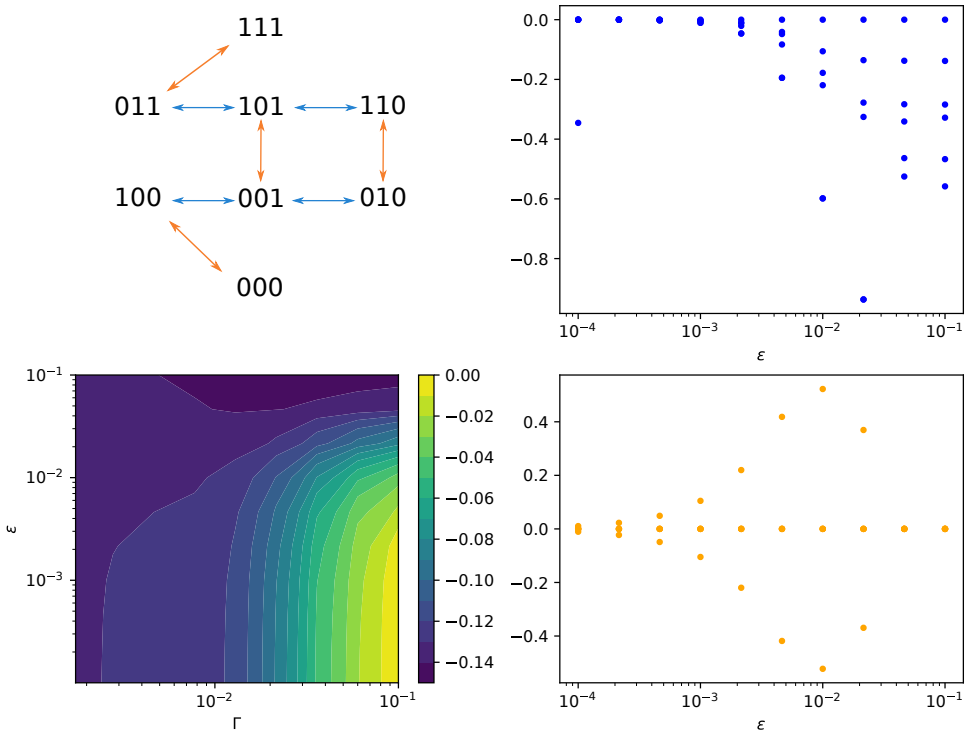

Figure 7.2.: (top, left) Possible transitions of the system generated by the collisional thermostat. Orange arrows represent local transitions (flips of the first qubit), and blue arrows represent transitions along the chain. (top, right) The real part of the six less damped eigenvalues of the $\mathbb{M}$ as a function of ε. (bottom, right) The imaginary part of the same eigenvalues. (bottom, left) The real part of the less damped eigenvalue of $\mathbb{M}$ as a function of ε and Γ. $\Gamma = 1/20$, $h = 2$, $\lambda = 1$, $\beta = 0.1$, $m = 0.1$, $L = 100$ and $\Delta k = 0.01$. In the last plot $\varepsilon = 10^{-3}$.

In figure 7.2 (bottom, right) I plot the imaginary part of the same eigenvalues, governing the oscillation frequency as a function of ε. There is always one eigenvalue with zero complex part, representing again the global steady state of the dynamics. For high ε the modes present high oscillation frequencies even if these modes are damped. Decreasing ε the frequency of the modes decreases until become zero. The physical interpretation of fig.7.2(right) explains the complete dynamics present in fig.7.1: for high ε the system is immediately damped into the oscillation-less global state, which is the only stable state. In the intermediate values of ε the transient increases, appearing system oscillations due to the chain free Hamiltonian evolution. When $\varepsilon \to 0$, since the system decays quickly to the local steady state, there already exists damped modes; however, the oscillations damp and the oscillation frequency becomes zero, freezing the system in the local equilibrium

state.

To study the role of the bombarding rate Γ in the modes damping, in fig.7.2(bottom, left) I represent the real part of the highest (the least damped) eigenvalue, apart from the zero eigenvalue; this eigenvalue represents, precisely the longest-lived eigenmode surviving before the global steady state. For low bombarding rate Γ, the eigenvalue is very negative, quickly damping the oscillations. In fact, if the system and environment interact infrequently, all the energy is dissipated through the qubit chain during the free evolution and the oscillations disappear. If Γ is large the chain is continuously evolving under fluctuations, and the oscillations damping disappears.

In conclusion, I found that the global equilibrium state is always the unique steady state of the system's evolution. However, during the transient, one can find local effects such as local thermalization, where only the local qubit affected by the thermostat achieves a steady state. Local thermalization requires a timescale separation between the local thermostat diffusion process and the global transport through the chain; if the first one is faster, the first qubit is always close to the local equilibrium and the rest of the chain presents the oscillations regarded in figure 7.1.

Non-local effects

The rapid interaction between the first qubit and the bath prevents any quantum coherence between it and the rest of the chain. However, as one can observe in the example with $N = 3$ qubits, the third and second qubits oscillate between $|01\rangle_{23}$ and $|10\rangle_{23}$. This suggests that the second and third qubits could be quantum correlated, even forming a Bell state.

To describe the quantum correlation of these qubits, one can use the *quantum concurrence*,

$$\mathcal{C} = \max(0, a_0 - a_1 - a_2 - a_3), \tag{7.7}$$

with a_i the eigenvalues of the Hermitian matrix $\sqrt{\sqrt{\rho_{23}}\hat{\rho}_{23}\sqrt{\rho_{23}}}$ in decreasing order. $\rho_{23} = \mathrm{Tr}_1\rho$ is the reduced matrix of the second and third qubit and $\hat{\rho}_{23} = (\sigma_y \otimes \sigma_y)\,\rho_{23}^*\,(\sigma_y \otimes \sigma_y)$. This magnitude was introduced in [Bennett et al., 1996] to represent a measure of the quantum entanglement between two qubits; in fact, it takes a value from 0 to 1, being 0 for non-entangled states and 1 for maximally entangled states such as the Bell states.

In addition, I define the magnitude

$$r_{ij} = \ln\left[\frac{\mathcal{P}\left(q_1 = |i\rangle\right)}{\mathcal{P}\left(q_1 = |j\rangle\right)}\right]. \tag{7.8}$$

Here $\mathcal{P}\left(q_1 = |i\rangle\right) = \sum_{ab}\langle iab|\,\rho\,|iab\rangle$ is the probability of observing the first qubit in the state $|i\rangle$. This quantity can be used to evaluate how far is the first qubit from equilibrium; in particular, $r_{10} = -\beta(e_1 - e_0)$ when the first qubit reaches thermal equilibrium.

Both quantities are represented in figure 7.3. As one can observe, the quantity r_{10} (top) reaches the equilibrium value after a short transient and remains in this state for the rest of the simulation. The second and third qubits are initialized in an uncorrelated state. The quantum correlation is created once the first qubit is in equilibrium, increasing the

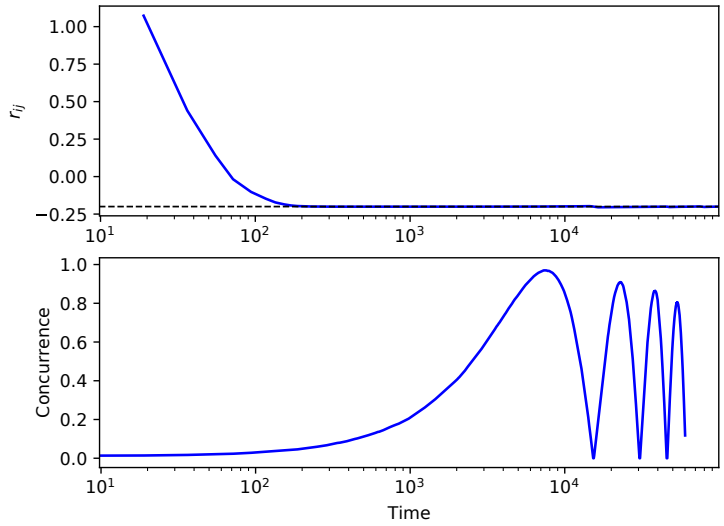

Figure 7.3.: (top) Ratio r_{10}. The black dashed line represents the equilibrium prediction $r_{10} = -\beta(e_1 - e_0)$. (bottom) Concurrence of the second and third qubits. $\Gamma = 1/20$, $h = 2$, $\lambda = 1$, $\beta = 0.1$, $m = 0.1$, $L = 100$, $\varepsilon = 10^{-3}$ and $\Delta k = 0.01$.

concurrence until it reaches a value close to one. This value indicates that the second and third qubits are forming a Bell state. After that, the concurrence starts oscillating, destroying and regenerating the quantum coherence.

7.1.2. Steady state

In this section, I will study (again) the relation of the thermostat with thermalization. In the last chapter, I prove that the scattering of wave particles leads to global thermalization if the system does not degenerate. Close to degeneration, one must consider extremely slow bombarding rates in order to prevent coherence in the steady state. The main difference between the current system and the previous chapter is, precisely, the presence of interesting behaviour close to degeneration.

Since the density matrix of the qubit chain is large, I will use the *quantum fidelity* to describe the global system in the steady state. The fidelity between states is a measure of the closeness of two quantum states; for pure states, this is just the projection of one state into the other. If both states are mixed, the fidelity, called Uhlmann fidelity, is the projection of two purifications of the states [Wilde, 2013]. The fidelity is always in the interval $0 \leq \mathcal{F} \leq 1$, being 0 if the two states are completely orthogonal and 1 if they are the same state. It can be computed using the formula

$$\mathcal{F}(\rho, \sigma) = \left(\mathrm{Tr} \sqrt{\sqrt{\rho}\sigma\sqrt{\rho}} \right)^2 , \tag{7.9}$$

In figure 7.4 I plot the quantum fidelity between the global thermal equilibrium

$\pi = \exp(-\beta H_S)/\mathcal{Z}$, with $\mathcal{Z} = \mathrm{Tr}\{\exp(-\beta H_S)\}$, and the global steady state obtained in the numerical simulations, as a function of the bombarding rate Γ and the wave packet width Δk. For a high bombarding rate, the thermostat interaction generates quantum

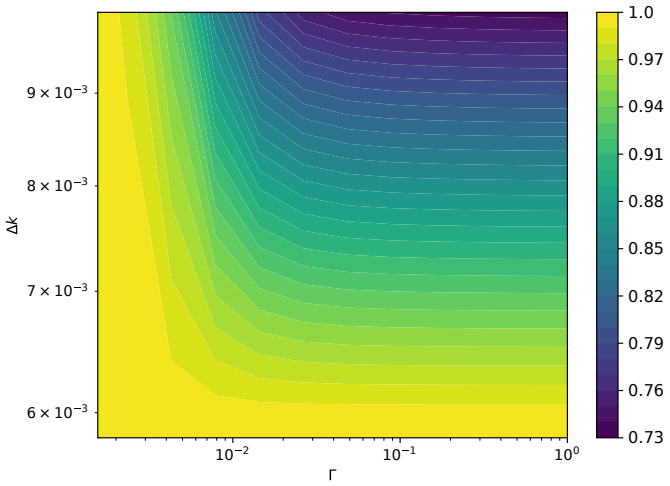

Figure 7.4.: Fidelity between thermal state π and the steady state of the dynamics obtained in numerical simulations, as a function of Γ and Δk. $h = 2$, $\lambda = 1$, $\beta = 0.1$, $m = 0.1$ and $L = 100$.

coherence, avoiding the system to approach the thermal state. Thermalization is only recovered with narrow packets, at low Δk. If one reduces the bombarding rate, the Poissonian thermostat is enough to recover thermal behaviour, even with broad packets.

However, as I mention under figure 7.2, the lower values of Γ damp the oscillating modes in the transient. In conclusion, fixed Δk, a thermostat describing these oscillations fails in predicting the global thermal state and vice versa. This result is very similar to that observed in the introduction of this chapter, where I state that LME are able to correctly treat the transient dynamics whereas GME treat correctly the steady state. In the next section, I elaborate on this comparison.

7.2. Comparison with master equations

In this last section of the chapter, I will compare the Poissonian thermostat with local and global master equations. Following the preceding example, the thermostat can be used to describe either the global steady state or the transient thermodynamics, but not both at the same time. Following this, I will start obtaining a master equation from the narrow packet approximation introduced in the last chapter; I will prove that this approximation properly describes global thermalization, and therefore, the narrow approximation is equivalent to the global master equations. Then, assuming broad packets, I will derive a local master equation.

7.2.1. Master equation with narrow packets

The thermalization with narrow packets was described in section 6.3. There I proved that the narrow approximation limits the possible transitions induced by the thermostat, reducing the scattering map to Eq. (6.35). Now, if the thermostat temperature is high, one can make use of the time of flight approximation, Eq. (6.10) to evaluate the transition amplitudes

$$t_{j'j} \simeq \langle e'_j | \, e^{-i\tau_j(k_0)(H_{\mathcal{S}}+V)} \, |e_j\rangle \,, \tag{7.10}$$

with

$$\tau_j(k) = \begin{cases} \dfrac{L}{\sqrt{2E/m}} & E > e_{max}, \\ 0 & E \leq e_{\max}. \end{cases} \tag{7.11}$$

Remember that $E = k^2/2m + e_j$ is the total energy in the collision. Assuming that the times of flight τ_j are small enough, one can expand

$$t_{j'j}(k_0) = \delta_{j'j} - i\tau_j(k_0)\hat{H}_{j'j} - \frac{\tau_j^2(k_0)}{2}\hat{H}^2_{j'j} + o(\tau^3). \tag{7.12}$$

Here I use $H = H_{\mathcal{S}} + V$. Then

$$\begin{aligned} t_{i'i}(k_0)t^*_{j'j}(k_0) = \delta_{j'j}\delta_{i'i} - i\tau_j\hat{H}_{j'j}\delta_{i'i} + i\tau_i\hat{H}_{i'i}\delta_{j'j} \\ -\frac{\tau_j^2}{2}\hat{H}^2_{j'j}\delta_{i'i} - \frac{\tau_i^2}{2}\hat{H}^2_{i'i}\delta_{j'j} + \tau_j\tau_i\hat{H}_{i'i}\hat{H}^*_{j'j}. \end{aligned} \tag{7.13}$$

Using Eq. (7.4) and inserting this result into the master equation, Eq. (7.5) one obtains

$$\begin{aligned} \dot{\rho}_{i'j'} &= -i\Delta_{i'j'}\rho_{i'j'} \\ &+\Gamma\left[-i\left\langle\tau_{j'}\right\rangle\hat{H}_{j'j'} + i\left\langle\tau_{i'}\right\rangle\hat{H}^*_{i'i'} - \frac{\left\langle\tau^2_{j'}\right\rangle}{2}\hat{H}^2_{j'j'} - \frac{\left\langle\tau^2_{i'}\right\rangle}{2}\hat{H}^2_{i'i'} + \left\langle\tau_{j'}\tau_{i'}\right\rangle\hat{H}_{i'i'}\hat{H}^*_{j'j'}\right]\rho_{i'j'} \\ &+\Gamma\sum_{i\neq i'}\delta_{i'j'}\left\langle\tau_i^2\right\rangle\hat{H}_{i'i}\hat{H}^*_{j'i}\rho_{ii}. \end{aligned} \tag{7.14}$$

This equation is, precisely, a GME expressed by components in the eigenbasis of $H_{\mathcal{S}}$, whose transition rates are given by the times of flight averages

$$\left\langle\tau_j\right\rangle\int dk_0\mu(k_0)\tau_j(k_0). \tag{7.15}$$

In fact, the non-diagonal terms $i' \neq j'$ evolve following the first line exclusively,

$$\begin{aligned} \dot{\rho}_{i'j'} &= -i\Delta_{i'j'}\rho_{i'j'} \\ &+\Gamma\left[-i\left\langle\tau_{j'}\right\rangle\hat{H}_{j'j'} + i\left\langle\tau_{i'}\right\rangle\hat{H}^*_{i'i'} - \frac{\left\langle\tau^2_{j'}\right\rangle}{2}\hat{H}^2_{j'j'} - \frac{\left\langle\tau^2_{i'}\right\rangle}{2}\hat{H}^2_{i'i'} + \left\langle\tau_{j'}\tau_{i'}\right\rangle\hat{H}_{i'i'}\hat{H}^*_{j'j'}\right]\rho_{i'j'}. \end{aligned} \tag{7.16}$$

As one can note, each component evolves independently from the rest. Then, the second term of the right-hand side damps these elements, preventing quantum coherence [Jacob et al., 2021]. Diagonal elements evolve according to the master equation

$$\dot{\rho}_{i'i'} = \Gamma \sum_i \left\langle \tau_i^2 \right\rangle \left[\hat{H}_{i'i} \hat{H}^*_{i'i} - \hat{H}^2_{i'i'} \right] \rho_{ii}. \tag{7.17}$$

Detailed balance

The local detailed balance recovering global thermalization is provided by the averages $\langle \tau_i^2 \rangle$. In order to prove it, one can write

$$\begin{aligned} e^{-\beta e_i} \langle \tau_i^2 \rangle &= \int_{k_{\max}}^{\infty} \frac{\beta k_0}{m} e^{-\beta \left(k_0^2/2m + e_i \right)} \tau_i(k_0) dk_0 \\ &= \beta m \int_{e_{\max}}^{\infty} \frac{e^{-\beta E}}{E} dE. \end{aligned} \tag{7.18}$$

We defined $k_{\max}$ satisfying $k_{\max}^2/2m + e_i = e_{\max}$ and made use of the change of variable $E = k_0^2 + e_i$. From the last equation, one recovers the local detailed balance

$$e^{-\beta e_i} \langle \tau_i^2 \rangle = e^{-\beta e'_i} \langle \tau_{i'}^2 \rangle \tag{7.19}$$

for any value of i, i'.

Therefore, the master equation obtained from the narrow approximation describes the global steady state correctly. However, since the quantum coherence decays exponentially, this equation is not able to describe the transient oscillations or the quantum correlation created in the chain.

7.2.2. Master equation with broad packets

Let's derive a master equation using broad packets. In this case, the integral on momentum in Eq. (7.4) can not be directly simplified: in order to treat this integral one must consider, again, the high-temperature limit where the kinetic energy of the ancillae is much higher than the chain level spacing $k_0 \gg 2m\Delta_{i'i}$. Within this approximation, the integral is simplified [Jacob et al., 2022]

$$\mathbb{S}_{ij}^{i'j'}(k_0) = \int dk |f(k - k_0)|^2 t_{i'i}(k) t^*_{j'j}(k). \tag{7.20}$$

Moreover, the interaction times $\tau_i(k)$ are approximated by $\tau_i(k) = mL/k$ for any value of index i. Then, we can write the scattering map in a basis-independent way

$$\mathbb{S}(k_0)\rho \simeq \int_{-\infty}^{\infty} dk |f(k - k_0)|^2 e^{-i\tau_i(k)\hat{H}} \rho e^{i\tau_j(k)\hat{H}}. \tag{7.21}$$

This process is very similar to that in section 5.2 where I derived a CPTP QME using the interaction-time model. In fact, in the high-temperature approximation, I am recovering

the interaction-time model[Filippov et al., 2020] which we already know that it is not capable to describe the steady state. Finally, expanding again the exponential and inserting Eq. (7.5), I finally obtain

$$\dot{\rho} = -i\left[H,\rho\right] - i\Gamma\langle\tau\rangle_B\left[\hat{H},\rho\right] + \Gamma\langle\tau^2\rangle_B\left[\hat{H}\rho\hat{H} - \frac{1}{2}\left\{\hat{H}^2,\rho\right\}\right]. \tag{7.22}$$

This is a local master equation where the diffusion term only affects the first qubit due to the action of the local potential V. The decay rates are given by the quantities

$$\langle\tau\rangle_B = \int dk_0 \mu_{\text{eff}}(k_0) \int_{-\infty}^{\infty} dk |f(k-k_0)|^2 \tau(k), \tag{7.23}$$

analogous for $\langle\tau^2\rangle_B$.

7.3. Discussion and conclusion

In this chapter, I utilize the quantum collisional thermostats developed in the previous chapter to investigate the behavior of a quantum system driven by its boundaries. In the first part, I analyze the transient behavior and steady state of a qubit chain separately. The duration of the transient depends on the system timescales. If the local action of the thermostat is much faster than the energy transport along the chain, the first qubit remains close to the equilibrium state, while the rest of the qubits become quantum correlated. Under this timescale separation, in fig.7.1 I observed quantum oscillations, similar to that found in experimental and theory works in several systems.

However, to recover global equilibrium and thermalize the system, one must dramatically reduce the bombarding rate close to degeneration, avoiding the timescale separation. As a consequence, the same thermostat cannot describe both the transient properties and the thermal global state simultaneously. The conclusion is that quantum collisional reservoirs can predict interesting physical behavior (quantum oscillations), but they cannot provide a unique model representing both global and local behavior simultaneously. Therefore, they fail in this regard, as do the quantum master equations.

In the second part, I explore the relationship between collisional reservoirs and global and local master equations. I derive a GME considering narrow wave packets, which are known to properly describe the thermal global steady state. In the same line, I derive a master equation considering broad packets, obtaining an LME; interestingly, considering the LME in the high-temperature limit, I recovered the interaction-time model discarded in chapter 5 because of the spurious performed work, and therefore, one must conclude that it is a useful tool in global systems to describe the transient phenomenon.

Conclusion

In this thesis, I have studied the thermodynamics of systems at the nanoscale from two different perspectives. In the first part, I analysed an experimental device, the *single electron resonator*; this device combines the movement on a nano-oscillator (a suspended carbon nanotube) with the stochastic transport of electrons. The main feature of this device is the strong *capacitive coupling* between the oscillator and the electric flow, generating a rich phenomenology, such as the frequency softening and *self-oscillations*. Due to the coupling with the noisy environment, the single electron transistor losses quantum coherence, and can be described by the Fokker-Planck equation derived in chapter 2.

In chapter 3 I studied the physics of self-oscillations in detail. Self-oscillations can be experimentally detected by observing the hysteresis behaviour in the electric current. In the bistable region, corresponding with the Coulomb diamond border, self-oscillations can start and disappear spontaneously because of thermal and electric fluctuations. In addition, the duration time of the self-oscillations before disappear is several billion times the oscillation period; this timescale separation can be explained using the theoretical model, which makes clear that in order to destroy self-oscillations, a thermal or electrical fluctuation must drive the oscillation below a certain amplitude. Similar results have been observed in the double-dot configuration.

After proving the dynamical model in the self-oscillations experiment, I used it to describe the device thermodynamics, identifying the *heat and work exchange* with the environment and deriving an *expression of the second law* in terms of the positiveness of the entropy production. The main result of this chapter is the analysis of the *information engine*, a working regime in which the chemical work extraction is provided by the information exchange between the oscillator and the electron transport.

After that, in chapter 5 I consider the study of *quantum collisional reservoirs*, a powerful class of models representing the action of a noisy environment on a target quantum system, based on the repeated action of smaller quantum systems (the ancillae) on the target. After explaining the general features of these models, I discuss the characteristics required by the collisional reservoir in order to recover genuine thermal behaviour, i.e. recover thermalization.

Considering the last discussion, in chapter 6 I study two implementations of thermal collisional reservoirs based on the scattering of wave packets. The first implementation, the *Poissonian thermostat*, deals with the spurious quantum coherence by dephasing the repeated interactions, recovering thermal equilibrium. The second implementation considers *narrow wave packets*, which can be proved to create no quantum coherence.

In chapter 7 I apply the collisional thermostat to a qubit chain, acting exclusively on the chain boundary. This allows me to approach the *local vs. global* problem, observing

how the local thermalization of a single qubit is disseminated along the qubit chain reaching global thermalization at very long times.

Perspective

Through the debate that concludes each chapter, I have opened up new questions that may inspire future work. To conclude, I want to highlight the main lines that I believe will be important in the future.

In the first part, I provide a solid thermodynamic framework for studying the single-electron transistor, but there are formal aspects that need to be formalised in the future, for example, the fluctuation theorem involving information flow. However, in my view, the focus should be on the experimental applications of the single-electron resonator: first, to observe the autonomous pumping of electrons in the experiment, evidencing the discovery of the information engine. Second, to fully consider the ability of the device to store and manipulate classical information beyond the Landauer erasure protocol proposed in chapter 4. From the point of view of theory, future discussion must be on the interpretation of thermodynamic processes at extremely low temperatures.

In the second law of the thesis, I proposed some open questions. Indeed, quantum collisional reservoir models based on wave packet scattering are useful tools to study a quantum system under continuous bombardment but fail when the system degenerates. In this limit, an important problem, such as the local vs. global problem explained in chapter 7, is far from being understood.

Appendices

A. Scattering map

In this appendix, I explore the properties of the scattering map that remained outstanding in the main text.

A.1. Transition amplitudes

The scattering map transition amplitudes in Eq. (5.34) were introduced in the main text in terms of the quantities β_{ij}, α_{ik}. In order to obtain them, one must impose the continuity conditions eqs.(5.23) in the scattering states at the boundary points $x = 0, L$, obtaining the following system of equations,

$$\begin{aligned} \sum_j \left(\delta_{ij} + \beta_{ij}\right) |s_j\rangle &= \sum_j \left(\alpha'_{ij} + \beta'_{ij}\right) |s'_j\rangle \,, \\ \sum_j \left(k_{ij}\delta_{ij} - k_{ij}\beta_{ij}\right) |s_j\rangle &= \sum_j \left(k'_{ij}\alpha'_{ij} - k'_{ij}\beta'_{ij}\right) |s'_j\rangle \,, \end{aligned} \tag{A.1}$$

at $x = 0$ and

$$\begin{aligned} \sum_j \left(\alpha'_{ij} e^{ik'_{ij}L} + \beta'_{ij} e^{-ik'_{ij}L}\right) |s'_j\rangle &= \sum_j \alpha''_{ij} e^{ik_{ij}L} |s_j\rangle \,, \\ \sum_j \left(k'_{ij}\alpha'_{ij} e^{ik'_{ij}L} - k'_{ij}\beta'_{ij} e^{-ik'_{ij}L}\right) |s'_j\rangle &= \sum_j k_{ij}\alpha''_{ij} e^{ik_{ij}L} |s_j\rangle \,. \end{aligned} \tag{A.2}$$

At $x = L$. Defining the vectors

$$\begin{cases} |a\rangle = \sum_j \delta_{ij} |s_j\rangle \,, & |b\rangle = \sum_j \beta_{ij} |s_j\rangle \,, \\ |a'\rangle = \sum_j \alpha'_{ij} |s'_j\rangle \,, & |b'\rangle = \sum_j \beta'_{ij} |s'_j\rangle \,, \\ |a''\rangle = \sum_j \alpha''_{ij} |s_j\rangle \,, & \end{cases} \tag{A.3}$$

and the operators $\mathbb{K}_0(E) = \sqrt{2m(E-H)}$, $\mathbb{K}(E) = \sqrt{2m(E-H-V)}$, the continuity equations can be rewritten in a compact fashion as

$$\begin{aligned} |a\rangle + |b\rangle &= |a'\rangle + |b'\rangle \,, \\ \mathbb{K}_0 \left(|a\rangle - |b\rangle\right) &= \mathbb{K} \left(|a'\rangle - |b'\rangle\right) \end{aligned} \tag{A.4}$$

and

$$\begin{aligned} e^{i\mathbb{K}L}\left|a'\right\rangle + e^{-i\mathbb{K}L}\left|b'\right\rangle =& e^{i\mathbb{K}_0 L}\left|a''\right\rangle, \\ \mathbb{K}\left(e^{i\mathbb{K}L}\left|a'\right\rangle - e^{-i\mathbb{K}L}\left|b'\right\rangle\right) =& \mathbb{K}_0 e^{i\mathbb{K}_0 L}\left|a''\right\rangle. \end{aligned} \tag{A.5}$$

Notice that the vectors $|a\rangle$ and $|b\rangle$ represent incoming and outgoing waves, as one can observe in figure A.1 From the last equation

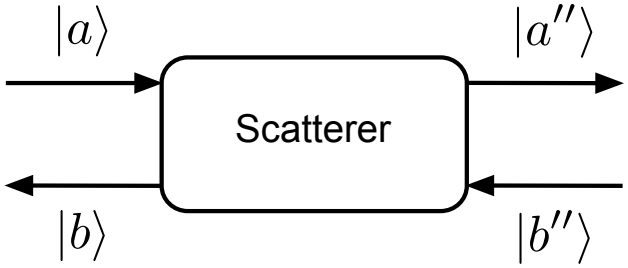

Figure A.1.: Incoming and outgoing waves in the scattering problem. Figure from [Tabanera et al., 2022].

$$e^{i\mathbb{K}L}\left|a'\right\rangle - e^{-i\mathbb{K}L}\left|b'\right\rangle = \mathbb{K}^{-1}\mathbb{K}_0 e^{i\mathbb{K}_0 L}\left|a''\right\rangle, \tag{A.6}$$

concluding

$$2e^{i\mathbb{K}L}\left|a'\right\rangle = \left(\mathbb{I} + \mathbb{K}^{-1}\mathbb{K}_0\right) e^{i\mathbb{K}_0 L}\left|a''\right\rangle \tag{A.7}$$

and

$$2e^{-i\mathbb{K}L}\left|b'\right\rangle = \left(\mathbb{I} - \mathbb{K}^{-1}\mathbb{K}_0\right) e^{i\mathbb{K}_0 L}\left|a''\right\rangle. \tag{A.8}$$

High energy limit

One can obtain the transition amplitudes $\alpha''_{ij}, \beta_{ij}$ directly from the last result using numerical methods. However, it will be useful to consider a very general approximation at high temperatures. In this regime, the kinetic energy of the particles is higher than the internal level spacing of the system, $k^2/2m \gg e_i, e'_i$, then $\mathbb{K}^{-1}\mathbb{K}_0 \simeq \mathbb{I}$. As a consequence, from Eq. (A.8) one obtains $|b'\rangle \sim 0$, and therefore, the outgoing wave is determined as

$$\left|a''\right\rangle = e^{-i\mathbb{K}_0 L} e^{i\mathbb{K}L}\left|a\right\rangle, \tag{A.9}$$

solving the scattering problem in terms of the initial condition $|a\rangle$. In addition, it implies that there are no reflected particles $|b\rangle \sim 0$. The WVO approximation presented in the main text,

$$t_{ij}(k) \simeq \alpha''_{ij} \simeq \left\langle s_j\right| e^{-i\mathbb{K}_0 L} e^{i\mathbb{K}L}\left|s_i\right\rangle \tag{A.10}$$

is obtained under this approximation.

A.2. Computing the scattering map

Expanding Eq. (5.27), one has the explicit expression

$$\mathbb{S}^{ij}_{i'j'}(t) = \int dx \frac{dkdk'}{2\pi} f(k-k_0) f^*(k'-k_0) \left[\alpha''_{i'i}(k)\alpha''^*_{j'j}(k') + \beta_{i'i}(k)\beta^*_{j'j}(k')\right] \\ e^{-i(k'-k)x_0} e^{-i[k_{l'l}(k)-k_{q'q}(k')]x} e^{-i[E_q(k')-E_l(k)]t}. \tag{A.11}$$

This quantity contains both the reflected and the transmitted waves in the intervals $x > L$ and $x < 0$. In the last term, we recognize the Dirac delta property

$$\int dx e^{-i[k_{j'j}(k)-k_{i'i}(k')]x} = 2\pi\delta[k_{i'i}(k) - k_{i'i}(k')]. \tag{A.12}$$

Integrating the delta (see below) in last integral one has

$$\mathbb{S}^{j'i'}_{lq}(t) = \int dk \frac{k_{l'l}(k)}{\kappa} f(k-k_0) f^*(\kappa-k_0) \\ \left[\alpha''_{i'i}(k)\alpha^*_{j'j}(\kappa) + \beta_{i'i}(k)\beta^*_{j'j}(\kappa)\right] e^{-i(\kappa-k)x_0} e^{-i[E_q(\kappa)-E_l(k)]t}, \tag{A.13}$$

with

$$\kappa = \sqrt{k^2 + 2m\left(e_l - e_q + e'_q - e'_l\right)}. \tag{A.14}$$

Finally, rearranging the complex exponentials in terms of $\tau = t - t_0$

$$-(\kappa-k)x_0 - [E_q(\kappa) - E_l(k)]t = \\ = -\Delta_{ql}t_0 - \Delta_{q'l'}\tau - (\kappa - k + \frac{k^2-\kappa^2}{2k_0})x_0, \tag{A.15}$$

and

$$\mathbb{S}^{l'q'}_{lq}(t) = e^{-i\Delta_{ql}t_0} e^{-i\Delta_{q'l'}\tau} \int dk \frac{k_{l'l}(k)}{\kappa} \left[\alpha''_{i'i}(k)\alpha^*_{j'j}(\kappa) + \beta_{i'i}(k)\beta^*_{j'j}(\kappa)\right] \\ f(k-k_0) f^*(\kappa-k_0) e^{-i\left(\kappa-k+\frac{k^2-\kappa^2}{2k_0}\right)x_0}. \tag{A.16}$$

A.2.1. Integration of Dirac delta

In order to integrate the Dirac delta one can consider the identity

$$\delta[k_{iq}(k') - a] = \frac{\delta(k'-\kappa)}{\left|\frac{dk_j}{dk'}(\kappa)\right|}. \tag{A.17}$$

Here κ is the solution of the equation

$$k_{iq}(\kappa) - a = 0, \\ \rightarrow \sqrt{2m\left(\frac{\kappa^2}{2m} + e_q - e_i\right)} = a, \\ \rightarrow \kappa = \sqrt{2m\left(\frac{a^2}{2m} + e_i - e_q\right)}. \tag{A.18}$$

Considering also

$$\frac{dk_{iq}}{dk'} = \frac{k'}{k_{iq}(k')}, \tag{A.19}$$

one has

$$\left|\frac{dk_i}{dk'}(\kappa)\right| = \frac{\kappa}{a}. \tag{A.20}$$

Finally

$$\delta[k_{iq}(k') - a] = \frac{a\delta(k' - \kappa)}{\kappa}. \tag{A.21}$$

B. Scattering of wave packets

The most intuitive way to implement the scattering map is using wave packets as ancillae [Taylor, 2006]. A wave packet is an envelope of plain waves with different linear momentum that travel as a unit. A wave packet initialized in $x_0 < 0$ is the pure state $|\Psi_{k_0}\rangle = \int dx \Psi_{k_0}(x) |x\rangle$ with

$$\Psi_{k_0}(x) = \int f(k - k_0) e^{-ik(x_0 - x)} dk. \tag{B.1}$$

The quantity $f(k - k_0)$ is an arbitrary function peaked around the central momentum k_0 defining the wave packet. If we consider a collisional reservoir whose ancillae $\mathcal{A}$ are wave packets, the central momentum k_0 will be a random variable. The initial density matrix of a single ancilla is $|\Psi_{k_0}\rangle \langle \Psi_{k_0}|$.

The joint state of the ancilla and target system $\mathcal{S}$ before the collision is $|e_j\rangle \otimes |\Psi_{k_0}\rangle$. During the collision, this state evolves under the unitary operator $\exp -iH_{\text{tot}}t$ defined by the Hamiltonian

$$H_{\text{tot}} = \frac{p^2}{2m} + H_{\mathcal{S}} + \chi_{[0,L]}(x)V, \tag{B.2}$$

described in the main text. To describe the evolution of these states, I must write the initial state in terms of the eigenstates of H_{tot}, id est, the scattering states Eq. (5.20),

$$\Psi_{ji} = (\langle x| \otimes \langle \psi_i(k, x)|) (|\Psi_{k0}\rangle \otimes |e_j\rangle) \tag{B.3}$$

The kinematics of the wave packets is determined by the evolution of the last components in each interval $x < 0$, $0 < x < L$ and $x > L$. This is

$$\begin{aligned}
\Psi_{ji}(x < 0, t) &= \int \frac{dk}{\sqrt{2\pi}} f(k - k_0) \left(\delta_{ji} e^{ik_{ji}x} + \beta_{ji} e^{-ik_{ji}x}\right) e^{-i[kx_0 + E_l(k)t]} \\
\Psi_{ji}(0 < x < L, t) &= \int \frac{dk}{\sqrt{2\pi}} f(k - k_0) \left(\alpha'_{ji} e^{ik'_{ji}x} + \beta'_{ji} e^{-ik'_{ji}x}\right) e^{-i[kx_0 + E_l(k)t]} \\
\Psi_{ji}(x > L, t) &= \int \frac{dk}{\sqrt{2\pi}} f(k - k_0) \alpha''_{ji} e^{ik_{ji}x} e^{-i[kx_0 + E_l(k)t]}.
\end{aligned} \tag{B.4}$$

Kinematics of the wave packets

In the following, $\phi(k, x)$ denotes the phase appearing in the complex exponential of each component, and remember that $f(k - k_0)$ is a narrow function packed around $k = k_0$ with width Δk. Notice that each component will vanish that points with many oscillations

inside the Δk interval. In other words, each component in Eq. (B.4) will have a relevant contribution in that x satisfying

$$\left|\frac{d\phi}{dk}(k_0, x)\right| 2\Delta k \gg 1. \tag{B.5}$$

Note that the phase is evaluated in k_0. The maximum of the wave packet appears at the point $\bar{x}$ defined by

$$\frac{d\phi}{dk}(k_0, \bar{x}) = 0. \tag{B.6}$$

This point can be understood as the classical position of the packet in the Euclidean space. If the packet is well localized in space, corresponding to Δk small, we can use the last equation to evaluate the packet contribution in different regions of space independently.

Region $x < 0$

In the interval $x < 0$, the phase associated with the incoming wave $\alpha_{ji} = \delta_{ji}$ in Eq. B.4 is $\phi(k, x) = -kx_0 + k_{ji}(k)x - E_l(k)$, therefore last relation becomes

$$\begin{aligned} \frac{d\phi}{dk}(k_0, \bar{x}) = -x_0 + \frac{dk_{ji}}{dk}\bar{x} - \frac{dE(j,k)}{dk}(k_0)t = 0 \\ \rightarrow \bar{x} = \frac{k_j(k_0)}{k_0}\left(x_0 + \frac{k_0}{m}t\right) \\ \rightarrow \bar{x} = x_0 + \frac{k_0}{m}t. \end{aligned} \tag{B.7}$$

In the second line we used $dk_j/dk = k/k_{ji}$ and $dE/dk = k/m$, and in the third we take $k_j(k)/k = 1$ because of the initial condition $\alpha_{ji} = \delta_{ji}$. Last result represents a packet moving rightward from x_0 with velocity k/m. At time $t_0 = m|x_0|/k_0$ the packet achieves $\bar{x} = 0$ and bounces.

Following the same steps, the phase associated with each β_{ji} gives us

$$\bar{x} = -\frac{k_j(k)}{k_0}\left(x_0 + \frac{k_0}{m}t\right). \tag{B.8}$$

This solution only appears in $x < 0$ only at times $t \leq t_0$, representing the bounced packets in the collision.

Region $x > L$

In the region $x > L$ each transition α''_{ji} have associated the phase $\phi(k, x) = -kx_0 + k_{ji}(k)x - E_l(k)$, therefore

$$\bar{x} = \frac{k_{ji}(k)}{k}\left(x_0 + \frac{k_0}{m}t\right). \tag{B.9}$$

Each solution represents a packet appearing in $x = L$ at different times given by $t_{Lji} = m(L/k_{ji} - x_0/k_0)$. These times depend on the incoming state and the outgoing state. The total time Δt required by a single collision to occur, is then delimited by

$$t_0 < \Delta t < t_{Lji} \tag{B.10}$$

for any value of i, j.

C. Non-equilibrium of the two qubit example

In this section, I explicitly derive some non-equilibrium properties of the example studied in section 6.3.2. The Hamiltonian $H_{\mathcal{S}} + H_{\mathcal{A}} + V$ in the eigenbasis of the free Hamiltonian $H_{\mathcal{S}} + H_{\mathcal{A}}$, $\{|00\rangle_{\mathcal{SA}}, |01\rangle_{\mathcal{SA}}, |10\rangle_{\mathcal{SA}}, |11\rangle_{\mathcal{SA}}\}$, reads

$$H = H_0 + H_{\mathcal{SA}} = \begin{pmatrix} \Omega & 0 & 0 & \xi \\ 0 & \Delta\omega & \Xi & 0 \\ 0 & \Xi & -\Delta\omega & 0 \\ \xi & 0 & 0 & -\Omega \end{pmatrix} \tag{C.1}$$

where $\Omega = \Delta_{\mathcal{S}}/2 + \Delta_{\mathcal{A}}/2$, $\Delta\omega = \Delta_{\mathcal{A}}/2 - \Delta_{\mathcal{S}}/2$, $\Xi = J_x + J_y$, and $\xi = J_x - J_y$. The block structure of this matrix allows only for transitions $|11\rangle_{\mathcal{SA}} \leftrightarrow |00\rangle_{\mathcal{SA}}$ and $|10\rangle_{\mathcal{SA}} \leftrightarrow |01\rangle_{\mathcal{SA}}$. The eigenvalues of H are $\pm\sqrt{\Omega^2 + \xi^2}$ and $\pm\sqrt{\Delta\omega^2 + \Xi^2}$.

If $J_x = J_y$, then $\xi = 0$ and the only permitted transitions are $|10\rangle_{\mathcal{SA}} \leftrightarrow |01\rangle_{\mathcal{SA}}$ and the probability that the system jumps from 0 to 1 in the random-interaction-time model with $\tau_{packet}(p_0) \equiv Lm/p_0$ reads:

$$p(j_{\mathcal{S}} = 0 \to j'_{\mathcal{S}} = 1) = \frac{e^{-\beta\Delta_{\mathcal{A}}/2}}{Z_{\mathcal{A}}} \int_{\sqrt{2me_{max}}}^{\infty} dp_0\, \mu(p_0) \left\langle 0\,1 \right| e^{-i\tau_{packet}(p_0)H} \left| 1\,0 \right\rangle \tag{C.2}$$

whereas

$$p(j_{\mathcal{S}} = 1 \to j'_{\mathcal{S}} = 0) = \frac{1}{Z_{\mathcal{A}}} \int_{\sqrt{2me_{max}}}^{\infty} dp_0\, \mu(p_0) \left\langle 1\,0 \right| e^{-i\tau_{packet}(p_0)H} \left| 0\,1 \right\rangle . \tag{C.3}$$

Then, the ratio verifies

$$\frac{p(j_{\mathcal{S}} = 0 \to j'_{\mathcal{S}} = 1)}{p(j_{\mathcal{S}} = 1 \to j'_{\mathcal{S}} = 0)} = e^{-\beta\Delta_{\mathcal{A}}/2} \tag{C.4}$$

and the system thermalizes in the resonant case, $\Delta_{\mathcal{A}}/2 = \Delta_{\mathcal{S}}/2$.

On the other hand, if $J_x = -J_y$, then $\Xi = 0$ and the only permitted transitions are $|00\rangle_{\mathcal{SA}} \leftrightarrow |11\rangle_{\mathcal{SA}}$. Hence,

$$p(j_{\mathcal{S}} = 1 \to j'_{\mathcal{S}} = 0) = \frac{e^{-\beta\Delta_{\mathcal{A}}/2}}{Z_{\mathcal{A}}} \int_{\sqrt{2me_{max}}}^{\infty} dp_0\, \mu(p_0) \left\langle 0\,0 \right| e^{-i\tau_{packet}(p_0)H} \left| 1\,1 \right\rangle \tag{C.5}$$

whereas

$$p(j_{\mathcal{S}} = 0 \to j'_{\mathcal{S}} = 1) = \frac{1}{Z_{\mathcal{A}}} \int_{\sqrt{2me_{max}}}^{\infty} dp_0\, \mu(p_0) \left\langle 1\,1 \right| e^{-i\tau_{packet}(p_0)H} \left| 0\,0 \right\rangle . \tag{C.6}$$

Now the ratio verifies

$$\frac{p(j_{\mathcal{S}} = 0 \to j'_{\mathcal{S}} = 1)}{p(j_{\mathcal{S}} = 1 \to j'_{\mathcal{S}} = 0)} = e^{\beta \Delta_{\mathcal{A}}/2} \tag{C.7}$$

which indicates that the steady state exhibit a population inversion with negative effective temperature $-\beta$, as shown in fig.6.4.

Bibliography

[Alicki and Horodecki, 2019] Alicki, R. and Horodecki, M. (2019). Information-thermodynamics link revisited. *J. Phys. A: Math. Theor.*, 52(20):204001.

[Allahverdyan et al., 2009] Allahverdyan, A. E., Janzing, D., and Mahler, G. (2009). Thermodynamic efficiency of information and heat flow. *J. Stat. Mech.: Theory Exp.*, 2009(09):P09011.

[Aminzare et al., 2019] Aminzare, Z., Holmes, P., and Srivastava, V. (2019). On Phase Reduction and Time Period of Noisy Oscillators. In *2019 IEEE 58th Conference on Decision and Control (CDC)*, pages 4717–4722. IEEE.

[Ares et al., 2016] Ares, N., Pei, T., Mavalankar, A., Mergenthaler, M., Warner, J. H., Briggs, G. A. D., and Laird, E. A. (2016). Resonant Optomechanics with a Vibrating Carbon Nanotube and a Radio-Frequency Cavity. *Phys. Rev. Lett.*, 117(17):170801.

[Armour et al., 2002] Armour, A. D., Blencowe, M. P., and Schwab, K. C. (2002). Entanglement and Decoherence of a Micromechanical Resonator via Coupling to a Cooper-Pair Box. *Phys. Rev. Lett.*, 88(14):148301.

[Armour et al., 2004] Armour, A. D., Blencowe, M. P., and Zhang, Y. (2004). Classical dynamics of a nanomechanical resonator coupled to a single-electron transistor. *Phys. Rev. B*, 69(12):125313.

[Aspelmeyer et al., 2014] Aspelmeyer, M., Kippenberg, T. J., and Marquardt, F. (2014). Cavity optomechanics. *Rev. Mod. Phys.*, 86(4):1391–1452.

[Aurell et al., 2012] Aurell, E., xn Gawdzki-i1c, K., Mejía-Monasterio, C., Mohayaee, R., and Muratore-Ginanneschi, P. (2012). Refined Second Law of Thermodynamics for Fast Random Processes. *J. Stat. Phys.*, 147(3):487–505.

[Bachtold et al., 2022] Bachtold, A., Moser, J., and Dykman, M. I. (2022). Mesoscopic physics of nanomechanical systems. *arXiv*.

[Barra, 2015] Barra, F. (2015). The thermodynamic cost of driving quantum systems by their boundaries. *Sci. Rep.*, 5(14873):1–10.

[Barzanjeh et al., 2022] Barzanjeh, S., Xuereb, A., Gröblacher, S., Paternostro, M., Regal, C. A., and Weig, E. M. (2022). Optomechanics for quantum technologies. *Nat. Phys.*, 18:15–24.

[Bashkirtseva et al., 2015] Bashkirtseva, I., Ryazanova, T., and Ryashko, L. (2015). Stochastic bifurcations caused by multiplicative noise in systems with hard excitement of auto-oscillations. *Phys. Rev. E*, 92(4):042908.

[Bedingham and Maroney, 2016] Bedingham, D. J. and Maroney, O. J. E. (2016). The thermodynamic cost of quantum operations. *New J. Phys.*, 18(11):113050.

[Bérut et al., 2012] Bérut, A., Arakelyan, A., Petrosyan, A., Ciliberto, S., Dillenschneider, R., and Lutz, E. (2012). Experimental verification of Landauer's principle linking information and thermodynamics. *Nature*, 483(7388):187–189.

[Bennett, 1982] Bennett, C. H. (1982). The thermodynamics of computation—a review. *Int. J. Theor. Phys.*, 21(12):905–940.

[Bennett, 2003] Bennett, C. H. (2003). Notes on Landauer's principle, reversible computation, and Maxwell's Demon. *Studies in History and Philosophy of Science Part B: Studies in History and Philosophy of Modern Physics*, 34(3):501–510.

[Bennett et al., 1996] Bennett, C. H., DiVincenzo, D. P., Smolin, J. A., and Wootters, W. K. (1996). Mixed-state entanglement and quantum error correction. *Phys. Rev. A*, 54(5):3824–3851.

[Bennett and Clerk, 2006] Bennett, S. D. and Clerk, A. A. (2006). Laser-like instabilities in quantum nano-electromechanical systems. *Phys. Rev. B*, 74(20):201301.

[Bennett et al., 2010] Bennett, S. D., Cockins, L., Miyahara, Y., Grütter, P., and Clerk, A. A. (2010). Strong Electromechanical Coupling of an Atomic Force Microscope Cantilever to a Quantum Dot. *Phys. Rev. Lett.*, 104(1):017203.

[Benyamini et al., 2014] Benyamini, A., Hamo, A., Kusminskiy, S. V., von Oppen, F., and Ilani, S. (2014). Real-space tailoring of the electron–phonon coupling in ultraclean nanotube mechanical resonators. *Nat. Phys.*, 10(2):151–156.

[Bezryadin et al., 1997] Bezryadin, A., Dekker, C., and Schmid, G. (1997). Electrostatic trapping of single conducting nanoparticles between nanoelectrodes. *Appl. Phys. Lett.*, 71(9):1273–1275.

[Blanter et al., 2004] Blanter, Ya. M., Usmani, O., and Nazarov, Yu. V. (2004). Single-Electron Tunneling with Strong Mechanical Feedback. *Phys. Rev. Lett.*, 93(13):136802.

[Breuer et al., 2002] Breuer, H.-P., Petruccione, F., et al. (2002). *The theory of open quantum systems*. Oxford University Press on Demand.

[Brillouin, 2013] Brillouin, L. (2013). *Science and information theory*. Courier Corporation.

[Bulnes Cuetara et al., 2011] Bulnes Cuetara, G., Esposito, M., and Gaspard, P. (2011). Fluctuation theorems for capacitively coupled electronic currents. *Phys. Rev. B*, 84(16):165114.

[Campbell and Vacchini, 2021] Campbell, S. and Vacchini, B. (2021). Collision models in open system dynamics: A versatile tool for deeper insights? *Europhys. Lett.*, 133(6):60001.

[Camposeo et al., 2001] Camposeo, A., Piombini, A., Cervelli, F., Tantussi, F., Fuso, F., and Arimondo, E. (2001). A cold cesium atomic beam produced out of a pyramidal funnel. *Opt. Commun.*, 200(1):231–239.

[Cattaneo et al., 2019] Cattaneo, M., Giorgi, G. L., Maniscalco, S., and Zambrini, R. (2019). Local versus global master equation with common and separate baths: superiority of the global approach in partial secular approximation. *New J. Phys.*, 21(11):113045.

[Caves, 1986] Caves, C. M. (1986). Quantum mechanics of measurements distributed in time. A path-integral formulation. *Phys. Rev. D*, 33(6):1643–1665.

[Caves and Milburn, 1987] Caves, C. M. and Milburn, G. J. (1987). Quantum-mechanical model for continuous position measurements. *Phys. Rev. A*, 36(12):5543–5555.

[Chiang et al., 2017] Chiang, K.-H., Lee, C.-L., Lai, P.-Y., and Chen, Y.-F. (2017). Electrical autonomous Brownian gyrator. *Phys. Rev. E*, 96(3):032123.

[Ciccarello et al., 2022] Ciccarello, F., Lorenzo, S., Giovannetti, V., and Palma, G. M. (2022). Quantum collision models: Open system dynamics from repeated interactions. *Phys. Rep.*, 954:1–70.

[Ciliberto et al., 2013] Ciliberto, S., Imparato, A., Naert, A., and Tanase, M. (2013). Heat Flux and Entropy Produced by Thermal Fluctuations. *Phys. Rev. Lett.*, 110(18):180601.

[Ciliberto et al., 2010] Ciliberto, S., Joubaud, S., and Petrosyan, A. (2010). Fluctuations in out-of-equilibrium systems: from theory to experiment. *J. Stat. Mech.: Theory Exp.*, 2010(12):P12003.

[Cirac and Zoller, 2000] Cirac, J. I. and Zoller, P. (2000). A scalable quantum computer with ions in an array of microtraps. *Nature*, 404:579–581.

[Claudon et al., 2010] Claudon, J., Bleuse, J., Malik, N. S., Bazin, M., Jaffrennou, P., Gregersen, N., Sauvan, C., Lalanne, P., and Gérard, J.-M. (2010). A highly efficient single-photon source based on a quantum dot in a photonic nanowire. *Nat. Photonics*, 4:174–177.

[Clausius, 1850] Clausius, R. (1850). Ueber die bewegende kraft der wärme und die gesetze, welche sich daraus für die wärmelehre selbst ableiten lassen. *Annalen der Physik*, 155(3):368–397.

[Clausius, 1865] Clausius, R. (1865). *Ueber verschiedene für die Anwendung bequeme Formen der Hauptgleichungen der mechanischen Wärmetheorie: vorgetragen in der naturforsch. Gesellschaft den 24. April 1865.* éditeur inconnu.

[Clerk et al., 2020] Clerk, A. A., Lehnert, K. W., Bertet, P., Petta, J. R., and Nakamura, Y. (2020). Hybrid quantum systems with circuit quantum electrodynamics. *Nat. Phys.*, 16:257–267.

[Cover et al., 1991] Cover, T. M., Thomas, J. A., et al. (1991). Entropy, relative entropy and mutual information. *Elements of information theory*, 2(1):12–13.

[De Chiara et al., 2018] De Chiara, G., Landi, G., Hewgill, A., Reid, B., Ferraro, A., Roncaglia, A. J., and Antezza, M. (2018). Reconciliation of quantum local master equations with thermodynamics. *New J. Phys.*, 20(11):113024.

[Degen et al., 2009] Degen, C. L., Poggio, M., Mamin, H. J., Rettner, C. T., and Rugar, D. (2009). Nanoscale magnetic resonance imaging. *Proc. Natl. Acad. Sci. U.S.A.*, 106(5):1313–1317.

[Dunlop et al., 2023] Dunlop, J., Cerisola, F., Tabanera-Bravo, J., and Anders, J. (2023). Multipurpose Quantum Thermodynamic Operations. *arXiv*.

[Earman and Norton, 1999] Earman, J. and Norton, J. D. (1999). Exorcist xiv: The wrath of maxwell's demon. part ii. from szilard to landauer and beyond. *Studies in History and Philosophy of Science Part B: Studies in History and Philosophy of Modern Physics*, 30(1):1–40.

[Eckmann and Mejía-Monasterio, 2022] Eckmann, J.-P. and Mejía-Monasterio, C. (2022). Revisiting the Monge Problem in the Landauer Limit. *Ann. Henri Poincaré*, pages 1–15.

[Ehrich et al., 2020] Ehrich, J., Esposito, M., Barra, F., and Parrondo, J. M. (2020). Micro-reversibility and thermalization with collisional baths. *Physica A: Statistical Mechanics and its Applications*, 552:122108.

[Eichler et al., 2011] Eichler, A., Chaste, J., Moser, J., and Bachtold, A. (2011). Parametric Amplification and Self-Oscillation in a Nanotube Mechanical Resonator. *Nano Lett.*, 11(7):2699–2703.

[Einstein, 1905] Einstein, A. (1905). Über die von der molekularkinetischen theorie der wärme geforderte bewegung von in ruhenden flüssigkeiten suspendierten teilchen. *Annalen der physik*, 4.

[Elouard et al., 2015] Elouard, C., Richard, M., and Auffèves, A. (2015). Reversible work extraction in a hybrid opto-mechanical system. *New J. Phys.*, 17(5):055018.

[Esposito and Schaller, 2012] Esposito, M. and Schaller, G. (2012). Stochastic thermodynamics for "Maxwell demon" feedbacks. *Europhys. Lett.*, 99(3):30003.

[Esposito and Van den Broeck, 2010] Esposito, M. and Van den Broeck, C. (2010). Three faces of the second law. I. Master equation formulation. *Phys. Rev. E*, 82(1):011143.

[Ficek et al., 1987] Ficek, Z., Tanaś, R., and Kielich, S. (1987). Quantum beats and superradiant effects in the spontaneous emission from two nonidentical atoms. *Physica A*, 146(3):452–482.

[Filippov et al., 2020] Filippov, S. N., Semin, G. N., and Pechen, A. N. (2020). Quantum master equations for a system interacting with a quantum gas in the low-density limit and for the semiclassical collision model. *Phys. Rev. A*, 101(1):012114.

[Filliger and Reimann, 2007] Filliger, R. and Reimann, P. (2007). Brownian Gyrator: A Minimal Heat Engine on the Nanoscale. *Phys. Rev. Lett.*, 99(23):230602.

[Fogedby and Imparato, 2018] Fogedby, H. C. and Imparato, A. (2018). Autonomous quantum rotator. *Europhys. Lett.*, 122(1):10006.

[Fokker, 1914] Fokker, A. D. (1914). Die mittlere energie rotierender elektrischer dipole im strahlungsfeld. *Annalen der Physik*, 348(5):810–820.

[Funo et al., 2019] Funo, K., Ueda, M., and Sagawa, T. (2019). Quantum Fluctuation Theorems. In *Thermodynamics in the Quantum Regime*, pages 249–273. Springer, Cham, Switzerland.

[Galindo and Pascual, 2012] Galindo, A. and Pascual, P. (2012). *Quantum mechanics I*. Springer Science & Business Media.

[Gallego et al., 2014] Gallego, R., Riera, A., and Eisert, J. (2014). Thermal machines beyond the weak coupling regime. *New J. Phys.*, 16(12):125009.

[Gardiner et al., 1985] Gardiner, C. W. et al. (1985). *Handbook of stochastic methods*, volume 3. springer Berlin.

[Geusic et al., 1967] Geusic, J. E., Schulz-DuBios, E. O., and Scovil, H. E. D. (1967). Quantum Equivalent of the Carnot Cycle. *Phys. Rev.*, 156(2):343–351.

[Giorgi et al., 2013] Giorgi, G. L., Plastina, F., Francica, G., and Zambrini, R. (2013). Spontaneous synchronization and quantum correlation dynamics of open spin systems. *Phys. Rev. A*, 88(4):042115.

[Gorelik et al., 1998] Gorelik, L. Y., Isacsson, A., Voinova, M. V., Kasemo, B., Shekhter, R. I., and Jonson, M. (1998). Shuttle Mechanism for Charge Transfer in Coulomb Blockade Nanostructures. *Phys. Rev. Lett.*, 80(20):4526–4529.

[Gorini et al., 1976] Gorini, V., Kossakowski, A., and Sudarshan, E. C. G. (1976). Completely positive dynamical semigroups of N-level systems. *J. Math. Phys.*, 17(5):821–825.

[Gross and Haroche, 1982] Gross, M. and Haroche, S. (1982). Superradiance: An essay on the theory of collective spontaneous emission. *Phys. Rep.*, 93(5):301–396.

[Guarnieri et al., 2020] Guarnieri, G., Morrone, D., Çakmak, B., Plastina, F., and Campbell, S. (2020). Non-equilibrium steady-states of memoryless quantum collision models. *Phys. Lett. A*, 384(24):126576.

[Hackermüller et al., 2004] Hackermüller, L., Hornberger, K., Brezger, B., Zeilinger, A., and Arndt, M. (2004). Decoherence of matter waves by thermal emission of radiation. *Nature*, 427:711–714.

[Hammerer et al., 2009] Hammerer, K., Wallquist, M., Genes, C., Ludwig, M., Marquardt, F., Treutlein, P., Zoller, P., Ye, J., and Kimble, H. J. (2009). Strong Coupling of a Mechanical Oscillator and a Single Atom. *Phys. Rev. Lett.*, 103(6):063005.

[Hanson et al., 2007] Hanson, R., Kouwenhoven, L. P., Petta, J. R., Tarucha, S., and Vandersypen, L. M. K. (2007). Spins in few-electron quantum dots. *Rev. Mod. Phys.*, 79(4):1217–1265.

[Haroche and Raimond, 2006] Haroche, S. and Raimond, J.-M. (2006). *Exploring the quantum: atoms, cavities, and photons*. Oxford university press.

[Heinze et al., 2003] Heinze, S., Radosavljević, M., Tersoff, J., and Avouris, Ph. (2003). Unexpected scaling of the performance of carbon nanotube Schottky-barrier transistors. *Phys. Rev. B*, 68(23):235418.

[Heinze et al., 2002] Heinze, S., Tersoff, J., Martel, R., Derycke, V., Appenzeller, J., and Avouris, Ph. (2002). Carbon Nanotubes as Schottky Barrier Transistors. *Phys. Rev. Lett.*, 89(10):106801.

[Hillery et al., 1984] Hillery, M., O'Connell, R. F., Scully, M. O., and Wigner, E. P. (1984). Distribution functions in physics: Fundamentals. *Phys. Rep.*, 106(3):121–167.

[Hofer et al., 2017] Hofer, P. P., Perarnau-Llobet, M., Miranda, L. D. M., Haack, G., Silva, R., Brask, J. B., and Brunner, N. (2017). Markovian master equations for quantum thermal machines: local versus global approach. *New J. Phys.*, 19(12):123037.

[Hornberger and Sipe, 2003] Hornberger, K. and Sipe, J. E. (2003). Collisional decoherence reexamined. *Phys. Rev. A*, 68(1):012105.

[Hornberger et al., 2003] Hornberger, K., Uttenthaler, S., Brezger, B., Hackermüller, L., Arndt, M., and Zeilinger, A. (2003). Collisional Decoherence Observed in Matter Wave Interferometry. *Phys. Rev. Lett.*, 90(16):160401.

[Horowitz and Esposito, 2014] Horowitz, J. M. and Esposito, M. (2014). Thermodynamics with Continuous Information Flow. *Phys. Rev. X*, 4(3):031015.

[Horowitz and Parrondo, 2011] Horowitz, J. M. and Parrondo, J. M. R. (2011). Thermodynamic reversibility in feedback processes. *Europhys. Lett.*, 95(1):10005.

[Hünenberger, 2005] Hünenberger, P. H. (2005). Thermostat Algorithms for Molecular Dynamics Simulations. In *Advanced Computer Simulation: Approaches for Soft Matter Sciences I*, pages 105–149. Springer, Berlin, Germany.

[Hüttel et al., 2010] Hüttel, A. K., Meerwaldt, H. B., Steele, G. A., Poot, M., Witkamp, B., Kouwenhoven, L. P., and van der Zant, H. S. J. (2010). Single electron tunnelling through high-Q single-wall carbon nanotube NEMS resonators. *Phys. Status Solidi B*, 247(11-12):2974–2979.

[Isacsson et al., 1998] Isacsson, A., Gorelik, L. Y., Voinova, M. V., Kasemo, B., Shekhter, R. I., and Jonson, M. (1998). Shuttle instability in self-assembled Coulomb blockade nanostructures. *Physica B*, 255(1):150–163.

[Ito, 1944] Ito, K. (1944). 109. Stochastic Integral. *Proceedings of the Imperial Academy*, 20(8):519–524.

[Jacob et al., 2021] Jacob, S. L., Esposito, M., Parrondo, J. M. R., and Barra, F. (2021). Thermalization Induced by Quantum Scattering. *PRX Quantum*, 2(2):020312.

[Jacob et al., 2022] Jacob, S. L., Esposito, M., Parrondo, J. M. R., and Barra, F. (2022). Quantum scattering as a work source. *Quantum*, 6:750.

[Jacobs, 2009] Jacobs, K. (2009). Second law of thermodynamics and quantum feedback control: Maxwell's demon with weak measurements. *Phys. Rev. A*, 80(1):012322.

[Jenkins, 2013] Jenkins, A. (2013). Self-oscillation. *Phys. Rep.*, 525(2):167–222.

[Kewming and Shrapnel, 2022] Kewming, M. J. and Shrapnel, S. (2022). Entropy production and fluctuation theorems in a continuously monitored optical cavity at zero temperature. *Quantum*, 6:685.

[Khivrich et al., 2019] Khivrich, I., Clerk, A. A., and Ilani, S. (2019). Nanomechanical pump–probe measurements of insulating electronic states in a carbon nanotube. *Nat. Nanotechnol.*, 14:161–167.

[Kindermann, 2011] Kindermann, M. (2011). Shuttle transport for single electrons. *Nat. Nanotechnol.*, 6:691–692.

[Knott and Tait, 1911] Knott, C. G. and Tait, P. G. (1911). *Life and Scientific Work of Peter Guthrie Tait: Cargill Gilston Knott*. University Press.

[Koenig et al., 2008] Koenig, D. R., Weig, E. M., and Kotthaus, J. P. (2008). Ultrasonically driven nanomechanical single-electron shuttle. *Nat. Nanotechnol.*, 3:482–485.

[Kolkowitz et al., 2012] Kolkowitz, S., Jayich, A. C. B., Unterreithmeier, Q. P., Bennett, S. D., Rabl, P., Harris, J. G. E., and Lukin, M. D. (2012). Coherent Sensing of a Mechanical Resonator with a Single-Spin Qubit. *Science*, 335(6076):1603–1606.

[Korotkov and Nazarov, 1991] Korotkov, A. N. and Nazarov, Yu. V. (1991). Single-electron tunneling coexisting with the barrier suppression. *Physica B*, 173(3):217–222.

[Koski et al., 2013] Koski, J. V., Sagawa, T., Saira, O.-P., Yoon, Y., Kutvonen, A., Solinas, P., Möttönen, M., Ala-Nissila, T., and Pekola, J. P. (2013). Distribution of entropy production in a single-electron box. *Nat. Phys.*, 9(10):644–648.

[Kosloff, 2013] Kosloff, R. (2013). Quantum Thermodynamics: A Dynamical Viewpoint. *Entropy*, 15(6):2100–2128.

[Kramers, 1940] Kramers, H. A. (1940). Brownian motion in a field of force and the diffusion model of chemical reactions. *Physica*, 7(4):284–304.

[Küng et al., 2012] Küng, B., Rössler, C., Beck, M., Marthaler, M., Golubev, D. S., Utsumi, Y., Ihn, T., and Ensslin, K. (2012). Irreversibility on the Level of Single-Electron Tunneling. *Phys. Rev. X*, 2(1):011001.

[Laird et al., 2012] Laird, E. A., Pei, F., Tang, W., Steele, G. A., and Kouwenhoven, L. P. (2012). A High Quality Factor Carbon Nanotube Mechanical Resonator at 39 GHz. *Nano Lett.*, 12(1):193–197.

[Landauer, 1961] Landauer, R. (1961). Irreversibility and heat generation in the computing process. *IBM journal of research and development*, 5(3):183–191.

[Landauer et al., 1991] Landauer, R. et al. (1991). Information is physical. *Physics Today*, 44(5):23–29.

[Langevin, 1908] Langevin, P. (1908). Sur la théorie du mouvement brownien. *Compt. Rendus*, 146:530–533.

[Lin et al., 2018] Lin, J., Guha, S., and Ramanathan, S. (2018). Vanadium Dioxide Circuits Emulate Neurological Disorders. *Front. Neurosci.*, 12.

[Lindblad, 1976] Lindblad, G. (1976). On the generators of quantum dynamical semigroups. *Commun. Math. Phys.*, 48(2):119–130.

[Liphardt et al., 2002] Liphardt, J., Dumont, S., Smith, S. B., Tinoco, Jr., I., and Bustamante, C. (2002). Equilibrium Information from Nonequilibrium Measurements in an Experimental Test of Jarzynski's Equality. *Science*, 296(5574):1832–1835.

[Maitland et al., 2015] Maitland, M., Grosskinsky, S., and Harris, R. J. (2015). Large deviation analysis of a simple information engine. *Phys. Rev. E*, 92(5):052136.

[Manzano et al., 2022] Manzano, G., Parrondo, J. M. R., and Landi, G. T. (2022). Non-Abelian Quantum Transport and Thermosqueezing Effects. *PRX Quantum*, 3(1):010304.

[Manzano et al., 2020] Manzano, G., Sánchez, R., Silva, R., Haack, G., Brask, J. B., Brunner, N., and Potts, P. P. (2020). Hybrid thermal machines: Generalized thermodynamic resources for multitasking. *Phys. Rev. Res.*, 2(4):043302.

[Marchegiani et al., 2016] Marchegiani, G., Virtanen, P., Giazotto, F., and Campisi, M. (2016). Self-Oscillating Josephson Quantum Heat Engine. *Phys. Rev. Appl.*, 6(5):054014.

[Markov, 2014] Markov, I. L. (2014). Limits on fundamental limits to computation. *Nature*, 512(7513):147–154.

[Matveev and Andreev, 2002] Matveev, K. A. and Andreev, A. V. (2002). Thermopower of a single-electron transistor in the regime of strong inelastic cotunneling. *Phys. Rev. B*, 66(4):045301.

[Maxwell, 1990] Maxwell, J. C. (1990). *The Scientific Letters and Papers of James Clerk Maxwell: Volume 1, 1846-1862*, volume 3. CUP Archive.

[Mayrhofer et al., 2021] Mayrhofer, R. D., Elouard, C., Splettstoesser, J., and Jordan, A. N. (2021). Stochastic thermodynamic cycles of a mesoscopic thermoelectric engine. *Phys. Rev. B*, 103(7):075404.

[Meerwaldt et al., 2012] Meerwaldt, H. B., Labadze, G., Schneider, B. H., Taspinar, A., Blanter, Ya. M., van der Zant, H. S. J., and Steele, G. A. (2012). Probing the charge of a quantum dot with a nanomechanical resonator. *Phys. Rev. B*, 86(11):115454.

[Mehboudi et al., 2019] Mehboudi, M., Sanpera, A., and Correa, L. A. (2019). Thermometry in the quantum regime: recent theoretical progress. *J. Phys. A: Math. Theor.*, 52(30):303001.

[Mejía-Monasterio et al., 2005] Mejía-Monasterio, C., Prosen, T., and Casati, G. (2005). Fourier's law in a quantum spin chain and the onset of quantum chaos. *Europhys. Lett.*, 72(4):520.

[Micadei et al., 2020] Micadei, K., Landi, G. T., and Lutz, E. (2020). Quantum Fluctuation Theorems beyond Two-Point Measurements. *Phys. Rev. Lett.*, 124(9):090602.

[Micchi et al., 2015] Micchi, G., Avriller, R., and Pistolesi, F. (2015). Mechanical Signatures of the Current Blockade Instability in Suspended Carbon Nanotubes. *Phys. Rev. Lett.*, 115(20):206802.

[Micchi et al., 2016] Micchi, G., Avriller, R., and Pistolesi, F. (2016). Electromechanical transition in quantum dots. *Phys. Rev. B*, 94(12):125417.

[Miller et al., 2020] Miller, H. J. D., Guarnieri, G., Mitchison, M. T., and Goold, J. (2020). Quantum Fluctuations Hinder Finite-Time Information Erasure near the Landauer Limit. *Phys. Rev. Lett.*, 125(16):160602.

[Moser et al., 2014] Moser, J., Eichler, A., Güttinger, J., Dykman, M. I., and Bachtold, A. (2014). Nanotube mechanical resonators with quality factors of up to 5 million. *Nat. Nanotechnol.*, 9:1007–1011.

[Moser et al., 2013] Moser, J., Güttinger, J., Eichler, A., Esplandiu, M. J., Liu, D. E., Dykman, M. I., and Bachtold, A. (2013). Ultrasensitive force detection with a nanotube mechanical resonator. *Nat. Nanotechnol.*, 8:493–496.

[Nazarov and Blanter, 2009] Nazarov, Y. V. and Blanter, Y. M. (2009). *Quantum transport: introduction to nanoscience*. Cambridge university press.

[Nord et al., 2002] Nord, T., Gorelik, L. Y., Shekhter, R. I., and Jonson, M. (2002). Electromechanics of charge shuttling in dissipative nanostructures. *Phys. Rev. B*, 65(16):165312.

[O'Connor et al., 2021] O'Connor, E., Vacchini, B., and Campbell, S. (2021). Stochastic Collisional Quantum Thermometry. *Entropy*, 23(12):1634.

[Palomaki et al., 2013] Palomaki, T. A., Harlow, J. W., Teufel, J. D., Simmonds, R. W., and Lehnert, K. W. (2013). Coherent state transfer between itinerant microwave fields and a mechanical oscillator. *Nature*, 495:210–214.

[Parrondo et al., 2015] Parrondo, J. M. R., Horowitz, J. M., and Sagawa, T. (2015). Thermodynamics of information. *Nature Physics*, 11(2). Number: 2 Publisher: Nature Publishing Group.

[Perarnau-Llobet et al., 2017] Perarnau-Llobet, M., Bäumer, E., Hovhannisyan, K. V., Huber, M., and Acin, A. (2017). No-Go Theorem for the Characterization of Work Fluctuations in Coherent Quantum Systems. *Phys. Rev. Lett.*, 118(7):070601.

[Pistolesi et al., 2021] Pistolesi, F., Cleland, A. N., and Bachtold, A. (2021). Proposal for a Nanomechanical Qubit. *Phys. Rev. X*, 11(3):031027.

[Planck, 1917] Planck, V. (1917). Über einen satz der statistischen dynamik und seine erweiterung in der quantentheorie. *Sitzungberichte der*.

[Rabl et al., 2009] Rabl, P., Cappellaro, P., Dutt, M. V. G., Jiang, L., Maze, J. R., and Lukin, M. D. (2009). Strong magnetic coupling between an electronic spin qubit and a mechanical resonator. *Phys. Rev. B*, 79(4):041302.

[Rau, 1963] Rau, J. (1963). Relaxation Phenomena in Spin and Harmonic Oscillator Systems. *Phys. Rev.*, 129(4):1880–1888.

[Ray and Crutchfield, 2023] Ray, K. J. and Crutchfield, J. P. (2023). Gigahertz Sub-Landauer Momentum Computing. *Phys. Rev. Appl.*, 19(1):014049.

[Reed et al., 2017] Reed, A. P., Mayer, K. H., Teufel, J. D., Burkhart, L. D., Pfaff, W., Reagor, M., Sletten, L., Ma, X., Schoelkopf, R. J., Knill, E., and Lehnert, K. W. (2017). Faithful conversion of propagating quantum information to mechanical motion. *Nat. Phys.*, 13:1163–1167.

[Rempe et al., 1990] Rempe, G., Schmidt-Kaler, F., and Walther, H. (1990). Observation of sub-Poissonian photon statistics in a micromaser. *Phys. Rev. Lett.*, 64(23):2783–2786.

[Rivas and Huelga,] Rivas, A. and Huelga, S. F. *Open Quantum Systems*. Springer, Berlin, Germany.

[Rocco et al., 2022] Rocco, R., del Valle, J., Navarro, H., Salev, P., Schuller, I. K., and Rozenberg, M. (2022). Exponential Escape Rate of Filamentary Incubation in Mott Spiking Neurons. *Phys. Rev. Appl.*, 17(2):024028.

[Rodrigues et al., 2019] Rodrigues, F. L. S., De Chiara, G., Paternostro, M., and Landi, G. T. (2019). Thermodynamics of Weakly Coherent Collisional Models. *Phys. Rev. Lett.*, 123(14):140601.

[Rosinberg and Horowitz, 2016] Rosinberg, M. L. and Horowitz, J. M. (2016). Continuous information flow fluctuations. *Europhys. Lett.*, 116(1):10007.

[Roulet et al., 2017] Roulet, A., Nimmrichter, S., Arrazola, J. M., Seah, S., and Scarani, V. (2017). Autonomous rotor heat engine. *Phys. Rev. E*, 95(6):062131.

[Rubio et al., 2021] Rubio, J., Anders, J., and Correa, L. A. (2021). Global Quantum Thermometry. *Phys. Rev. Lett.*, 127(19):190402.

[Rutten et al., 2009] Rutten, B., Esposito, M., and Cleuren, B. (2009). Reaching optimal efficiencies using nanosized photoelectric devices. *Phys. Rev. B*, 80(23):235122.

[Sánchez and Büttiker, 2011] Sánchez, R. and Büttiker, M. (2011). Optimal energy quanta to current conversion. *Phys. Rev. B*, 83(8):085428.

[Sánchez et al., 2010] Sánchez, R., López, R., Sánchez, D., and Büttiker, M. (2010). Mesoscopic Coulomb Drag, Broken Detailed Balance, and Fluctuation Relations. *Phys. Rev. Lett.*, 104(7):076801.

[Sachs, 1987] Sachs, R. G. (1987). *The physics of time reversal*. University of Chicago Press.

[Sagawa and Ueda, 2010] Sagawa, T. and Ueda, M. (2010). Generalized Jarzynski Equality under Nonequilibrium Feedback Control. *Phys. Rev. Lett.*, 104(9):090602.

[Sagawa and Ueda, 2012] Sagawa, T. and Ueda, M. (2012). Nonequilibrium thermodynamics of feedback control. *Phys. Rev. E*, 85(2):021104.

[Saira et al., 2012] Saira, O.-P., Yoon, Y., Tanttu, T., Möttönen, M., Averin, D. V., and Pekola, J. P. (2012). Test of the Jarzynski and Crooks Fluctuation Relations in an Electronic System. *Phys. Rev. Lett.*, 109(18):180601.

[Sakurai and Napolitano, 2014] Sakurai, J. and Napolitano, J. (2014). Modern quantum mechanics. 2-nd edition. *Person New International edition*, page 35.

[Sayrin et al., 2011] Sayrin, C., Dotsenko, I., Zhou, X., Peaudecerf, B., Rybarczyk, T., Gleyzes, S., Rouchon, P., Mirrahimi, M., Amini, H., Brune, M., Raimond, J.-M., and Haroche, S. (2011). Real-time quantum feedback prepares and stabilizes photon number states. *Nature*, 477:73–77.

[Sazonova et al., 2004] Sazonova, V., Yaish, Y., Üstünel, H., Roundy, D., Arias, T. A., and McEuen, P. L. (2004). A tunable carbon nanotube electromechanical oscillator. *Nature*, 431(7006):284–287.

[Scali et al., 2021] Scali, S., Anders, J., and Correa, L. A. (2021). Local master equations bypass the secular approximation. *Quantum*, 5:451.

[Schaller et al., 2010] Schaller, G., Kießlich, G., and Brandes, T. (2010). Low-dimensional detector model for full counting statistics: Trajectories, back action, and fidelity. *Phys. Rev. B*, 82(4):041303.

[Schmid et al., 2012] Schmid, D. R., Stiller, P. L., Strunk, C., and Hüttel, A. K. (2012). Magnetic damping of a carbon nanotube nano-electromechanical resonator. *New J. Phys.*, 14(8):083024.

[Schmid et al., 2015] Schmid, D. R., Stiller, P. L., Strunk, Ch., and Hüttel, A. K. (2015). Liquid-induced damping of mechanical feedback effects in single electron tunneling through a suspended carbon nanotube. *Appl. Phys. Lett.*, 107(12):123110.

[Schneider et al., 2012] Schneider, B. H., Etaki, S., van der Zant, H. S. J., and Steele, G. A. (2012). Coupling carbon nanotube mechanics to a superconducting circuit. *Sci. Rep.*, 2(599):1–5.

[Scovil and Schulz-DuBois, 1959] Scovil, H. E. D. and Schulz-DuBois, E. O. (1959). Three-Level Masers as Heat Engines. *Phys. Rev. Lett.*, 2(6):262–263.

[Seah et al., 2019] Seah, S., Nimmrichter, S., Grimmer, D., Santos, J. P., Scarani, V., and Landi, G. T. (2019). Collisional Quantum Thermometry. *Phys. Rev. Lett.*, 123(18):180602.

[Seifert, 2005] Seifert, U. (2005). Entropy Production along a Stochastic Trajectory and an Integral Fluctuation Theorem. *Phys. Rev. Lett.*, 95(4):040602.

[Sekimoto, 1998] Sekimoto, K. (1998). Langevin Equation and Thermodynamics. *Prog. Theor. Phys.*, 130:17–27.

[Sekimoto, 2010] Sekimoto, K. (2010). *Stochastic energetics*, volume 799. Springer.

[Serra-Garcia et al., 2016] Serra-Garcia, M., Foehr, A., Molerón, M., Lydon, J., Chong, C., and Daraio, C. (2016). Mechanical Autonomous Stochastic Heat Engine. *Phys. Rev. Lett.*, 117(1):010602.

[Shannon, 1948] Shannon, C. E. (1948). A mathematical theory of communication. *Bell System Technical Journal*, 27(3):379–423.

[Shiraishi and Sagawa, 2015] Shiraishi, N. and Sagawa, T. (2015). Fluctuation theorem for partially masked nonequilibrium dynamics. *Phys. Rev. E*, 91(1):012130.

[Smoluchowski, 1927] Smoluchowski, M. (1927). Experimentell nachweisbare, der üblichen thermodynamik widersprechende molekularphänomene. *Pisma Mariana Smoluchowskiego*, 2(1):226–251.

[Sommerfeld, 1916] Sommerfeld, A. (1916). Zur Quantentheorie der Spektrallinien. *Ann. Phys.*, 356(17):1–94.

[Stoliar et al., 2021] Stoliar, P., Schneegans, O., and Rozenberg, M. J. (2021). Implementation of a Minimal Recurrent Spiking Neural Network in a Solid-State Device. *Phys. Rev. Appl.*, 16(3):034030.

[Strasberg, 2022] Strasberg, P. (2022). *Quantum Stochastic Thermodynamics: Foundations and Selected Applications*. Oxford University Press.

[Strasberg et al., 2013] Strasberg, P., Schaller, G., Brandes, T., and Esposito, M. (2013). Thermodynamics of a Physical Model Implementing a Maxwell Demon. *Phys. Rev. Lett.*, 110(4):040601.

[Strasberg et al., 2017] Strasberg, P., Schaller, G., Brandes, T., and Esposito, M. (2017). Quantum and Information Thermodynamics: A Unifying Framework Based on Repeated Interactions. *Phys. Rev. X*, 7(2):021003.

[Strasberg et al., 2021] Strasberg, P., Wächtler, C. W., and Schaller, G. (2021). Autonomous Implementation of Thermodynamic Cycles at the Nanoscale. *Phys. Rev. Lett.*, 126(18):180605.

[Szilard, 1929] Szilard, L. (1929). Über die entropieverminderung in einem thermodynamischen system bei eingriffen intelligenter wesen. *Zeitschrift für Physik*, 53(11-12):840–856.

[Tabanera et al., 2022] Tabanera, J., Luque, I., Jacob, S. L., Esposito, M., Barra, F., and Parrondo, J. M. R. (2022). Quantum collisional thermostats. *New J. Phys.*, 24(2):023018.

[Tabanera-Bravo et al., 2023] Tabanera-Bravo, J., Parrondo, J. M., Esposito, M., and Barra, F. (2023). Thermalization and dephasing in collisional reservoirs. *arXiv preprint arXiv:2302.06429*.

[Tabanera-Bravo et al., 2022] Tabanera-Bravo, J., Vigneau, F., Monsel, J., Aggarwal, K., Bresque, L., Fedele, F., Cerisola, F., Briggs, G. A. D., Anders, J., Aufèves, A., Parrondo, J. M. R., and Ares, N. (2022). Stability of long-sustained oscillations induced by electron tunneling. *arXiv*.

[Taylor, 2006] Taylor, J. R. (2006). *Scattering theory: the quantum theory of nonrelativistic collisions*. Courier Corporation.

[Toral and Colet, 2014] Toral, R. and Colet, P. (2014). *Stochastic numerical methods: an introduction for students and scientists*. John Wiley & Sons.

[Treutlein et al., 2014] Treutlein, P., Genes, C., Hammerer, K., Poggio, M., and Rabl, P. (2014). Hybrid Mechanical Systems. In *Cavity Optomechanics*, pages 327–351. Springer, Berlin, Germany.

[Trotzky et al., 2012] Trotzky, S., Chen, Y.-A., Flesch, A., McCulloch, I. P., Schollwöck, U., Eisert, J., and Bloch, I. (2012). Probing the relaxation towards equilibrium in an isolated strongly correlated one-dimensional Bose gas. *Nat. Phys.*, 8:325–330.

[Turek and Matveev, 2002] Turek, M. and Matveev, K. A. (2002). Cotunneling thermopower of single electron transistors. *Phys. Rev. B*, 65(11):115332.

[Urgell et al., 2020] Urgell, C., Yang, W., De Bonis, S. L., Samanta, C., Esplandiu, M. J., Dong, Q., Jin, Y., and Bachtold, A. (2020). Cooling and self-oscillation in a nanotube electromechanical resonator. *Nat. Phys.*, 16:32–37.

[Usmani et al., 2007] Usmani, O., Blanter, Ya. M., and Nazarov, Yu. V. (2007). Strong feedback and current noise in nanoelectromechanical systems. *Phys. Rev. B*, 75(19):195312.

[van der Wiel et al., 2002] van der Wiel, W. G., De Franceschi, S., Elzerman, J. M., Fujisawa, T., Tarucha, S., and Kouwenhoven, L. P. (2002). Electron transport through double quantum dots. *Rev. Mod. Phys.*, 75(1):1–22.

[Van Houten et al., 1992] Van Houten, H., Beenakker, C. W. J., and Staring, A. A. M. (1992). Coulomb-Blockade Oscillations in Semiconductor Nanostructures. In *Single Charge Tunneling*, pages 167–216. Springer, Boston, MA, Boston, MA, USA.

[Vigneau et al., 2022] Vigneau, F., Monsel, J., Tabanera, J., Aggarwal, K., Bresque, L., Fedele, F., Cerisola, F., Briggs, G. A. D., Anders, J., Parrondo, J. M. R., Auffèves, A., and Ares, N. (2022). Ultrastrong coupling between electron tunneling and mechanical motion. *Phys. Rev. Res.*, 4(4):043168.

[Vinjanampathy and Anders, 2016] Vinjanampathy, S. and Anders, J. (2016). Quantum thermodynamics. *Contemp. Phys.*, 57(4):545–579.

[Von Smoluchowski, 1906] Von Smoluchowski, M. (1906). Zur kinetischen theorie der brownschen molekularbewegung und der suspensionen. *Annalen der physik*, 326(14):756–780.

[Wächtler et al., 2020] Wächtler, C. W., Bastidas, V. M., Schaller, G., and Munro, W. J. (2020). Dissipative nonequilibrium synchronization of topological edge states via self-oscillation. *Phys. Rev. B*, 102(1):014309.

[Wächtler et al., 2019] Wächtler, C. W., Strasberg, P., Klapp, S. H. L., Schaller, G., and Jarzynski, C. (2019). Stochastic thermodynamics of self-oscillations: the electron shuttle. *New J. Phys.*, 21(7):073009.

[Wang et al., 2017] Wang, Y., Micchi, G., and Pistolesi, F. (2017). Sensitivity of the mixing-current technique for the detection of mechanical motion in the coherent tunnelling regime. *J. Phys.: Condens. Matter*, 29(46):465304.

[Wang and Pistolesi, 2017] Wang, Y. and Pistolesi, F. (2017). Sensitivity of mixing-current technique to detect nanomechanical motion. *Phys. Rev. B*, 95(3):035410.

[Weiss and Zwerger, 1999] Weiss, C. and Zwerger, W. (1999). Accuracy of a mechanical single-electron shuttle. *Europhys. Lett.*, 47(1):97.

[Wen et al., 2018] Wen, Y., Ares, N., Pei, T., Briggs, G. A. D., and Laird, E. A. (2018). Measuring carbon nanotube vibrations using a single-electron transistor as a fast linear amplifier. *Appl. Phys. Lett.*, 113(15):153101.

[Wen et al., 2020] Wen, Y., Ares, N., Schupp, F. J., Pei, T., Briggs, G. A. D., and Laird, E. A. (2020). A coherent nanomechanical oscillator driven by single-electron tunnelling. *Nat. Phys.*, 16:75–82.

[Wilde, 2013] Wilde, M. M. (2013). *Quantum information theory*. Cambridge University Press.

[Willick and Baugh, 2020] Willick, K. and Baugh, J. (2020). Self-driven oscillation in Coulomb blockaded suspended carbon nanotubes. *Phys. Rev. Res.*, 2(3):033040.

[Wilson-Rae et al., 2004] Wilson-Rae, I., Zoller, P., and xn Imamolu-4s3c, A. (2004). Laser Cooling of a Nanomechanical Resonator Mode to its Quantum Ground State. *Phys. Rev. Lett.*, 92(7):075507.

[Wiseman and Milburn, 2009] Wiseman, H. M. and Milburn, G. J. (2009). *Quantum measurement and control*. Cambridge university press.

[Wolpert, 2019] Wolpert, D. H. (2019). The stochastic thermodynamics of computation. *J. Phys. A: Math. Theor.*, 52(19):193001.

[Woodside and McEuen, 2002] Woodside, M. T. and McEuen, P. L. (2002). Scanned Probe Imaging of Single-Electron Charge States in Nanotube Quantum Dots. *Science*, 296(5570):1098–1101.

[Yeo et al., 2014] Yeo, I., de Assis, P.-L., Gloppe, A., Dupont-Ferrier, E., Verlot, P., Malik, N. S., Dupuy, E., Claudon, J., Gérard, J.-M., Auffèves, A., Nogues, G., Seidelin, S., Poizat, J.-Ph., Arcizet, O., and Richard, M. (2014). Strain-mediated coupling in a quantum dot–mechanical oscillator hybrid system. *Nat. Nanotechnol.*, 9:106–110.